Periodontal pathobiology and defective cell-autonomous mineralization in X-linked hypophosphatemia

Benjamin R. Coyac

UNIVERSITÉ PARIS DESCARTES

MEMBRE DE USPC Université Sorbonne Paris Cité

Université Paris Descartes

École doctorale Bio Sorbonne Paris Cité

Craniofacial Pathologies, Imaging and Biotherapies Laboratory/EA2496

Periodontal Pathobiology and Defective Cell-Autonomous Mineralization in X-linked Hypophosphatemia

By Benjamin R. Coyac

Thèse de Doctorat en Physiopathologie

Dirigée par le Professeur Catherine Chaussain

Présentée et soutenue publiquement le jeudi 6 avril 2017

Devant un jury composé de :

Rapporteur :	Docteur Laurent Beck,	CR
Rapporteur :	Professeur Agnès Bloch-Zupan,	PU-PH
Examinateur :	Professeur Philippe Bouchard,	PU-PH
Directeur de thèse :	Professeur Catherine Chaussain,	PU-PH
Invité :	Docteur Claire Bardet,	MCF

Abstract

Title: Periodontal Pathobiology and Defective Cell-Autonomous Mineralization in X-linked Hypophosphatemia

Abstract: X-linked hypophosphatemia (XLH) is a rare X-linked dominant disorder caused by inactivating mutations in the *PHEX* gene. The impairment of PHEX protein leads to an increase in FGF23, a circulating factor that causes systemic loss of phosphate. The rachitic skeleton of patients with XLH displays short stature and osteomalacia. Dental defects include poorly mineralized dentin and spontaneous dental abscesses. Little is known about the periodontal condition of XLH and if patients are more prone to develop periodontitis, eventually leading to tooth loss. Although the exact function and substrate of PHEX are not known, it has been shown *in vitro* that PHEX could interact with SIBLING proteins such as MEPE or OPN, both involved in the regulation of bone and dentin mineralization, but it is not yet clear if the defects in the calcified extracellular matrices of XLH are caused by systemic hypophosphatemia only, or also by local consequences of the absence of PHEX. The aim of this doctoral dissertation was to explore the pathobiology of the XLH periodontium and to determine the impact of PHEX deficiency at the local level in a model of human biomineralization where phosphate supply could be adjusted and normalized. We first examined 34 adults with XLH in a case-control study and observed that periodontitis frequency and severity were increased in individuals with late or incomplete supplementation in phosphate and vitamin D analogs. The periodontium was then analyzed in XLH dental roots and further characterized in the *Hyp* mouse, the murine model of XLH. We performed a model of tooth movement adaptation leading to the formation of cellular cementum and a model of periodontal breakdown and repair to investigate the impact of XLH on the pathobiology of periodontal tissues. Our results showed strongly affected XLH/*Hyp* periodontal phenotype and impaired pathobiology and suggested that the key role played by OPN in bone could not be generalized to other periodontal mineralized tissues. In order to determine the role of PHEX in local human mineralization, dense collagen gels were seeded with primary human dental pulp cells harvested from XLH patients displaying *PHEX* mutations and age-matched healthy individuals. Cell-seeded gels were cultured up to 24 days under osteogenic conditions and controlled phosphate medium concentrations. Our results showed that despite normal phosphate concentrations, PHEX deficiency led to decreased quantity and quality of the mineral phase and a pathologic accumulation and processing of OPN. Overall the original contributions of this doctoral dissertation consist in the demonstration of a higher susceptibility of XLH patients to periodontitis and in the evidence of a local effect of PHEX deficiency in the pathologic intrinsic mineralization from XLH osteogenic cells.

Keywords: PHEX, X-linked hypophosphatemia, mineralization, dental pulp cells, collagen hydrogels, periodontium, cementum, osteopontin, periodontal breakdown and repair, alveolar bone, overeruption

Résumé

Titre : Physiopathologie parodontale et défauts de minéralisation dans le rachitisme vitamino-résistant hypophosphatémique

Résumé : Le rachitisme vitamino-résistant hypophosphatémique (RVRH) est une maladie génétique rare causée par des mutations du gène *PHEX*. La perte de fonction de la protéine PHEX conduit à l'augmentation du FGF23, une hormone circulante qui agit sur le rein et entraine une perte systémique de phosphate. Le squelette rachitique des patients atteints de RVRH présente des déformations osseuses et une ostéomalacie. La dentine hypominéralisée des patients est à l'origine d'abcès dentaires fréquents, mais le statut parodontal des patients RVRH est mal connu, de même que leur risque de développer une parodontite pouvant aboutir à la perte des dents. La fonction et le substrat de la protéine PHEX ne sont pas identifiés avec exactitude. Il a été montré *in vitro* que PHEX avait la capacité d'interagir et de dégrader des protéines membres de la famille des SIBLINGs comme MEPE ou OPN, toutes les deux impliquées dans la régulation de la minéralisation des tissus osseux et dentinaires, mais on ne sait pas si *in vivo* les défauts de minéralisation observés résultent principalement de l'hypophosphatémie systémique ou bien également des effets directs de l'absence de PHEX sur les protéines régulatrices de la minéralisation. L'objectif de cette thèse a consisté à s'intéresser à la physiopathologie du parodonte dans le RVRH ainsi qu'à déterminer quel était l'impact de la mutation de *PHEX* dans un modèle de biominéralisation humaine où les conditions de concentration en phosphate pouvaient être ajustées et normalisées. Nous avons d'abord analysé le statut parodontal de 34 patients RVRH dans une étude clinique cas-témoins et ainsi montré que les malades dont la supplémentation en phosphate et vitamine D était tardive ou incomplète présentaient une fréquence et une sévérité accrues de maladie parodontale. Le phénotype parodontal du RVRH a alors été étudié sur des échantillons humains et sur le modèle murin du RVRH, la souris HYP. Nous avons réalisé un modèle d'égression dentaire de façon à permettre une apposition du cément cellulaire, ainsi qu'un modèle de résorption et de réparation osseuses parodontales afin de caractériser l'impact du RVRH sur la physiopathologie parodontale. Nos résultats ont montré que le phénotype parodontal et sa physiopathologie étaient très perturbés dans le rachitisme vitamino-résistant hypophosphatémique et chez la souris HYP, nous avons aussi pu mettre en évidence que le rôle pathologique majeur joué par l'ostéopontine dans le tissu osseux au cours du RVRH ne pouvait pas être généralisé aux autres tissus minéralisés du parodonte. De façon à identifier le rôle de PHEX dans la minéralisation matricielle locale indépendamment de la phosphatémie systémique, nous avons ensemencé des matrices de collagène dense avec des cellules primaires humaines issues de patients RVRH comparés à des contrôles que nous avons cultivés pendant 24 jours en conditions ostéogéniques avec des concentrations en phosphate identiques. Nos résultats ont montré que malgré une concentration normale en phosphate, la perte de fonction de la protéine PHEX entrainait une diminution de la quantité et de la qualité de la phase minérale et une accumulation et une dégradation pathologiques de la protéine OPN. Les contributions originales de ce travail de thèse doctorale ont consisté à démontrer sur le plan clinique et biologique la susceptibilité accrue du rachitisme hypophosphatémique lié à l'X quant au risque de développer une maladie parodontale, ainsi qu'à apporter la preuve d'un rôle pathologique de l'absence de PHEX indépendant de la phosphatémie sur des cultures primaires humaines.

Mots-clefs : Rachitisme hypophosphatémique lié à l'X, PHEX, hydrogels de collagène, cellules souches pulpaires, ostéopontine, parodonte, modèle de résorption et d'apposition parodontales, os alvéolaire, cément, modèle d'égression

“Let me be contented in everything except in the great science of my profession. Never allow the thought to arise in me that I have attained to sufficient knowledge, but vouchsafe to me the strength, the leisure and the ambition ever to extend my knowledge. For art is great, but the mind of man is ever expanding.”

The Prayer of Maimonides

« Vivez dans la paix sereine des laboratoires et des bibliothèques. Vous n’y trouverez pas toujours la gloire, vous n’y trouverez jamais la fortune, mais vous y sentirez cette douceur d’être chaque jour quelque chose de plus que la veille et d’avoir apporté dans le monde votre part de vérité. »

Émile Duclaux

Acknowledgments

I thank the jury external examiners, Dr. Laurent Beck and Pr. Agnès Bloch-Zupan for accepting to review this dissertation.

I thank Pr. Catherine Chaussain, Pr. Philippe Bouchard and Dr. Claire Bardet for their supervision and support during my graduate training.

I thank the Fondation pour la Recherche Médicale *that supported my work and provided my doctoral scholarship (PhD grant FDM20140731354).*

I thank Pr. Jean-Louis Saffar for sharing his expertise and for his guidance since 2009 when I joined his laboratory.

I thank Pr. Marc D. McKee for welcoming me at McGill University where I experienced great moments of science and friendship.

I wish to acknowledge Dr. Tchilalo Boukpessi, Dr. Benjamin Salmon and Pr. Sibylle Vital for their kindness and guidance all along my years at Paris Descartes University, both in research and clinics.

I acknowledge Dr. Maxime Ghighi, Dr. Frédéric Chamieh and Dr. Bassam Hassan who I enjoyed working with every day at the lab and at the Rothschild Hospital, Paris.

I thank Dr. Brigitte Baroukh, Annie Llorens and Mahéva Garcia for their daily help and kindness during these last years of experiments.

I wish to acknowledge my family, for their love and support.

Table of Contents

List of figures

List of tables

Glossary of abbreviations and symbols

ADAM: A Disintegrin and Metalloprotease

ADHR: Autosomal dominant hypophosphatemia

ANKH: Progressive ankyloses protein homolog

ASARM: Acidic serine- and aspartate-rich motif

BMP: Bone morphogenetic protein

Ca^{2+}: Calcium

CDC/AAP: Center for Disease Control and Prevention/American Academy of Periodontology

CPPD: Calcium pyrophosphate dihydrate

CR: Calcium sensing receptor

DBP: Vitamin D binding protein

DSPP: Dentin sialophosphoprotein

ECM: Extracellular matrix

FAM20C: Family with sequence similarity 20, member C

FBS: Fetal bovine serum

FGF23: Fibroblast growth factor 23

FRP4: Frizzled related peptide-4

HAP: Hydroxyapatite

HERS: Hertwig epithelial root sheath

HPP: Hypophosphatasia

IGF-1: Insulin-like growth factor-1

IgG: Immunoglobulin G

IL-1: Interleukin-1

KO: Knock out

MEPE: Matrix extracellular phosphoglycoprotein

Mg^{2+}: Magnesium

mRNA: Messenger ribonucleic acid

Na^{+}: Sodium

NHANES: National Health and Nutrition Examinations Surveys

NPP1: Ectonucleotide pyrophosphatase/phosphodiesterase 1

NPT2a: Sodium-phosphate co-transporter Type 2a

OPG: Osteoprotegerin

OPN: Osteopontin

PCR: Polymerase chain reaction

PDL: Periodontal ligament

PGE_2: prostaglandin E_2

PHEX: Phosphate-regulating gene with homologies to endopeptidases on the X chromosome

PHOSPHO1: Phosphoethanolamine/phosphocholine phosphatase

P_i: Inorganic or orthophosphate

PMN: Polymorphonuclear neutrophil

PP_i: Pyrophosphate

PTH: Parathyroid hormone

RANKL: Receptor activator of nuclear factor kappa-B ligand

SIBLING: Small Integrin-Binding-Ligand-N-linked Glycoprotein

TIO: Tumor-induced osteomalacia

TNAP: Tissue nonspecific alkaline phosphatase

TNF: Tumor necrosis factor

VDR: Vitamin D receptor

WT: Wild type

XLH: X-linked Hypophosphatemia

1,25-$(OH)_2D_3$: Active vitamin D, calcitriol

2D: Two-dimensional

3D: Three-dimensional

1 General Introduction

1.1 Introduction

First described in 1937 (Albright et al. 1937), X-linked hypophosphatemic rickets (XLH) inheritance was detailed in 1958 (Winters et al. 1991). XLH is the most common form of hypophosphatemia, occurring in 3.9-5 per 100,000 live births. The genetic basis of XLH was elucidated as mutations in *PHEX* (phosphate-regulating gene with homologies to endopeptidases on the X chromosome) in the 1990s (The HYP consortium). To date, 338 mutations have been described (PHEX database: www.PHEXdb.mcgill.ca). The *PHEX* gene encodes a M13 family member of membrane-bound metalloproteases present in osteoblasts, osteocytes and odontoblasts but not in kidney tubules (Beck et al. 1997). PHEX controls phosphate homeostasis through an unknown mechanism involving fibroblast growth factor 23 (FGF23), and thus contributes to regulate renal phosphate reabsorption.

PHEX loss-of-function mutations manifest clinically as rickets in children and as osteomalacia in adults, with defective growth, deformed bone shape, hampered hearing function and multiple dental abscesses (Carpenter et al. 2011; Linglart et al. 2014). PHEX being expressed in cells that orchestrate mineralization of bones and teeth, every mineralized tissue might be affected in XLH, possibly extending the scope of pathologic phenotypes already described in the disease. The periodontium is the interface between tooth organs and jaw bones (maxilla and mandible). It is composed of mineralized tissues (i.e. alveolar bone and dental cementum) and soft tissues (i.e. collagenous periodontal ligament and gingiva). The periodontium absorbs constrains of chewing function or dental trauma and adapts the tooth to its changing environment during tooth movements in passive eruption or orthodontic therapy. It can be irreversibly destroyed by periodontitis, a multifactorial inflammatory disease that affects 46% of individuals over 30 years old (Eke et al. 2015). Only one case series described the periodontal condition of 10 XLH patients (Ye et al. 2011). This lack of information regarding the periodontal condition and phenotype of XLH is to be compared with hypophosphatasia (HPP), another genetic disease characterized by osteomalacia, for which extensive data have been published regarding the specific susceptibility of HPP patients to develop periodontitis.

In addition to its role in controlling FGF23 hormone, and thus phosphate reabsorption, PHEX is believed to regulate collagen biomineralization in extracellular matrices of calcified tissues by controlling Small Integrin-Binding-Ligand-N-linked Glycoproteins (SIBLING) homeostasis. Direct function of PHEX on local mineralization remains a hypothesis when it relates to human mineralized tissues as this role has only been demonstrated *in vitro* with recombinant peptides/proteins and murine cells (Addison et al. 2010; Addison et al. 2008; Barros et al. 2013; Salmon et al. 2013) or *in vivo* where it is not possible to isolate the putative direct effect of PHEX impairment (independent from phosphate variations) from the pathologic contribution of systemic hypophosphatemia on the disturbed SIBLING proteins homeostasis and the observed local mineralization defects (Barros et al. 2013).

1.2 Thesis outline

The present section (**Section 1**) consists of a general overview of X-linked hypophosphatemia and highlights the gaps in our understanding of the extent and pathobiology of the disease. A thesis outline is presented, followed by a description of the aim, the research hypothesis and the objectives. In addition, a summary of original contributions ends the first section. **Section 2** provides a detailed review of biological principles underlying the field of pathological mineralization as it relates to phosphate and a description of the periodontium, along with an exhaustive description of the current state-of-the-art. Topics discussed include phosphate homeostasis, biomineralization and associated disorders, and a description of the periodontium and periodontitis. In particular, Section 2 outlines the specific relationship between biomineralization disorders and periodontal diseases. **Section 3** offers a description of the statement of the problem, highlighting the motivations behind this doctoral research. **Section 4** introduces the processing of human and murine tissues and details the experimental models of ligature-induced periodontal breakdown and repair and of tooth movement adaptation. Finally, the mechanism of production of dense collagen gels via the plastic compression technique with primary dental pulp cells is detailed. **Section 5** deals with the observational study of XLH patients with a comparison based on their compliance with the treatment for XLH. **Section 6** investigates the periodontal phenotype of XLH/*Hyp* with a

characterization of the adaptive capacity of *Hyp* periodontium to alveolar bone healing and tooth movement. An investigation on the phosphate variation-independent impact of PHEX impairment in a model of human biomineralization is reported in **Section 7**. **Section 8** provides a general discussion of the work undertaken in this thesis with overall conclusions and future perspectives. In **Section 9**, references are presented. Finally, in **Section 10**, additional co-authored published papers related to the work of this dissertation are provided.

1.3 Aim, Research hypothesis, Objectives

The aim of this doctoral research was to study the periodontal pathobiology in X-linked hypophosphatemic patients and to explore the effect of PHEX impairment on cell-autonomous intrinsic mineralization in order to determine if PHEX had a direct role in the defective matrix mineralization displayed *in vivo*, in addition to the detrimental hypophosphatemia. The global hypothesis underlying this thesis is that **"skeletal defects of X-linked hypophosphatemic rickets extend to the periodontium, providing a specific susceptibility to periodontitis and *PHEX* loss-of-function mutations locally impair extracellular matrix mineralization in addition to systemic hypophosphatemia."**

Within this research, three different objectives were established, which were to:

1. Measure the extent and severity of periodontitis in a population of X-linked hypophosphatemic patients and to evaluate the effect of the treatment for XLH in the susceptibility to periodontitis.

2. Characterize the periodontal tissues and physiology in XLH teeth and *Hyp* mice, the murine counterpart of XLH.

3. Evaluate the impact of *PHEX* loss-of-function mutations, independently to surrounding hypophosphatemia, in terms of mineral phase formation and quality and in terms of SIBLING proteins processing.

In order to meet the first objective, an epidemiological observational case-control study was designed to compare XLH patients' periodontal status with different compliance to treatment of XLH (Phosphate supplementation and vitamin D analogs). Three groups were compared: no use of XLH treatment – no use of XLH treatment during adulthood – use of XLH treatment during childhood and adulthood. Clinical, radiographic and histologic examinations were performed, followed by a statistical analysis between groups. The overall frequency and severity of periodontitis in XLH patients were compared with existing data from the National Health and Nutrition Examination Survey on the prevalence, extent and severity of periodontitis among the US adult population (Eke et al. 2015).

To achieve the second objective, dental tissues from XLH patients and *Hyp* mice (the murine analog of XLH), were compared with age- and sex-matched control individuals and WT mice. Every tissue involved in the periodontal attachment apparatus (i.e. alveolar bone, acellular and cellular cementum, periodontal ligament) was described using imaging, histology, immunohistochemistry and Raman spectroscopy. The alveolar bone healing and periodontal adaptive function to passive eruption were further investigated in the *Hyp* mouse, using two experimental models: a modified ligature-induced model of periodontal breakdown and repair and a model of tooth over-eruption/cellular cementum formation.

To meet the third objective, primary dental pulp cells from XLH patients and control individuals were cultured in a three-dimensional *in vitro* collagen model of human mineralization (Coyac et al. 2013) under normalized phosphate medium concentration. After 24 days of culture, the mineral phase quantity was measured with imaging, histology and biochemical quantification, the mineral phase quality was evaluated through ultrastructural microscopy and Raman spectroscopy, and the molecular processing of XLH and Control cell-seeded scaffolds was assessed with immunohistochemistry, western blots and immunogold labeling.

1.4 Summary of original contributions

The original contribution to the advancement of knowledge in the research area of craniofacial pathologies are summarized by the following publications:

- Biosse Duplan M, **Coyac BR**, Bardet C, Zadikian C, Rothenbuhler A, Kamenicky P, Briot K, Linglart A, Chaussain C. 2016. Phosphate and vitamin d prevent periodontitis in x-linked hypophosphatemia. **Journal of dental research**.

This article confirmed a previous case series showing a higher frequency and severity of periodontal diseases among XLH patients. In addition, it indicated that conventional XLH management begun during childhood and continued during adulthood could effectively prevent or treat periodontitis in these patients.

- **Benjamin R. Coyac**, Guillaume Falgayrac, Brigitte Baroukh, Lotfi Slimani, Jérémy Sadoine, Guillaume Penel, Martin Biosse-Duplan, Thorsten Schinke, Agnès Linglart, Marc D. McKee, Catherine Chaussain, Claire Bardet. Impaired oral bone healing and adaptation to tooth movement in X-linked Hypophosphatemia. **Submitted to a peer-reviewed journal**.

Extensive characterization of XLH and *Hyp* periodontal tissues was provided in this paper. It was shown that contrary to a previous report (Boukpessi et al. 2016)(Appendix), osteopontin is not an etiologic factor to the defective mineralization and formation of periodontal mineralized tissues. In addition, the defective *Hyp* periodontium was tested in experimental models of alveolar bone healing following ligature-induced breakdown, and in a model of unloaded tooth over-eruption following antagonist teeth extraction, triggering cellular cementum apposition. In both models, *Hyp* periodontium presented impaired healing and adaptive responses.

- **Benjamin R. Coyac**, Guillaume Falgayrac, Betty Hoac, Lotfi Slimani, Guillaume Penel, Agnès Linglart, Marc D. McKee, Catherine Chaussain, Claire Bardet. Impaired Cell-autonomous Mineralization in X-linked Hypophosphatemia. **Submitted to a peer-reviewed journal**.

The development of a model of mineralization obtained from primary human pulp cells (Coyac et al. 2013) (Appendix 1) enabled to test the direct impact of PHEX deficiency in conditions of “normophosphatemia”. This article demonstrated that regardless of surrounding phosphate concentration, XLH cells presented a reduced mineral phase with impaired quality and an accumulation of osteopontin.

2 Background and literature review

2.1 Phosphate metabolism

2.1.1 Overview of calcium and phosphate metabolism

Calcium (Ca^{2+}) and phosphate (P_i, inorganic or orthophosphate, as opposed to organophosphate compounds such as adenosine triphosphate) balance is primarily controlled by parathyroid hormone (PTH) and the active form of vitamin D ($1\alpha,25\text{-}(OH)_2D_3$, calcitriol). Approximately 60% of calcium in the plasma is filtered in the kidney. Forty percent of plasma calcium is bound to proteins, or complexed with anions. Most of Ca^{2+} reabsorption (more than 60%) occurs in the proximal tubule and is independent of any hormonal control. Forty percent of calcium reabsorption is made in the distal convoluted tubule and early in the cortical collecting duct through hormonal control. When plasma calcium is low, the secretion of PTH from the parathyroid glands increases. PTH increases Ca^{2+} reabsorption by stimulating channels in the nephron. In addition, PTH increases the activity of 1-α-hydroxylase enzyme that activates $25\text{-}(OH)D_3$ to $1\alpha,25\text{-}(OH)_2D_3$, which then increases Ca^{2+} and P_i ion absorption in the gastrointestinal tract.

Phosphate is involved in skeletal development, in bones and teeth mineralization, in the composition of cell membranes, in the structure of nucleotides, phosphoproteins, phospholipids and phosphoglycans or as a source of energy bonds in adenosine triphosphates. Eighty-five percent of phosphate resides in bone, primarily compounded with calcium Ca^{2+}, in hydroxyapatite (HAP) crystals that are deposited on and in the collagen matrix (Landis and Jacquet 2013) and soft tissues only contain about 1% of the total phosphate in extracellular fluids (Drezner 2013). Phosphate homeostasis is essential for normal development, maintenance, and repair of teeth and skeletal tissues. Phosphate is present in a large variety of foods, and most of the P_i load is absorbed in the small intestine. From blood, phosphate is incorporated into mineralized tissues matrices or into cells, or excreted from the body in urine through hormonal regulation targeting the kidney. The impact of hormonal regulation mediated by $1\alpha,25\text{-}(OH)_2D_3$ is minor relative to the dietary load, and so the maintenance of circulating plasma level is largely performed through the

excretion and reabsorption of the renal glomerular filtrate in the proximal tubule, rather than absorption in the gastrointestinal tract. Unlike Ca^{2+}, phosphate ion reabsorption is decreased by PTH. Thus, when plasma Ca^{2+} level is low and PTH and Ca^{2+} reabsorption are increased, as a result phosphate ion excretion is increased (Drezner 2013). Renal P_i reabsorption concerns nearly 90% of the glomerular filtrate. It is mostly mediated by the sodium-phosphate co-transporter Type 2a (NPT2a) in the proximal tubules. The expression of co-transporter proteins regulates reabsorption (Murer et al. 1999; Murer et al. 1998) and is affected by dietary phosphate load: hyperphosphatemia decreases the expression of NPT2a and hypophosphatemia increases its expression. PTH increases endocytosis of NPT2a from the cell membrane (Nashiki et al. 2005a). In the proximal tubule, PTH induces mRNA expression of 25-hydroxy-vitamin D and 1-α hydroxylase, and thus increases the production of $1\alpha,25\text{-}(OH)_2D_3$ which will mobilize P_i stored in the bone matrix. Although PTH is seen as an important physiological regulator of renal P_i excretion, the balance between dietary intake and renal excretion is maintained in conditions of hyper and hypoparathyroidism, suggesting an intrinsic proximal tubule regulation of the excretion in response to dietary load (Foster et al. 2008; Levi et al. 1994).

Several other hormones display secondary effects on P_i tubular reabsorption: insulin-like growth factor (IGF-1), insulin, thyroid hormone and epidermal growth factor (EGF) enhance phosphate reabsorption, and transforming growth factor alpha (TGFα), calcitonin, parathyroid hormone related peptide (PTHrP) and glucocorticoids inhibit phosphate reabsorption. In addition to dietary load and reabsorption of the glomerular filtrate, other conditions affect circulating P_i levels, such as sepsis and insulin therapy (Foster et al. 2008).

The parathyroid-intestinal-kidney-bone axis is believed to regulate the homeostasis of Ca^{2+} and P_i with molecules such as PTH, $1\alpha,25\text{-}(OH)_2D_3$ and calcitonin acting via a self-limiting feed-back loop mechanism. Ca^{2+} levels were believed to be paramount in influencing the actions of these molecules, and P_i levels were thought to follow the flow of Ca^{2+} in order to maintain electrical balance. It has become clear that the regulation of P_i levels is under as strict control as Ca^{2+} by newly discovered agents.

Recently, the study of renal phosphate wasting disorders such as tumor-induced osteomalacia (TIO), X-linked hypophosphatemic rickets (XLH) or autosomal dominant hypophosphatemia (ADHR), has enabled the characterization of hormones that specifically regulate P_i homeostasis, i.e. phosphate-regulating protein with homologies to endopeptidases on the X chromosome (PHEX), fibroblast growth factor 23 (FGF23) (Quarles 2003; Rowe 2012; 2015; White et al. 2006), secreted frizzled related peptide-4 (FRP4) (Berndt et al. 2003; Berndt and Kumar 2009; Berndt et al. 2006; Vaes et al. 2005; White et al. 2006), matrix extracellular phosphoglycoprotein (MEPE) (Argiro et al. 2001; Fisher and Fedarko 2003; MacDougall et al. 2002; Quarles 2003; Rowe 2012; 2015; Rowe et al. 2000; White et al. 2006), and fibroblast growth factor 7 (FGF7) (Berndt et al. 2005; Carpenter et al. 2005). Both FGF23 and FRP4 have been shown to inhibit 25-$(OH)D_3$ 1-α-hydroxylase activity, that normally increased in conditions causing hypophosphatemia, and are thus considered ''phosphatonins'': a label attributed to factors that increase renal loss of phosphate and inhibit active vitamin D synthesis (Berndt et al. 2005; Econs and Drezner 1994). Notably, factors that alter Ca^{2+} and P_i plasma levels affect both PTH and 1α,25-$(OH)_2D_3$ levels, adding complexity to studies that aim at defining the processes by which factors regulating plasma phosphate levels modulate mineral homeostasis.

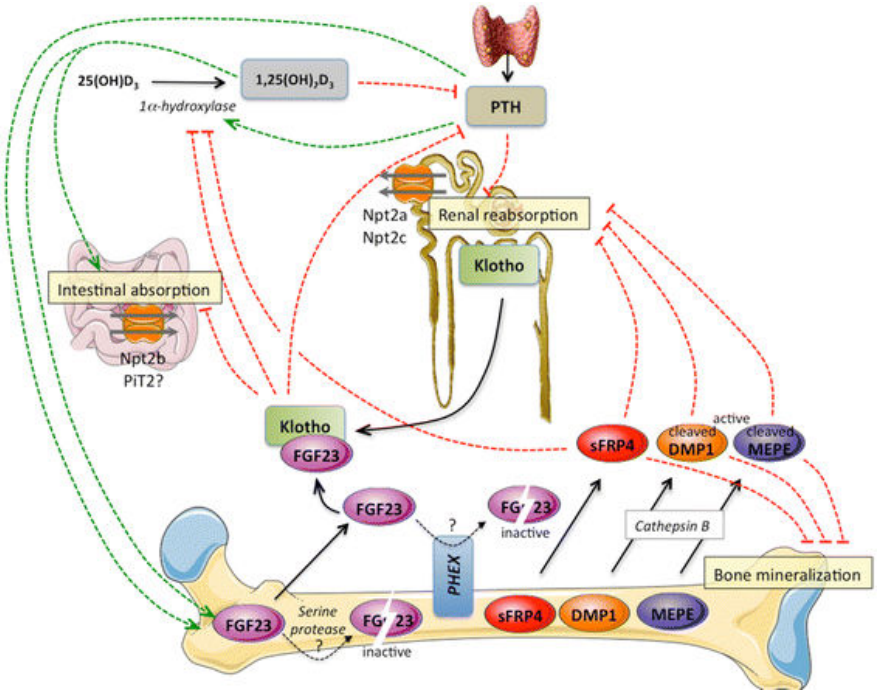

Figure 1 Regulators of Phosphate Homeostasis

Regulators inhibit (red lines) or increase (green lines) phosphate absorption/reabsorption and skeletal mineralization

Reprinted from Khoshniat et al., 2011, with permission from Springer

2.1.2 The tooth: an organ sensitive to phosphate homeostasis

The teeth and their supporting tissues are epithelial-mesenchymal organs composed of four mineralized tissues: highly mineralized enamel in the outer crown, resilient dentin surrounding the pulp chamber, layers of cementum that cover the root and are essential for attachment of the tooth via the periodontal ligament, and alveolar bone anchoring the teeth in the bony sockets via the periodontal ligament (Nanci 2012; Nanci and Bosshardt 2006). Studies on developmental disorders in humans and on gene mutation and knock out (KO) in mouse models indicate that systemic and local factors modulating P_i homeostasis seem to differentially control formation of oral mineralized tissues (Boukpessi et al. 2006; Chaussain-Miller et al. 2003; Fong et al. 2009; Foster et al. 2007; Nociti et al. 2002; Onishi et al. 2007; Opsahl Vital et al. 2012; Toyosawa et al. 2004; van den Bos et al. 2005; Ye et al. 2004; Ye et al. 2008) providing insight into the specific roles of key regulators of P_i homeostasis during development, maintenance, disease, repair and regeneration of dental tissues.

2.1.3 Systemic regulators of phosphate homeostasis

2.1.3.1 Vitamin D

Vitamin D was discovered in 1920 and its chemical structure characterized in 1932, and was found to be critical for bone formation and Ca^{2+} regulation (Brockmann 1936; Mellanby 1921). The vitamin D precursor is produced in the skin in response to ultraviolet light, and as part of food intake (Goldblatt and Soames 1923). This pre-vitamin D_3 molecule (cholecalciferol) must undergo two sequential hydroxylations to yield to the active metabolite 1α,25-$(OH)_2D_3$ (calcitriol). Vitamin D binding protein (DBP) first moves pre-vitamin D_3 molecule through the bloodstream to the liver. In the liver, pre-vitamin D_3 molecule receives a hydroxyl group at carbon 25 position, from the action of cytochrome P450 25-hydroxylase enzymes such as CYP27A1 (Oftebro et al. 1981). 25(OH)D_3 then moves to the proximal kidney tubule to receive another hydroxylation at the 1α position via cytochrome P450 1-α-hydroxylase (CYP27B1) (Henry and Norman 1974). This renal enzyme is stimulated by PTH in response to low Ca^{2+} levels in the plasma, or low 1α,25-$(OH)_2D_3$ levels (Brown et al. 1995). 1α,25-$(OH)_2D_3$ finally moves with DBP to its target tissues. Parathyroid gland then inhibits the release of PTH in a negative feed-back loop (Russell et al. 1993). The

1α,25-$(OH)_2D_3$ receptor (VDR) is located in the cytosol of targeted cells. Once inside the cell, 1α,25-$(OH)_2D_3$ binds to VDR and forms a heterodimer with the retinoid X receptor. This complex moves to the nucleus and binds to the promoters of 1α,25-$(OH)_2D_3$ target genes, acting as either an enhancer or a repressor (Prüfer et al. 2000). 1α,25-$(OH)_2D_3$ exerts its effects on mineral homeostasis in the intestine by increasing the absorption of Ca^{2+} and the expression of NaP_i2b enabling the reabsorption of P_i, and in the kidney where it increases the expression of NaP_i2c and the reabsorption of P_i from the glomerular filtrate (Barthel et al. 2007; Capuano et al. 2005; Hoenderop et al. 2005; Peng et al. 1999). 1α,25-$(OH)_2D_3$ also indirectly increases the plasma Ca^{2+} levels by stimulating bone marrow stromal cells to produce RANKL, thus inducing osteoclastogenesis (Udagawa et al. 1990). Apart from its role in mineral homeostasis, 1α,25-$(OH)_2D_3$ has direct effects on osteoblastic differentiation, stimulating the expression of osteocalcin, tissue-nonspecific alkaline phosphatase (TNAP) and osteopontin (OPN) (Anderson et al. 2013). 1α,25-$(OH)_2D_3$ also works together with the Wnt and Notch signaling proteins to promote osteoblastic differentiation (Fretz et al. 2007).

Nutritional deficiency in vitamin D is characterized by rickets, hypocalcemia and secondary hyperparathyroidism (Nagpal et al. 2005). Mice lacking the 1-α-hydroxylase gene present rickets and osteomalacia, with secondary hyperparathyroidism, hypocalcemia, and hypophosphatemia (Panda et al. 2001). Humans with familial hypophosphatemic rickets, characterized by low circulating 1α,25-$(OH)_2D_3$ concentrations, have teeth with dentin defects resulting from unmerged calcospherites (Chaussain-Miller et al. 2003). Treatment of these patients with 1α,25-$(OH)_2D_3$ and increased dietary P_i results in a normalization of dentin mineralization(Chaussain-Miller et al. 2007).

2.1.3.2 Parathyroid hormone

The primary structure of PTH was identified in 1970 (Niall et al. 1970), it is a 84 amino acid protein, but its biological activity resides in the amino terminal 34 residues (Rosenblatt et al. 1978; Tregear et al. 1973). PTH is secreted from the parathyroid gland based on serum Ca^{2+} levels which are detected by the calcium sensing receptor (CR). Low levels of Ca^{2+} inhibit CR activity, allowing PTH to be released into the circulation to achieve downstream effects (Riccardi et al. 1995). A major action of PTH is to increase osteoblastic production of receptor activator of nuclear factor kappa-B ligand (RANKL) (Suda et al. 1999), and so

indirectly increase the osteoclastic activity to release Ca^{2+} from bone resorption (Kondo et al. 2002). PTH also induces osteoblasts to secrete osteoprotegerin (OPG), a RANK decoy ligand that inhibits osteoclasts activation (Fu et al. 2002). In addition, PTH stimulates the formation of $1\alpha,25\text{-}(OH)_2D_3$ which results in both increased Ca^{2+} absorption in the intestine and reabsorption in the kidney, and stimulates the endocytosis of NaP_i2a transporters, thus reducing the reabsorption of P_i in the kidney (Nashiki et al. 2005b). High levels of Ca^{2+} stimulate the CR which inhibits PTH release, and increases calcitonin release from the thyroid, inhibiting osteoclasts activity (Fudge and Kovacs 2004). There is some evidence that PTH has direct effects on dental cells. Both odontoblasts and cementoblasts present cell surface PTH receptors (Lundgren et al. 1998; Tenorio and Hughes 1996).

2.1.3.3 Calcitonin

Calcitonin promotes renal excretion of Ca^{2+} by decreasing its tubular reabsorption (Sexton et al. 1999). In addition, calcitonin increases the transcription of the 1-α-hydroxylase gene (*CYP27B1*) in the proximal tubule of the kidney, and so increases the renal conversion of $25(OH)D_3$ to $1,25(OH)_2D_3$ (Zhong et al. 2009). Unlike PTH, calcitonin is a major regulator of 1α-hydroxylase and plasma levels of $1,25(OH)_2D_3$ in the normocalcemic state (Shinki et al. 1999). Calcitonin is also an inhibitor of bone resorption that acts by inhibiting osteoclast activity (Del Fattore et al. 2008). Despite these documented effects, the role of calcitonin remains debated. The absence of any obvious bone or calcium pathobiology in patients with low levels of calcitonin led some investigators to think of calcitonin as a vestigial hormone (Davey and Findlay 2013).

2.1.4 Phosphate transporters

P_i movement into the cell does not occur by simple diffusion. Na^+-coupled P_i cotransporters mediate the transport of P_i across cell membranes (Khoshniat et al. 2011; Murer et al. 2000; Werner and Kinne 2001). Na^+-P_i cotransporters are grouped into two genetically distinct families. The SLC34 family comprises SLC34A1 (NaP_i2a), SLC34A2 (NaP_i2b) and SLC34A3 (NaP_i2c). The SLC20 family comprises SLC20A1 (PiT-1) and SLC20A2 (PiT-2).

NaP_i2a (encoded by the *SLC34A1* gene) is located at the brush border of the renal proximal tubular epithelial cells and is responsible for the renal reabsorption of P_i. It is a target for most humoral factors regulating P_i homeostasis (Beck et al. 1998b; Murer et al. 2003; Prie et al. 2009). NaP_i2b (encoded by the *SLC34A2* gene) is the main transporter for intestinal P_i absorption, it is not detected in renal tissues (Hilfiker et al. 1998; Sabbagh et al. 2009). NaP_i2c (encoded by the *SLC34A3* gene) is localized in the same cells as NaP_i2a and is also involved in P_i and Ca^{2+} homeostasis and in bone mineralization by modulating the 1α,25-$(OH)_2D_3$/FGF23 axis (Kido et al. 2013; Segawa et al. 2009a; Segawa et al. 2009b).

SLC20 proteins are functionally distinct from SLC34 proteins, with PiT-1 being less sensitive to pH compared to SLC34 proteins. Unlike SLC34 proteins that are exclusively Na^+ driven, for PiT-1, lithium ion can replace sodium ion as the driving cation (Ravera et al. 2007). SLC20 proteins are widely expressed, yet their cell specific localization in different organs remains unclear (Collins et al. 2004; Nishimura and Naito 2008). The cellular localization at the apical membrane of proximal tubular epithelia is established for PiT-2 (Villa-Bellosta et al. 2009). In the small intestine, both PiT-1 and PiT-2 are expressed (Bai et al. 2000; Giral et al. 2009; Kavanaugh and Kabat 1996; Li et al. 2006; Ravera et al. 2007). In both small intestine and kidney, the contribution of PiT-1 & 2 might represent ~5% of transepithelial P_i transport (Forster et al. 2011; Villa-Bellosta and Sorribas 2010).

PiT-1 expression in osteoblasts and other cells is regulated by P_i availability and factors including IGF-1 or BMP2 that suggest a role in vascular and bone physiology (Forster et al. 2011; Li and Giachelli 2007; Miyamoto et al. 2011; Yoshiko et al. 2007a; Zoidis et al. 2004). In addition to a role in phosphate homeostasis, PiT-1 might be involved in hyperphosphatemia induced calcification of blood vessels (Lau et al. 2010; Shanahan et al. 2011), as well as in parathyroid function (Tatsumi et al. 1998). Functions independent of transport have emerged for PiT-1, such as cell proliferation and mitosis (Beck et al. 2009), liver development (Beck et al. 2010), anemia and growth (Festing et al. 2009).

PiT-2 expression does not respond to P_i starvation or treatment with PTH or 1α,25-$(OH)_2D_3$, but PiT-2 may play a role in P_i reabsorption (Villa-Bellosta et al. 2009). In kidney, its apical abundance is regulated by dietary intake of P_i (Villa-Bellosta et al. 2009), potassium deficiency (Breusegem et al. 2009) and PTH (Picard et al. 2010). Analysis in a family with familial idiopathic basal ganglia calcification (Fahr disease) identified loss of function

mutations in the *SLC20A2* gene that represent the molecular basis for disturbed P_i homeostasis in the brain of these patients, implicating the involvement of PiT-2 in brain (Wang et al. 2012).

2.1.5 Emerging regulators of phosphate homeostasis

2.1.5.1 PHEX

PHEX (Phosphate-regulating gene with homologies to endopeptidases on the X chromosome) is an endopeptidase of unknown physiological substrate. PHEX expression is limited to osteoblasts, osteocytes and odontoblasts, suggesting a role in the mineralization process (Ruchon et al. 2000). *PHEX* mutations were found responsible for XLH after positional cloning method (HYP Consortium, 1995). XLH is the most common form of rickets in humans and is characterized by hypophosphatemia, reduced growth and altered 1α,25-$(OH)_2D_3$ levels (Rasmussen and Tenenhouse 1995). The *Hyp* mouse is a natural mutant homologous to human XLH, (Eicher et al. 1976), it also presents a reduction in body weight, shortened bones with rachitic splaying at the epiphysis and a widening of the growth plate due to an expansion of the hypertrophic zone, and an increase in unmineralized osteoid, with lower serum P_i and 1α,25-$(OH)_2D_3$ levels, and increased PTH levels compared to wild type mouse (WT), however the *Hyp* mouse is normocalcemic. Transgenic expression of *Phex* in the *Hyp* mouse restores the bone phenotype, without improving the P_i metabolism deficiencies (Erben et al. 2005a; Zelenchuk et al. 2014b), that is directly impacted by an over-expression of FGF23, primarily by osteocytes. FGF23 has been shown to be responsible for much of the pathogenesis in the *Hyp* mouse (Liu et al. 2006).

2.1.5.2 MEPE

MEPE (Matrix extracellular phosphoglycoprotein) was identified in tumor-induced osteomalacia (TIO), and is a member of the SIBLING (Small Integrin-Binding Ligand N-linked Glycoprotein) family (McKee et al. 2013). MEPE expression in osteocytes, odontoblasts, hypertrophic chondrocytes and in the callus of bone fractures suggests a function in skeletal and dental mineralization (Argiro et al. 2001; Rowe et al. 2000). The expression of MEPE is increased in XLH patients and in the *Hyp* mouse (Rowe 2012; 2015). In addition, the *Mepe*$^{-/-}$ mouse displays an increase in cortical and trabecular bone (Liu et al. 2005), indicating that

MEPE functions as an inhibitor of mineralization upon normal levels of P_i and 1α,25-$(OH)_2D_3$. Like other SIBLINGs, the functional portion of MEPE is the acidic serine-aspartate rich associated Motif (ASARM) (Martin et al. 2008). It was previously supposed that MEPE was a PHEX substrate that could release its ASARM motif upon cleavage, but further studies showed that MEPE is not a substrate of PHEX, and PHEX seems to protect MEPE (and DMP1) from cleavage by cathepsin B, which frees ASARM motifs (Rowe 2012; 2015). *In vitro* studies show that PHEX can cleave ASARM peptides, thus inhibiting the inhibitory effect of ASARM on hydroxyapatite crystal growth (Addison et al. 2008). The hypomineralization in the *Hyp* mouse might be a combination of increased MEPE expression with a lack of PHEX-mediated protection from degradation of MEPE, producing an excess of ASARM peptides. Mice null for *Phex* and for *Mepe* were crossed, and the offsprings did not have a correction of the hypomineralization, neither of hypophosphatemia and low 1α,25-$(OH)_2D_3$ levels (Liu et al. 2005). And so, MEPE is not the main phosphatonin defining the mineralization phenotype in *Hyp* mouse and XLH.

2.1.5.3 FGF23

Among the 22 members of the FGF family, the *FGF23* gene is localized to human chromosome 12p13 and encodes the 251-amino acid FGF23 protein (Yamashita et al. 2000). FGF23 functions as a phosphatonin, affecting P_i levels directly or by regulating the actions of 1α,25-$(OH)_2D_3$. FGF23 decreases the expression of NaP_i2a and NaP_i2c transporters, and so decreases P_i reabsorption in the kidney. In addition, FGF23 decreases the expression of 1-α-hydroxylase in the kidney, thus reducing the levels of 1α,25-$(OH)_2D_3$ and stimulating the expression of 24-hydroxylase, which is catabolic for 1α,25-$(OH)_2D_3$ (Roy et al. 1994; Segawa et al. 2003; Shimada et al. 2004b). FGF23 is primarily expressed in osteoblasts and osteocytes in bone, odontoblasts and cementoblasts in teeth, and growth plate chondrocytes (Riminucci et al. 2003; Yoshiko et al. 2007b). Signaling by FGF is mediated by FGF receptors (FGFR) that propagate a signal cascade which stimulates the FGF effector genes in the nucleus (Ornitz et al. 1996; Werner et al. 1992). The binding of FGF23 to FGFRs is enhanced by Klotho (Urakawa et al. 2006). Klotho is mainly produced in the distal convoluted tubules of the kidney (Kuro-o et al. 1997) where is acts as a membrane-bound

co-receptor for FGF23, allowing it to bind to fibroblast growth factor receptors 1, 3 and 4 and to contribute to phosphate homeostasis (Kurosu et al. 2006).

The over-expression of FGF23 is responsible for the development of multiple diseases characterized by P_i wasting, low levels of 1α,25-$(OH)_2D_3$, and bone mineralization defects including rickets/osteomalacia, such as ADHR (autosomal dominant hypophosphatemic rickets), tumor-induced osteomalacia (TIO), autosomal recessive hypophosphatemic rickets (ARHR), and XLH in humans, and the *Hyp* phenotype in mice with a *Phex* mutation. These various endocrine conditions suggest that the observed phenotypes may not result from direct effects of the mutated genes (e.g. loss of PHEX or DMP1) but are rather associated with high levels of FGF23 (Foster et al. 2008). It was hypothesized that FGF23 was a PHEX substrate, but this assumption was refuted (Quarles 2003). It is now believed that a natural substrate of PHEX controls FGF23 expression and this unprocessed factor in the absence of PHEX results in the over-expression of FGF23 in XLH/*Hyp* (McKee et al. 2013; Rowe 2012; 2015).

Knockout mouse models investigated the participation of FGF23 in the *Hyp* mouse by producing a *Hyp/Fgf23* KO cross (Liu et al. 2006; Sitara et al. 2004). The compound mice had a resolution of rickets with no detectable expression of FGF23, hyperphosphatemia, high levels of 1α,25-$(OH)_2D_3$, low PTH and normal Ca^{2+} level, but still presented shortened bones and osteomalacia. So much of the phenotype in the *Hyp* mouse is due to the FGF23 over-expression, and its removal superimposes the *Fgf23* KO phenotype onto the *Hyp* mouse (Liu et al. 2006; Sitara et al. 2004).

2.1.5.4 αKlotho

αKlotho is a transmembrane protein detectable in a variety of tissues, with abundant expression in the kidney, parathyroid glands and in brain choroid plexus. Several isoforms of the αKlotho exist: the membrane bound form is a 130 kDa glycoprotein comprised of a large extracellular domain that directly interacts with FGF23, in addition to a short intracellular region that is not capable of signaling in isolation (Matsumura et al. 1998). The membrane bound Klotho serves as a co-receptor and promotes FGF23 signaling via the recruitment of

canonical FGF receptors (FGFRs) for renal phosphate handling (Goetz et al. 2010; Urakawa et al. 2006) and for vitamin D regulation mediated through FGFR3 and FGFR4 (Kurosu et al. 2006; Li et al. 2011). A 110 kDa form of αKlotho is cleaved by the α-secretases ADAM10 and 17 (Bloch et al. 2009) and secreted. Whereas FGFRs present a wide tissue distribution, the restricted αKlotho expression enables the specificity of FGF23 on its target organs. αKlotho also promotes FGFR high affinity to circulating FGF23 (Kuro and Moe 2016). A human case with loss-of-function mutations in the *αKLOTHO* gene was identified (Ichikawa et al. 2007) presenting a syndrome resembling familial tumoral calcinosis, including hyperphosphatemia, in spite of high serum intact FGF23 levels.

2.1.5.5 DMP1

DMP1 is member of the SIBLING protein family (Fisher and Fedarko 2003). It is expressed in odontoblasts, mature osteoblasts and in osteocytes (George et al. 1994; Toyosawa et al. 2001). The acidic domains of DMP1 form β-like sheets capable of binding Ca^{2+} ions and of initiating crystal nucleation *in vitro*. *In vivo,* DMP1 was shown to play a major role in predentin mineralization (He et al. 2003). In addition, DMP1 functions as a signaling factor: its overexpression in mesenchymal cells localizes to the nucleus and induces the transcription of *DSPP* gene and an odontoblast phenotype (Narayanan et al. 2003; Narayanan et al. 2001). DMP1 requires proteolytic cleavage to become active or is rapidly degraded; the protease responsible for this cleavage remains unknown (Qin et al. 2003).

Autosomal recessive hypophosphatemic rickets (ARHR) is a P_i wasting disorder caused by mutations in the *DMP1* gene (Farrow et al. 2007). Osteocytes' production of FGF23 is increased in the *Dmp1* knockout mouse with both dental and skeletal phenotypes of rickets and osteo/dentinomalacia (Feng et al. 2006; Ling et al. 2005). In the periodontium of the *Dmp1* null mouse, there is a hypomineralization of dentin, an enlargement of the pulp chamber, dentinal tubule abnormalities, a reduced expression of *Dspp*, and an impaired periodontium including defective alveolar bone, periodontal ligament, and cementum (Ye et al. 2004; Ye et al. 2005; Ye et al. 2008). Similar to XLH/*Hyp* phenotype, ARHR displays hypophosphatemia resulting from an increased expression of FGF23 by osteocytes (Feng et al. 2006). This suggests that FGF23 is under the control of DMP1. The connection between DMP1 and PHEX is unknown. FGF23, MEPE, PHEX, and DMP1 are all expressed in osteocytes

in normal conditions, suggesting a major role for osteocytes in regulating systemic P_i levels (Dallas et al. 2013).

2.1.5.6 Secreted frizzled-related protein 4

Tumor Induced Osteomalacia (TIO) is a rare paraneoplastic syndrome associated with mesenchymal tumors releasing phosphaturic factors causing hypophosphatemia, osteomalacia and abnormal 1,25-$(OH)_2D_3$ metabolism (Imel and Econs 2005). Besides FGF23, FGF7 and MEPE, secreted frizzled-related protein 4 (sFRP4) was also found to be responsible for the symptoms observed in TIO (Berndt et al. 2003). sFRP4 is highly upregulated in tumorous tissue, it inhibits phosphate transport in the opossum kidney cell line as well as *in vivo* (Berndt et al. 2003; Berndt et al. 2006). However, mice lacking *sfrp4* do not show any impaired systemic phosphate homeostasis (Christov et al. 2011). Thus, the relevance of sFRP4 for phosphate homeostasis remains to be clarified.

2.1.6 Local cellular regulators/ion transporters regulating P_i/PP_i homeostasis

2.1.6.1 Tissue nonspecific Alkaline Phosphatase

Among the four alkaline phosphatase isozymes, tissue nonspecific alkaline phosphatase (TNAP) is found in liver, kidney, bone and tooth (Millán 2006). TNAP activity produces phosphate (P_i) from the hydrolysis of pyrophosphate (PP_i) and other substrates. TNAP is of major importance in skeletal mineralization as it removes a mineralization inhibitor: PP_i, and increases the local concentration of P_i (Murshed et al. 2005). Biologically controlled-mineralization is in part regulated by the P_i:PP_i ratio, with regulators like TNAP that determine the microenvironmental P_i and PP_i levels. TNAP is present on cell membranes of osteoblasts and at the surface of matrix vesicles, plasma circulating levels are also measurable. Hypophosphatasia (HPP) results from dysfunctional or low levels of TNAP, causing poor mineralization, rickets and osteomalacia (Whyte 1994; Whyte 2010). In *Tnap* (*Akp2*) knockout mice, bones display a decreased mineral density (Beertsen et al. 1999). A recombinant TNAP enzyme replacement therapy approach targeting bone was able to rescue skeletal and dental defects in *Tnap* KO mice (Millan et al. 2008), which contrasted with failures of previous systemic infusions of TNAP into HPP patients (Weninger et al. 1989;

Whyte et al. 1984), suggesting that local, pericellular function of TNAP is more critical than circulating plasma levels in the development of mineralized tissues. TNAP is highly expressed in the periodontium, by cementoblasts, osteoblasts, and ligament fibroblasts (Groeneveld et al. 1995). TNAP deficiency causes cementum aplasia or severe hypoplasia, especially in the more coronal acellular cementum region, compromising periodontal attachment and resulting in premature exfoliation of still-rooted teeth (Bruckner et al. 1962; Chapple 1993; van den Bos et al. 2005).

2.1.6.2 Progressive ankylosis protein

The mouse progressive ankylosis gene (*Ank*), analogous to *ANKH* in humans, encodes for a transporter of intracellular PP_i to the extracellular space (Ho et al. 2000). Loss-of-function mutations in *ANKH* result in low levels of PP_i in the pericellular environment, with high intracellular PP_i, in contrast to *TNAP* deficiency, which causes increased PP_i outside cells (Ho et al. 2000; Terkeltaub 2001). Mutations in *ANKH* have been associated with a variety of skeletal defects. Excess levels of PP_i result in pathological calcium pyrophosphate dihydrate (CPPD) elaboration (Netter et al. 2004; Ryan 2001) leading to chondrocalcinosis, where CPPD are deposited within articular cartilage and cause pain and arthritis. Additional dominant mutations in *ANKH* have been linked to craniometaphyseal dysplasia resulting in overgrowth and sclerosis of the craniofacial bones and abnormal modeling of long bone metaphysis with mineralization defects (Nurnberg et al. 2001; Reichenberger et al. 2001). A hypercementosis phenotype was identified in the *Ank* knockout mice. While periodontal ligament, dentin, and alveolar bone are unaffected, cementum formation is increased (Nociti et al. 2002).

2.1.6.3 Plasma Cell Membrane Glycoprotein 1

The protein PC-1 (coded by ectonucleotide pyrophosphatase/phosphodiesterase 1, *NPP1* gene) is a membrane-bound enzyme that generates PP_i from triphosphates and so also regulates extracellular PP_i level. Mutations in *NPP1* result in low extracellular PP_i, and a phenotype resembling those with *ANKH* deficiency (Johnson et al. 2000; Terkeltaub 2001). The hypermineralization observed in *Pc-1* deficient mice is more severe than in *Ank* deficient mice because of the localization of PC-1 in matrix vesicles (Hessle et al. 2002; Johnson et al. 2001; Vaingankar et al. 2004). Humans with mutations in *NPP1* present pathologies resulting

from deficient PP_i, including craniometaphyseal dysplasia and idiopathic infantile arterial calcification (Nurnberg et al. 2001; Reichenberger et al. 2001; Rutsch and Terkeltaub 2005). While *ANK* and *PC-1* increase PP_i in cell environment, TNAP activity decreases PP_i to release P_i. In this sense, *PC-1* and *ANK* can be seen as natural antagonists to *TNAP* in terms of regulating P_i:PP_i levels and mineralization (Foster et al. 2008; Harmey et al. 2004).

2.1.6.4 Phosphoethanolamine/phosphocholine phosphatase

Phosphoethanolamine/phosphocholine phosphatase (PHOSPHO1) is an enzyme present in mineralized tissue cells and in matrix vesicles that exhibits phosphatase activity on phosphoethanolamine and phosphocholine (Roberts et al. 2007; Roberts et al. 2004). Inside the vesicle of mineralization, phosphate accumulates through the combined action of transporters (TNAP and NPP1) and through its production by PHOSPHO1 until sufficient amounts are present for precipitation to occur (Nakano et al. 2003; Roach 1999).

2.1.7 Phosphate as a signaling molecule

2.1.7.1 Effect of phosphate on osteoblasts

The rate at which mineralization occurs during mineralized tissues formation and bone remodeling is partly dependent on the local availability of Ca^{2+} and P_i (Bellows et al. 1992; Hansen et al. 1976). In the absence or in case of abnormal absorption or reabsorption of these ions, mineralization is impaired, resulting in the formation of poorly mineralized bone that is characteristic of osteomalacia in adults or rickets in children (Kumar and Riggs 1980). However, P_i is also a signaling molecule capable of modulating multiple cellular functions in bone (Khoshniat et al. 2011). During the osteoblastic differentiation, the expression level of alkaline phosphatase (ALP) increases. In the presence of organic phosphates, such as β-glycerophosphate, ALP contributes to the local liberation of phosphate, thus leading to an increased P_i concentration in the extracellular environment (Bellows et al. 1992). Phosphate in the extracellular milieu serves as a signal for a shift in cell function/differentiation, in addition to acting as one of the building blocks for hydroxyapatite mineral. A regulation of osteopontin expression by ALP-generated P_i prevents excessive mineralization before osteoblasts cease proliferation (Beck et al. 1998a; Beck et al. 2000).

2.1.7.2 Effect of phosphate on osteoclasts

At sites of bone resorption, active osteoclasts are exposed to high concentrations of P_i and Ca^{2+} as HAP is dissolved in the acidic environment within the limits of the ruffled border. High P_i level inhibits osteoclastogenesis and osteoclasts function (Mozar et al. 2008), and studies on mice under hypophosphatemic conditions have suggested that low P_i may also inhibit osteoclasts number and activity (Hayashibara et al. 2007). Osteoclastogenesis from WT marrow cells was decreased under both low and high P_i conditions, while osteoclastogenesis was not impaired in *Hyp* mouse marrow cells under normal P_i conditions.

2.2 Biomineralization

2.2.1 Overview of extracellular matrices of the teeth and periodontium

Bone, dentin and cementum are similar regarding the composition of their extracellular matrices. However, unlike bone, dentin and cementum are not resorbed as part of a remodeling process, and they are not involved in the regulation of systemic mineral ion homeostasis that occurs during resorption of bone (Opsahl Vital et al. 2012). All three tissues present an extracellular matrix mainly composed of type I collagen, and all are 50-70% mineralized with a carbonate-substituted apatitic mineral. During the formation of collagenous mineralized tissues (i.e. osteogenesis, dentinogenesis, cementogenesis), the assembly of extracellular matrix and its following mineralization occur through highly ordered steps with a lag time between matrix deposition and mineralization. Throughout this process, extracellular matrix proteins are secreted and assembled into the fibrillar scaffold, making it receptive to mineral deposition (McKee et al. 2005; McKee et al. 2013). These events are orchestrated by the osteoblasts, the odontoblasts and the cementoblasts associated with a thin layer of unmineralized matrix (i.e. osteoid, predentin and cementoid, respectively) which subsequently mineralizes at the mineralization front. Additional mineral maturation like carbonation into the hydroxyapatite lattice slowly occurs over time (Boskey and Coleman 2010; Cazalbou et al. 2004). The organic phase will also undergo a maturation process involving proteolytic degradation that provides an adequate functional state (Kaartinen et al. 2002; Kaartinen et al. 2005).

2.2.2 Collagen matrix mineralization

Collagenous mineralized tissues are composite materials determined in dimensional scales starting from the protein-nanocrystal interface and extending into the anatomical macroscale of bone and tooth structures. They consist in an organic network of proteins that interweave as a scaffold for mineral deposition, providing hardness and toughness (McKee et al. 2005). Ca^{2+} and P_i complex together as crystalline salts to mineralize extracellular matrix in bones and teeth. Heterogeneous minerals are also deposited at isolated locations within, at the surface of, and between collagen fibrils (Landis et al. 1996a). This process is very controlled at the molecular level. Indeed, the nanoscale deposition of billions of plate-like crystallites (crystalline substituted hydroxyapatite) within the soft organic matrix provides toughness and flexibility of bones and allows deformation during mechanical challenge (Rey et al. 2009). The collagen fibrils with interwoven noncollagenous protein assemblies present interconnected pores that extend throughout the extracellular matrix and are filled with apatitic crystals. The mineral is not only nucleated in nanoscale volumes within fibrillar collagen (intrafibrillar collagen mineralization), but also interfibrillarly. In the interfibrillar compartment, there is an abundance of noncollagenous proteins, and mineral crystals dimensions are larger (McKee and Nanci 1995). The two different extracellular compartments provide different limitations on biomineralization. At each compartment, mineral crystal is nucleated and its growth is regulated locally by concentrations of mineral ions and by the presence or absence of mineral nucleators and inhibitors, so that crystalized minerals do not grow beyond the nanometer range (Glimcher 2006; McKee et al. 2013).

Mineral crystals typically are platelet-shaped crystallites with dimensions that vary upon their physical location within the structure of the pre-established extracellular matrix (Landis et al. 1996b). Eighty percent of mineral is located external to the collagen fibrils, with dimensions of 5 nm thick, 65 nm wide and at least 200 nm long (McNally et al. 2012). Regarding intrafibrillar mineralization, matrix interaction domains and charge groups have been described in fibrillar type I collagen (Silver and Landis 2011) allowing mineral placement within the holes zones in the interior of the collagen fibrils, but much less is known about the chemical environment contributing to mineral crystal nucleation and propagation between the fibrils (interfibrillar mineralization) (McKee et al. 2013).

The mineral-binding proteins comprise the SIBLING family. These noncollagenous proteins are thought to guide the mineralization process, and are located primarily between the collagen fibrils. While crystal deposition within the collagen fibril (intrafibrillar mineralization) is thought to occur independently from that occurring between the fibrils (interfibrillar mineralization), a recent proposal suggests that crystals formed at the surface of collagen fibrils might migrate within the fibril, thus linking inter- and intrafibrillar mineralizations (Toroian et al. 2007).

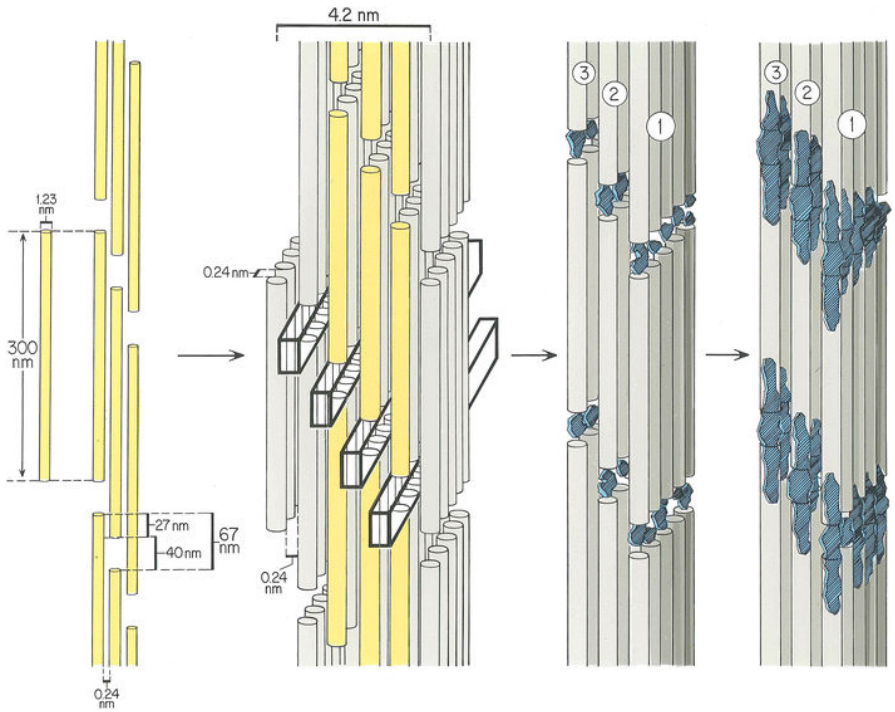

Figure 2 Intrafibrillar Collagen Mineralization

The pore spaces (0.24 nm) between adjacent collagen molecules constitute narrow regions. A single collagen molecule assembles into a 2D aggregate, cross-links into a quarter-staggered array with characteristic hole (40 nm) and overlap (27 nm) zones. 3D assemblages occur of all hole and overlap zones so that channels are created. Once nucleated in the collagen hole zones, the crystals, grow in their c-crystal axis direction. The largest developing face of the crystals lie parallel to each other and to the associated collagen molecules. Reprinted from Landis & Jacquet, 2013, with permission from Springer

2.2.3 Pyrophosphate and the phosphate:pyrophosphate ratio in mineralization

Pyrophosphate (PP_i) is composed of two molecules of phosphate (P_i). PP_i regulates physiologic and pathologic mineralization by acting as an inhibitor of crystal precipitation and growth (Addison et al. 2007; Fleisch and Bisaz 1962; Fleisch et al. 1966; Meyer 1984; Murshed et al. 2005; Termine et al. 1970). PP_i adsorbs to HAP and antagonizes the ability of P_i to crystallize with Ca^{2+} to form additional HAP, and thus inhibits the elongation of HAP crystal (Terkeltaub 2001). For normal mineral deposition to proceed, a tight balance between the P_i and PP_i levels must be maintained. Early *in vitro* studies performed in aqueous solutions at pH 7.4, temperature 37°C, concentrations of Na^+, Mg^{2+} and Ca^{2+} of 140, 0.5 and 1.0 mM respectively, determined that HAP is formed when the P_i:PP_i ratio is greater than 100 (Cheng and Pritzker 1983).

Local tissue concentrations of pyrophosphate are controlled by regulatory enzymes and transporters. The tissue-nonspecific alkaline phosphatase (TNAP) hydrolyzes pyrophosphate, thus providing a mechanism to control the concentration of this mineralization inhibitor. TNAP is highly expressed by osteo/odontogenic cells and it is critical for proper skeletal mineralization (McKee et al. 2013; Whyte 1994). Loss-of-function mutations in *ALPL* (the human gene encoding TNAP) cause hypophosphatasia (HPP), a disease characterized by poor skeletal and dental mineralization (Reibel et al. 2009; Whyte 2008). In contrast, two proteins can increase pyrophosphate concentration: the progressive ankylosis transmembrane protein (ANK) and the enzyme ectonucleotide pyrophosphatase phosphodiesterase 1 (NPP1). ANK regulates the transport of intracellular pyrophosphate to the extracellular space (Gurley et al. 2006; Ho et al. 2000; Johnson et al. 2003) and NPP1 increases extracellular PP_i by hydrolysis of nucleotide triphosphates (Johnson et al. 1999). Pyrophosphate removal by TNAP activity thus antagonizes provision of PP_i by ANK and NPP1, thereby creating a mutual regulation of phosphate and pyrophosphate levels to control mineralization (Harmey et al. 2004).

2.2.4 Matrix vesicles and mineralization

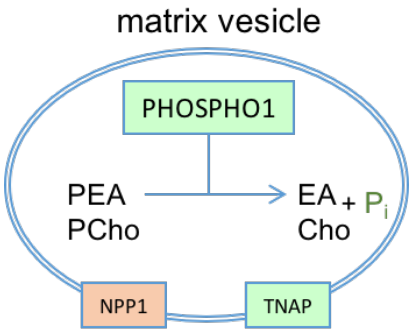

Figure 3 Matrix Vesicle

Green and red stand for mineralization promoters and inhibitors, respectively. (PCho) phosphocholine, (PEA) phosphoethanolamine, (P_i) phosphate

Inside the matrix vesicle, calcium phosphate accumulates until precipitation is possible. The precipitate is then converted to an intermediate, octa-calcium phosphate, crystals of which are transformed into less soluble hydroxyapatite (Sauer and Wuthier 1988). The vesicle membrane then breaks down, releasing preformed hydroxyapatite into the extracellular fluid (Roberts et al. 2004). The formation of hydroxyapatite crystals inside matrix vesicles is favored by phosphate accumulation through two mechanisms: the phosphoethanolamine/phosphocholine phosphatase-mediated intravesicular production; and the influx of phosphate mediated by transporters. The transported phosphate is primarily produced pericellularly by the adenosine triphosphatase activity of TNAP or NPP1 (Yadav et al. 2011). Other sources of phosphate are found in organophosphate compounds like adenosine triphosphate and polyphosphates (Hoac et al. 2013; Omelon et al. 2009). TNAP and NPP1 support the next step of collagen-mediated extravesicular mineralization, which is driven by the extracellular phosphate/pyrophosphate ratio and by the presence of the collagenous fibrillar scaffold, with further regulation of crystal growth by noncollagenous proteins of the SIBLING family. Investigators in the bone mineralization field are divided between collagen-mediated and matrix vesicle-mediated mechanisms of mineralization, but both are not exclusive (McKee et al. 2013).

2.2.5 Noncollagenous extracellular matrix proteins and mineralization

2.2.5.1 The SIBLING protein family

A collagen fibril matrix by itself does not have the capacity to induce mineralization from a solution of calcium and phosphate ions at the appropriate pH, degree of saturation and temperature (Nudelman et al. 2013). In order to mineralize the collagenous matrix, two major processes are involved: the removal of pyrophosphate by alkaline phosphatase for the induction of mineralization, and the biological control of crystal growth by noncollagenous proteins and their peptides that allows promotion or inhibition of crystal growth (George and Veis 2008; Qin et al. 2004). Most noncollagenous proteins in the skeleton and in teeth are highly acidic phosphoproteins that bind to mineral through negatively charged phosphate groups in order to regulate crystal growth during the interfibrillar mineralization process. The SIBLING proteins family (small integrin-binding ligand N-linked glycoproteins) (Fisher and Fedarko 2003) is a subcategory of the secreted calcium-binding phosphoprotein family (Kawasaki and Weiss 2006). The SIBLING family is encoded by genes located on chromosome 4 in humans (loci 20-21), it comprises dentin sialophosphoprotein (DSPP), dentin matrix protein 1 (DMP1), bone sialoprotein (BSP), osteopontin (OPN), statherin, and matrix extracellular phosphoglycoprotein (MEPE). In mineralized tissues, crystal growth is inhibited by direct binding of certain SIBLING proteins/peptides to crystal surfaces (Addison et al. 2010; Giachelli and Steitz 2000). In addition, some SIBLING proteins/peptides are associated with specific sites on collagen molecules to promote the nucleation and growth of apatite crystals (He et al. 2005; Traub et al. 1992). Genes encoding SIBLING proteins are well-conserved during evolution; their importance in the regulation of tissues biomineralization is also confirmed by studies using transgenic mice and the identification of human mutations on SIBLINGs that are linked to diseases (Alford and Hankenson 2006; McKee et al. 2013).

2.2.5.2 The acidic serine- and aspartate-rich motif

Proteins of the SIBLING family have an acidic serine- and aspartate-rich motif (ASARM) which is highly conserved across species (Martin et al. 2008; Rowe 2012). The ASARM region encloses serine residues that can be phosphorylated, and abundant acidic aspartate and

glutamic acid residues (Rowe et al. 2000). The ASARM motif is located in the C-terminal region of SIBLINGs, excluding osteopontin where it is located in the mid-region of the protein sequence. ASARM appears to have evolved to regulate mineralization, extending from eggshell to mammalian bone (Bardet et al. 2010). Its functions seem to have been extended to transduce and to suppress FGF23 signaling in mammals (Liu et al. 2007). In normal osteo/dentinogenesis, MEPE can be enzymatically cleaved resulting in the release of free ASARM peptides into the extracellular matrix (Martin et al. 2008). Osteopontin is also involved in enzymatic cleavage that produces ASARM-containing peptides (Barros et al. 2013). These acidic peptides are highly resistant to proteolysis, and are strong inhibitors of mineralization. However, ASARM peptides can also be cleaved and thus cleared from the local matrix environment where mineralization is designed to occur, by the PHEX enzyme (Addison et al. 2010; Addison et al. 2008; Barros et al. 2013). PHEX can bind to MEPE at the ASARM site, protecting these proteins from proteolytic cleavage by other enzymes (Rowe 2012; 2015). Once released, the ASARM peptide itself becomes a substrate for PHEX with numerous internal cleavage sites, thus promoting mineralization. In this way, PHEX enzyme tightly controls mineralization at the local level in the extracellular matrix (Rowe et al. 2005). Furthermore, PHEX could negatively or positively influence FGF23 expression and so plasma P_i levels by binding DMP1 or cleaving ASARM. In addition, PHEX could indirectly influence the degradation of FGF23 via Klotho, and thus control plasma P_i level (Atkins et al. 2011; Martin et al. 2011; Rowe 2015).

The complex links between PHEX, FGF23, DMP1, ASARM, Klotho and MEPE in the control of P_i homeostasis requires further study (Addison and McKee 2010).

2.3 Disorders of phosphate metabolism and mineralization

2.3.1 Hypophosphatasia

Hypophosphatasia (HPP) is a heritable disorder featuring hypomineralization of the skeleton and teeth (Fraser 1957; Whyte 2008; 2010) characterized by deficiency of TNAP activity. TNAP deficiency leads to the accumulation of PP_i and a reduced P_i:PP_i ratio, impairing HAP formation and crystal propagation. HPP affects all races and displays wide-ranging expressivity, with clinical manifestations spanning stillbirth with complete absence of skeletal mineralization, to early tooth loss as the only symptom. Subnormal extracellular

concentrations of P_i cause nearly all types of rickets or osteomalacia, but HPP is an exception where the circulating levels of P_i are usually normal or elevated. Despite high levels of TNAP in bone, cartilage, liver, kidney, and adrenal tissue in healthy individuals, HPP appears to disrupt only mineralized tissues. Approximately 200 mutations in *TNAP*, transmitted in various combinations by autosomal recessive inheritance or by autosomal dominant inheritance occur in HPP. Current nosology classifies five principal forms of HPP. Individuals without skeletal features but dental defects only are said to have “odonto-HPP”. Typically, the earlier the signs and symptoms, the worse the outcome. Perinatal HPP is always fatal. Infantile HPP often features clinical and radiographic deterioration with nearly 50% of infants dying from respiratory compromise. Childhood HPP may improve when growth plates fuse. Adult HPP causes recurrent and lingering orthopedic difficulties (Linglart and Biosse-Duplan 2016; Whyte 2010). Although several approaches have been attempted, there is no established medical treatment. Since 2015, a recombinant mineral-targeted alkaline phosphatase (asfotase alfa) is under investigation for enzyme replacement therapy, and is now approved for pediatric-onset HPP (Whyte 2017).

2.3.2 X-linked hypophosphatemia

2.3.2.1 Clinical presentation

X-linked hypophosphatemia (X-linked hypophosphatemic rickets, XLH) is a genetic disorder whose major symptom is a hypomineralized skeleton and dentition. It is the most common form of heritable rickets. Impaired bone mineralization manifests in children as rickets with severe skeletal deformities, and in adults as osteomalacia (the accumulation of unmineralized osteoid) (Carpenter et al. 2011).

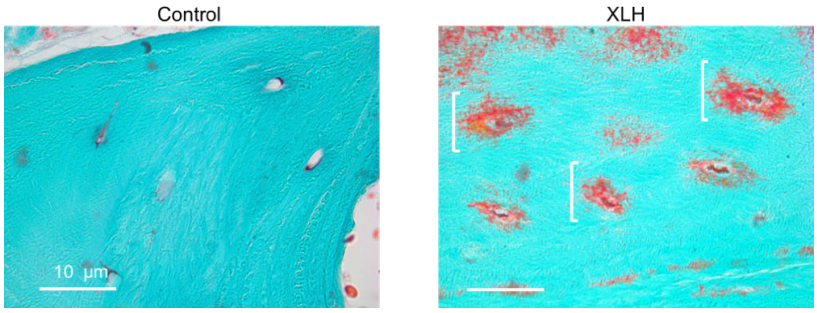

Figure 4 Osteomalacia in XLH appendicular bone

Unmineralized (orange) osteoid accumulates in periosteocytic lesions in XLH undecalcified bone tissue

Document B. R. Coyac, EA2496

Clinical manifestations vary in severity; patients present in childhood with progressive bowing of the legs, antero-medial rotational torsion of tibiae, and short stature leading to deformities in growing children. These abnormalities can be improved with medical therapy, but usually do not entirely resolve. Metaphyseal changes of rickets are usually evident on radiographs of the distal femur when a child presents with XLH. A major feature in these patients is the occurrence of spontaneous tooth abscesses both in the deciduous and permanent dentition, in teeth without any signs of trauma or decay (Chaussain-Miller et al. 2003; Seow et al. 1984). Although patients' teeth look clinically normal, X-rays show a thin enamel layer and a radiolucent dentin layer, the latter associated with enlarged pulp chambers with prominent pulp horns extending up to the dentino-enamel junction. Histologic examination shows extensive enamel cracking and fissuring, and unmerged dentin calcospherites separated by large unmineralized interglobular spaces (Chaussain-Miller et al. 2007; Murayama et al. 2000) where the dentin matrix contains degraded fragments of MEPE, MEPE-ASARM peptide, DMP1 and osteopontin (Boukpessi et al. 2006; Salmon et al. 2014). Abnormal dentin mineralization and enamel cracks may lead to rapid pulp necrosis with periapical complications (Chaussain-Miller et al. 2007). XLH is often misdiagnosed as nutritional rickets, metaphyseal dysplasia, and physiologic bowing.

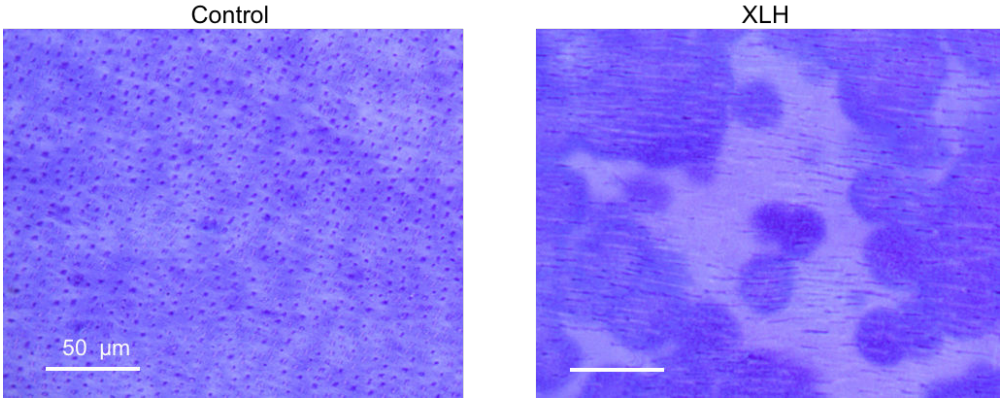

Figure 5 "Dentinomalacia" in XLH tooth

XLH dentin show unmerged calculospherites with unmineralized regions (light blue)

Document B. R. Coyac, EA2496

2.3.2.2 Genetics

In 1995, the *PEX* gene, located on chromosome Xp22.1-22.2 in humans and later renamed *PHEX* (phosphate-regulating gene with homologies to endopeptidases on the X chromosome), was identified as the etiology of XLH (The HYP consortium). Recently, a large cohort of 118 pedigrees representing 56 familial cases and 62 sporadic cases of X-linked hypophosphatemia revealed that *PHEX* mutations were involved in 87% of familial cases, and also in 72% of sporadic cases (Gaucher et al. 2009b). Regarding the other genetic mutations associated with familial hypophosphatemic rickets, *FGF23* mutations are the cause of autosomal dominant hypophosphatemic rickets (ADHR consortium), *DMP1* mutations (Lorenz-Depiereux et al. 2006a) and *SLC34A* mutations (Bergwitz et al. 2006; Lorenz-Depiereux et al. 2006b) are the causes of recessive autosomal hypophosphatemic rickets, and loss-of-function mutations in the *NPP1* gene and a translocation involving the *Klotho* gene were assumed to be associated with hypophosphatemic rickets (Brownstein et al. 2008; Levy-Litan et al. 2010; Lorenz-Depiereux et al. 2010).

DISEASE	Gene	Transmission	Main Features
X-linked Hypophosphatemic Rickets	*PHEX*	X-linked	Hypophosphatemic rickets
Autosomal Dominant Hypophosphatemic Rickets	*FGF23*	Autosomal dominant	Hypophosphatemic rickets
Autosomal Recessive Hypophosphatemic Rickets	*DMP1*	Autosomal recessive	Hypophosphatemic rickets
Autosomal Recessive Hypophosphatemic Rickets	*NPP1*	Autosomal recessive	Hypophosphatemic rickets + arterial calcifications
Autosomal Recessive Hypophosphatemic Rickets	*FAM20C*	Autosomal recessive	Hypophosphatemia + osteosclerosis

Table 1 Major Forms of Genetic Hypophosphatemic Rickets

2.3.2.3 Biochemical findings

Hypophosphatemia and low to normal circulating 1α,25-$(OH)_2D_3$ levels are typical biochemical findings. Serum alkaline phosphatase activity is elevated in children, but not to the degree observed in nutritional rickets with 1α,25-$(OH)_2D_3$ deficiency. Serum calcium is normal, as is circulating 25$(OH)D_3$. Radiographic images exclude diagnoses of physiologic bowing and skeletal dysplasia. Evidence of renal phosphate wasting is obtained before committing patients to treatment: a 2-hour fasting urine specimen, together with a blood sample collected at the midpoint of the urine collection period is used to calculate the percentage of tubular reabsorption of phosphate, and to determine the maximum tubular threshold for phosphate (Carpenter et al. 2011).

2.3.2.4 Pathobiology

The basic physiologic defect in XLH is impaired proximal renal tubular reabsorption of phosphate. This defect is due to reduced expression of sodium-phosphate cotransporters (NaP_i2a and NaP_i2c) on the apical surface of proximal renal tubule cells. Loss-of-function of PHEX results in elevated circulating FGF23 by an unknown mechanism. FGF23 suppresses transcription of the genes encoding NaP_i2a and NaP_i2c. A direct consequence of elevated FGF23 levels is the abnormally regulated vitamin D axis. FGF23 can down-regulate CYP27B1 (which encodes 1-α-hydroxylase), and up-regulate CYP24A1 (encoding the 24-hydroxylase) (Shimada et al. 2004a), thereby resulting in inappropriate low levels of $1\alpha,25\text{-}(OH)_2D_3$, due to decreased synthesis and increased catabolism. FGF23 acts through specific FGF receptors (FGFRs) on the basolateral surface of renal tubular cells. To transduce its signal, FGF23 must form a ternary complex with a cognate FGFR and the Klotho protein (Farrow and White 2010; Hu et al. 2010; Urakawa et al. 2006). The precise downstream pathway mediating the altered expression of NaP_i2 and the vitamin D hydroxylases has not been clarified. In addition to its function in systemic P_i homeostasis, PHEX seems to be involved in the binding and proteolytic processing of the proteins and peptides regulating mineralization. In the absence of PHEX activity, inhibitory osteopontin protein fragments accumulate to inhibit mineralization in XLH/*Hyp* appendicular bone (Barros et al. 2013; Boukpessi et al. 2016). MEPE-derived ASARM peptides have been shown to inhibit in a dose-dependent manner the mineralization of human primary osteoblast cultures grown under differentiating conditions (Atkins et al. 2011) and experiments both *in vivo* and *in vitro* have confirmed the capacity of MEPE-derived ASARM peptides to inhibit both dentin mineralization and odontoblast differentiation (Salmon 2012; Salmon et al. 2013). These pathologic features in extracellular matrices of mineralized tissues might directly result from the impairment of PHEX, independently of the surrounding hypophosphatemia, as it has been shown *in vitro* with osteoblasts from the *Hyp* mouse (Xiao et al. 1998) and *in vivo* by producing compound mice from *Hyp/Fgf23* knockout cross (Liu et al. 2006; Sitara et al. 2004) and by inducing transgenic expression of *Phex* in the *Hyp* mouse (Erben et al. 2005b; Zelenchuk et al. 2014a).

2.3.2.5 Treatment

XLH was initially termed “vitamin D resistant rickets” due to the lack of therapeutic response to vitamin D in dosages that would cure nutritional rickets. The finding that renal phosphate wasting was the principal pathophysiologic abnormality led to the use of phosphate replacement regimens, which resulted in partial correction of skeletal lesions but led to hyperparathyroidism. Since the 1970s, combining active vitamin D analogs with a balanced dose of phosphate has become the mainstay of therapy. Careful monitoring to avoid toxicity is required. Most affected children and symptomatic or severely affected adults are candidates for treatment. Most children with XLH are treated from the time of diagnosis until growth is complete (Carpenter et al. 2011; Linglart et al. 2014).

The disease spectrum is heterogeneous, with some individuals minimally affected even without treatment. Hypophosphatemia and low to normal serum $1\alpha,25\text{-}(OH)_2D_3$ levels result from increased FGF23 levels. Current treatment with activated vitamin D metabolites and phosphate salts attempts to correct these deficiencies. Both vitamin D (calcitriol or alfacalcidol) and phosphate are usually required, current recommendations are a calcitriol dosage of 20 to 30 ng/kg/day in 2-3 divided doses, and an elemental phosphorus dose of 20-40 mg/kg/day (in 3-5 divided doses) (Carpenter et al. 2011; Linglart et al. 2014). Phosphate dosages may require titration to minimize abdominal pain or diarrhea. Treatment during growth partially corrects leg deformities, decreases the number of required surgeries, and improves adult height. Early initiation of treatment appears to optimize height outcomes (Linglart et al. 2014; Makitie et al. 2003). There is uncertainty regarding optimal doses, and concerns regarding the side effects of nephrocalcinosis, hypercalciuria and hyperparathyroidism (Verge et al. 1991). Changes in body size, growth velocity, and skeletal mineralization necessitate periodic dose adjustments (Linglart et al. 2014). Growth hormone has been used as adjunctive therapy, but given the lack of adequately controlled trials, there is no clear benefits of this therapy.

The primary goals of treatment are to correct rickets/osteomalacia, radiographic abnormalities, and skeletal deformities, but not to normalize the serum phosphate concentration, which is not a practical goal in children with XLH (Carpenter 1997) and that

could lead to secondary hyperparathyroidism. Nephrocalcinosis, hypercalcemia or hypercalciuria are indications to reduce the calcitriol dose. The most useful biomarker for skeletal response is serum alkaline phosphatase activity, which is moderately elevated before treatment and decreases with treatment, serving as a surrogate marker for bone healing.

The goals of treatment in adults are to reduce pain symptoms, the extent of osteomalacia and to improve fracture healing or surgical recovery (Sullivan et al. 1992). Like pediatric XLH, adults are treated with calcitriol and phosphate. Treatment is individualized for each patient depending on age, body weight, parathyroid status and renal function. Many adults with XLH have enthesopathy (Liang et al. 2009), which does not improve with treatment. This includes paraspinal enthesopathy and spinal ligament calcification that can lead to spinal cord compression and unbearable pain. Current medical management does not prevent or reverse this complication either. Joint replacement surgery, especially knees and hips, is common in adults because of the high frequency of degenerative joint disease and enthesopathy. Orthopedic surgery is recommended to correct bone deformities. The time of healing can be shortened with medical treatment: 3 to 6 months before the operation and continued for 6-9 months afterwards (Linglart et al. 2014).

Endodontic disease, particularly dental abscesses prevention, require good dental hygiene including regular use of interdental brushes. No specific dental treatment has been shown to prevent this complication. Whether resin sealants or topical fluoride could help reduce the incidence of dental abscesses needs further study (Douyere et al. 2009; Weyant et al. 2013).

2.3.2.6 Novel therapies

In the recent years, monoclonal antibodies targeted against FGF23 have been generated (Yamazaki et al. 2008). When administered intravenously to *Hyp* mice, FGF23 antibodies promoted growth and ameliorated mineralization and cartilage development (Aono et al. 2009). The elaboration of a humanized antibody (KRN23, human monoclonal IgG_1 antibody) showed, in XLH patients, increased serum P_i, increased renal tubular reabsorption rate of phosphate/glomerular filtration rate, and increased $1\alpha,25\text{-}(OH)_2D_3$ in all subjects (Imel et al. 2015). A Phase 3 clinical trial is ongoing in the USA and Canada. However, anti-FGF23

antibodies will probably not rescue the putative direct impact of PHEX deficiency on calcified tissue mineralization that depends on MEPE- or OPN-derived ASARM peptides presence in the extracellular matrix. In addition, FGF23 prevents ectopic calcification through the control of the calcium-phosphate product. Precise modulation of FGF23 signaling will be necessary to avoid off-target actions of FGF23 antibodies (Linglart et al. 2014).

2.4 The periodontium

2.4.1 Overview of the periodontium

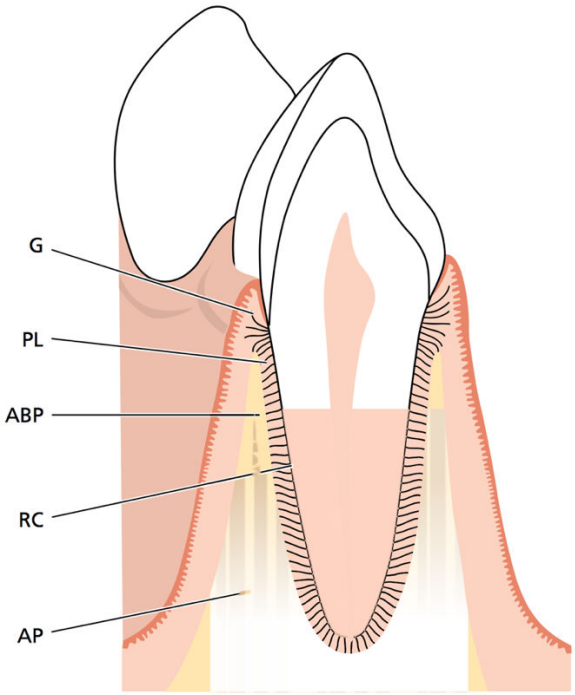

Figure 6 The Periodontium

(G) Gingiva, (PL) Periodontal ligament, (ABP) Alveolar bone proper, (RC) Root cementum, (AP) Alveolar process.

Reprinted from Lang and Lindhe, 2015, with permission from John Wiley & Sons

The periodontium (peri: around, odontos: tooth), also called the attachment apparatus or the supporting tissues of the teeth, constitutes a developmental, biologic and functional unit comprising tissues supporting and investing the tooth: root cementum, periodontal ligament, alveolar bone lining the tooth socket, and the dentogingival junction (a portion of the gingiva facing the tooth). Each of the periodontal components displays a very specialized

structure that directly defines function. The main function of the periodontium is to attach the tooth to the bone tissue of the jaws and to maintain the integrity of the surface of the masticatory mucosa of the oral cavity (Lang and Lindhe 2015; Nanci and Bosshardt 2006).

2.4.2 Embryology of the periodontium

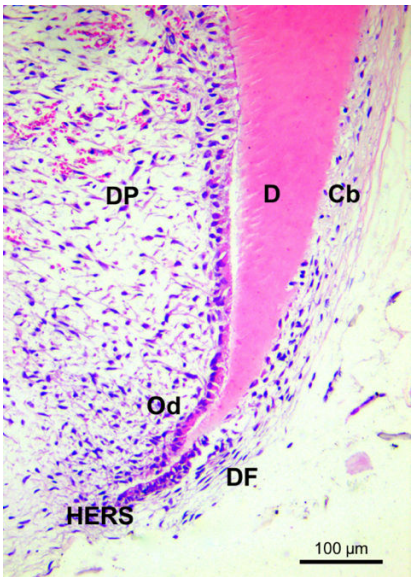

Figure 7 Epithelial Root Sheath

(D) Dentin, (Cb) Cementoblasts, (Od) Odontoblasts, (DP) Dental papilla, (DF) Dental follicle, (HERS) Hertwig Epithelial Root Sheath

Document B. R. Coyac, EA2496

The development of periodontal tissues occurs during the development and formation of teeth when cells from the neural crests migrate into the first branchial arch in early embryonic phases. The neural crest cells form a band of ectomesenchyme beneath the epithelium of the stomatodeum. Epithelial-ectomesenchymal interactions lead to the formation of the dental lamina and a series of processes are initiated, described as bud stage, cap stage and bell stage with the development of the root, resulting in the formation of a tooth and its surrounding periodontal tissues, including the alveolar bone proper. During the cap stage, a condensation of ectomesenchymal cells in relation to the dental epithelium forms the dental follicle that gives rise to the periodontium (McCauley and Somerman 2012). The development of the root and the periodontal supporting tissues follows that of the crown. Epithelial cells of the external and internal dental epithelium proliferate in an apical direction, forming a double layer of cells called Hertwig's epithelial root sheath. The

odontoblasts forming the dentin of the root differentiate from ectomesenchymal cells in the dental papilla. The dentin forms in an apical direction, producing the shape of the root. Ectomesenchymal cells of the dental follicle and in contact with the root surface differentiate into cementoblasts and start to form cementum. The remaining parts of the periodontium are formed by cells lateral to the cementum. Some of them differentiate into fibroblasts and form the periodontal ligament, while others become osteoblasts and form the alveolar bone proper in which the periodontal fibers are anchored (Lang and Lindhe 2015).

2.4.3 The anatomy of periodontal tissues

2.4.3.1 Dentogingival junction

The dentogingival junction is the gingiva facing the tooth, it is an adaptation of the oral mucosa that comprises epithelial and connective tissue components. The epithelium is divided into three compartments: gingival, sulcular and junctional epithelium, and the connective tissue comprises superficial and deep compartments. The junctional epithelium seals off periodontal tissues from the oral environment. Its integrity is essential for maintaining a healthy periodontium. Periodontal disease hallmark is the apical migration of the junctional epithelium (Nanci and Bosshardt 2006).

2.4.3.2 Periodontal ligament

The periodontal ligament is the soft, highly vascularized and cellularized connective tissue that surrounds the roots of the teeth and joins the root cementum with the socket bony wall. The width of the periodontal ligament is approximately 0.25 mm and is the narrowest at the mid-root level. The periodontal ligament allows forces from the masticatory function and dental trauma to be distributed to and absorbed by the alveolar process via the alveolar bone proper. The periodontal ligament is essential for tooth mobility, that is determined by the width, height, and quality of the periodontal ligament (Lang and Lindhe 2015; Nanci and Bosshardt 2006).

2.4.3.3 Cementum

The cementum is a specialized mineralized tissue that covers the root surface. After HERS becomes disrupted, cells from the dental follicle exposed to the root dentin receive the signal to differentiate into cementoblasts, to secrete cementum ECM and to orchestrate ECM mineralization (Foster and Somerman 2012). Unlike bone, the cementum does not contain blood or lymph vessels, has no innervation, does not undergo physiologic resorption or remodeling, but is characterized by continuing deposition throughout life (Colard et al. 2016; Huang et al. 2016). It attaches the principal periodontal ligament fibers to the root and contributes to the process of repair after damage to the root surface. It also serves to adjust the tooth position to new requirements. Different forms of cementum have been described (Bosshardt and Selvig 1997; Nanci and Bosshardt 2006), that can be found mixed together.

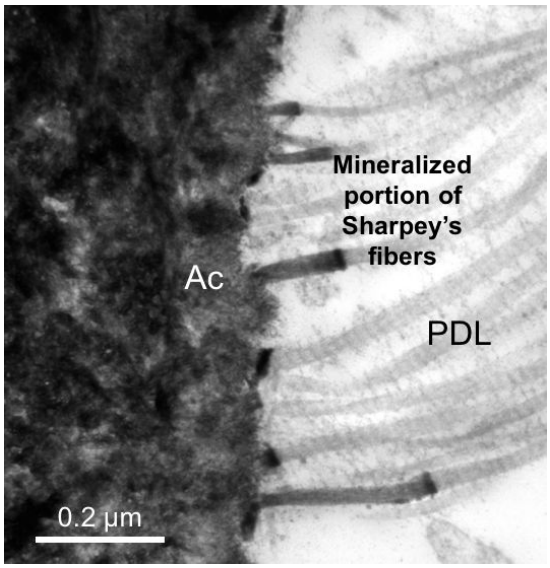

Figure 8 Acellular cementum

(Ac) Acellular cementum, (PDL) Periodontal ligament

Document B. R. Coyac, EA2496

2.4.3.3.1 Acellular cementum

Acellular extrinsic fiber cementum is found in the coronal and middle portions of the root. This type of cementum is critical for attachment of the tooth to the periodontal ligament as it contains bundles of Sharpey's fibers connecting the tooth with the bundle bone (alveolar bone proper). Acellular afibrillar cementum is found mainly at the cervical portion of the enamel.

2.4.3.3.2 Cellular cementum

Cellular cementum is a thick, bone-like tissue that adjusts tooth position by modeling at the root tip as crown enamel is worn down during life, it also serves as a repair tissue that fills dental root resorptive lacunae and fractures. Cellular mixed stratified cementum occurs in the apical third of the roots and in the furcation areas. It contains both extrinsic and intrinsic fibers as well as cementocytes. Cellular intrinsic fiber cementum is found mainly in resorption lacunae and it contains intrinsic fibers and cementocytes.

2.4.3.4 Alveolar bone

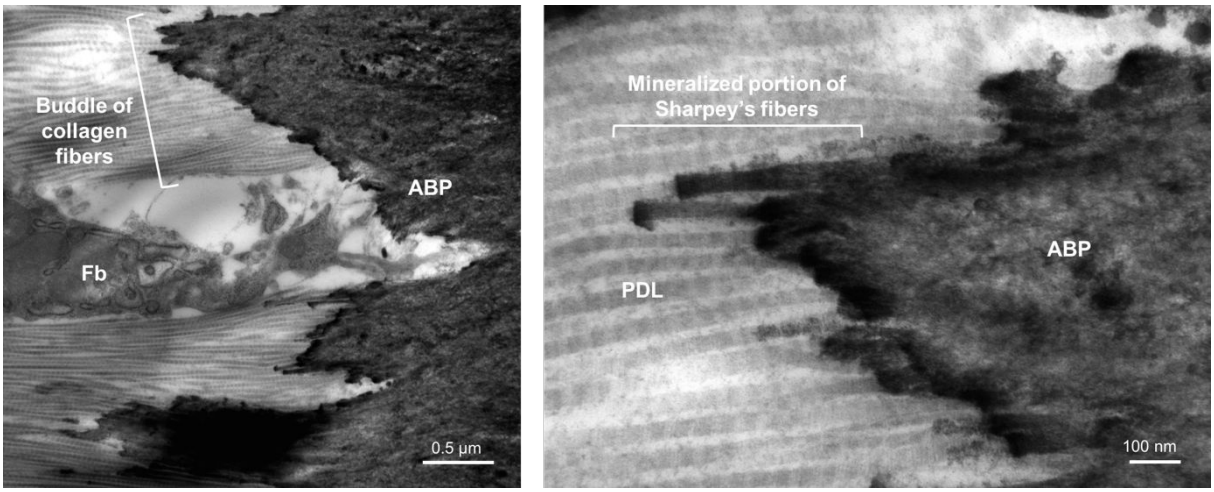

Figure 9 Periodontal Ligament-Alveolar Bone Anchorage

(Fb) Fibroblast, (ABP) Alveolar bone proper, (PDL) Periodontal ligament

Document B. R. Coyac, EA2496

The alveolar process of the maxilla and the mandible contains the sockets (alveoli) for the teeth. It consists of outer cortical plates of compact bone, a central cancellous bone, and bone lining the alveolus. Bone tissue in the periodontium and craniofacial complex is similar to bone elsewhere (McKee et al. 2012), but its origin is different, with much of it deriving from neural crest cells (Nanci 2012). Alveolar bone is lost in the absence of a tooth, suggesting specific local regulatory mechanisms. Another specific feature is its high remodeling rate (Saffar et al. 1997; Tricker and Garetto 1997) resulting from large and frequent mastication forces exerted by the masseter muscles. Such forces transduced via the tooth and the suspensory periodontal ligament to the bone result in the requirement for particularly ductile bone lining the tooth alveolus. This bone lining the alveolus is called alveolar bone proper, it has a unique structure appearing as a thin fringe of bone

accommodating the many insertions of the periodontal ligament. It is also described as bundle bone (Avery 2011) that provides a robust suspensory attachment function (McCulloch et al. 2000). The cortical plates consist of lamellae supported by Haversian systems. They are thinner in the maxilla and thicker on the buccal aspect of mandibular premolars and molars. The trabecular bone occupying the central part of the alveolar process also consists of bone disposed in lamellae, with Haversian systems present in the largest trabeculae. Yellow marrow fills the intertrabecular spaces, although there can also be some red hematopoietic marrow. The remodeling process of alveolar bone is similar to that of bone in general (Baron 2000), with some specificity: resorption is asynchronous so that periodontal ligament attachment is lost only focally, for short periods of time. During tooth migration, bone lost by resorption on one surface of the tooth socket is balanced by bone formation along the opposite surface. This bone balance, together with the continued deposition of cementum throughout life act to maintain a constant relationship between the root surface and the alveolar socket (Saffar et al. 1997). Within bone, distinct cell populations include osteogenic precursor cells, osteoblasts, osteoclasts, osteocytes, and hematopoietic elements of bone marrow (McKee et al. 2013).

2.4.3.4.1 Osteoblasts

Osteoblasts are the primary cells responsible for the formation of bone; they synthesize the organic extracellular matrix components and orchestrate the mineralization of the matrix. Osteoblasts are located on bone surfaces where they secrete matrix and eventually differentiate into two different cell types: bone lining cells or osteocytes. Bone lining cells are elongated cells that cover a surface of bone tissue and exhibit no synthetic activity. The osteoprogenitor cells are present in the bone marrow, in the endosteum, and in the periosteum that covers the bone surface. Such cells possess the capacity to proliferate and differentiate into osteoblasts. The differentiation of osteoblasts from osteoprogenitor cells are dependent on osteoinductive growth factors, such as bone morphogenetic proteins, insulin-like growth factor, platelet-derived growth factor, or fibroblast growth factor (Lang and Lindhe 2015; Marie 2008).

2.4.3.4.2 Osteocytes

Osteocytes are stellate-shaped cells embedded within the mineralized matrix in lacunae. They maintain a network of dendrites that extend through cylindrical encased compartments termed canaliculi (Bonewald 2011). Osteocytes translate mechanical signals into biochemical mediators that participate to anabolic and catabolic events within bone. Osteocytes participate in the regulation of plasma Ca^{2+} homeostasis and sense mechanical loading and transmit this information to other cells within bone tissue to further orchestrate osteoblastic and osteoclastic functions. Different bone diseases and disorders affect the arrangement of the osteocyte lacunocanalicular system, causing significant alterations to this important cellular network (Bonewald 2012; Lang and Lindhe 2015).

2.4.3.4.3 Osteoclasts

The bone formation activity is coupled to bone resorption that is initiated and maintained by osteoclasts. They are specialized multinucleated cells originating from the mononuclear phagocyte lineage, that develop and adhere to bone matrix and then secrete acid and lytic enzymes to degrade the mineral and organic components of bone. Macrophage colony-stimulating factor is required to engage the cells in the monocyte lineage and ensure their proliferation and the expression of the RANK (receptor activator of NF-κB) receptor. At this stage, the cells require the presence of RANKL (receptor activator of NF-κB ligand), a member of the TNF (tumor necrosis factor) family of cytokines, produced by stromal cells and osteoblasts, to commit to the osteoclast lineage and progress in their differentiation program (Baron 2000; Baron et al. 2012).

2.5 Periodontal diseases

2.5.1 Epidemiology

2.5.1.1 Periodontitis and tooth loss

Periodontitis is a complex chronic inflammatory disease of the supporting tissues of the teeth in which there is an imbalance between the host's immune system and the oral bacterial load. In susceptible individuals, certain microbial pathogens can proliferate, leading

to the induction of inflammatory reactions. These inflammatory reactions irreversibly destroy the periodontium. If left untreated, teeth lose their ligamentous support and alveolar bone is resorbed, the affected teeth become mobile and are eventually lost. The normal oral microbiota protects the host from extrinsic pathogens and the immune system controls bacterial proliferation to maintain homeostasis. The complex interplay between environmental factors, the microbiota in the oral cavity, the immune system, and lifestyle factors (smoking, stress, diet, etc.) is largely regulated by genes and underlies the changes to which the host's physiology must adapt to maintain health (Bartold and Van Dyke 2013; Ebersole et al. 2013; Genco and Borgnakke 2013). In this context, constitutional defects in periodontal tissues represent a detrimental factor, as it is the case in (odonto/)hypophosphatasia (Armitage 1999; Chapple 1993).

2.5.1.2 Prevalence of periodontal diseases

Cross-sectional studies in adults from geographically different areas and involving large-sized samples reveal that severe forms of periodontitis affect a limited portion of the population in the Western world, not exceeding 10-15%. This fraction increases considerably with age and reaches a peak at the age of 50-60 years. The increased loss of periodontally affected teeth occurring after this age explains the decline in prevalence. Data from the National Health and Nutrition Examinations Surveys (NHANES) 2009-2012 estimated that about 46% of the United States of America dentate adults aged 30 years and older had periodontitis, with 8.9% having severe periodontitis and 37.1% having less severe periodontitis (Eke et al. 2012). These estimates in the USA appear to be much lower than those reported from certain European populations. For example, a large population based study in West Pomerania used the original CDC/AAP no/mild, moderate, and severe case definition among 3,255 persons aged 20-79 years, assessing four sites on all teeth other than third molars in two quadrants (Zhan et al. 2014). They found 20% (versus 8.9% in NHANES 2009–2012) with severe and 35.3% (versus 30.9%) moderate periodontitis, leaving less than half (44.7%) the population with only mild or no periodontitis. This is in spite of the inclusion of individuals up to ten years younger than the NHANES participants and the exclusion of those 80 years and older. In France, Bourgeois et al. reported a total prevalence of periodontal disease of 31.5%, with 2.3% displaying a periodontal pocket ≥ 6mm (Bourgeois et al. 1999).

2.5.1.3 Risk factors for periodontitis

The NHANES examined large nationally representative, stratified, multistage probability samples in the United States of America (Albandar et al. 1999; Eke et al. 2015; Eke et al. 2012), their data showed that the prevalence of deep pockets and advanced periodontal attachment loss was more pronounced in Hispanic (63.5%) and non-Hispanic black (59.1%), followed by non-Hispanic Asian American (50.0%), and the lowest in non-Hispanic white adult subjects. Thus, current evidence suggests that the prevalence of severe periodontitis is not uniformly distributed among various races, ethnicities or socioeconomic groups. In addition, periodontal disease is not evenly distributed in the population and not only correlated to supragingival plaque levels; instead, the majority of the subjects examined exhibits negligible periodontal problems, while a limited group is affected by advanced disease (Lang and Lindhe 2015). The huge variability in progression of periodontitis in a seemingly homogeneous population shows that upon a same load of periodontal pathogens, all individuals are not equally susceptible to periodontitis, and variables other than age and plaque are important determinants of periodontal deterioration over time. Individual risk factors change the susceptibility and resistance of individuals to periodontitis. They include smoking and poorly controlled diabetes, and possibly obesity, stress, osteopenia, inadequate Ca^{2+} and $1\alpha,25\text{-}(OH)_2D_3$ levels, race and genetic factors (Genco and Borgnakke 2013).

2.5.2 Pathogenesis of Periodontitis

The bacteria in dental plaque, including *Porphyromonas gingivalis, Tannerella forsythia*, *Treponema denticola* and *Aggregatibacter actinomycetemcomitans* are the cause of periodontitis (Socransky et al. 1998); however, not all individuals with high amount of plaque and bacteria will develop periodontitis. In some people, due to environmental factors, their own innate susceptibility or both, there is loss of connective tissue and bone, apical migration of the junctional epithelium, and development of periodontitis (Lang and Lindhe 2015). Disease expression and progression reflects the interplay between the bacteria, the host's immune system and environmental factors. Tissue destruction is the outcome of the inflammatory response to the patient's specific individual microbiota (Cullinan et al. 2001; Seymour and Taylor 2004).

2.5.2.1 Periodontal lesions

The development of the periodontal disease is classified into the initial, early, established and advanced lesions (Page and Schroeder 1976). The established lesion presents a predominance of plasma cells within the periodontal connective tissue (Mackler et al. 1977; Seymour and Greenspan 1979). Connective tissue breakdown leads to periodontal ligament detachment, allowing the junctional epithelium to migrate and extend towards the apical direction, thus forming a periodontal pocket. Polymorphonuclear neutrophils (PMNs) migrate through the pocket epithelium into the periodontal pocket and form a barrier against the plaque biofilm. Increased permeability and ulceration of the pocket epithelium allows the penetration of microbial products, leading to the continued production of inflammatory cytokines such as interleukin-1 (IL-1), tumor necrosis factor-alpha (TNF-α), and prostaglandin E_2 (PGE_2) (Gemmell et al. 1997), perpetuating the inflammatory process (Lang and Lindhe 2015). In consequence, both connective tissue and alveolar bone are destroyed (Reynolds and Meikle 1997).

2.5.2.2 Inflammation-induced bone resorption

The upregulated production of proinflammatory mediators in periodontitis activates RANKL expression pathways (Cochran 2008; Hienz et al. 2015). Both IL-1 and TNF-α regulate the balance of RANKL and OPG. Increased IL-1β production by B cells contributes to alveolar bone resorption. Upon stimulation, osteoblasts produce RANKL. RANKL-activated osteoclasts produce a number of acids and hydrolases that decalcify the mineral content of the alveolar bone and break down the organic matrix. The osteoclasts further resorb bone.

2.5.3 Periodontal wound healing

Periodontal wound healing is considered to be more complex than epidermal wound healing because of the interfaces between periodontal tissues and the transgingival position of the tooth. Periodontal wound healing seeks to create a new connection to the non-vascularized, non-vital and permanently contaminated hard tissue of the root surface.

Successful periodontal treatment requires a decontaminated root surface. Therapy includes both non-surgical and surgical modalities (Heitz-Mayfield and Lang 2013). While the healing

of gingival epithelia and their underlying connective tissues is achieved in weeks, the healing of periodontal ligament, root cementum, and alveolar bone generally occurs over months. Following the healing of gingiva, a reduction of its volume causes both gingival recession and reduction of the periodontal pocket depth. PDL is shown to regenerate on newly formed cementum created by cementoblasts originating from the PDL granulation tissue (Karring et al. 1985). Furthermore, alveolar bone modeling occurs following the stimulation of mesenchymal cells from the gingival connective tissue, which are transformed into osteoprogenitor cells by locally expressed BMPs (Krebsbach et al. 2000; Sykaras and Opperman 2003). Following periodontal treatment, the down-growth of the epithelium along the root surface reaches the level of the PDL before the latter has regenerated with new layers of cementum and newly inserted connective tissue fibers. Therefore, in order to enable and promote the healing towards the rebuilding of cementum and PDL, the formation of a long junctional epithelium must be delayed (Melcher 1976). In addition, the granulation tissue derived from PDL cells has to be given both space and time to format and mature to new cementum and ligament (Lang and Lindhe 2015).

2.5.3.1 Alveolar bone repair

Although it is a continuous process, bone repair can be divided into three phases: inflammation, reparative, and remodeling phases (Hadjidakis and Androulakis 2006). It starts with the formation of a blood clot. Cytokines released from injured cells recruit inflammatory cells, macrophages begin phagocytosis of damaged tissues and cells for the clearance of wound debris. Osteoclasts resorb damaged bone and mesenchymal cells differentiate into osteoblasts. The RANKL:OPG ratio is reduced. Osteoblasts produce a collagenous scaffold consisting in a soft callus, which is slowly mineralized to form a hard callus composed of immature woven bone. Woven bone is eventually remodeled into mature lamellar bone mediated by osteoblast-osteoclast coupling. Adequate $1\alpha,25\text{-}(OH)_2D_3$ and Ca^{2+} are critical for proper bone repair, their levels may dictate the rate of repair. The time for the remodeling stage varies depending upon individual bone metabolism, but usually requires months from the time of injury (Lang and Lindhe 2015; Pagni et al. 2012).

2.5.3.2 Alveolar bone regeneration

Repair process replaces lost tissue with immature tissue and does not completely restore function. In contrast, regeneration process aims at restoring the original structure and function of a tissue (Galliot et al. 2017). Therapeutic strategies to promote bone regeneration include bone grafting from various sources, epithelial-occlusive barrier membranes, antiresorptive therapies, anabolic agents, and growth factors to promote osteoblastic differentiation and proliferation. Assessment of alveolar bone regeneration following therapy is often documented by measurements made on radiographs obtained in a standardized and reproducible manner or by a re-entry operation (Lang and Lindhe 2015; Pagni et al. 2012).

2.6 Disorders of mineralization and the periodontium

2.6.1 Hypophosphatasia

TNAP activity in the normal periodontium is high, with wide expression in the periodontal ligament cells and cementoblasts (Foster et al. 2013; Foster et al. 2015; Groeneveld et al. 1993; 1995). Observations that root acellular cementum is defective in HPP, resulting in compromised attachment of the tooth root to surrounding alveolar bone (Bruckner et al. 1962; Chapple 1993) along with the loss of primary rooted teeth led to consider pyrophosphate as an essential regulator of tooth root acellular cementum development and mineralization (Nociti et al. 2002), and as a key determinant defining the hard-soft interface between the cementum and the periodontal ligament (Foster et al. 2012). Studies suggest that the acellular extrinsic fiber cementum of the cervical portion of the root is the most severely affected by the pyrophosphate dysregulation, while the apically located cellular intrinsic fiber cementum is generally unaffected (Foster et al. 2012; Foster et al. 2014a; Foster and Somerman 2012). Dysplasia and aplasia of acellular cementum is considered the cause for the early exfoliation of rooted primary teeth (Bruckner et al. 1962; el-Labban et al. 1991; Hu et al. 2000). Irregular crown dentin mineralization and enlarged pulp chambers have also been described. These features have also been found in the *Alpl*$^{-/-}$ mouse (Foster et al. 2014a; Reibel et al. 2009; Rodrigues et al. 2012; van den Bos et al. 2005). Loss of

acellular cementum structure and function lead to ligament detachment after tooth eruption in *Alpl*$^{-/-}$ mice. A root dentin defect was also identified in the *Alpl*$^{-/-}$ mouse model for infantile HPP (Foster et al. 2013; McKee et al. 2011a). Increased production of the SIBLING protein OPN has been reported to contribute to skeletal mineralization defects in *Alpl*$^{-/-}$ mice (Harmey et al. 2004; Harmey et al. 2006) and may play a similar role in the human condition (Bloch-Zupan 2016; Linglart and Biosse-Duplan 2016).

2.6.2 X-linked hypophosphatemia

The major dental focus in XLH patients has been on the tooth abnormalities alone, and only a few studies have explored their periodontal status. A clinical study (a case series) has reported the periodontal condition of ten adults with familial hypophosphatemic rickets (Ye et al. 2011). They showed that 70% of the patients presented periodontal attachment loss (including alveolar bone loss) higher than 5 mm, which is much higher than reported values for extensive attachment loss prevalence of 8.9% in the general adult population (Eke et al. 2012), suggesting that patients with hypophosphatemic rickets are prone to increased periodontal diseases. In addition, the *Hyp* mouse was shown to present a reduced acellular cementum thickness and osteoidosis in the alveolar bone (Fong et al. 2009; Koehne et al. 2013). In periodontal disease, during pathologic bone resorption (Cochran 2008), mineral crystals are dissolved and the soft extracellular matrix is degraded. And so, mineral-bound proteins and peptides such as ASARM might be released and redistributed systemically in the plasma (Bresler et al. 2004). While tissue-resident PHEX may be able to degrade some of this increased inhibitory ASARM (Addison et al. 2010; Addison et al. 2008) to promote bone healing and mineralization, in XLH the enzymatic capacity of PHEX being impaired, bone healing might be altered and circulating phosphate levels negatively affected (McKee et al. 2013).

3 Statement of the problem

Constitutional defects in the periodontium of genetic diseases affecting the local P_i:PP_i ratio – such as hypophosphatasia (HPP) – have been shown to result in an impaired periodontal condition, with the loss of rooted deciduous teeth (Armitage 1999; Chapple 1993). The extensively studied periodontal pathobiology of HPP has contributed to a better dental care of affected patients (Linglart and Biosse-Duplan 2016). On the opposite, possibly because of the striking oral abscesses found in X-linked hypophosphatemia (Chaussain-Miller et al. 2007; Chaussain-Miller et al. 2003) masking other aspects of oral health, the XLH periodontal condition has not been described in more than two studies. One case series (Ye et al. 2011) and one animal study (Fong et al. 2009) suggest both a defective periodontium and a specific susceptibility of XLH patients to periodontitis. Many questions persist as it is not known to what extent the XLH periodontium is affected by PHEX deficiency and phosphate wasting, if current systemic treatments impact the periodontal status of XLH patients and if the XLH periodontium is fully functional as it relates to adaptive tooth movements or alveolar bone repair. These questions extend beyond the scope of periodontology as the periodontium is critical in orthodontic movements or for dental implant placement.

This dissertation investigates the periodontal condition of XLH patients and its variations depending on the age of onset and type of systemic treatment for XLH, and it provides an extensive description of the attachment apparatus in XLH and *Hyp* mice tissues. In addition, using experimental models, this doctoral research assesses two critical functions of the periodontium that might be affected in XLH: adaptation to tooth movement and alveolar bone repair capacities.

Since the finding that X-linked hypophosphatemic rickets was mediated by an increase in FGF23, treatment strategies aimed at counteracting consequences of FGF23 excess, i.e. oral phosphorus supplementation with multiple daily intakes to compensate for renal phosphate wasting and active vitamin D analogs to counter the 1,25-$(OH)_2D_3$ deficiency (Carpenter et al. 2011; Linglart et al. 2014). However, the treatment compliance, especially in children, is hard to obtain and needs to be monitored to avoid intestinal discomfort, secondary

hyperparathyroidism, hypercalciuria and nephrocalcinosis. New treatments, currently under development (phase 3 trial for adults), consist in inactivating FGF23 through the use of monoclonal antibodies (Imel et al. 2015). This approach responds to constraints from supplementations and faulty compliance, but it will not consider the alleged direct impact of PHEX deficiency on calcified tissues mineralization, thus leaving aside a whole pathologic aspect of the disease. Accumulating data point to a local and direct aspect of PHEX deficiency, evidenced by MEPE- or OPN-derived ASARM peptides presence in the ECM (Barros et al. 2013; Salmon et al. 2014), but these studies are questioned because of their models: whether using recombinant proteins *in vitro*, or murine and human tissue samples where it is impossible to discriminate if the pathological mechanism originates from local PHEX deficiency or from systemic hypophosphatemia. In this doctoral research, we developed an *in vitro* model of human biomineralization using primary dental pulp cells where mineralization assays could be performed while adjusting surrounding levels of phosphate in the culture media, aiming at assessing for the first time with human cells from XLH patients, the existence or not of PHEX deficiency-related local defects independent of FGF23-mediated hypophosphatemia.

4 Materials and Methods

4.1 *In vivo:* Human teeth and *Hyp* mouse

4.1.1 Human teeth

Human permanent teeth from 7 XLH patients and from gender- and age-matched control individuals extracted prior to orthodontic treatments were collected in the dental departments of Paris Nord Val de Seine Hospitals, AP-HP, France. Informed consent was obtained from patients in agreement with French law (agreement n°DC-2009-927, Cellule Bioéthique DGRI/A5). Teeth were fixed for 7 days at 4°C in 4% paraformaldehyde solution at pH 7.2–7.4, followed by microwave-assisted decalcification in 4.13% EDTA for ~3 months. Decalcified teeth were embedded in Paraplast, sectioned (at 7 µm) in the coronoapical axis and stained with toluidine blue (pH 7.2).

4.1.2 Animals

Hyp mice were obtained from the Jackson Laboratory. Heterozygous female and WT male breedings were carried out and tail snips were collected for genotyping. DNA was extracted from the snips using DNeasy Blood and Tissue Kit (Qiagen, France) and the genotype was determined by PCR using primers for *Phex* gene (Sheen et al. 2012). Offspring males with the *Phex* gene-null mutant phenotype ($Hyp^{-/0}$) were maintained under the same conditions as those for the WT mice. Three-month old littermate WT and $Hyp^{-/0}$ mice were examined in this study. Chemical methods were used for sacrificing mice according to the ethical protocol approved by the Animal Care Committee of French Veterinary Services (DPP Haut de Seine, France: agreement number C-9204901). *Hyp* males and wild-type (WT) littermates were sacrificed by cervical dislocation or included in the experimental models at 90 days postnatal. If included in an experimental model, mice were intraperitoneally anesthetized with a mixture of ketamine (80mg/kg) and xylazine (10 mg/kg). All experimental procedures involving animals were approved by the Institutional Animal Care and Use Committee at Paris Descartes University (APAFiS #5214). All mice were housed in standard conditions of temperature (23 ± 2°C) in a light-controlled environment, and provided water and standard pelleted food *ad libitum*.

Protocol for *Hyp* mice tail genotyping

Primer	Sequence	Tm (°C)	MW
WT/R	5'-GAT GAA AAG CCT GCA GTT-3'	50.6	5,547.7
WT/F	5'-CAG GTC ACA TGC TTA CAG-3'	50.4	5,483.6
HYP/R	5'-ACA TTT CTT GGG TGC AAA GGT G-3'	56.3	6,805.5
HYP/F	5'-GAC AGA GTC AAA TTC TGG CCC-3'	55.9	6,415.2

Table 2 List of Primers Sequences for Hyp *Genotyping*

Taq Polymerase: Invitrogen™ Platinum™ DNA Polymerase (ThermoFisher).

Expected bands:

- 1 band at 351 bp: *Hyp*
- 1 band at 235 bp: WT

Master Mix	1 rxn	PCR Cycle for **25 µL**:	
MQ H20	15.15 µL	94°C – 5 min	
10X Buffer	2.5 µL	94°C – 30 sec	x **36 cycles**
10 mM dNTPs	0.5 µL	58°C – 30 sec	
10 µM WT/F primer	1 µL	72°C – 30 sec	
10 µM WT/R primer	1 µL	72°C – 5 min	
10 µM Hyp/F primer	1 µL	4°C – hold	
10 µM Hyp/R primer	1 µL		
50 mM $MgCl_2$	0.75 µL		
Taq (Invitrogen Platinum)	0.1 µL		
Final Volume	**23 µL**		

Add **2µL** tail DNA to each reaction

2.2% agarose gel

94V (20-25min)

4.1.3 Micro-computed Tomography Dataset Acquisition

Live animals were anesthetized (isoflurane, induction at 3–4% under airflow of 0.8–1.5 L/min; 1.5–2% under 400–800 ml/min thereafter) and scanned using a high-resolution X-ray micro-CT device (Quantum FX Caliper, Life Sciences, Perkin Elmer, Waltham, MA, United

States). Three-dimensional acquisitions were performed with a field of view of 10 mm diameter, using an isotropic voxel size of 20x20x20 μm^3 (90 kV, 160 microA, 180s). The trabecular bone morphometric indices were calculated according to guidelines published by the American Society for Bone and Mineral Research (Bouxsein et al. 2010). Morphometric measurements were performed using Skyscan software (v1.13.5.1, Kontich, Belgium).

- Bone volume fraction or bone volume/tissue volume ratio (BV/TV, %) to estimate the percentage of segmented mineralized volume to the total volume of interest, i.e. the white to black voxel ratio of the binary images.
- Trabecular number (Tb.N, mm^{-1}) to measure the average number of mineralized structures per unit length.

4.1.4 Cone-Beam Computed Tomography (CBCT)

CBCT scans from 3 XLH patients and 3 control individuals imaged before wisdom teeth removal were collected (Planmeca ProMax® 3D Max, Helsinki, Finland). Image analysis comprised four steps: alignment, cropping, thresholding and bone analysis. The inter-radicular areas of the 2 first mandibular molars were cropped in each 2D section of the stack with the dedicated shape tool of the Skyscan software (v1.13.5.1, Kontich, Belgium). These regions-of-interest included the trabecular bone above the inferior alveolar nerve canal in the basal bone. The trabecular bone morphometric indices were extrapolated to investigate the micro-architecture of alveolar bone (Panmekiate et al. 2015). Calculation of the 3D structural parameters followed the guidelines published by the American Society for Bone and Mineral Research (Bouxsein et al. 2010). Morphometric measurements were performed using the Skyscan software (v1.13.5.1, Kontich, Belgium).

4.1.5 Murine Tissue Specimen Preparation

After dissection, maxillas and mandibles were fixed in 70% ethanol at 4°C and dehydrated in a graded ethanol series. Undecalcified samples were embedded in methyl methacrylate (Merck, Rahway, NJ). Dental crowns were abraded using grinding paper discs (P400, 3M) and specimens were embedded a second time prior to sectioning in a sagittal orientation. Serial sections, 4 µm thick, were cut on a microtome (Polycut E microtome, Leica, Wetzlar, Germany) sagittal to the second maxillary molar buccal roots and to the second mandibular

molar roots. A series of consecutive sections were stained respectively with toluidine blue (pH 3.8), von Kossa reagent (5% silver nitrate solution, Sigma-Aldrich, St Louis, MO), Masson's trichrome stain and Sirius red staining.

4.1.6 Light Microscopy

Tissues were analyzed in a LEITZ DM-RBE microscope (Leica, Germany) set for transmitted light illumination, or polarized light, and equipped with a Sony DXC-950 CCD camera. Fluorochrome-based indices of murine bone and cellular cementum formation were measured in sections photographed under ultraviolet light. Double labeling allowed the measurement of the amount of bone or cellular cementum formed between the two dye injections. The mean distance between the two labels was determined using previously described parameters (Vignery and Baron 1980). The daily mineral apposition rate (MAR) was calculated using these parameters and ImageJ software (NIH, Bethesda, MD).

4.1.7 Enzyme Histochemistry

Tartrate-resistant acid phosphatase (TRAP) was detected by using 2.5 mM naphthol-ASTR-phosphate (Sigma-Aldrich, St Louis, MO), 0.36 M N–N-dimethyl-formamide (Sigma-Aldrich, St Louis, MO), and 4 mM salt in pH 5.2 acetate buffer. Nonosteoclastic acid phosphatase activity was inhibited with 100 mM L(+)-tartaric acid (Sigma-Aldrich, St Louis, MO) added to the substrate solution. Alkaline phosphatase (ALP) was used to reveal the layer of osteogenic cells (pre-osteo/cementoblasts and osteo/cementoblasts) by incubating the sections with naphthol ASTR phosphate (Sigma-Aldrich, St Louis, MO) and diazonium fast blue RR salt (Sigma-Aldrich, St Louis, MO) for 30 min at 37°C (pH 9) in the presence of $MgCl_2$.

4.1.8 Immunohistochemistry

Paraffin sections were dewaxed in xylene and sections embedded in methyl methacrylate were deplastified. After rehydration in a graded ethanol series to pure distilled water, sections were blocked using 5% normal horse serum/PBS-T. Sections were incubated for 12 hours at 4°C with goat anti-human OPN antibody (R&D Systems, Minneapolis, MN, USA) diluted 1:20 in 2.5% normal horse serum/PBS-T or in rabbit anti-PHEX peptide (NH_2-

CMINQYSNYYWKKAGL-$CONH_2$) kindly provided by Peter S. Rowe (Martin et al. 2008) diluted 1:50 in 2.5% normal horse serum/PBS-T. Sections were washed and then incubated with peroxidase-conjugated anti-IgG diluted 1:1000 in the same buffer. Peroxidase activity was detected using a diaminobenzadine substrate kit from Abcam (Cambridge, MA, USA) following the manufacturer's instructions. Control incubations to assess nonspecific staining consisted of the same procedure except that the primary antibody was substituted by nonimmune serum (these control incubations resulted in nonspecific staining, data not shown).

Immunohistochemistry protocol

1. Incubate sections 30 min to 1h at 37°C
2. Deparaffinise tissue sections:
   - Xylene I (8 min) (50 mL)
   - Xylene II (8 min)

   Deplastify, for undecalcified samples:
   - 2-Methoxyethyl acetate I (30 min)
   - 2-Methoxyethyl acetate II (30 min)
3. Incubate slides in acetone at -20°C for 10 min
4. Hydrate tissue sections, on a shaker
   - 100% Ethanol (5 min, x2)
   - 90% Ethanol (5 min)
   - 70% Ethanol (5 min)
   - 50% Ethanol (5 min)
   - 20% Ethanol (5 min)
   - H_2O (5 min, x2)
5. If quenching of endogenous peroxidase activity is required, incubate sections at 37°C for 1 hour in 3% H_2O_2 in methanol (5mL 30% H_2O_2 + 45mL MeOH)
6. Wash slides in 0.1% Triton or Tween in PBS for 5 minutes (50ul of Tween 20 + 50mL of PBS)
7. Incubate sections for 1 hour at 37°C with diluted normal serum (Vector kit: Yellow-labeled bottle 1) for blocking. Vector Elite PK-6200
   10uL/1 mL buffer (PBST)
   1 drop (50uL)/5 mL buffer
8. Blot excess serum from sections

9. Incubate sections overnight at 4°C with primary antiserum (antibody) diluted in buffer (PBST)
   Concentrations of primary antibody in PBST: 1/100 or 1/50 or 1/20
10. Wash slides in 0.1% PBST for 15 minutes, with rotation, x3
11. Incubate sections for 2 hours at 37°C with diluted biotinylated secondary antibody solution (Vector kit: blue-labeled bottle): 1 drop (50uL) yellow (NHS) + 2.5 mL buffer + 1 drop (50uL) blue
12. Wash slides in 0.1% PBST for 15 minutes, with rotation
13. Wash slides in 0.1% PBST for 15 minutes, with rotation, x2
14. Incubate sections at 37°C for 1 hour with VECTASTAIN ABS Reagent (silver bottle): 1 drop A + 2.5 mL buffer + 1 drop B
15. Wash slides in 0.1% PBST for 5 minutes
16. Incubate sections at 37°C in peroxidase substrate solution (AEC kit) until desired stain intensity develops (typically 8-10 minutes for most antibodies, can be 30 minutes). AEC SK-4205 To 5 mL diluent, add 2 drops of #1, 3 drops of #2 and 2 drops of 3#
17. Immerse slides in water for 2 minutes
18. Counterstain with hematoxylin (20 seconds to 4 minutes), rinse with gently running water for 7 minutes and add Invitrogen Clearmount mixed with water (1:1) on the wet slide
19. Let dry the Clearmount overnight at 37°C, the surface must be perfectly flat
20. Take images
21. Incubate sections at 60°C for one hour to dry it perfectly.
22. Put drops of Eukitt on cover slips, add the cover slips on the Clearmount layer of the slide, without touching the Clearmount swelling on the edges
23. Let dry for a few hours and store forever

4.1.9 Transmission Electron Microscopy

For ultrastructural characterization by transmission electron microscopy (TEM), murine maxillae were fixed with 1% glutaraldehyde (Electron Microscopy Sciences, Hatfield, PA, USA) and 2% paraformaldehyde in PBS for 1 hour at room temperature and then overnight at 4°C, and then dehydrated through a graded ethanol series. Samples were embedded in

epoxy resin (Electron Microscopy Sciences). 90-nm-thick sections obtained with a Reichert Ultracut S (Leica, Germany) were placed on formvar-coated nickel grids (Electron Microscopy Sciences) and conventionally stained with uranyl acetate and lead citrate (Electron Microscopy Sciences) at room temperature. Observations and images were collected using a JEOL 1011 transmission electron microscope operating at 80 kV and equipped with a GATAN Erlangshen camera 1000.

4.1.10 Raman Microspectroscopy

Human teeth from 4 XLH patients and 3 control individuals, and the whole maxillae including periodontium from 5 *Hyp* and 5 WT mice, were harvested and fixed in 70% ethanol solution for 48 hours. Human samples were air-dried at room temperature and murine samples were embedded in methyl methacrylate (Merck, Rahway, NJ). All samples were cut in the sagittal plane and progressively polished with silicium carbides and diamond suspension (Escil®, Chavassieu, France). Raman analyses were carried out on a Labram HR800 microspectrometer (Horiba Gr, Jobin Yvon, Lille, France). The spectrometer was equipped with a diode laser (λ= 785 nm), an air-cooled CDD (1024×256 pixels) and a ×100 objective (NA= 0.90, Olympus, France). The illumination spot size was ~1 µm. Spectral acquisitions were done in the 300-1700 cm^{-1} range. The total acquisition time for each spectrum was 1 min with an integration time of 30 s and 2 accumulations. Each spectrum was treated with smoothing filtering (filter width: 3; and polynomial order: 2) with Labspec software (Horiba GR, Jobin Yvon, Lille, France). A total of 30 spectra were obtained per tissue in each sample. Physico-chemical variables were recorded as described previously (Colard et al. 2016). Briefly, mineralization was evaluated as the mineral-to-organic ratio (υ_1 (PO_4)/$\delta(CH_2)$-wag), carbonation was evaluated as Type-B carbonate substitution (υ_1 (CO_3)/υ_1 (PO_4) bands), and crystallinity was the inverse of the full width at half maximum intensity (FWHM) of the ν_1PO_4 band (1/FWHM de υ_1 (PO_4)). All data analyses were performed using Matlab R2010a (Mathworks, Inc., Natick, MA, USA).

Five physicochemical variables linked to pathophysiological behavior of bone (Colard et al. 2016; Mandair and Morris 2015) were determined from Raman spectra:

1- Mineral-to-organic ratio = intensity ratio between ν_1PO_4 (960 cm^{-1}) to the $\delta(CH_2)$ side chains of collagen molecules (1450cm^{-1}) bands. The mineral to organic ratio reflects the relative amount of mineral par amount of organic matrix and described the mineral content of mineralized tissues;

2- Monohydrogen phosphate content= intensity ratio between ν_3 HPO_4 (1003cm^{-1}) and ν_1PO_4 bands. The monohydrogen phosphate (HPO_4) content reflects the conversion of nonapatitic precursors into apatitic mineral and consequently is related to the mineral bone maturity;

3- Crystallinity= inverse of the full width at half maximum intensity (FWHM) of the ν_1PO_4 band. The crystallinity reflects mineral crystal size and order; this is increased during mineralization from initial amorphous calcium phosphate phases to well-ordered apatite forms.

4- Type-B carbonate substitution= intensity ratio between B-type CO_3 (1071cm^{-1}) and ν_1PO_4 bands. This non-stoichiometric substitution of PO_4 ions in the crystal lattice (called type-B substitution) promotes structural changes occurring within the crystal lattice (vacancies, shape and symmetry changes of the mineral crystal).

5- Hydroxyproline-to-proline ratio= intensity ratio between proline (855cm^{-1}) and hydroxyproline bands (870cm^{-1}). The hydroxyproline-to-proline ratio gives an assessment of the collagen posttranslational modifications. The hydroxyproline-to-proline ratio had been suggested to be linked with the mineralization pattern.

4.1.11 Statistical analysis

Results are given as the mean ±SD. Comparison between groups was performed using Student's *t*-test or nonparametric tests when the number of data/samples was lower than 30 to fit the normal law (Kruskal-Wallis test followed, if significant, by group comparisons with the Mann-Whitney U test) using R 3.3.2 software. Differences between groups were considered significant when $p<0.05$. For Raman spectroscopy, the *x* value of relative gain/loss for each variable of each human or animal sample was treated as a single statistical unit.

4.2 Experimental Models

4.2.1 Model of alveolar bone breakdown and repair

Periodontal breakdown was achieved as described previously (Abe and Hajishengallis 2013): 5-0 synthetic absorbable undyed braided suture (Ethicon, Inc. 2008) was tied as a ligature around second maxillary molars using a triple-knot for up to four days to induce alveolar bone resorption (Kantarci et al. 2015). At day 4, ligatures were removed to allow bone healing. Mice were injected intraperitoneally with demeclocycline (Sigma-Aldrich, 30 mg/kg) at day 7 and day 13 post-surgery, and sacrificed at day 15.

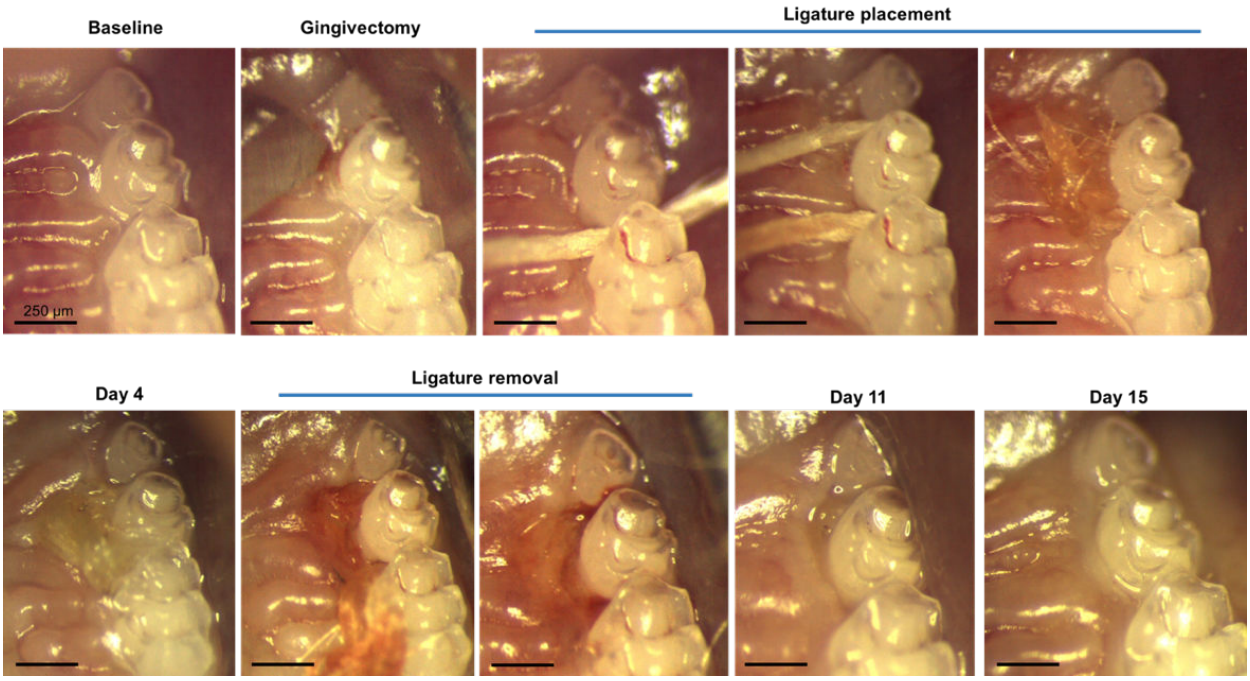

Figure 10 Ligature placement and removal

Document B. R. Coyac, EA2496

Alveolar bone loss and repair measurement

Two-dimensional alveolar bone resorption/formation was measured longitudinally as the distance between the top of the bone septum and the bottom of the pulp-chamber floor at the furcation area between the 2 buccal roots of the maxillary second molar. Five slices were measured per animal to cover the entire width of the two buccal roots. Measurements were performed at days 0, 4, 7, 11, 13, 15 on the same experimental WT and *Hyp* mice.

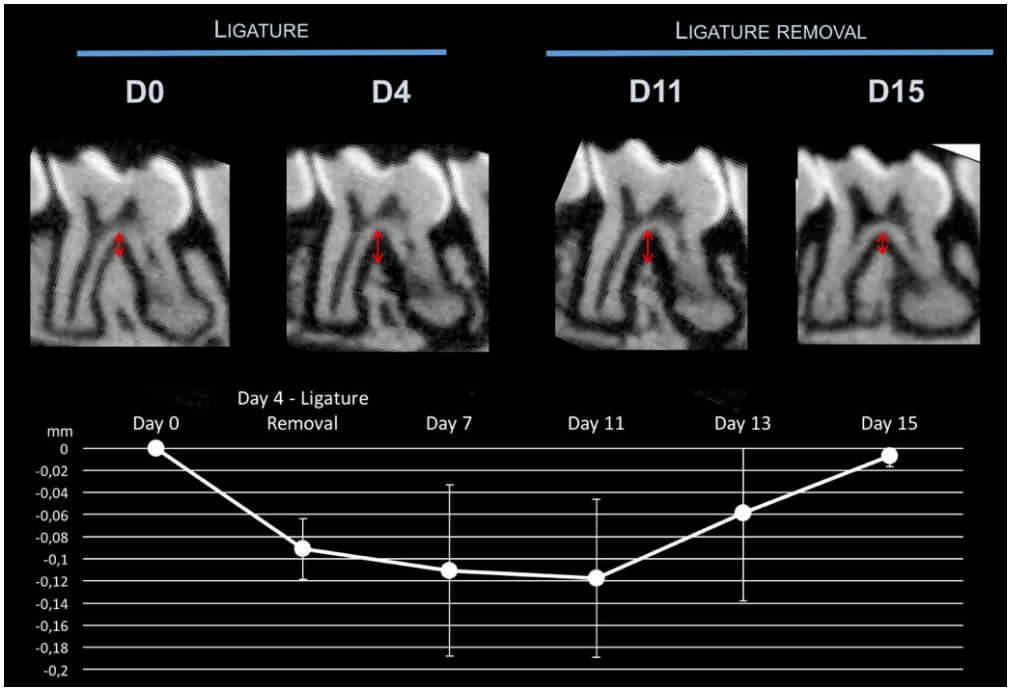

Figure 11 Radiographic follow-up of alveolar bone breakdown and repair

Document B. R. Coyac, EA2496

4.2.2 Model of tooth movement adaptation

Experimentally-induced appositional growth of cellular cementum was performed as previously described (Salmon et al. 2016): cellular cementum formation on the tooth apex of mandibular molars was stimulated by the extraction of opposing maxillary molars. Extraction of maxillary molars removed mandibular molars from occlusion (i.e. they become unloaded), putting them into super-eruption and promoting increased appositional growth of cellular cementum on the tooth apex.

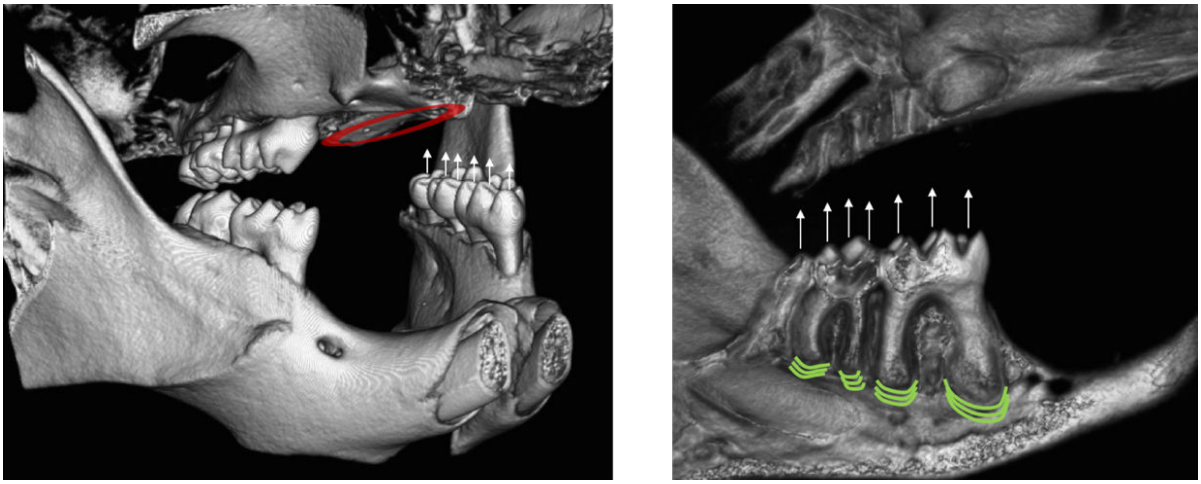

Figure 12 Model of tooth overeruption/cementum formation

Document B. R. Coyac, EA2496

4.3 *In vitro:* 3-dimensional cell culture model

4.3.1 Patients information and Human teeth

XLH was diagnosed at the collaborating institutions based on the disorder's characteristic findings and a pattern of X-linked dominant disease transmission and positive *PHEX* mutation analysis. Teeth were obtained from the Dental Department of Academic Hospitals Paris Nord Val de Seine, AP-HP, France. Deciduous and permanent teeth were extracted for orthodontic reasons from three XLH patients and 3 sex- and age-matched healthy young individuals (11 and 15 years of age) with informed and oral consents from the patients and the parents according to ethical guidelines set by the French law (agreement n°DC-2009-927, *Cellule Bioéthique* DGRI/A5, 6477, subject N°16-024).

4.3.2 Culture of human dental pulp cells

After decontamination with povidone-iodine solution (Betadine, Meda Pharma, France), teeth were sectioned longitudinally and exposed pulp tissues were collected and enzymatically digested with type I collagenase (3 mg/ml; Worthington Biochem, Freehold, NJ, USA) and dispase (4 mg/ml; Boehringer Mannheim, Germany). Cells were treated following an established protocol (Gronthos et al. 2011; Miura et al. 2003): cells were seeded at a density of $10^4/cm^2$, and the cultures were maintained with Dulbecco's Modified Eagle Medium 1 g/L D-Glucose (DMEM; Invitrogen, Grand island, NY, USA) supplemented with 10% fetal bovine serum (FBS; Invitrogen), 1% penicillin/streptomycin (PS; Invitrogen), at 37°C with 5% CO_2. The medium was refreshed the next day after initial cell attachment and then twice every week. Cells were detached by trypsinization at 70-80% confluence (0.25% trypsin EDTA solution Sigma-Aldrich, St. Louis, MO, USA) and re-plated at the same density. For all experiments, pulp cells were used at passage 3.

4.3.3 Preparation of dense collagen gels and osteo/odontogenic cell differentiation

Sterile, rat-tail tendon-derived type I collagen (2.10 mg/mL of protein in 0.1% acetic acid) was used as starting materials and developed as previously described (Coyac et al. 2013). 3.6 mL of sterile rat-tail collagen type I at a protein concentration of 2.01 mg/mL in 0.1% acetic

acid was mixed with 0.9 mL of ×10 DMEM (Dulbecco's Modified Eagle Medium) and neutralized by drop-wise addition of 5 M NaOH to ~pH 7.4. After neutralization, dental pulp cells, either from control individuals or XLH patients were seeded within the hydrogels at a density of 150×10^3 cells/mL of collagen solution, immediately prior to gel polymerization. Cellularized collagen solutions were poured in 4-well plates (0.9 mL/well of 4.5 mm height×16 mm diameter) to produce dense planar discs. Gelation was achieved by allowing the solutions to set at 37°C in a 5% CO_2 incubator for 30 min. Highly hydrated hydrogels (with < 0.5 weight % fibrillar collagen density) were removed from the molds and dense gels were produced by plastic compression (PC) as previously reported (Brown et al. 2005; Coyac et al. 2013). Briefly, highly hydrated gels were placed on a stack of blotting paper, nylon mesh, and metal mesh, and subjected to PC using an unconfined compressive stress of 0.5 kPa for 5 min, to remove the excess casting fluid. After compression, dense discs (16 mm diameter) were transferred to 12-well plates and cultured under static conditions for 24 days. Ctrl and XLH cellularized scaffolds were cultured in osteogenic medium (DMEM media supplemented with 300 µM L-ascorbic acid sodium salt, 10 nM dexamethasone, 4% fetal bovine serum, and 1% penicillin/streptomycin) either supplemented with 10% β-glycerophosphate (+P) or no β-glycerophosphate supplementation (-P). A same batch of FBS was used for all experiments.

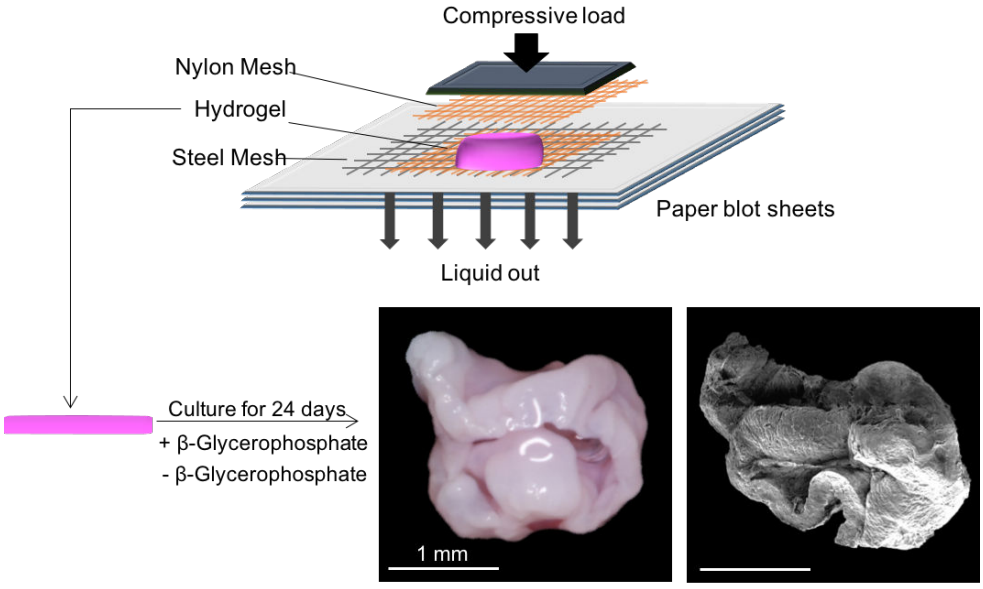

Figure 13 Compression of highly hydrated cellularized hydrogels

Document B. R. Coyac, EA2496

Protocol for dense collagen gels seeded with dental pulp cells preparation

Materials

- Sterile rat-tail tendon derived type I collagen: 2.07mg/mL of protein in 0.6% acetic acid (First Link Ltd., West Midlands, UK) or homemade sterile rat-tail tendon derived type I collagen: 2mg/mL of protein in 0.1% acetic acid.
  Following steps are designed for 0.1% acetic acid.
- 10x minimum essential medium (MEM10X)
- 5N NaOH, filtered
- Sterile nylon and metal mesh
- Sterile paper and forceps
- Sterile glass slides for load (1kN/m^2)
- DMEM 10% FBS 1% PS with osteogenic additives
- Cells in DMEM 10% FBS, 1% PS
- PBS
- Trypsin
- Tripan blue
- Hemocytometer
- 12-well plates
- 4-well plates

Methods

1- Cell density: 150.000 cells/mL of collagen

In one 50mL tube, prepare 3.6mL of collagen, so there is a need of:

150.000 x 3.6 = 540.000 cells for 1 tube (= for 4 scaffolds).

Collect 540.000 cells x (X+1) in 250µL x (X+1) of DMEM 10% FBS, 1% PS

(X= number of 50mL tubes required)

2- Master mix: 10xMEM + 5N NaOH

- 10xMEM= 965µL x (X+1)
- 5N NaOH= 10µL x (X+1)

*Note: for 0.6% acetic acid, proportions of the master mix are 0.9*mL 10xMEM and 75µL 5N NaOH

Gel preparation: on ice, make it fast before it jellifies

1- Add 3.6mL of collagen in a 50mL sterile tube
2- Add 975µL of master mix to the collagen I
3- Mix gently by doing circular moves
4- Adjust pH to 7.4 (cherry color) by adding 5-10µL and 1µL of 5N NaOH drops
5- Mix gently each time
6- Once the desired pH is reached (cherry color)
7- Add the cell suspension (540.000 cells in 250µL of DMEM) and mix
8- Pour 900µL of the solution on each well of a 4-well plate
9- Place the well plate in the incubator for 30min
10- Once jellified, place the 4 gels on a series of nylon and metal mesh and paper blot
11- Apply a stress of 1kN/m^2 by placing 3 glass slides on top of 2 gels
12- Wait for 5min and transfer the gels to a 12-well plate w/DMEM 10%FBS, 1%PS

4.3.4 Microscopy analyses of scaffolds and cells

After 24 days of culture, scaffolds were rinsed in PBS (-Ca, -P) and fixed in 70% ethanol at 4°C and dehydrated in a graded ethanol series. Undecalcified samples were embedded in methyl methacrylate (Merck, Rahway, NJ). Serial sections, 4µm thick were cut on a microtome (Polycut E microtome, Leica, Wetzlar, Germany). Series of consecutive sections were stained respectively with toluidine blue (pH 3.8), with von Kossa reagent (5% silver nitrate solution, Sigma-Aldrich). Light microscopy (LEITZ DM-RBE microscope, Leica, Germany, equipped with a Sony DXC-950 CCD camera) was used to examine Ctrl and XLH dental pulp cells-seeded scaffolds. For scanning electron microscopy (SEM) and transmission electron microscopy (TEM), scaffolds were rinsed in PBS (-Ca, -P) and fixed in 1% glutaraldehyde (Electron Microscopy Sciences, Hatfield, PA, USA) and 2% paraformaldehyde in PBS for 1 hour at room temperature and then overnight at 4°C, and then dehydrated through a graded ethanol series. SEM and TEM were performed to analyze scaffold microstructure as well as cellular morphology and mineralization. Energy-dispersive X-ray spectroscopy (EDS) was performed for elemental analysis of mineral, and crystalline structure of the mineral was assessed by Raman spectroscopy.

4.3.5 Immunogold labeling for OPN

LR White acrylic resin (London Resin Company, Berkshire, UK) embedded scaffolds were polymerized in block molds at 55°C for 2 days. Grid-mounted sections (80 nm) were cut on an ultramicrotome and incubated with goat anti-human OPN antibody, followed by rabbit anti-goat secondary antibody and then protein A-colloidal gold (14 nm) conjugate (Dr. G. Posthuma, University of Utrecht, Utrecht, The Netherlands), and then conventional staining with uranyl acetate and lead citrate. Sections were viewed in a FEI Technai 12 transmission electron microscope (FEI, Hillsboro, OR, USA) operating at 120 kV and equipped with a 792 Bioscan 1k x_1k wide-angle multiscan CCD camera (Bioscan, Pleasanton, CA, USA). Control incubations to assess nonspecific binding of gold particles consisted of the same procedure except the primary antibody was omitted or substituted by non-immune serum.

4.3.6 Western Blotting

Flash-frozen cell-seeded scaffolds were crushed in liquid nitrogen and solubilized in 10 volulmes of lysis buffer containing 8 M Urea, 2 M Thiourea, 4% CHAPS, 50 mM DTE. After centrifugation (100 000 × *g* for 45 min at 6 °C), the supernatants were collected and, in order to remove DTT, all samples were treated with 2D Clean-Up kit (GE healthcare) according to the manufacturer's instructions. The resultant dry pellets were suspended into lysis buffer without DTT, and the pH was set to 8.5 with 1.5 M Tris-base. Protein concentration of samples was estimated according to the manufacturer's instructions using a commercial Bradford reagent (Quick Start Bradford protein assay, Bio-Rad) and samples were stored at −80°C until use. A 15-µg quantity of total protein extracts of each sample was separated by SDS-PAGE on a gradient gel (Biorad stain free anyKd), transferred to a polyvinylidene difluoride membrane, and iBind Flex Invitrogen Thermo Fisher. The membrane was probed with goat anti-human OPN antibody diluted 1:1000 (AF 1433, R&D Systems, Minneapolis, MN, USA). Membrane was then incubated with horseradish peroxidase-conjugated anti-goat secondary antibody and visualized with ECL Select^{TM} Prime Western Blotting Detection Reagent (GE Healthcare, Buckinghamshire, UK). Quantitation of digitized images of immunoblots was done using ImageJ software.

4.3.7 Micro-computed Tomography Dataset Acquisition

Scaffolds were scanned using a high-resolution X-ray micro-CT device (Quantum FX Caliper, Life Sciences, Perkin Elmer, Waltham, MA, United States). Three-dimensional acquisitions were performed using an isotropic voxel size of 40x40x40 μm^3 (90 kV, 160 microA, 180 s). Morphometric measurements were performed using Skyscan software (v1.13.5.1, Kontich, Belgium). Measurements were performed at Days 24 on 12 scaffolds in each group (Ctrl +P, -P and XLH +P, -P).

5 Paper 1: Higher severity and frequency of periodontitis in XLH patients with erratic phosphate and vitamin D treatments

Journal of Dental Research
1–8

DOI: 10.1177/0022034516677528
jdr.sagepub.com

Phosphate and Vitamin D Prevent Periodontitis in X-Linked Hypophosphatemia

M. Biosse Duplan[1,2,3], B.R. Coyac[4*], C. Bardet[4*], C. Zadikian[1,2], A. Rothenbuhler[3,5], P. Kamenicky[3,5], K. Briot[3,6], A. Linglart[3,5], and C. Chaussain[1,3,4**]**

Abstract

X-linked hypophosphatemia (XLH) is a rare genetic skeletal disease where increased phosphate wasting in the kidney leads to hypophosphatemia and prevents normal mineralization of bone and dentin. Here, we examined the periodontal status of 34 adults with XLH and separated them according to the treatment they received for hypophosphatemia. We observed that periodontitis frequency and severity were increased in adults with XLH and that the severity varied according to the hypophosphatemia treatment. Patients who benefited from an early and continuous vitamin D and phosphate supplementation during their childhood presented less periodontal attachment loss than patients with late or incomplete supplementation. Continued hypophosphatemia treatment during adulthood further improved the periodontal health. Extracted teeth from patients with late or incomplete supplementation showed a strong acellular cementum hypoplasia when compared with age-matched healthy controls. These results show that XLH disturbs not only bone and dentin formation but also cementum and that the constitutional defect of the attachment apparatus is associated with attachment loss.

Keywords: hypophosphatemic rickets, periodontal disease, dental cementum, alveolar bone loss, periodontal attachment loss, osteomalacia

Introduction

X-linked hypophosphatemia (XLH) is a rare genetic disorder characterized by hypophosphatemia, rickets in children, and/or osteomalacia in adults. It belongs to a larger group of genetic hypophosphatemia with autosomal dominant hypophosphatemic rickets and autosomal recessive HR. XLH affects 1 out of 20,000 births (Feng et al. 2013). In XLH, elevated signaling of the phosphate-regulating hormone FGF23 in the kidney leads to phosphate wasting and hypophosphatemia (Bergwitz and Jüppner 2010). Reduced circulating levels of phosphate disturbs the mineralization of bones and teeth, resulting in various clinical manifestations. These include bone pain, deformities and fractures, growth failure, spontaneous endodontic abscesses, and hearing loss in children and adults (Linglart et al. 2014). Infection of the dental pulp tissue results from enamel microcracks and poor dentin mineralization that allow microbial invasion (Chaussain-Miller et al. 2003; Chaussain-Miller et al. 2007). Treatment options are currently limited, aimed at counteracting consequences of FGF23 excess, with oral phosphate supplementation with multiple daily intakes and vitamin D analogs (Linglart et al. 2014). In a majority of pediatric patients, this treatment will improve active rickets, allow proper mineralization of the bone and dentin matrix, and partially restore the growth velocity (Linglart et al. 2014). Potential benefits on other mineralized tissues are unknown. However, compliance to oral treatment is a major issue, and young adults often stop treatment at the end of growth. There is no consensus of the therapeutic benefits of phosphate supplementation and vitamin D analogs in adults, although the

[1]Service d'Odontologie, Hôpital Bretonneau, HUPNVS, AP-HP, Paris, France
[2]Faculté de Chirurgie Dentaire, Université Paris Descartes, Montrouge, France
[3]Centre de Référence des Maladies Rares du Métabolisme du Calcium et du Phosphore, Plateforme d'expertise Paris Sud Maladies rares, filière OSCAR, Hôpital Bicêtre-Paris Sud, AP-HP, Le Kremlin Bicêtre, France
[4]EA 2496, Faculté de Chirurgie Dentaire, Université Paris Descartes, Montrouge, France
[5]Service d'endocrinologie, Hôpital Bicêtre, HUPS, AP-HP, Le Kremlin Bicêtre, France
[6]Service de Rhumatologie, Hôpital Cochin, HUPC, AP-HP, Paris, France
*Authors contributing equally to this article
**Authors contributing equally to this article

Corresponding Author:
M. Biosse Duplan, Service d'Odontologie, Hôpital Bretonneau, 23 rue Joseph de Maistre, 75018 Paris, France.
Email: martin.biosse-duplan@parisdescartes.fr

hypophosphatemia persists throughout life and data have shown the immediate recurrence of osteomalacia after the cessation of the treatment (Sullivan et al. 1992).

The periodontium relies on 2 mineralized tissues, alveolar bone and cementum, to attach the tooth to the bone tissue of the jaw. Constitutional defects of these tissues, as caused by genetic diseases, have been shown to result in periodontal attachment loss and eventually tooth loss. This is the case for patients with hypophosphatasia (Chapple 1993), a genetic disease where mineralization of bones and teeth can be severely disturbed (Linglart and Biosse-Duplan 2016). The attachment loss in hypophosphatasia arises from cementum aplasia or hypoplasia that prevents normal insertion of the periodontal ligament fibers on the root surface (van den Bos et al. 2005).

XLH could also result in attachment loss. The examination of 10 adults with presumptive XLH showed a significant increased prevalence and severity of periodontitis, with the presence of bone loss, deep pockets, and severe attachment loss (Ye et al. 2011). Periodontal defects were also consistently observed in the different murine models of hypophosphatemic rickets, with evidence of reduced thickness of acellular cementum (Ye et al. 2008; Fong et al. 2009), reduced cellular cementum (Wang et al. 2012), and defective alveolar bone matrix (Ye et al. 2008; Sun et al. 2011). It is unknown if similar defects exist in XLH patients.

Here, we examined the periodontal status of 34 adults with XLH and separated them according to the treatment that they received for XLH. We also analyzed and compared the cementum characteristics of extracted teeth from the same patients and age-matched controls.

Materials and Methods

Study Population

This study was carried out in the frame of the French Reference Center for Rare calcium and phosphate metabolism disorders (French Reference Center for Rare Calcium and Phosphate Metabolism Disorders, Paris, France). It was approved by its ethical committee, and all the patients gave their informed consent to participate (agreement CNIL 1920371 and 1915179). All patients aged ≥18 y who were referred to the Odontology Department of Bretonneau Hospital, Paris, France, by an endocrinologist for oral examination after diagnosis of XLH received a complete periodontal examination. Diagnosis of XLH was made by the patient's endocrinologist, based on clinical presentation and biochemical profile. Most patients had a genetic confirmation. History of XLH treatment—including type of treatment, age at onset of treatment, years with treatment, and compliance—was provided by the endocrinologist and the patient.

All adult patients with XLH were prospectively clinically and radiographically assessed during a 4-y period (January 2012 to 2016), and parameters were gathered and analyzed. Exclusion criteria included 1) diagnosis of another form of genetic hypophosphatemia than XLH, 2) presence of other diseases likely to affect the periodontium (e.g., diabetes), 3) edentulism, and 4) patients with a history of periodontal treatment (nonsurgical and/or surgical). Smoking history was recorded. Patients were stratified into 3 groups according to whether they had used and were using oral phosphate supplementation and vitamin D analogs:

Group 1 (childhood intermittent): No use, intermittent use, or use of only phosphate or vitamin D analog during childhood.
Group 2 (childhood full): Continuous use during childhood of both phosphate and vitamin D and no use during adulthood.
Group 3 (childhood and adulthood): Continuous use during childhood and continuous or intermittent use during adulthood of both phosphate and vitamin D.

Intermittent use was defined as a treatment started after the age of 5 y, stopped before the age of 17 y, and/or discontinued for more than a few months between 5 and 17 y. The daily doses of phosphorus supplements ranged between 40 and 60 mg/kg/d. The dose of vitamin D analogs depended on growth velocity (1–3 μg/d, alfacalcidol; or 0.5–1.5 μg/d, calcitriol).

Examination Protocol

Clinical Examination. A comprehensive oral examination, including periodontal charting, was performed. Full-mouth clinical measurements of the distance from the free gingival margin to the base of the sulcus (pocket depth [PD], measured to the next millimeter) and the distance from the cement-enamel junction to the gingival margin (recession) were collected with a manual UNC-15 periodontal probe. The clinical attachment level was calculated as probing depth + recession. Six measurements were made from the buccal and lingual aspects of each tooth. A dichotomous full-mouth bleeding score was recorded as the percentage of total bleeding surfaces upon probing (Ainamo and Bay 1975). A dichotomous full-mouth plaque score was recorded as the percentage of total surfaces with plaque (O'Leary et al. 1972). One single examiner (M.B.D.) carried out all measurements.

We used the Center for Disease Control and Prevention and American Academy of Periodontology consensus 3-level classification for periodontitis definition (Eke, Page et al. 2012). Based on the periodontal charting, each case was classified independently into 1 of the 4 categories (no periodontitis and mild, moderate, and severe periodontitis) by 2 examiners (M.B.D. and C.Z.). Interexaminer concordance was 100%.

Radiographic Examination and Bone Loss Assessments. All participants received a panoramic radiograph or a set of 21 long-cone periapical radiographs, unless they provided a recent radiograph (<1 y). Bone loss was classified as localized or generalized (affecting ≤30% or >30% of the teeth, respectively) and mild, moderate, or severe (bone loss ≤1/3, >1/3 to ≤1/2, or >1/2 of the root length, respectively; van der Velden 2005). When the severity of the bone loss varied in the different

Table 1. Selected Patient Characteristics Included in the Study.

Characteristics	*n* (%)[a]
Age, y	
Mean	36.2
Max	59.4
Min	20.8
Sex	
Male	8 (23.5)
Female	26 (76.5)
Smoking status	
Current smoker	11 (32.4)
Former smoker	3 (8.8)
No smoker	20 (58.8)
Genetic mutation	
PHEX	26 (76.5)
Unknown	8 (23.5)
Treatment with phosphorous and vitamin D analogs	
Childhood only: intermittent compliance	9 (26.5)
Childhood only: full compliance	12 (35.3)
Childhood and adulthood	13 (38.2)

[a]Values presented as *n* (%) unless otherwise noted.

quadrants, the worst quadrant was selected. Two examiners (M.B.D. and C.Z.) carried out all measurements independently. Interexaminer concordance was 100%.

Teeth

Permanent teeth were collected from XLH patients and from sex- and age-matched controls, extracted during periodontal, restorative, or orthodontic treatments. All teeth were collected with patient's informed and oral consent in agreement with ethical guidelines set by French law (Loi Bioéthique 2004-800, agreement DC-2009-927, Cellule Bioéthique DGRI/A5).

Histologic Staining. Immediately after extraction, teeth were fixed for 7 d at 4°C in 4% paraformaldehyde solution at pH 7.2 to 7.4 and were decalcified in 4.13% EDTA for ~1 mo in a decalcification microwave. Decalcified teeth were embedded in Paraplast, sectioned (7 µm), and stained for hematoxylin and eosin. Teeth were sectioned in the longitudinal (cervico-apical) plane to facilitate orientation. Histomorphometry of the cementum was carried out with MetaMorph 7 and ImageJ softwares. Acellular cementum thickness was measured on a standardized length of the root (1,000 µm), starting around 300 µm from the cementoenamel junction.

Immunostaining. For immunohistochemistry, paraffin sections were dewaxed in xylene, hydrated in a graded ethanol series to pure distilled water, and blocked with 5% bovine serum albumin/tris-buffered saline-T (BSA/TBS-T). Sections were incubated for 1 h at room temperature with goat anti-human osteopontin (OPN) antibody (AF1433; R&D Systems) diluted 1:20 in 5% BSA/TBS-T, washed, and then incubated with horseradish peroxidase–conjugated anti-goat IgG diluted 1:1,000 in the same buffer. Peroxidase activity was detected with a diaminobenzidine substrate kit from Abcam following the manufacturer's instructions. Sections were counterstained with toluidine blue. Negative controls were prepared by omitting the primary antibody.

Statistical Analysis

Differences between groups were assessed with unpaired *t* tests for pairwise comparisons and analysis of variance for multiple comparisons or Fisher's exact test. The significance threshold was set at $P \leq 0.05$. Statistical analyses were performed with GraphPad PRISM 5.03. All values are shown as mean ± SD.

Results

Thirty-nine adult patients diagnosed with presumptive XLH were prospectively examined. One patient was excluded because of a diagnosis of autosomal dominant hypophosphatemic rickets, 3 patients because they were edentulous, and 1 patient because he had received periodontal treatment before the clinical examination. No patient was excluded because of the presence of diabetes. Thus, 34 patients were included in the study (Table 1). Periodontal charting was missing for 2 patients, and radiographic examination was missing for 1 patient. The mean age was 36.2 y (max: 59.4, min: 20.8). Eleven patients were current smokers (32.4%), 3 former smokers (8.8%), and 20 no smokers (58.8%). A majority of patients were women (76.5%), which was expected since XLH is inherited in an X-linked dominant manner. *PHEX* mutations were detected in 26 patients (76.5%). The clinical and biochemical profile and inheritance of the 8 other patients are compatible with XLH. Per the history of XLH treatment provided by the endocrinologist and the patients, XLH patients were classified in 3 groups: group 1 (childhood intermittent, $n = 9$), group 2 (childhood full, $n = 12$), and group 3 (childhood and adulthood, $n = 13$). The mean ages of groups 1, 2, and 3 were, respectively, 44.8, 34.4, and 32.0 y ($P \leq 0.005$ between groups 1 and 2; $P \leq 0.001$ between groups 1 and 3). The percentages of women in groups 1, 2, and 3 were 88.9%, 50%, and 92.3%, respectively ($P \leq 0.05$ between groups 2 and 3). The percentages of patients who smoked were 11.1%, 25.0%, and 53.8%, respectively (not significant).

Clinical Examination

The mean numbers of teeth present in groups 1 (childhood intermittent), 2 (childhood full), and 3 (childhood and adulthood) were 21.6, 26.9, and 28.1, respectively (Fig. 1). Group 1 had on average 8 teeth other than third molars absent, compared with group 2 (2.7, $P \leq 0.01$) and group 3 (1.4, $P \leq 0.01$; Fig. 1).

Using the last Center for Disease Control and Prevention–American Academy of Periodontology case definition of periodontitis (Eke, Page et al. 2012), we observed that XLH patients frequently presented with periodontitis: 78.1% of the patients were affected with a moderate (53.1%) or severe

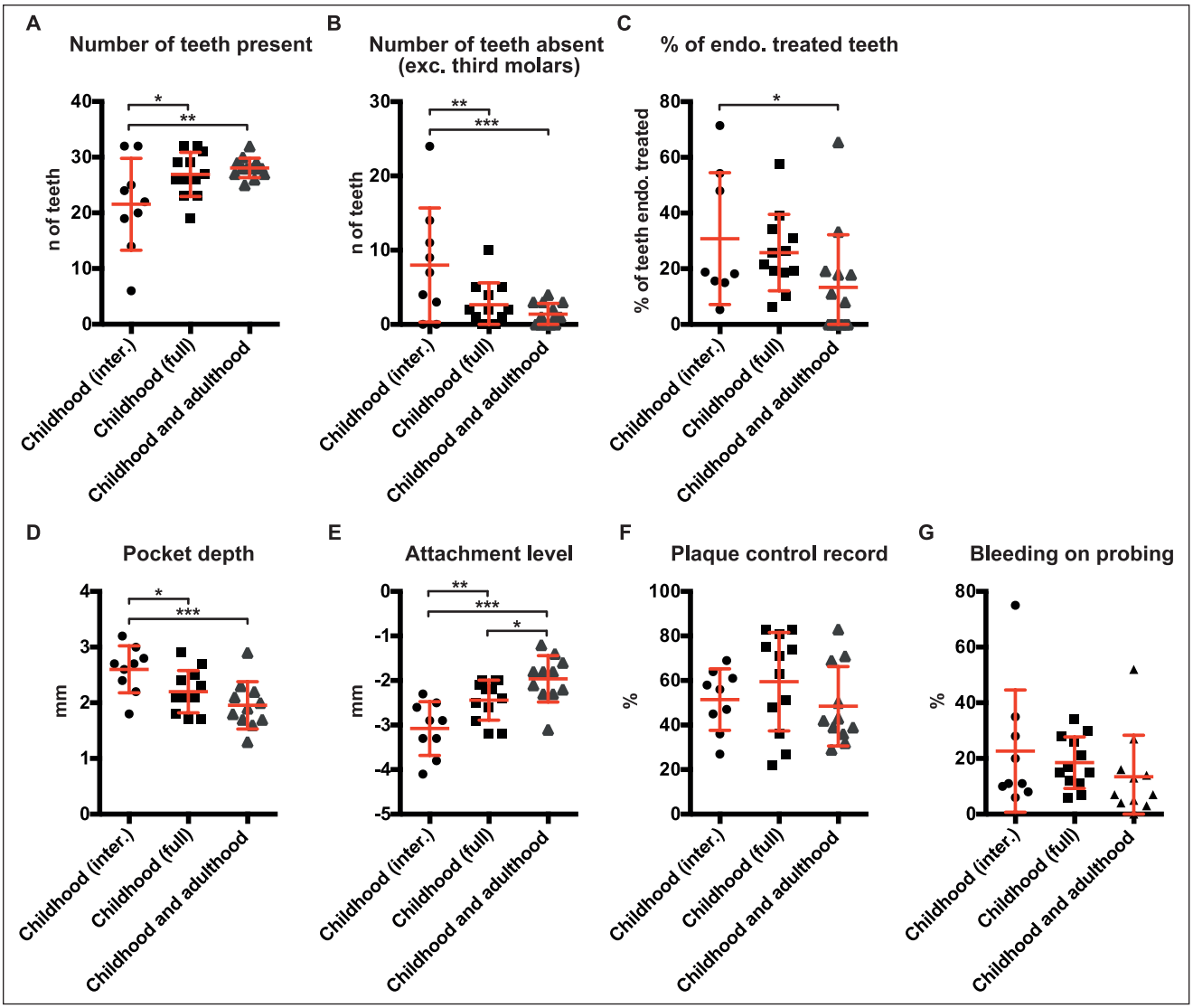

Figure 1. Comparison of the number of teeth present (**A**), the number of teeth absent (excluding third molars; **B**), the percentage of endodontically treated teeth (**C**), the mean pocket depth (**D**), the mean attachment level (**E**), and the plaque control record (**F**) and bleeding on probing (**G**) scores in group 1 (intermittent treatment during childhood), group 2 (treatment with full compliance during childhood), and group 3 (treatment with full compliance during childhood and treatment during adulthood). The number of endodontically treated and absent teeth decreases with the duration of the treatment, as do the mean pocket depth and attachment loss, despite similar plaque control. Lines connecting 2 groups indicate statistically significant differences. All statistically significant differences are indicated. *$P \leq 0.05$; **$P \leq 0.01$; ***$P \leq 0.005$.

(25.0%) form. The frequency of periodontitis varied among the 3 groups, with 100% of patients from groups 1 and 2 affected, compared with 36.4% in the group 3 (Table 2). Fifty-six percent of patients ($n = 5$) from group 1 had severe periodontitis, compared with 25% ($n = 3$) and 0% in the groups 2 and 3.

The mean PD was increased in group 1 (2.6 mm) compared with groups 2 and 3 (2.2 mm; $P \leq 0.05$ and 1.96 mm; $P \leq 0.005$, respectively; Fig. 1). The mean level of attachment was −3.1 mm in group 1, compared with −2.4 ($P \leq 0.01$) and −1.97 mm ($P \leq 0.001$) in groups 2 and 3, respectively (Fig. 1). Mean plaque control records were not different among the 3 groups, with 51.4%, 59.5%, and 48.4% of teeth surfaces with plaque in groups 1, 2, and 3 (not significant), while the bleeding index was 22.7%, 18.5%, and 13.4% in groups 1, 2, and 3, respectively (not significant; Fig. 1).

Radiographic Examination

The mean percentages of endodontically treated teeth in groups 1 (childhood intermittent), 2 (childhood full), and 3 (childhood and adulthood) were 30.8%, 25.8%, and 13.3% ($P \leq 0.05$ vs. group 1), respectively (Figs. 1 and 2, Table 2).

Generalized alveolar bone loss was frequent in XLH patients, with 81.8% affected. Half the patients in group 1

Table 2. Prevalence and Severity of Periodontitis and Presence of Bone Loss and Intrabony Defects among the Patients with Hypophosphatemic Rickets.

	Proportion of Life with Treatment, *n* (%)		
	Childhood Only: Intermittent Compliance	Childhood Only: Full Compliance	Childhood and Adulthood
Periodontitis			
No	0	0	7 (63.6)
Mild	0	0	0
Moderate	4 (44.4)	9 (75)	4 (36.4)
Severe	5 (55.6)	3 (25)	0 (0)
Bone loss: generalized			
No	0	1 (8.3)	5 (38.5)
Mild	3 (37.5)	6 (50)	7 (53.8)
Moderate	1 (12.5)	3 (25)	1 (7.7)
Severe	4 (50)	2 (16.7)	0
Presence of intrabony defect			
No	0	3 (25)	10 (69.2)
Yes	8 (100)	9 (75)	4 (30.8)

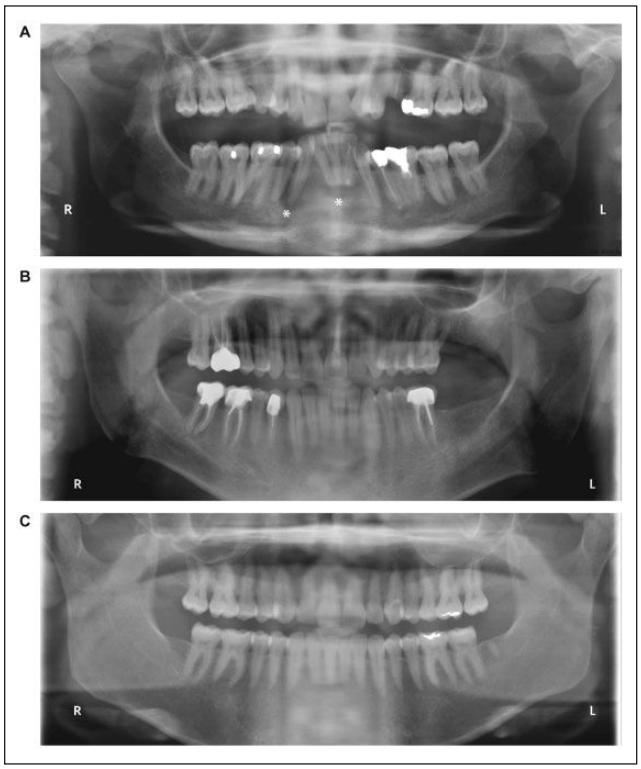

Figure 2. Representative panoramic radiographs of patients with X-linked hypophosphatemia (XLH) in groups 1, 2, and 3: (**A**) A 48-y-old woman with XLH from group 1 (intermittent treatment during childhood). Note the signs of several endodontic infections (*) and the presence of endodontically treated teeth and generalized alveolar bone loss. (**B**) A 40-y-old man with XLH from group 2 (treatment with full compliance during childhood). Note the presence of endodontically treated teeth and generalized alveolar bone loss. (**C**) A 39-y-old woman with XLH from group 3 (treatment with full compliance during childhood and treatment during adulthood). Note the absence of endodontically treated teeth and absence of alveolar bone loss.

($n = 4$) had severe generalized bone loss, compared with 16.7% ($n = 2$) and 0% in groups 2 and 3, respectively (Table 2, Fig. 2). Infraosseous defects were more frequent in group 1 (100%, $n = 8$) and group 2 (75%, $n = 9$) than in group 3 (30.8%, $n = 4$; Table 2, Fig. 2).

Histologic Analysis

Seven permanent teeth from XLH patients were collected. All but 1 tooth were from XLH patients who had received intermittent phosphate supplementation and vitamin D analogs during childhood only. Seven teeth from controls matched for tooth number, age, and sex were also collected. Acellular cementum was identified on sections stained with HE or immunolabeled for OPN. We observed that the thickness of acellular cementum was decreased in XLH patients compared with controls (−62.5%; $P \leq 0.005$; Fig. 3). The only XLH tooth that presented with an acellular cementum thicker on average than a control tooth belonged to an XLH patient who had been treated with full compliance during childhood.

Discussion

It is established that genetic bone diseases can affect other mineralized tissues, including those of the tooth, in particular dentin (Opsahl Vital et al. 2012; Foster et al. 2014). Only recently, observations mostly obtained with transgenic mouse models have demonstrated that genetic anomalies of the mineralization process can lead to a defective periodontium (Foster et al. 2013; McKee et al. 2013; Linglart and Biosse-Duplan 2016). Among the periodontal tissues, acellular cementum seems exquisitely sensitive to the changes in the local mineral metabolism (Foster et al. 2012). Here, we show with the largest cohort prospectively assessed so far that the genetic skeletal disorder XLH affects acellular cementum and causes attachment loss.

We analyzed the clinical records of 39 adults with XLH, one of the largest groups of adult patients with this rare disease (Connor et al. 2015; Che et al. 2016). Like Ye and colleagues

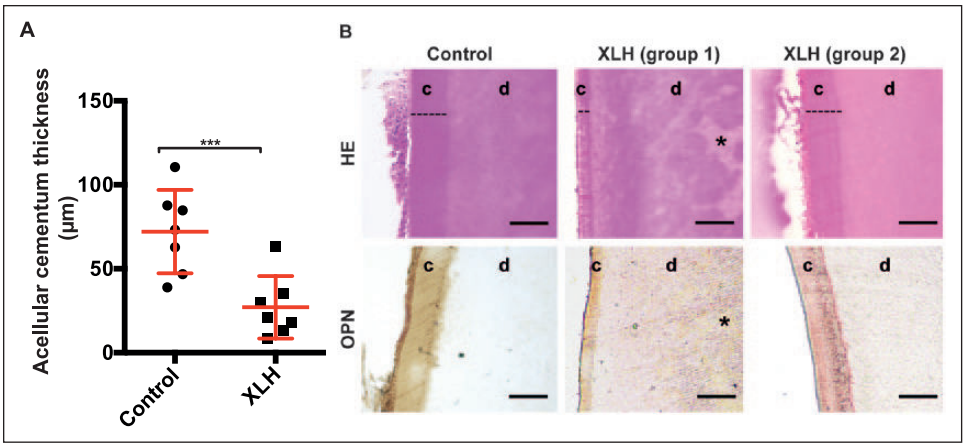

Figure 3. Analysis of acellular cementum thickness in permanent teeth of healthy controls and patients with X-linked hypophosphatemia (XLH) from group 1 (intermittent treatment during childhood) and group 2 (treatment with full compliance during childhood) (**A**). Representative micrographs of sections of teeth from a healthy control and XLH patients from groups 1 and 2 (**B**). Cementum (c) and dentin (d) are identified following hematoxylin and eosin (HE) staining and osteopontin (OPN) immunolabeling. Note that in the tooth from group 1, dentin displays unmineralized areas (*) lightly stained with HE and where OPN accumulates. ***$P \leq 0.005$.

(Ye et al. 2011), we first observed that patients with XLH exhibited more frequent and severe periodontitis. More than 75% of the XLH patients included in our study had periodontitis, with nearly 25% having severe periodontitis. This is much higher than that in the general US population, where 46% of adults have periodontitis, with 8.9% having severe periodontitis (Eke et al. 2015). Among adults with XLH, 63.6% had at least 1 site with attachment loss ≥5 mm, compared with 43.4% and 46.7% of US and French adults (Bourgeois et al. 2007; Eke, Dye et al. 2012). In 27.3% of patients with XLH, the attachment loss ≥5 mm occurred in ≥5% of the sites, compared with 18.2% of the US adults (Eke, Dye et al. 2012). The negative effect of periodontitis on quality of life is considerable and increases with the severity of the disease (Needleman et al. 2004). Periodontitis therefore likely contributes to the impaired quality of life experienced by adults with XLH (Che et al. 2016).

We then observed that periodontitis severity varied extensively among XLH patients (Fig. 2). Conventional management of XLH with daily intake of vitamin D analogs and phosphate supplements during growth not only has a substantial beneficial effect on the skeleton but also improves mineralization of dentin and decreases the occurrence of endodontic infection (Chaussain-Miller et al. 2003; Chaussain-Miller et al. 2007; Connor et al. 2015). However, the clinical benefits during childhood depend on the onset, compliance, and duration of the treatment, and there is no consensus on the benefits of continuing treatment during adulthood (Linglart et al. 2014). We hypothesized that periodontitis severity would depend on the duration of the XLH treatment, and we separated the patients into 3 groups based on whether they had used and were using oral phosphate supplementation and vitamin D analogs during growth and adulthood. As expected, the number of endodontically treated and absent teeth, partially reflecting episodes of endodontic abscesses, decreased with the duration of the treatment. Importantly, the 3 edentulous patients (mean age, 60.1 y) who were excluded from our study would all have been classified in group 1. The prevalence and severity of periodontitis in the group of patients who had been treated during childhood and adulthood (group 3) were lower than in the groups treated during growth only (groups 1 and 2), despite similar plaque control. The increased percentage of smokers in group 3 could also negatively affect periodontal health, as it is well established that the prevalence and severity of periodontitis are increased in smokers (Bergström 2004) and therefore partially mask the benefit of hypophosphatemia treatment. Periodontitis severity also varied depending on the compliance of treatment during childhood (group 1 vs. group 2). More than half the patients from group 3 exhibited no periodontitis, and none had severe periodontitis. At odds with group 3, more than half the patients from group 1 had severe periodontitis. It therefore appears that the presence and severity of periodontitis in adults with XLH are correlated to the extent of vitamin D and phosphate supplementation. It should be noted that the proportion of adult life with supplementation varied extensively in group 3, from patients supplemented for only a few months during pregnancy or after a surgical intervention to those who had been supplemented continuously during adulthood. Of this later subgroup, 5 of 6 patients presented with no periodontitis. These findings could constitute an additional argument in favor of the maintenance of this medical treatment in adults. One limitation of our study might come from the age difference observed among groups, since the exposure to periodontitis risks factors and accumulation of attachment loss increase with age (Schätzle et al. 2003). Most patients from group 1 were born before 1975, the start of the current therapy of XLH in France, and therefore did not benefit from an early management. Importantly, no patient in this study was treated or had been treated with the antibody against FGF23, KRN23, a promising experimental treatment for XLH currently under clinical investigation in adults (Carpenter et al. 2014). The benefits of this new treatment on the periodontium and, more generally, on the oral health of patients affected with XLH are unknown.

How does XLH increase the prevalence and severity of periodontitis? One possibility is that XLH could affect the formation and homeostasis of cementum and alveolar bone, the 2 mineralized tissues of the periodontium. Indeed, we observed a significant reduction of acellular cementum thickness in XLH. This

cementum primary role is to anchor the root in the alveolar bone. Similar hypoplasia of acellular cementum has been observed in different clinical situations where it contributes to attachment loss: hypophosphatasia (van den Bos et al. 2005), Coffin-Lowry syndrome (Norderyd and Aronsson 2012), and localized aggressive periodontitis (Bimstein et al. 1998). Reduced thickness of acellular cementum was observed in the murine models of XLH and autosomal recessive HR (Ye et al. 2008; Fong et al. 2009). The cementum hypoplasia was absent on the root obtained from a patient with XLH that had been properly treated during childhood, suggesting that phosphate and vitamin D supplementation improves the cementum formation in XLH as in the case of dentin (Chaussain-Miller et al. 2007). In this study, OPN was used as a marker to distinguish acellular cementum from dentin. This acidic calcium-binding extracellular matrix phosphoprotein is highly expressed in acellular cementum, where it may allow a robust anchorage of the periodontal collagen fibers (McKee et al. 2013). As OPN fragments have been shown to accumulate in bones of mice with *Phex* mutation (Barros et al. 2013) and unmineralized tooth dentin of patients with XLH (Boukpessi et al. 2006), it may be important in the future to investigate the status of OPN in both cellular and acellular cementum. Defects in alveolar bone caused by XLH have not been explored in the present study and cannot be excluded. We have indeed noted a high frequency of intrabony defects in XLH patients. The expected alveolar bone phenotype in adults with untreated XLH would be osteomalacia, whose influence on periodontal attachment level is unknown.

A recent study unveiled that high levels of FGF23, the elevated hormone responsible for renal phosphate wasting in XLH, impairs neutrophil recruitment into inflamed tissues (Rossaint et al. 2016). Neutrophils are key players in the host immune response to the bacterial biofilm in periodontitis, acting as a first-line defense with their phagocytic function (Hajishengallis and Hajishengallis 2014). Leukocyte recruitment in XLH has not been explored to date. If defective, it could contribute, along with impaired acellular cementum formation, to the observed periodontal attachment loss, as in various syndromes (Khocht and Albandar 2014) or aggressive periodontitis (Ryder 2010).

In conclusion, our findings suggest that XLH in adults could increase the prevalence and severity of periodontitis and that these manifestations could result from a cementum hypoplasia. Conventional XLH management begun during childhood and continued during adulthood could prevent the periodontal defects. In patients with XLH, periodontal health evaluation should be integrated in routine clinical examination, and evaluation of the extent of the vitamin D analogs and phosphate treatment after growth should help to effectively prevent or treat periodontitis in these patients.

Author Contributions

M. Biosse Duplan, contributed to design, data acquisition, analysis, and interpretation, wrote the manuscript; B.R. Coyac, contributed to data acquisition and analysis, critically revised the manuscript; C. Bardet, contributed to design, data analysis, and interpretation, critically revised the manuscript; C. Zadikian, A. Rothenbuhler, P. Kamenicky, and K. Briot, contributed to data acquisition and analysis, critically revised the manuscript; A. Linglart, contributed to design, data acquisition, analysis, and interpretation, critically revised the manuscript; C. Chaussain, contributed to design, data acquisition, analysis, and interpretation, wrote the manuscript. All authors gave final approval and agree to be accountable for all aspects of the work.

Acknowledgments

The author(s) received no financial support and declare no potential conflicts of interest with respect to the authorship and/or publication of this article.

References

Ainamo J, Bay I. 1975. Problems and proposals for recording gingivitis and plaque. Int Dent J. 25(4):229–235.

Barros NMT, Hoac B, Neves RL, Addison WN, Assis DM, Murshed M, Carmona AK, McKee MD. 2013. Proteolytic processing of osteopontin by PHEX and accumulation of osteopontin fragments in Hyp mouse bone, the murine model of X-linked hypophosphatemia. J Bone Miner Res. 28(3):688–699.

Bergström J. 2004. Tobacco smoking and chronic destructive periodontal disease. Odontol Soc Nippon Dent Univ. 92(1):1–8.

Bergwitz C, Jüppner H. 2010. Regulation of phosphate homeostasis by PTH, vitamin D, and FGF23. Annu Rev Med. 61:91–104.

Bimstein E, Wagner M, Nauman RK, Abrams RG, Shapira L. 1998. Root surface characteristics of primary teeth from children with prepubertal periodontitis. J Periodontol. 69(3):337–347.

Boukpessi T, Septier D, Bagga S, Garabedian M, Goldberg M, Chaussain-Miller C. 2006. Dentin alteration of deciduous teeth in human hypophosphatemic rickets. Calcif Tissue Int. 79(5):294–300.

Bourgeois D, Bouchard P, Mattout C. 2007. Epidemiology of periodontal status in dentate adults in France, 2002–2003. J Periodontal Res. 42(3):219–227.

Carpenter TO, Imel EA, Ruppe MD, Weber TJ, Klausner MA, Wooddell MM, Kawakami T, Ito T, Zhang X, Humphrey J, et al. 2014. Randomized trial of the anti-FGF23 antibody KRN23 in X-linked hypophosphatemia. J Clin Invest. 124(4):1587–1597.

Chapple IL. 1993. Hypophosphatasia: dental aspects and mode of inheritance. J Clin Periodontol. 20(9):615–622.

Chaussain-Miller C, Sinding C, Septier D, Wolikow M, Goldberg M, Garabedian M. 2007. Dentin structure in familial hypophosphatemic rickets: benefits of vitamin D and phosphate treatment. Oral Dis. 13(5):482–489.

Chaussain-Miller C, Sinding C, Wolikow M, Lasfargues JJ, Godeau G, Garabédian M. 2003. Dental abnormalities in patients with familial hypophosphatemic vitamin D-resistant rickets: prevention by early treatment with 1-hydroxyvitamin D. J Pediatr. 142(3):324–331.

Che H, Roux C, Etcheto A, Rothenbuhler A, Kamenicky P, Linglart A, Briot K. 2016. Impaired quality of life in adults with X-linked hypophosphatemia and skeletal symptoms. Eur J Endocrinol. 174(3):325–333.

Connor J, Olear EA, Insogna KL, Katz L, Baker S, Kaur R, Simpson CA, Sterpka J, Dubrow R, Zhang JH, et al. 2015. Conventional therapy in adults with X-linked hypophosphatemia: effects on enthesopathy and dental disease. J Clin Endocrinol Metab. 100(10):3625–3632.

Eke PI, Dye BA, Wei L, Slade GD, Thornton-Evans GO, Borgnakke WS, Taylor GW, Page RC, Beck JD, Genco RJ. 2015. Update on prevalence of periodontitis in adults in the United States: NHANES 2009 to 2012. J Periodontol. 86(5):611–622.

Eke PI, Dye BA, Wei L, Thornton-Evans GO, Genco RJ; CDC Periodontal Disease Surveillance Workgroup. 2012. Prevalence of periodontitis in adults in the United States: 2009 and 2010. J Dent Res. 91(10):914–920.

Eke PI, Page RC, Wei L, Thornton-Evans G, Genco RJ. 2012. Update of the case definitions for population-based surveillance of periodontitis. J Periodontol. 83(12):1449–1454.

Feng JQ, Clinkenbeard EL, Yuan B, White KE, Drezner MK. 2013. Osteocyte regulation of phosphate homeostasis and bone mineralization underlies the pathophysiology of the heritable disorders of rickets and osteomalacia. Bone. 54(2):213–221.

Fong H, Chu EY, Tompkins KA, Foster BL, Sitara D, Lanske B, Somerman MJ. 2009. Aberrant cementum phenotype associated with the hypophosphatemic hyp mouse. J Periodontol. 80(8):1348–1354.

Foster BL, Nagatomo KJ, Nociti FH, Fong H, Dunn D, Tran AB, Wang W, Narisawa S, Millán JL, Somerman MJ. 2012. Central role of pyrophosphate in acellular cementum formation. PloS One. 7(6):e38393.
Foster BL, Nociti FH, Somerman MJ. 2014. The rachitic tooth. Endocr Rev. 35(1):1–34.
Foster BL, Soenjaya Y, Nociti FH Jr, Holm E, Zerfas PM, Wimer HF, Holdsworth DW, Aubin JE, Hunter GK, Goldberg HA, et al. 2013. Deficiency in acellular cementum and periodontal attachment in Bsp null mice. J Dent Res. 92(2):166–172.
Hajishengallis E, Hajishengallis G. 2014. Neutrophil homeostasis and periodontal health in children and adults. J Dent Res. 93(3):231–237.
Khocht A, Albandar JM. 2014. Aggressive forms of periodontitis secondary to systemic disorders. Periodontol 2000. 65(1):134–148.
Linglart A, Biosse-Duplan M. 2016. Hypophosphatasia. Curr Osteoporos Rep. 14(3):95–105.
Linglart A, Biosse-Duplan M, Briot K, Chaussain C, Esterle L, Guillaume-Czitrom S, Kamenicky P, Nevoux J, Prié D, Rothenbuhler A, et al. 2014. Therapeutic management of hypophosphatemic rickets from infancy to adulthood. Endocr Connect. 3(1):R13–R30.
McKee MD, Hoac B, Addison WN, Barros NM, Millán JL, Chaussain C. 2013. Extracellular matrix mineralization in periodontal tissues: noncollagenous matrix proteins, enzymes, and relationship to hypophosphatasia and X-linked hypophosphatemia. Periodontol 2000. 63(1):102–122.
Needleman I, McGrath C, Floyd P, Biddle A. 2004. Impact of oral health on the life quality of periodontal patients. J Clin Periodontol. 31(6):454–457.
Norderyd J, Aronsson J. 2012. Hypoplastic root cementum and premature loss of primary teeth in Coffin-Lowry syndrome: a case report. Int J Paediatr Dent. 22(2):154–156.
O'Leary TJ, Drake RB, Naylor JE. 1972. The plaque control record. J Periodontol. 43(1):38.
Opsahl Vital S, Gaucher C, Bardet C, Rowe PS, George A, Linglart A, Chaussain C. 2012. Tooth dentin defects reflect genetic disorders affecting bone mineralization. Bone. 50(4):989–997.
Rossaint J, Oehmichen J, Van Aken H, Reuter S, Pavenstädt HJ, Meersch M, Unruh M, Zarbock A. 2016. FGF23 signaling impairs neutrophil recruitment and host defense during CKD. J Clin Invest. 126(3):962–974.
Ryder MI. 2010. Comparison of neutrophil functions in aggressive and chronic periodontitis. Periodontol 2000. 53:124–137.
Schätzle M, Löe H, Lang NP, Heitz-Mayfield LJ, Bürgin W, Anerud A, Boysen H. 2003. Clinical course of chronic periodontitis: III. Patterns, variations and risks of attachment loss. J Clin Periodontol. 30(10):909–918.
Sullivan W, Carpenter T, Glorieux F, Travers R, Insogna K. 1992. A prospective trial of phosphate and 1,25-dihydroxyvitamin D3 therapy in symptomatic adults with X-linked hypophosphatemic rickets. J Clin Endocrinol Metab. 75(3):879–885.
Sun Y, Lu Y, Chen L, Gao T, D'Souza R, Feng JQ, Qin C. 2011. DMP1 processing is essential to dentin and jaw formation. J Dent Res. 90(5):619–624.
van den Bos T, Handoko G, Niehof A, Ryan LM, Coburn SP, Whyte MP, Beertsen W. 2005. Cementum and dentin in hypophosphatasia. J Dent Res. 84(11):1021–1025.
van der Velden U. 2005. Purpose and problems of periodontal disease classification. Periodontol 2000. 39:13–21.
Wang X, Wang S, Lu Y, Gibson MP, Liu Y, Yuan B, Feng JQ, Qin C. 2012. FAM20C plays an essential role in the formation of murine teeth. J Biol Chem. 287(43):35934–35942.
Ye L, Liu R, White N, Alon US, Cobb CM. 2011. Periodontal status of patients with hypophosphatemic rickets: a case series. J Periodontol. 82(11):1530–1535.
Ye L, Zhang S, Ke H, Bonewald LF, Feng JQ. 2008. Periodontal breakdown in the Dmp1 null mouse model of hypophosphatemic rickets. J Dent Res. 87(7):624–629.

6 Paper 2: Impaired oral bone healing and tooth movement adaptation in X-linked hypophosphatemia

Impaired oral bone healing and adaptation to tooth movement in X-linked hypophosphatemia

ONE SENTENCE SUMMARY: Periodontal attachment complex is deeply affected in XLH, impairing bone repair and cementum adaptation to tooth movement.

Benjamin R. Coyac[1,2], Guillaume Falgayrac[3], Brigitte Baroukh[1], Lotfi Slimani[1], Jérémy Sadoine[1], Guillaume Penel[3], Martin Biosse-Duplan[4,5], Thorsten Schinke[6], Agnès Linglart[5,7], Marc D. McKee[8], Catherine Chaussain[1,4,5†], Claire Bardet[1†*]

[1]: EA2496, Faculty of Dentistry, Paris Descartes University, Montrouge, France.

[2]: Department of Periodontics and Implant Dentistry, Rothschild Hospital, AP-HP, Paris, France.

[3]: Univ. Lille, Univ. Littoral Côte d'Opale, EA 4490 - PMOI – Physiopathologie des Maladies Osseuses Inflammatoires, F-59000 Lille, France.

[4]: Department of Odontology, Bretonneau Hospital PNVS, AP-HP, Paris, France.

[5]: APHP, Reference Center for rare disorders of the Calcium and Phosphate Metabolism, filière OSCAR and Plateforme d'Expertise Maladies Rares Paris-Sud, Hôpital Bicêtre Paris Sud, Le Kremlin Bicêtre, France.

[6]: Department of Osteology and Biomechanics, University Medical Center Hamburg-Eppendorf, Hamburg, Germany.

[7]: INSERM U1169, Hôpital Bicêtre, Le Kremlin Bicêtre, and Université Paris-Saclay, France.

[8]: Faculties of Dentistry and Medicine, Department of Anatomy and Cell Biology, McGill University, Montreal, Canada.

[†]: Co-last authors

[*]**Corresponding author:** Claire Bardet (claire.bardet@parisdescartes.fr), EA 2496, Faculty of Dentistry, Paris Descartes University, 1 rue Maurice Arnoux, 92120 Montrouge, France; Tel/fax: 33158076724

ABSTRACT

X-linked hypophosphatemia (XLH) is a rare skeletal disorder caused by inactivating mutations in the *PHEX* gene. PHEX deficiency leads to renal phosphate wasting and hypophosphatemia, as well as impaired mineralization of bone and dentin resulting in severe skeletal manifestations. Recent clinical studies point to a higher susceptibility of XLH patients to periodontitis. In the present study, we characterized the periodontal phenotype of XLH patients and the Hyp mouse, the murine analog of the disease. The pathobiology of periodontal tissues was investigated in the Hyp mouse using a model of periodontal breakdown and repair, and a model of tooth movement adaptation inducing cementum formation. The examination of XLH/Hyp tooth root showed hypoplasia of cellular and acellular cementum associated with a lack of periodontal ligament attachment. All periodontal mineralized tissues had an immature apatitic mineral phase. In addition, OPN accumulation was observed in unmineralized bone and tooth extracellular matrix in a tissue-specific manner, most notably in the pericellular matrix surrounding osteocyte lacunae, while it was only faintly expressed in the XLH/Hyp acellular cementum, suggesting that the key role played by OPN in bone cannot be generalized to every mineralized tissue. The study of both experimental models applied here to the Hyp mouse revealed that cellular cementum apposition as well as bone resorption and formation/repair were dramatically altered in the Hyp mice compared to the same manipulations applied to wild-type mice. Our results show a major XLH phenotype in the periodontium whose pathobiology is susceptible to periodontal disorders.

INTRODUCTION

X-linked hypophosphatemia (XLH) is a rare inborn error of metabolism characterized by renal phosphate wasting and defective mineralization of the skeleton and dentition (Carpenter 2012; McKee et al. 2013; Opsahl Vital et al. 2012). XLH occurs because of loss-of-function mutations in the *PHEX* gene (phosphate-regulating gene with homologies to endopeptidases on the X chromosome), which encodes a zinc metallo-endopeptidase (Francis et al. 1997; Rowe 1997; Tenenhouse 1999) expressed by bone (osteoblasts and osteocytes) and tooth (odontoblasts) cells (Ruchon et al. 1998). Skeletal complications of XLH include rickets and osteo/dentinomalacia, with clinical symptoms including delayed walking, leg bowing (genu varum) or knock knees (genu valgum), growth failure and dental defects, where in the latter case, patients experience "spontaneous" dental abscesses in the absence of dental caries or trauma (Boukpessi et al. 2006; Carpenter 2012; Chaussain-Miller et al. 2007). In addition to systemically low circulating phosphate levels causing hypomineralization (osteoidosis), local extracellular matrix accumulation of mineralization-inhibiting proteins (osteopontin) and peptide fragments (ASARM peptides; Acidic Serine- and Aspartate-Rich Motif) likely also contributes to the osteo- and dentino-malacia (Barros et al. 2013; Boukpessi et al. 2010; Boukpessi et al. 2016).

Periodontitis is an infectious oral disease that irreversibly destroys the attachment of the teeth in the jaw bones by adversely affecting the periodontal tissues, including tooth cementum, the periodontal ligament and the alveolar bone circumscribing the tooth socket (Meyle and Chapple 2015). Periodontal disease affects nearly 50% of adults over 30 years old and represents a major cause for tooth loss (Eke et al. 2015). Although development and progression of periodontal disease characteristically involves bacterial infection of the periodontium, the etiology is multifactorial, and different individuals are affected to variable

degrees (Bouchard et al. 2016; Seymour and Taylor 2004; Van der Velden et al. 2006). Amongst other clinical manifestations resulting from hypophosphatemia, accumulating evidence suggests a higher susceptibility of XLH patients to periodontitis (Biosse Duplan et al. 2016; McKee et al. 2013; Ye et al. 2011). Two clinical studies suggested a higher prevalence of periodontitis in XLH patients with 75% of XLH patients displaying periodontal loss of attachment compared with nearly 50% in the general population, especially when their systemic supplementation treatment with phosphate and vitamin D analogs was erratic. Strengthening this hypothesis, reduced acellular cementum thickness and a higher frequency of intrabony defects were recently reported in patients with XLH (Biosse Duplan et al. 2016). Consistent with this, cementum hypoplasia occurs in the murine model of XLH (Fong et al. 2009; Foster et al. 2014a).

Besides the renal phosphate wasting, mineralized tissue defects are associated with loss of PHEX activity that normally regulates mineralization of the extracellular matrix locally by maintaining mineralized matrix homeostasis through the cleavage of inhibitory osteopontin (OPN) and ASARM peptides of the family of acidic noncollagenous SIBLING proteins (Small Integrin-Binding Ligand, N-linked Glycoproteins) (Fisher and Fedarko 2003; Martin et al. 2008; Qin et al. 2004; Rowe 2012). Of the SIBLING proteins, OPN is the most-studied in mineralized tissues where it inhibits mineralization by binding to calcium and apatitic mineral crystals in bones and teeth, and also at sites of ectopic pathologic calcification (Boukpessi et al. 2016; Kaartinen et al. 2007; McKee et al. 2013). Not only is OPN additionally involved in bone remodeling by mediating osteoclast attachment (Ek-Rylander and Andersson 2010; Ek-Rylander et al. 1994; Koyama et al. 2006; Nagao et al. 2011), but OPN has been described as a key factor for bone healing, acting as an opsonin facilitating clearance of bone debris by phagocytosis after surgical wounding, and by

contributing to the formation of a cement line at the wound margin to integrate newly formed repair bone with the existing bone (McKee and Nanci 1995; McKee et al. 2011b; Pedraza et al. 2008). In XLH patients, OPN has been proposed as a key player in the etiology of the mineralization defects (Boukpessi et al. 2016). Mineralization-inhibiting, full-length OPN was shown to accumulate in the hypomineralized matrix of appendicular bone, especially in the hypomineralized lacuno-canalicular defects of the periosteocytic lesions often referred to as osteocyte "halos" in humans (Boukpessi et al. 2016), in mouse bone (Barros et al. 2013), and in the tooth in interglobular dentin residing between unmerged calcospherites (Boukpessi et al. 2010; Salmon et al. 2014). However, the role of OPN in periodontal tissues, specifically in acellular and cellular cementum, and more generally in the pathobiology of the periodontium in XLH patients (including periodontitis), remains understudied.

In the present study, we analyzed how PHEX deficiency affects periodontal tissues in XLH patients resulting in a higher susceptibility to periodontitis. The periodontal phenotype associated with XLH was explored in human samples and characterized in greater depth using observations from the Hyp mouse, together with two experimental manipulations (ligature induction of periodontal breakdown, and tooth movement triggering cementum formation induced by loss of occlusion); the XLH mouse model Hyp harbors a *Phex* mutation, and phenocopies the biochemical and clinical features of XLH.

RESULTS

Periodontal phenotype of XLH patients and Hyp mice

In order to understand the higher susceptibility of XLH patients to periodontitis (Biosse Duplan et al. 2016; Ye et al. 2011), the different tissues of the periodontium were critically analyzed by various approaches in XLH teeth and Hyp mice. We first determined that all the extracellular matrix-secreting cells of the mineralized tissues we were examining in the periodontium (in both control human and WT mouse tissues) expressed *PHEX*/*Phex*, including not only odontoblasts, osteoblasts and osteocytes, but also the cellular cementum-forming cells – the cementoblasts and cementocytes (Appendix 1).

Observations of tooth roots revealed that XLH teeth had a thinner and poorly mineralized acellular cementum (panel A in Fig. 1), consistent with what has been reported previously (Biosse Duplan et al. 2016). In Hyp mice, the acellular cementum also was thinner (panel B in Fig. 1, a,b). Sirius red staining of molar periodontium observed by polarized light microscopy revealed poor ligament anchorage in Hyp mice affecting both the alveolar bone and dental attachment (cementum) sites (Fig. 1c-e). Quantitatively, 59% percent of the root surface was anchored by periodontal ligament in Hyp mice, compared to 94% in WT mice. Showing a similar decrease, 41% of the Hyp alveolar bone surface was involved in the insertion of periodontal ligament versus 74% in WT. These regions of poorly attached collagen fibers showed broadly dispersed ligament cells compared with well-aligned WT cells organized along the ligament fibers (insets in Fig. 1c,d). TEM analysis confirmed at the ultrastructural level the lack of attachment of Hyp ligament collagen fibrils which compared to the well-aligned insertions into acellular cementum of WT mice showed irregularly arranged (and sometimes parallel to the root surface) fibrils facing uneven, distorted

protrusions of abnormal acellular cementum having unmineralized matrix regions (possibly a portion of Sharpey's fiber terminations) in an irregular cementum layer (Fig. 1f,g).

We then analyzed the cellular cementum, the thicker form of cell-containing layered cementum which is located at the apical third of the root and which mainly forms gradually after tooth eruption. This tissue was thinner in XLH patients with small pockets of unmineralized matrix (panel A in Fig. 2, a-d). Similar observations were obtained in the cellular cementum of Hyp mice (panel B in Fig. 2, e-h).

The appendicular bone is known to be osteomalacic in both patients with XLH (Rowe 1997) and Hyp mice, and the murine alveolar bone was found to be hypomineralized with accumulation of osteoid (Fong et al. 2009; Koehne et al. 2013). Here, CBCT showed abnormal alveolar bone microarchitecture in XLH patients (Appendix 2) and in Hyp mice, with decreased bone volume over total volume, and lower trabecular number (panel A in Fig. 3). Osteomalacia of Hyp alveolar bone was shown by the von Kossa staining reaction for mineral, and conventional toluidine blue staining revealed a thick layer of osteoid matrix (panel B in Fig. 3, a,b), and TEM showed enlarged unmineralized perilacunar matrix surrounding osteocytes in the Hyp samples as recently described in XLH patient appendicular bone (Fig. 3c,d), (Boukpessi et al. 2016).

In order to characterize the mineral phase of XLH/Hyp periodontal tissues, physico-chemical parameters were analyzed by Raman spectroscopy revealing a significantly decreased mineral/organic ratio, increased Type-B carbonate substitution and decreased crystallinity in XLH patient acellular and cellular cementum (panel A in Fig. 4), and Hyp alveolar bone (panel B in Fig. 4), when compared to controls. Analysis by Raman spectroscopy showed that the collagenous matrix of XLH/Hyp tissues did not show any modification of composition (data not shown). These results indicate that all XLH mineralized

periodontal tissues have an immature apatitic mineral phase associated with an intact collagenous phase.

Unlike bone, OPN does not accumulate in XLH/Hyp cementum

OPN has recently been shown to accumulate in the extracellular matrix of XLH/Hyp bone, where it is thought to inhibit mineralization locally (Barros et al. 2013; Boukpessi et al. 2016). In order to determine whether OPN might also be involved in the impairment of mineralization in the periodontal tissues of XLH/Hyp patients and mice, OPN immunohistochemistry was performed on sections of the periodontium. In this case, strong positive OPN immunostaining serves as a marker to distinguish cementum from dentin (D'Errico et al. 1997), and weaker staining was observed in XLH patient cementum when compared to human control cementum both at the level of the acellular and cellular cementum (panel A in Fig. 5, a-d). In control human cellular cementum, OPN immunostaining localized primarily to sequential boundaries of appositional growth layers (Fig. 5c). In contrast, XLH cellular cementum showed only weak OPN staining (Fig. 5d), whereas in both cases the staining was generally confined to Tome's granular layer of dentin at the dentino-cemental junction. Similar results were found in murine cementum (panel B in Fig. 5, e-h). Immunohistochemistry for OPN confirmed an abnormal distribution of this protein in the lacuno-canalicular system of Hyp alveolar bone compared to WT alveolar bone. In Hyp bone, OPN accumulated in the enlarged periosteocytic lesions of Hyp samples (Fig. 5j). These results indicate that OPN was not similarly affected in each mineralized tissue of XLH periodontium, and that OPN accumulation was not necessary for cementum impairment in XLH.

Hyp cementum formation is altered in a model of tooth movement adaptation

Experimentally-induced apposition of cellular cementum in mandibular molars was studied by the extraction of maxillary molars as an approach to release mandibular molars from occlusal forces (panel A in Fig. 6) (Salmon et al. 2016). Histological sections made of the periodontium after dual calcein fluorochrome injections into the mice revealed that cellular cementum formation was altered in the Hyp mice. In this case, one thick blurry line formed by the incorporation of fluorochrome markers in the Hyp mice, whereas two distinct sequential fluorescent labels were observed in WT mice resulting from ongoing cellular cementum apposition and mineralization (panel B in Fig. 6, Appendix 3a'). The formation rate of cellular cementum was significantly reduced in Hyp mice (1.83 *vs* 3.82 µm/24 h, $p<0.05$ for all) (panel B in Fig. 6). Higher magnification of undecalcified sections stained with Toluidine blue showed a wide and uneven margin of "cementoid" in Hyp cellular cementum (panel C in Fig. 6, a,d, Appendix 3b). ALP staining at the sites of formation revealed a thick osteo/cementogenic layer at the margin of WT cellular cementum (Fig. 5b), whereas the staining was lighter and spread into the cementoid of Hyp cellular cementum (Fig. 5e). During cellular cementum-induced apposition, OPN signal was absent in Hyp cementum although it was moderately localized in the appositional growth lines of WT cellular cementum (Fig. 6c,f). These results indicate that despite the presence of ALP (a mineralization promoter) and the absence of OPN (a mineralization inhibitor), the formation of cellular cementum induced by tooth overeruption was altered in the Hyp mouse.

***Hyp* alveolar bone remodeling is impaired in a model of periodontal breakdown and repair**

Experimentally-induced alveolar bone resorption and apposition were performed to understand the higher susceptibility to periodontal breakdown in XLH (Abe and

Hajishengallis 2013). In this model, a ligature is placed on the second maxillary molars for 4 days to induce bone resorption. Then, the ligature is removed to allow the healing process (Appendix 4A). Longitudinal radiographic follow-up of the level of alveolar bone in the furcation zone revealed a milder resorption in Hyp mice when compared to WT mice at day 4 (-21 µm *vs* -91 µm, $p<0.05$ for all) (panel A in Fig. 7, Appendix 4B). Following ligature removal, the transition into the apposition phase was delayed in Hyp mice as shown by micro-CT measurements at day 15 (-170 µm *vs* -7 µm, $p<0.05$) (panel A in Fig. 7, Appendix 4B). In addition, an intense TRAP staining was observed in the Hyp alveolar bone at this time point (Fig. 7f) indicating persistent alveolar bone resorption, whereas faint activity was detected in WT bone. A single demeclocyclin-labeled line had formed during the apposition of Hyp repairing periodontal bone, whereas two distinct lines were observed in WT bone (Fig. 7i,j). Further histological analysis of undecalcified samples showed impaired mineralization of newly formed bone matrix in this region (Fig. 7h). When periodontal bone formed after ligature removal, OPN was localized at bone surfaces in WT mice at day 15, whereas it accumulated in unmineralized newly formed matrix regions in Hyp bone (Fig. 7m,n). This unmineralized enlarged osteoid bone matrix was ALP positive, whereas only the osteogenic layer was stained in WT samples (Fig. 7k,l). These results indicate that periodontal bone repair is altered in the Hyp mouse. Despite extracellular matrix deposition, the newly formed alveolar bone remained unmineralized, showing strong ALP activity and OPN expression.

DISCUSSION

Recent clinical studies have shown that adult patients with XLH have a higher susceptibility to periodontitis (Biosse Duplan et al. 2016; Ye et al. 2011). Here, we demonstrate that loss of PHEX activity dramatically alters the periodontal phenotype in humans and in the Hyp mouse, the murine model of XLH. In addition, we show that periodontal tissue formation and healing are both disturbed in XLH/Hyp.

Alveolar bone in Hyp mouse jaws is decreased, hypomineralized and abnormally structured, as has been previously reported for Hyp appendicular bone (Liu et al. 2016; Macica et al. 2016). This similarity between distinct anatomical sites suggests that despite the different embryological origins of these bones and their different functions and loading conditions, hypophosphatemia nevertheless manifests itself similarly – as osteomalacia and structural change – at both sites. Noteworthy in this regard, although the microarchitecture of XLH/Hyp alveolar bone suggested osteopenic/osteoporotic bone (Brandi 2009; Farr and Khosla 2015), our radiographic findings (radiolucency) clearly correspond to the osteomalacia, rather than to other bone parameters. This is also consistent with the observed immature apatitic mineral phase revealed by Raman spectroscopy in the XLH/Hyp mineralized periodontal tissues (*i.e*. acellular and cellular cementum, and alveolar bone), characterized by decreased mineralization and crystallinity levels and increased carbonate-B substitution. In physiological conditions, the carbonate content increases with maturation in bioapatite. The higher carbonate content in XLH may compensate the low phosphate content in XLH patients. Thus, a compensative mechanism should appear during crystal lattice formation in phosphate site (Type-B carbonation). Our data are in agreement with the decreased Raman mineral phase signal recently reported for Hyp cortical appendicular bone, which was further decreased by pregnancy and lactation (Macica et al. 2016). Of note, while

we show here that OPN accumulates in the alveolar bone matrix as previously shown for XLH/Hyp appendicular and jaw bone (Barros et al. 2013; Boukpessi et al. 2016; Marie and Glorieux 1983), its expression was very low in acellular and cellular cementum. These data suggest that OPN accumulation is not part of the etiology for the impaired mineralization of XLH cementum, but rather a bone- and dentin-specific marker of XLH, likely for bone reflecting the involvement in mineral metabolism.

Alveolar bone and acellular cementum (and to some extent cellular cementum) – which are the extremity components of the periodontal attachment apparatus ensuring appropriate tooth anchoring within the jaws – are linked together by the unmineralized periodontal ligament whose collagen fibers are inserted at both ends into mineralized tissues to accommodate the forces of functional occlusal loading during mastication (Naveh et al. 2013; Naveh et al. 2012a; Naveh et al. 2012b). Here, we have identified a defective ligament attachment in the Hyp tooth root showing abnormal fiber anchorage. While we show that *PHEX* mutations result in hypoplasia of XLH/Hyp tooth cementum and osteomalacia of periodontal alveolar bone with a poor ligament anchorage, this pathologic phenotype is not as severe as the one described for odontohypophosphatasia (Foster et al. 2012; Foster et al. 2015). Indeed, it has been reported that loss-of-function mutations in the tissue-nonspecific alkaline phosphatase gene *(ALPL, TNSALP)* gene led to an absence of acellular cementum formation (McKee et al. 2013; van den Bos et al. 2005). Unlike what has been reported for hypophosphatasia (Linglart and Biosse-Duplan 2016), no spontaneous tooth loss has been reported for patients with XLH, in either our own extensive clinical observations nor the literature (Carpenter 2012; McKee et al. 2013; Opsahl Vital et al. 2012), indicating that the tooth anchorage in XLH/Hyp, although altered, remains sufficient to maintain the tooth in its alveolar socket.

We have demonstrated an impaired healing capacity of Hyp periodontal bone in a model of periodontal breakdown and repair. To initially induce bone resorption, we selected a tooth ligature model rather than a model adding exogenous bacteria (Abe and Hajishengallis 2013) as it has been shown that the addition of *Porphyromonas gingivalis*, a bacteria extensively studied in the context of periodontitis (Haffajee and Socransky 1994; Hajishengallis et al. 2015), had little effect on murine alveolar bone resorption (de Molon et al. 2014; Kimura et al. 2000; Saadi-Thiers et al. 2013). Ligature placement and removal, which we adopted as our model, allowed the sequential study of alveolar bone repair following initial periodontal breakdown. The delayed resorption of bone, and the reduced activity of osteoclasts, observed in the Hyp periodontal bone may be explained by a lower activity (and/or accessibility) of osteoclasts to the poorly mineralized bone matrix, where unmineralized bone surfaces (osteoidosis) render a surface inappropriate for osteoclast attachment and induction of the required osteoclastic cellular resorption machinery. In this context, hypophosphatemia has been already proposed to reduce osteoclast differentiation and function (Hayashibara et al. 2007).

In the repair stage of our modified ligature-induced periodontitis model, Hyp mouse bone healing was dramatically delayed while the WT alveolar bone repaired *restitution ad integrum*. In the Hyp bone matrix, the delayed healing was associated with persistent ALP activity and OPN accumulation, which may play a role in osteoclast activation (Rodriguez et al. 2014). Thus, OPN accumulation during the repair phase might be involved in the persistence of resorption observed at day 15 in repairing Hyp bone. These data showing disturbance of alveolar bone resorption and repair processes in Hyp mice could explain, at least in part, the higher susceptibility of XLH patients to periodontitis and intrabony defects,

and the poor response to periodontal treatment encountered in patients with erratic phosphate and vitamin D analog treatment (Biosse Duplan et al. 2016).

Our observations have revealed a profound disruption of adaptation to tooth movement in the Hyp mouse. Cellular cementum, although poorly explored especially under pathologic conditions, is known to serve as an adaptive tissue capable of moving teeth in the jaws (sometimes referred to as passive eruption) that compensates for decreasing alveolar bone mass and alveolar crest height with aging, following orthodontic movements of teeth, and as a callus for root microfractures after a dental trauma (Cvek et al. 2004; Huang et al. 2016; Nanci 2012). Of note, we revealed cementum-secreting cells expressed PHEX in normal teeth, suggesting that the cellular cementum is also likely affected in the pathobiology of XLH. Similar to what has been described for XLH dentin (Boukpessi et al. 2010; Salmon et al. 2014), this tissue also displayed hypoplasia and “cementomalacia”, with the presence of unmineralized regions of cementum. When cementum formation was induced by our experimental procedure (removal of occlusal forces) resulting in the egression of the mandibular teeth, we observed only a weak mineralization response at the apical region of Hyp roots with strong ALP activity as compared to control teeth, and undetectable OPN by immunohistochemistry. Thus, the undetectable OPN level in the Hyp cementum versus the high amount of OPN observed in the healing Hyp bone highlight the tissue specificity of OPN expression, suggesting that OPN’s influence might be a bone-specific factor contributing to the decreased healing response of Hyp mineralized tissues.

Overall, our data support the observation that adult patients with XLH present with a higher susceptibility of developing periodontitis, while also suggesting that XLH patients will likely not be able to mount an appropriate adaptive and healing response to orthodontic treatments and trauma. This prospect is particularly important for clinicians to consider,

since XLH patients have a frequent need for orthodontic procedures during adolescence where occlusal disorders result from early loss of hypomineralized, infected primary teeth (Chaussain-Miller et al. 2003; Schwartz et al. 1988). Taken together, our results indicate that the periodontium of patients with XLH is less prone to adapt to trauma or orthodontic treatments, which both involve bone remodeling and cementum apposition. Further clinical work is needed in this area to extend the findings that we have presented here.

Currently, systemic phosphate and vitamin D supplementation seems to reduce periodontal disease risk in XLH patients (Biosse Duplan et al. 2016), as it does for other dental and skeletal complications (Chaussain-Miller et al. 2007; Chaussain-Miller et al. 2003; Linglart et al. 2014). Although such pharmacological treatment may also allow certain orthodontic therapies in XLH patients (Kawakami and Takano-Yamamoto 1997), further studies are needed to investigate in greater depth the effect of this supplementation and the effect of the recently introduced monoclonal antibody (KRN23) treatment (against FGF23) on the XLH periodontium, and whether these effects are sustained over a lifetime.

MATERIALS AND METHODS

Human teeth

Human permanent teeth from XLH patients and from gender- and age-matched control individuals extracted prior to orthodontic treatments were collected in the dental departments of Paris Nord Val de Seine Hospitals, AP-HP, France. Informed consent was obtained from patients in agreement with French law (agreement n°DC-2009-927, Cellule Bioéthique DGRI/A5). Teeth were fixed for 7 days at 4°C in 4% paraformaldehyde solution at pH 7.2–7.4, followed by microwave-assisted decalcification in 4.13% EDTA for ~3 months. Decalcified teeth were embedded in Paraplast, sectioned (at 7 µm) in the coronoapical axis and stained with toluidine blue (pH 7.2).

Animals

Hyp mice were obtained from the Jackson Laboratory. Heterozygous female and wild-type (WT) male breedings were carried out and tail snips were collected for genotyping. DNA was extracted from the snips using DNeasy Blood and Tissue Kit (Qiagen, France) and the genotype was determined by PCR using primers for *Phex* gene (Sheen et al. 2012). Offspring males with the *Phex* gene-null mutant phenotype ($Hyp^{-/0}$) were maintained under the same conditions as those for the WT mice. 3-month old littermate WT and $Hyp^{-/0}$ mice were examined in this study. Chemical methods were used for sacrificing mice according to the ethical protocol approved by the Animal Care Committee of French Veterinary Services (DPP Haut de Seine, France: agreement number C-9204901). Hyp males and wild-type (WT) littermates were sacrificed by cervical dislocation or included in the experimental models at 90 days postnatal. If included in an experimental model, mice were intraperitoneally anesthetized with a mixture of ketamine (80mg/kg) and xylazine (10 mg/kg). All

experimental procedures involving animals were approved by the Institutional Animal Care and Use Committee at Paris Descartes University (APAFiS #5214). All mice were housed in standard conditions of temperature (23 ± 2°C) in a light-controlled environment, and provided water and standard pelleted food *ad libitum*.

Experimental periodontal healing model

periodontal breakdown was achieved as previously described (Abe and Hajishengallis 2013). Briefly, 5-0 synthetic absorbable undyed braided suture (Ethicon, Inc. 2008) was tied as a ligature around second maxillary molars using a triple-knot for up to four days to induce alveolar bone resorption (Kantarci et al. 2015). At day 4, ligatures were removed to allow bone healing (Appendix 4, panel A). Mice were injected intraperitoneally with demeclocycline (Sigma-Aldrich, 30 mg/kg) at day 7 and day 13 post-surgery, and sacrificed at day 15.

Experimental model of tooth movement adaptation

Experimentally-induced appositional growth of cellular cementum was performed as previously described (Salmon et al. 2016). Briefly, appositional growth of cellular cementum induced on the tooth apex of mandibular molars was stimulated by the extraction of opposing maxillary molars (Fig. 6, panel A). Calcein (Sigma-Aldrich, St Louis, MO, 30 mg/kg) was injected intraperitoneally at day 3 and at day 9 (24 hours before sacrifice).

Micro-computed tomography dataset acquisition

Live animals were anesthetized (isoflurane, induction at 3–4% under airflow of 0.8–1.5 L/min; 1.5–2% under 400–800 ml/min thereafter) and scanned using a high-resolution X-ray micro-CT device (Quantum FX Caliper, Life Sciences, Perkin Elmer, Waltham, MA, United States). Three-dimensional acquisitions were performed with a field of view of 10 mm

diameter, using an isotropic voxel size of 20x20x20 μm^3 (90 kV, 160 microA, 180 s). The trabecular bone morphometric indices were calculated according to guidelines published by the American Society for Bone and Mineral Research (Bouxsein et al. 2010). Morphometric measurements were performed using Skyscan software (v1.13.5.1, Kontich, Belgium). Two-dimensional alveolar bone resorption/formation was measured longitudinally on the same experimental live WT and Hyp mice at days 0, 4, 7, 11, 13, 15, as the distance between the top of the bone septum and the bottom of the pulp-chamber floor at the furcation area between the 2 buccal roots of the maxillary second molar (panel B in Appendix 4). Five slices were measured per animal to cover the entire width of the two buccal roots.

Cone-Beam computed tomography (CBCT)

CBCT scans from 3 XLH patients and 3 control individuals imaged before wisdom teeth removal were collected (Planmeca ProMax® 3D Max, Helsinki, Finland). Image analysis comprised four steps: alignment, cropping, thresholding and bone analysis. The inter-radicular areas of the 2 first mandibular molars were cropped in each 2D section of the stack with the dedicated shape tool of the Skyscan software (v1.13.5.1, Kontich, Belgium). These regions-of-interest included the trabecular bone above the inferior alveolar nerve canal in the basal bone. The trabecular bone morphometric indices were extrapolated to investigate the micro-architecture of alveolar bone (Panmekiate et al. 2015). Calculation of the 3D structural parameters followed the guidelines published by the American Society for Bone and Mineral Research (Bouxsein et al. 2010). Morphometric measurements were performed using the Skyscan software (v1.13.5.1, Kontich, Belgium).

Murine tissue specimen preparation

After dissection, maxillas and mandibles were fixed in 70% ethanol at 4°C and dehydrated in a graded ethanol series. Undecalcified samples were embedded in methyl methacrylate (Merck, Rahway, NJ). Dental crowns were abraded using grinding paper discs (P400, 3M) and specimens were embedded a second time prior to sectioning in a sagittal orientation. Serial sections, 4 µm thick, were cut on a microtome (Polycut E microtome, Leica, Wetzlar, Germany) sagittal to the second maxillary molar buccal roots and to the second mandibular molar roots. A series of consecutive sections were stained respectively with toluidine blue (pH 3.8), von Kossa reagent (5% silver nitrate solution, Sigma-Aldrich, St Louis, MO), Masson's trichrome stain and Sirius red staining.

Light microscopy

Tissues were analyzed in a LEITZ DM-RBE microscope (Leica, Germany) set for transmitted light illumination, or polarized light, and equipped with a Sony DXC-950 CCD camera. Fluorochrome-based indices of murine bone and cellular cementum formation were measured in sections photographed under ultraviolet light. Double labeling allowed the measurement of the amount of bone or cellular cementum formed between the two dye injections. The mean distance between the two labels was determined using previously described parameters (Vignery and Baron 1980). The daily mineral apposition rate (MAR) was calculated using these parameters and ImageJ software (NIH, Bethesda, MD).

Enzyme histochemistry

Tartrate-resistant acid phosphatase (TRAP) was detected by using 2.5 mM naphthol-ASTR-phosphate (Sigma-Aldrich, St Louis, MO), 0.36 M N–N-dimethyl-formamide (Sigma-Aldrich, St Louis, MO), and 4 mM salt in pH 5.2 acetate buffer. Nonosteoclastic acid

phosphatase activity was inhibited with 100 mM L(+)-tartaric acid (Sigma-Aldrich, St Louis, MO) added to the substrate solution. Alkaline phosphatase (ALP) was used to reveal the layer of osteogenic cells (pre-osteo/cementoblasts and osteo/cementoblasts) by incubating the sections with naphthol ASTR phosphate (Sigma-Aldrich, St Louis, MO) and diazonium fast blue RR salt (Sigma-Aldrich, St Louis, MO) for 30 min at 37°C (pH 9) in the presence of $MgCl_2$.

Immunohistochemistry

Paraffin sections were dewaxed in xylene and sections embedded in methyl methacrylate were deplasticized. After rehydration in a graded ethanol series to pure distilled water, sections were blocked using 5% normal horse serum/PBS-T. Sections were incubated for 12 hours at 4°C with goat anti-human OPN antibody (R&D Systems, Minneapolis, MN, USA) diluted 1:20 in 2.5% normal horse serum/PBS-T or in rabbit anti-PHEX peptide (NH_2-CMINQYSNYYWKKAGL-$CONH_2$) kindly provided by Peter S. Rowe (Martin et al. 2008) diluted 1:50 in 2.5% normal horse serum/PBS-T. Sections were washed and then incubated with peroxidase-conjugated anti-IgG diluted 1:1000 in the same buffer. Peroxidase activity was detected using a diaminobenzadine substrate kit from Abcam (Cambridge, MA, USA) following the manufacturer's instructions. Control incubations to assess nonspecific staining consisted of the same procedure except that the primary antibody was substituted by nonimmune serum (these control incubations resulted in nonspecific staining, data not shown).

Transmission electron microscopy

For ultrastructural characterization by transmission electron microscopy (TEM), murine maxillae were fixed with 1% glutaraldehyde (Electron Microscopy Sciences, Hatfield, PA, USA) and 2% paraformaldehyde in PBS for 1 hour at room temperature and then

overnight at 4°C, and then dehydrated through a graded ethanol series. Samples were embedded in epoxy resin (Electron Microscopy Sciences). 90-nm-thick sections obtained with a Reichert Ultracut S (Leica, Germany) were placed on formvar-coated nickel grids (Electron Microscopy Sciences) and conventionally stained with uranyl acetate and lead citrate (Electron Microscopy Sciences) at room temperature. Observations and images were collected using a JEOL 1011 transmission electron microscope operating at 80 kV and equipped with a GATAN Erlangshen camera 1000.

Raman microspectroscopy

Human teeth from 4 XLH patients and 3 control individuals, and the whole maxillae including periodontium from 5 *Hyp* and 5 WT mice, were harvested and fixed in 70% ethanol solution for 48 hours. Human samples were air-dried at room temperature and murine samples were embedded in methyl methacrylate (Merck, Rahway, NJ). All samples were cut in the sagittal plane and progressively polished with silicium carbides and diamond suspension (Escil®, Chavassieu, France). Raman analyses were carried out on a Labram HR800 microspectrometer (Horiba Gr, Jobin Yvon, Lille, France). The spectrometer was equipped with a diode laser (λ= 785 nm), an air-cooled CDD (1024×256 pixels) and a ×100 objective (NA= 0.90, Olympus, France). The illumination spot size was ~1 µm. Spectral acquisitions were done in the 300-1700 cm^{-1} range. The total acquisition time for each spectrum was 1 min with an integration time of 30 s and 2 accumulations. Each spectrum was treated with smoothing filtering (filter width: 3; and polynomial order: 2) with Labspec software (Horiba GR, Jobin Yvon, Lille, France). A total of 30 spectra were obtained per tissue in each sample. Physico-chemical variables were recorded as described previously (Colard et al. 2016). Briefly, mineralization was evaluated as the mineral-to-organic ratio (υ_1

(PO_4)/δ(CH_2)-wag), carbonation was evaluated as Type-B carbonate substitution (υ_1 (CO_3)/υ_1 (PO_4) bands), and crystallinity was the inverse of the full width at half maximum intensity (FWHM) of the ν_1PO_4 band (1/FWHM de υ_1 (PO_4)). All data analyses were performed using Matlab R2010a (Mathworks, Inc., Natick, MA, USA).

Statistical analysis

Results are given as the mean ±SD. Comparison between groups was performed using Student's *t*-test or nonparametric tests when the number of data/samples was lower than 30 to fit the normal law (Kruskal-Wallis test followed, if significant, by group comparisons with the Mann-Whitney U test) using R 3.3.2 software. Differences between groups were considered significant when $p<0.05$. For Raman spectroscopy, the *x* value of relative gain/loss for each variable of each human or animal sample was treated as a single statistical unit.

REFERENCES

1. S. Opsahl Vital, C. Gaucher, C. Bardet, P. S. Rowe, A. George, A. Linglart, C. Chaussain, Tooth dentin defects reflect genetic disorders affecting bone mineralization. *Bone* **50**, 989-997 (2012).
2. M. D. McKee, B. Hoac, W. N. Addison, N. M. Barros, J. L. Millan, C. Chaussain, Extracellular matrix mineralization in periodontal tissues: Noncollagenous matrix proteins, enzymes, and relationship to hypophosphatasia and X-linked hypophosphatemia. *Periodontology 2000* **63**, 102-122 (2013).
3. T. O. Carpenter, The expanding family of hypophosphatemic syndromes. *Journal of bone and mineral metabolism* **30**, 1-9 (2012).
4. P. S. Rowe, The PEX gene: its role in X-linked rickets, osteomalacia, and bone mineral metabolism. *Experimental nephrology* **5**, 355-363 (1997).
5. F. Francis, T. M. Strom, S. Hennig, A. Boddrich, B. Lorenz, O. Brandau, K. L. Mohnike, M. Cagnoli, C. Steffens, S. Klages, K. Borzym, T. Pohl, C. Oudet, M. J. Econs, P. S. Rowe, R. Reinhardt, T. Meitinger, H. Lehrach, Genomic organization of the human PEX gene mutated in X-linked dominant hypophosphatemic rickets. *Genome research* **7**, 573-585 (1997).
6. H. S. Tenenhouse, X-linked hypophosphataemia: a homologous disorder in humans and mice. *Nephrology, dialysis, transplantation : official publication of the European Dialysis and Transplant Association - European Renal Association* **14**, 333-341 (1999).
7. A. F. Ruchon, M. Marcinkiewicz, G. Siegfried, H. S. Tenenhouse, L. DesGroseillers, P. Crine, G. Boileau, Pex mRNA is localized in developing mouse osteoblasts and odontoblasts. *The journal of histochemistry and cytochemistry : official journal of the Histochemistry Society* **46**, 459-468 (1998).
8. T. Boukpessi, D. Septier, S. Bagga, M. Garabedian, M. Goldberg, C. Chaussain-Miller, Dentin alteration of deciduous teeth in human hypophosphatemic rickets. *Calcified tissue international* **79**, 294-300 (2006).
9. C. Chaussain-Miller, C. Sinding, D. Septier, M. Wolikow, M. Goldberg, M. Garabedian, Dentin structure in familial hypophosphatemic rickets: benefits of vitamin D and phosphate treatment. *Oral diseases* **13**, 482-489 (2007).
10. N. M. Barros, B. Hoac, R. L. Neves, W. N. Addison, D. M. Assis, M. Murshed, A. K. Carmona, M. D. McKee, Proteolytic processing of osteopontin by PHEX and accumulation of osteopontin fragments in Hyp mouse bone, the murine model of X-linked hypophosphatemia. *Journal of bone and mineral research : the official journal of the American Society for Bone and Mineral Research* **28**, 688-699 (2013).
11. T. Boukpessi, C. Gaucher, T. Leger, B. Salmon, J. Le Faouder, C. Willig, P. S. Rowe, M. Garabedian, O. Meilhac, C. Chaussain, Abnormal presence of the matrix extracellular phosphoglycoprotein-derived acidic serine- and aspartate-rich motif peptide in human hypophosphatemic dentin. *The American journal of pathology* **177**, 803-812 (2010).
12. T. Boukpessi, B. Hoac, B. R. Coyac, T. Leger, C. Garcia, P. Wicart, M. P. Whyte, F. H. Glorieux, A. Linglart, C. Chaussain, M. D. McKee, Osteopontin and the dento-osseous pathobiology of X-linked hypophosphatemia. *Bone*, (2016).
13. J. Meyle, I. Chapple, Molecular aspects of the pathogenesis of periodontitis. *Periodontology 2000* **69**, 7-17 (2015).

14. P. I. Eke, B. A. Dye, L. Wei, G. D. Slade, G. O. Thornton-Evans, W. S. Borgnakke, G. W. Taylor, R. C. Page, J. D. Beck, R. J. Genco, Update on Prevalence of Periodontitis in Adults in the United States: NHANES 2009 to 2012. *Journal of periodontology* **86**, 611-622 (2015).
15. U. Van der Velden, F. Abbas, S. Armand, B. G. Loos, M. F. Timmerman, G. A. Van der Weijden, A. J. Van Winkelhoff, E. G. Winkel, Java project on periodontal diseases. The natural development of periodontitis: risk factors, risk predictors and risk determinants. *Journal of clinical periodontology* **33**, 540-548 (2006).
16. G. J. Seymour, J. J. Taylor, Shouts and whispers: An introduction to immunoregulation in periodontal disease. *Periodontology 2000* **35**, 9-13 (2004).
17. P. Bouchard, M. C. Carra, A. Boillot, F. Mora, H. Range, Risk Factors in Periodontology: a Conceptual Framework. *Journal of clinical periodontology*, (2016).
18. L. Ye, R. Liu, N. White, U. S. Alon, C. M. Cobb, Periodontal status of patients with hypophosphatemic rickets: a case series. *Journal of periodontology* **82**, 1530-1535 (2011).
19. M. Biosse Duplan, B. R. Coyac, C. Bardet, C. Zadikian, A. Rothenbuhler, P. Kamenicky, K. Briot, A. Linglart, C. Chaussain, Phosphate and Vitamin D Prevent Periodontitis in X-Linked Hypophosphatemia. *Journal of dental research*, (2016).
20. B. L. Foster, F. H. Nociti, Jr., M. J. Somerman, The rachitic tooth. *Endocrine reviews* **35**, 1-34 (2014).
21. H. Fong, E. Y. Chu, K. A. Tompkins, B. L. Foster, D. Sitara, B. Lanske, M. J. Somerman, Aberrant cementum phenotype associated with the hypophosphatemic hyp mouse. *Journal of periodontology* **80**, 1348-1354 (2009).
22. P. S. Rowe, The chicken or the egg: PHEX, FGF23 and SIBLINGs unscrambled. *Cell biochemistry and function* **30**, 355-375 (2012).
23. C. Qin, O. Baba, W. T. Butler, Post-translational modifications of sibling proteins and their roles in osteogenesis and dentinogenesis. *Critical reviews in oral biology and medicine : an official publication of the American Association of Oral Biologists* **15**, 126-136 (2004).
24. A. Martin, V. David, J. S. Laurence, P. M. Schwarz, E. M. Lafer, A. M. Hedge, P. S. Rowe, Degradation of MEPE, DMP1, and release of SIBLING ASARM-peptides (minhibins): ASARM-peptide(s) are directly responsible for defective mineralization in HYP. *Endocrinology* **149**, 1757-1772 (2008).
25. L. W. Fisher, N. S. Fedarko, Six genes expressed in bones and teeth encode the current members of the SIBLING family of proteins. *Connective tissue research* **44 Suppl 1**, 33-40 (2003).
26. M. T. Kaartinen, M. Murshed, G. Karsenty, M. D. McKee, Osteopontin upregulation and polymerization by transglutaminase 2 in calcified arteries of Matrix Gla protein-deficient mice. *The journal of histochemistry and cytochemistry : official journal of the Histochemistry Society* **55**, 375-386 (2007).
27. M. Nagao, T. N. Feinstein, Y. Ezura, T. Hayata, T. Notomi, Y. Saita, R. Hanyu, H. Hemmi, Y. Izu, S. Takeda, K. Wang, S. Rittling, T. Nakamoto, K. Kaneko, H. Kurosawa, G. Karsenty, D. T. Denhardt, J. P. Vilardaga, M. Noda, Sympathetic control of bone mass regulated by osteopontin. *Proceedings of the National Academy of Sciences of the United States of America* **108**, 17767-17772 (2011).
28. Y. Koyama, S. R. Rittling, K. Tsuji, K. Hino, R. Salincarnboriboon, T. Yano, Y. Taketani, A. Nifuji, D. T. Denhardt, M. Noda, Osteopontin deficiency suppresses high phosphate

load-induced bone loss via specific modulation of osteoclasts. *Endocrinology* **147**, 3040-3049 (2006).
29. B. Ek-Rylander, G. Andersson, Osteoclast migration on phosphorylated osteopontin is regulated by endogenous tartrate-resistant acid phosphatase. *Experimental cell research* **316**, 443-451 (2010).
30. B. Ek-Rylander, M. Flores, M. Wendel, D. Heinegard, G. Andersson, Dephosphorylation of osteopontin and bone sialoprotein by osteoclastic tartrate-resistant acid phosphatase. Modulation of osteoclast adhesion in vitro. *The Journal of biological chemistry* **269**, 14853-14856 (1994).
31. M. D. McKee, C. E. Pedraza, M. T. Kaartinen, Osteopontin and wound healing in bone. *Cells, tissues, organs* **194**, 313-319 (2011).
32. M. D. McKee, A. Nanci, Postembedding colloidal-gold immunocytochemistry of noncollagenous extracellular matrix proteins in mineralized tissues. *Microscopy research and technique* **31**, 44-62 (1995).
33. C. E. Pedraza, L. G. Nikolcheva, M. T. Kaartinen, J. E. Barralet, M. D. McKee, Osteopontin functions as an opsonin and facilitates phagocytosis by macrophages of hydroxyapatite-coated microspheres: implications for bone wound healing. *Bone* **43**, 708-716 (2008).
34. B. Salmon, C. Bardet, B. R. Coyac, B. Baroukh, J. Naji, P. S. Rowe, S. Opsahl Vital, A. Linglart, M. D. McKee, C. Chaussain, Abnormal osteopontin and matrix extracellular phosphoglycoprotein localization, and odontoblast differentiation, in X-linked hypophosphatemic teeth. *Connective tissue research* **55 Suppl 1**, 79-82 (2014).
35. T. Koehne, R. P. Marshall, A. Jeschke, B. Kahl-Nieke, T. Schinke, M. Amling, Osteopetrosis, osteopetrorickets and hypophosphatemic rickets differentially affect dentin and enamel mineralization. *Bone* **53**, 25-33 (2013).
36. J. A. D'Errico, R. L. MacNeil, T. Takata, J. Berry, C. Strayhorn, M. J. Somerman, Expression of bone associated markers by tooth root lining cells, in situ and in vitro. *Bone* **20**, 117-126 (1997).
37. C. R. Salmon, A. P. Giorgetti, A. F. Paes Leme, R. R. Domingues, E. A. Sallum, M. C. Alves, T. N. Kolli, B. L. Foster, F. H. Nociti, Jr., Global proteome profiling of dental cementum under experimentally-induced apposition. *Journal of proteomics* **141**, 12-23 (2016).
38. T. Abe, G. Hajishengallis, Optimization of the ligature-induced periodontitis model in mice. *Journal of immunological methods* **394**, 49-54 (2013).
39. C. M. Macica, H. E. King, M. Wang, C. L. McEachon, C. W. Skinner, S. M. Tommasini, Novel anatomic adaptation of cortical bone to meet increased mineral demands of reproduction. *Bone* **85**, 59-69 (2016).
40. E. S. Liu, J. S. Martins, A. Raimann, B. T. Chae, D. J. Brooks, V. Jorgetti, M. L. Bouxsein, M. B. Demay, 1,25-Dihydroxyvitamin D Alone Improves Skeletal Growth, Microarchitecture, and Strength in a Murine Model of XLH, Despite Enhanced FGF23 Expression. *Journal of bone and mineral research : the official journal of the American Society for Bone and Mineral Research* **31**, 929-939 (2016).
41. J. N. Farr, S. Khosla, Skeletal changes through the lifespan--from growth to senescence. *Nature reviews. Endocrinology* **11**, 513-521 (2015).
42. M. L. Brandi, Microarchitecture, the key to bone quality. *Rheumatology (Oxford, England)* **48 Suppl 4**, iv3-8 (2009).

43. P. J. Marie, F. H. Glorieux, Relation between hypomineralized periosteocytic lesions and bone mineralization in vitamin D-resistant rickets. *Calcified tissue international* **35**, 443-448 (1983).
44. G. R. Naveh, R. Shahar, V. Brumfeld, S. Weiner, Tooth movements are guided by specific contact areas between the tooth root and the jaw bone: A dynamic 3D microCT study of the rat molar. *Journal of structural biology* **177**, 477-483 (2012).
45. G. R. Naveh, V. Brumfeld, R. Shahar, S. Weiner, Tooth periodontal ligament: Direct 3D microCT visualization of the collagen network and how the network changes when the tooth is loaded. *Journal of structural biology* **181**, 108-115 (2013).
46. G. R. Naveh, N. Lev-Tov Chattah, P. Zaslansky, R. Shahar, S. Weiner, Tooth-PDL-bone complex: response to compressive loads encountered during mastication - a review. *Archives of oral biology* **57**, 1575-1584 (2012).
47. B. L. Foster, K. J. Nagatomo, F. H. Nociti, Jr., H. Fong, D. Dunn, A. B. Tran, W. Wang, S. Narisawa, J. L. Millan, M. J. Somerman, Central role of pyrophosphate in acellular cementum formation. *PloS one* **7**, e38393 (2012).
48. B. L. Foster, C. R. Sheen, N. E. Hatch, J. Liu, E. Cory, S. Narisawa, T. Kiffer-Moreira, R. L. Sah, M. P. Whyte, M. J. Somerman, J. L. Millan, Periodontal Defects in the A116T Knock-in Murine Model of Odontohypophosphatasia. *Journal of dental research* **94**, 706-714 (2015).
49. T. van den Bos, G. Handoko, A. Niehof, L. M. Ryan, S. P. Coburn, M. P. Whyte, W. Beertsen, Cementum and dentin in hypophosphatasia. *Journal of dental research* **84**, 1021-1025 (2005).
50. A. Linglart, M. Biosse-Duplan, Hypophosphatasia. *Current osteoporosis reports* **14**, 95-105 (2016).
51. G. Hajishengallis, R. J. Lamont, D. T. Graves, The enduring importance of animal models in understanding periodontal disease. *Virulence* **6**, 229-235 (2015).
52. A. D. Haffajee, S. S. Socransky, Microbial etiological agents of destructive periodontal diseases. *Periodontology 2000* **5**, 78-111 (1994).
53. R. S. de Molon, E. D. de Avila, A. V. Boas Nogueira, J. A. Chaves de Souza, M. J. Avila-Campos, C. R. de Andrade, J. A. Cirelli, Evaluation of the host response in various models of induced periodontal disease in mice. *Journal of periodontology* **85**, 465-477 (2014).
54. S. Kimura, A. Nagai, T. Onitsuka, T. Koga, T. Fujiwara, H. Kaya, S. Hamada, Induction of experimental periodontitis in mice with Porphyromonas gingivalis-adhered ligatures. *Journal of periodontology* **71**, 1167-1173 (2000).
55. K. Saadi-Thiers, O. Huck, P. Simonis, P. Tilly, J. E. Fabre, H. Tenenbaum, J. L. Davideau, Periodontal and systemic responses in various mice models of experimental periodontitis: respective roles of inflammation duration and Porphyromonas gingivalis infection. *Journal of periodontology* **84**, 396-406 (2013).
56. T. Hayashibara, T. Hiraga, A. Sugita, L. Wang, K. Hata, T. Ooshima, T. Yoneda, Regulation of osteoclast differentiation and function by phosphate: potential role of osteoclasts in the skeletal abnormalities in hypophosphatemic conditions. *Journal of bone and mineral research : the official journal of the American Society for Bone and Mineral Research* **22**, 1743-1751 (2007).
57. D. E. Rodriguez, T. Thula-Mata, E. J. Toro, Y. W. Yeh, C. Holt, L. S. Holliday, L. B. Gower, Multifunctional role of osteopontin in directing intrafibrillar mineralization of collagen and activation of osteoclasts. *Acta biomaterialia* **10**, 494-507 (2014).

58. L. Huang, B. Salmon, X. Yin, J. A. Helms, From restoration to regeneration: periodontal aging and opportunities for therapeutic intervention. *Periodontology 2000* **72**, 19-29 (2016).
59. M. Cvek, I. Mejare, J. O. Andreasen, Conservative endodontic treatment of teeth fractured in the middle or apical part of the root. *Dental traumatology : official publication of International Association for Dental Traumatology* **20**, 261-269 (2004).
60. A. Nanci, Ten Cate's Oral Histology, Development, Structure, and Function. (2012).
61. S. Schwartz, C. R. Scriver, T. M. Reade, E. D. Shields, Oral findings in patients with autosomal dominant hypophosphatemic bone disease and X-linked hypophosphatemia: further evidence that they are different diseases. *Oral surgery, oral medicine, and oral pathology* **66**, 310-314 (1988).
62. C. Chaussain-Miller, C. Sinding, M. Wolikow, J. J. Lasfargues, G. Godeau, M. Garabedian, Dental abnormalities in patients with familial hypophosphatemic vitamin D-resistant rickets: prevention by early treatment with 1-hydroxyvitamin D. *The Journal of pediatrics* **142**, 324-331 (2003).
63. A. Linglart, M. Biosse-Duplan, K. Briot, C. Chaussain, L. Esterle, S. Guillaume-Czitrom, P. Kamenicky, J. Nevoux, D. Prie, A. Rothenbuhler, P. Wicart, P. Harvengt, Therapeutic management of hypophosphatemic rickets from infancy to adulthood. *Endocrine connections* **3**, R13-30 (2014).
64. M. Kawakami, T. Takano-Yamamoto, Orthodontic treatment of a patient with hypophosphatemic vitamin D-resistant rickets. *ASDC journal of dentistry for children* **64**, 395-399 (1997).
65. C. R. Sheen, G. O. Pilarowski, W. Wang, J. L. Millan, Molecular characterisation of the Hyp deletion and an improved assay for its detection. *Bone* **50**, 592-595 (2012).
66. A. Kantarci, H. Hasturk, T. E. Van Dyke, Animal models for periodontal regeneration and peri-implant responses. *Periodontology 2000* **68**, 66-82 (2015).
67. M. L. Bouxsein, S. K. Boyd, B. A. Christiansen, R. E. Guldberg, K. J. Jepsen, R. Muller, Guidelines for assessment of bone microstructure in rodents using micro-computed tomography. *Journal of bone and mineral research : the official journal of the American Society for Bone and Mineral Research* **25**, 1468-1486 (2010).
68. S. Panmekiate, N. Ngonphloy, T. Charoenkarn, T. Faruangsaeng, R. Pauwels, Comparison of mandibular bone microarchitecture between micro-CT and CBCT images. *Dento maxillo facial radiology* **44**, 20140322 (2015).
69. A. Vignery, R. Baron, Dynamic histomorphometry of alveolar bone remodeling in the adult rat. *The Anatomical record* **196**, 191-200 (1980).
70. T. Colard, G. Falgayrac, B. Bertrand, S. Naji, O. Devos, C. Balsack, Y. Delannoy, G. Penel, New Insights on the Composition and the Structure of the Acellular Extrinsic Fiber Cementum by Raman Analysis. *PloS one* **11**, e0167316 (2016).

ACKNOWLEDGMENTS The authors thank Jean-Marc Masse and Alain Schmitt (Insitut Cochin, Paris 14, France) and Annie Llorens (EA2496) for their help with the microscopy methods. **FUNDINGS** This work was supported by grants from University Paris Descartes and *Fondation pour la Recherche Médicale* for Life Imaging Facility of Paris Descartes University (*Plateforme d'Imageries du Vivant - PIV*) (FRM DGE20111123012). BRC was supported by "La fondation pour la Recherche Médicale" (PhD grant FDM20140731354) (France). **AUTHOR CONTRIBUTIONS** BRC, CC and CB designed the study. BRC and GF performed the Raman spectroscopy experiments. BRC and CB performed the surgeries. BRC, LS and JS performed the *in vivo* radiographic follow-up of all samples. BRC and BB performed other experiments of the study. TS provided the mouse model. BRC, MBD, AL and CC followed the patients and collected the bone and tooth specimens. BRC, MDM, CC and CB contributed to the analysis of the data and the drafting of the manuscript. All authors reviewed and approved the final version of the manuscript. **COMPETING INTERESTS** MDM is a member of the *FRQ-S Network for Oral and Bone Health Research*, and the *McGill Centre for Bone and Periodontal Research*.

FIGURE LEGENDS

Fig. 1: Aberrant acellular cementum phenotype associated with periodontal ligament lack of attachment in XLH/Hyp

Panel A. Light microscopy of the upper third cervico-apical section of a control (Ctrl) individual and an XLH patient. Unmineralized areas from unmerged dentin calcospherites can be seen in the XLH dentin (white arrows). Note the reduced thickness of XLH acellular cementum (double-headed arrows), confirmed statistically (n=8 teeth/patient per group, $p<0.05$). AC, acellular cementum; DEN, dentin. (scale bars, 50 μm).

Panel B. Histology sections (Toluidine blue-stained) of WT (a) and Hyp (b) mice of the first and second maxillary molars in the sagittal plane. (Scale bars, 100 μm). Insets show higher magnification revealing thinner Hyp acellular cementum (Scale bars, 10 μm). Interdental septa of WT (c) and Hyp (d) mice were stained with Sirius red and observed under polarized light used to visualize birefringent collagen fibers of periodontal tissues in mandibular first molar roots. Mineralized structures of bone and dental roots appear as shiny red whereas organized periodontal collagen fibers of the ligament appear as yellow-green. Dark regions (asterisk) of poorly organized and sparsely embedded collagen fibers unattached to the root and alveolar bone tissue can be seen in the Hyp periodontium. (scale bars, 25 μm). The insets are Goldner's trichrome-stained regions similar to those indicated by the white rectangles to confirm the presence of cells and fibers in the dark regions, and their lack of orientation and organization. (scale bars, 20 μm). Quantification of bone and root surfaces involved in the attachment of periodontal ligament in WT and Hyp mice (e). Compared with WT mice, Hyp ligament displays a lack of anchorage of two thirds of the surface of

attachment of WT ligament, on both bone and cementum sides. (n=10 per group, $p<0.05$). Transmission electron microscopy in WT (f) and Hyp (g) periodontal acellular cementum confirm the presence of unattached periodontal ligament fibers (dashed-line area) running parallel to the tooth surface near unmineralized regions of acellular cementum (asterisk) in the Hyp mouse. (scale bars, 25 nm). DEN, dentin; AC, acellular cementum; AB, alveolar bone; PDL, periodontal ligament.

Fig. 2: Aberrant cellular cementum phenotype associated with XLH/*Hyp*

Panel A. Histology sections (Toluidine blue-stained) of control (Ctrl) individual (a) and XLH patient (b) of the apical tip of molar roots in the sagittal plane. Cellular cementum (CC) is thinner in the XLH patient (bracket). (scale bars, 100 µm)**.** Light microscopy of sagittal sections of Ctrl (c) and XLH (d) teeth. XLH cellular cementum appears roughly granular with hypomineralized interglobular patterns, magnified in the inset (arrowheads), typically found in XLH dentin (scale bars, 20 µm; inset, 5 µm).

Panel B. Von Kossa staining for mineral (black) followed by Toluidine blue staining of WT (e) and *Hyp* (f) cellular cementum at the apices of dental roots (scale bars, 50 µm). Note in the magnified regions of the white rectangles (g, h) the irregular margin of Hyp cellular cementum mineralization front (h, white arrows) and the enlarged cementocyte lacunae (h, brackets), (scale bars, 10 µm). CC, cellular cementum; AB, Alveolar bone; DEN, dentin; PDL, periodontal ligament.

Fig. 3: Periodontal bone in the Hyp mouse

Panel A. Bone microarchitecture of the Hyp periodontium. Three-dimensional reconstructions (upper images) created from micro-computed tomography (µ-CT) sections of maxillary second molars of 12-week-old WT (left) and Hyp (right) mice. Two-dimensional sagittal section (lower images) of the upper images. Note the lower density of mineralized bone tissue (asterisks) in the Hyp mouse with a higher number of trabeculae (arrow) in the WT mouse. Trabecular bone microarchitecture indices of the alveolar bone of WT and Hyp mice show significant reduced bone volume fraction (Bv/Tv) and trabecular number (Tb.N) in the Hyp mouse (each bar is the mean ±SD, n=28 animals per group, $p<0.05$).

Panel B. Osteomalacic alveolar bone in the Hyp mouse. Histological sections of the maxillary second molar of a 12-week-old WT (a) and Hyp (b) mouse. The Hyp alveolar bone displays osteomalacic characteristics, with large regions of unmineralized osteoid, indicated by light blue staining (arrowheads) surrounding the black staining of the von Kossa reaction in toluidine blue staining (vK + TB), not found in the WT mouse. A wide region of unmineralized predentin layer is observed along the root canals of the Hyp mouse radicular pulp (asterisks), as described in human XLH temporary teeth (Boukpessi et al. 2006). (scale bars, 100 µm). Transmission electron microscopy in WT (c) and Hyp (d) periodontal bone confirmed the periosteocytic lesion with the presence of a wider, umineralized perilacunar matrix surrounding osteocytes in Hyp bone (double-headed arrow). DEN, dentin; CC, cellular cementum; AB, alveolar bone. (scale bars, 0.5 µm).

Fig. 4: Raman mineral phase characteristics of XLH/Hyp periodontium

Panel A. Comparison of the relative gain/loss of Raman spectroscopy variables in human XLH patient and corresponding control (Ctrl) acellular and cellular cementum: relative values show mineral-to-organic ratio (Mineralization), Type-B CO_3 substitution (Carbonation) and Crystallinity. Asterisks indicate a significant difference (n=90 measures from 3 human tissues/animals per group, $p<0.05$).

Panel B. Comparison of the relative gain/loss of Raman spectroscopy variables in the Hyp alveolar bone and its corresponding WT groups. Asterisks indicate a significant difference (n=90 measures from 3 human tissues/animals per group, $p<0.05$).

Fig. 5: Tissue-specific expression of osteopontin in XLH

Panel A. Human XLH and control (Ctrl) cementum. Whereas OPN is strongly localized in the Ctrl acellular cementum (a), the signal for OPN in XLH acellular cementum is much weaker (b). In both groups, OPN localizes to Tome's granular layer of dentin at the dentino-cemental junction (arrows) (Scale bars, 50 μm). Although a strong immunostaining for OPN in Ctrl cellular cementum occurs as appositional growth lines (c, asterisks), in XLH cellular cementum (d), OPN staining is weak and localizes primarily in Tome's granular layer of dentin (arrows) (scale bars, 100 μm).

Panel B. Murine immunolocalization of OPN in methyl methacrylate sections from undecalcified samples. Like in human samples, while WT acellular cementum is stained for OPN (e, red, black arrows), no signal can be found in Hyp acellular cementum (f). (scale bars, 10 μm). Whereas OPN is also present in WT cellular cementum (g), it is absent in Hyp cellular cementum (h). (scale bars, 25 μm). While the strongest immunostaining for OPN in WT bone

occurs at bone surfaces and around osteocytes (i), in Hyp periodontal bone, OPN prominently localizes to the pericellular hypomineralized "halo" area around osteocytes, also known as the periosteocytic lesions (j, brackets). (scale bars, 20 μm). DEN, dentin; AC, acellular cementum; AB, alveolar bone; PDL, periodontal ligament.

Fig. 6: Impaired formation of cellular cementum in the Hyp mouse

Panel A. 3-dimensional and sagittal plane of μ-CT imaging. Upper left molars have been removed (left image, red oval) to allow the overeruption of lower left molars (white arrows) from lack of occlusion and to facilitate the compensating formation of cellular cementum at the apical tip of the molar roots (right image, sequential green lines).

Panel B. Calcein labeling of cellular cementum apposition. Calcein labels appear as two distinct and spaced apart layers indicating formation and mineralization of WT cellular cementum (left image), whereas irregular thick blurry layers labeled with calcein are revealed in Hyp cellular cementum (right image). (scale bars, 20 μm). Measurements of the mineral apposition rate of WT and Hyp cellular cementum show WT mouse cementum formation (3.8 μm/day) is nearly twice the amount of formation in the Hyp mouse (1.8 μm/day) (each bar is the mean ±SD, n=9 teeth per group, $p<0.05$).

Panel C. Toluidine blue staining of cellular cementum at the lower third of WT and Hyp molar roots. Note the accumulation of an unmineralized cementoid layer at the margin of Hyp cellular cementum (d, arrowheads). ALP dark purple staining is present in the osteogenic layer facing WT cellular cementum (b), whereas the staining extends into Hyp cementum tissue (e, white dotted-line). Immunohistochemical localization of OPN (red) in unmineralized sections of WT (c) and Hyp cellular cementum (f). Whereas a strong

immunostaining for OPN in WT cellular cementum occurs in the appositional growth lines (asterisks), in Hyp cellular cementum, OPN signal is essentially absent. (scale bars, 20 μm).

Fig. 7: Delayed pathologic Hyp alveolar bone remodeling in a model of periodontal breakdown and repair

Panel A. μ-CT images of the furcation areas of WT (left images) and Hyp (right images) mouse second maxillary molars at day 4 after ligature placement (upper images) and 11 days after ligature removal (day 15, lower images). The graph indicates longitudinal variations of the distance (double-headed arrows) between the roof of the furcation zone (dotted white lines) and the top of the inter-radicular alveolar septum (solid white line). Asterisks indicate a significant statistical difference at day 0. Crosses indicate a significant statistical difference between WT and Hyp mice at the indicated time-points. (each bar is the mean ±SD, n=10 animals per group, $p<0.05$).

Panel B. Histology of impaired Hyp remodeling. The TRAP reaction stains for osteoclast cells that indicate an increased activity of resorption at day 4 after ligature placement in WT and Hyp mice compared with TRAP activity at baseline in both groups (a, b). Whereas TRAP staining decreases in WT mice (e) 11 days after ligature removal (day 15), substantial resorption remains in Hyp mice (f). At day 15, bone formation during periodontal repair is less in Hyp than WT mice. Von Kossa staining for mineral (black) and Toluidine blue staining show the accumulation of osteoid at the site of repair in Hyp mouse (h, white arrowheads). Whereas demeclocycline injected at different intervals reveals two different layers of apposition in the WT mouse furcation septum (i), only one light band is seen in the Hyp mouse (j). The osteogenic layer stained with ALP reaction is present at the margin of WT

newly formed alveolar bone, whereas it is also present into the periodontal bone unmineralized matrix of Hyp mouse (l, white arrowheads). While OPN is localized to the borders of the newly formed WT bone (m), it is strongly accumulated in the bone matrix of Hyp periodontium (n). DEN, dentin; AB, alveolar bone. (scale bars, 25 µm)

Fig. 1

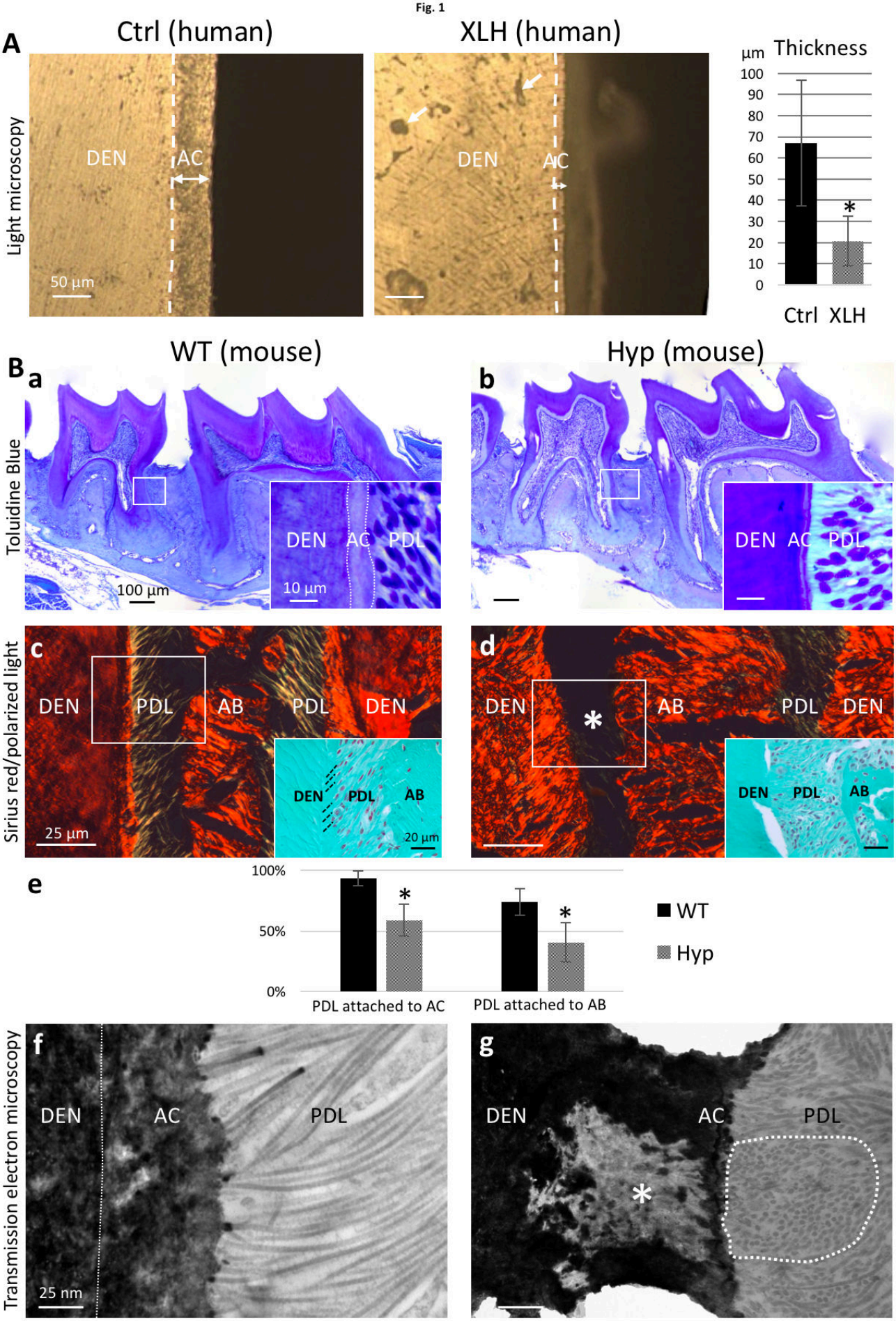
A
Ctrl (human)
XLH (human)
Light microscopy
DEN
AC
50 µm
Thickness
µm
100
90
80
70
60
50
40
30
20
10
0
*
Ctrl XLH
B
WT (mouse)
Hyp (mouse)
a
b
Toluidine Blue
DEN AC PDL
100 µm
10 µm
c
d
Sirius red/polarized light
DEN PDL AB PDL DEN
25 µm
20 µm
e
100%
50%
0%
PDL attached to AC
PDL attached to AB
WT
Hyp
f
g
Transmission electron microscopy
DEN AC PDL
25 nm

Fig. 2

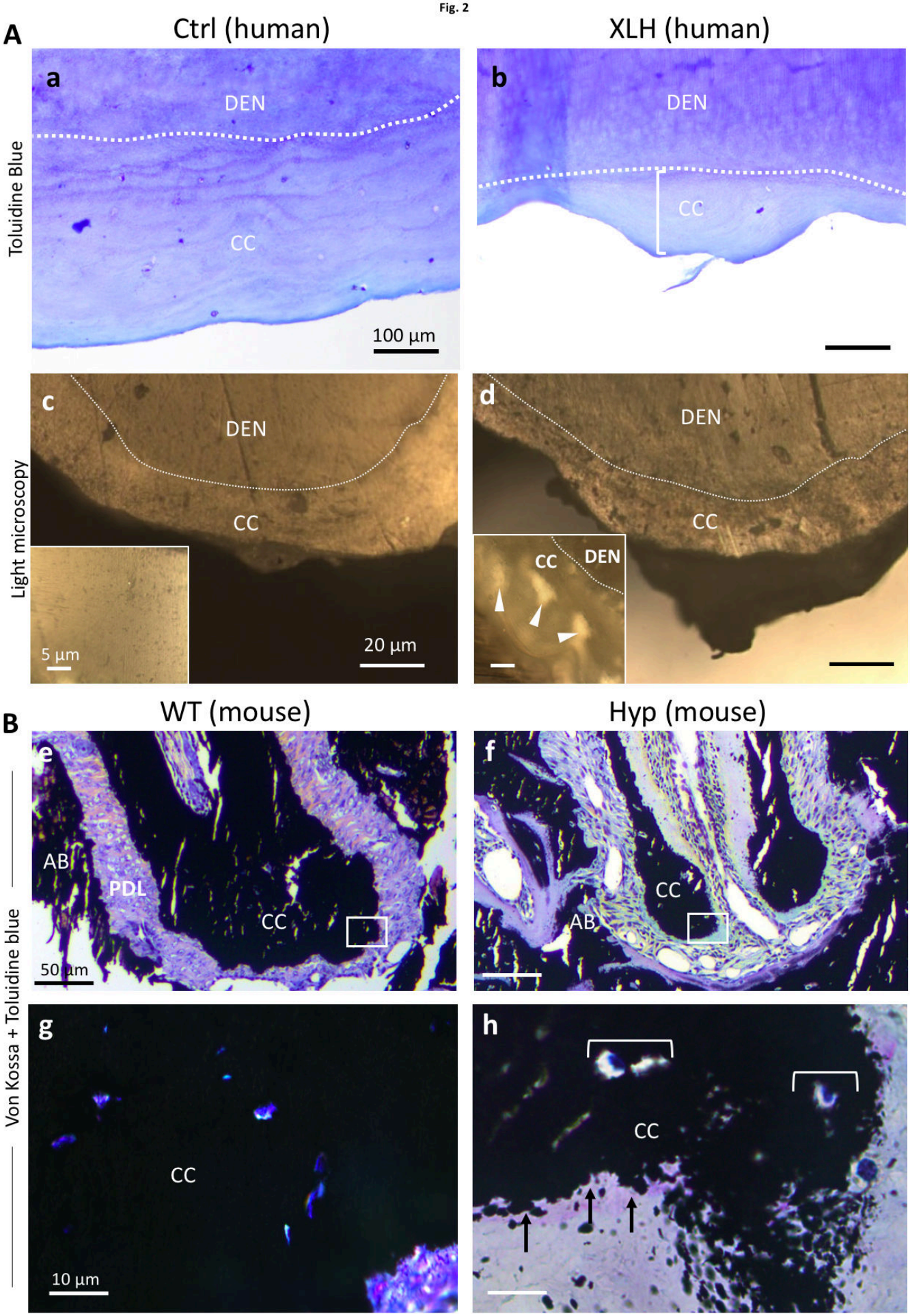
A
Ctrl (human)
XLH (human)
Toluidine Blue
a
DEN
CC
100 µm
b
DEN
CC
Light microscopy
c
DEN
CC
5 µm
20 µm
d
DEN
CC
CC
DEN
B
WT (mouse)
Hyp (mouse)
Von Kossa + Toluidine blue
e
AB
PDL
CC
50 µm
f
CC
AB
g
CC
10 µm
h
CC

Fig. 3

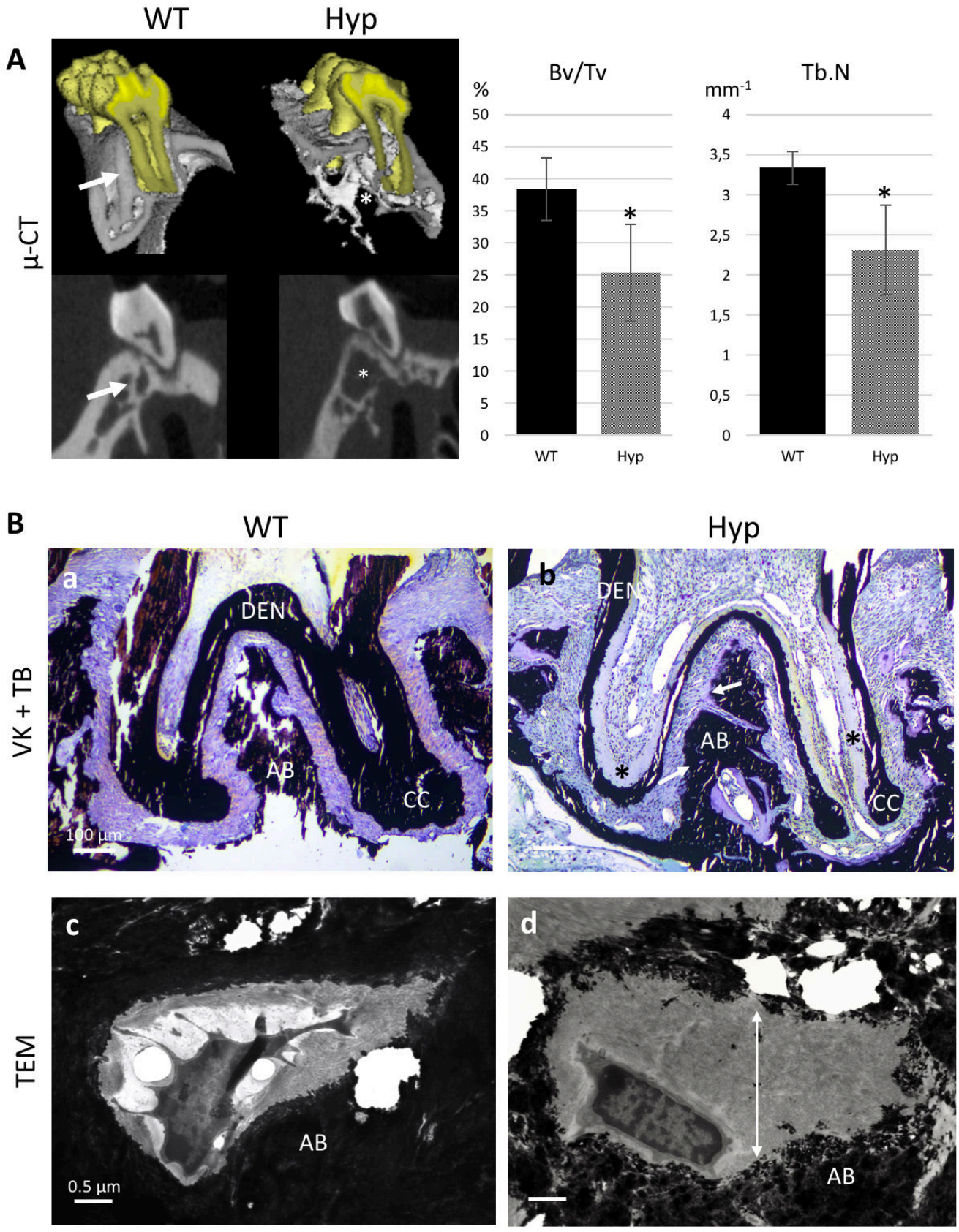
A
WT
Hyp
µ-CT
Bv/Tv
%
50
45
40
35
30
25
20
15
10
5
0
WT
Hyp
Tb.N
mm-1
4
3,5
3
2,5
2
1,5
1
0,5
0
WT
Hyp
B
WT
Hyp
VK + TB
a
DEN
AB
CC
100 µm
b
DEN
AB
CC
TEM
c
AB
0.5 µm
d
AB

Fig. 4

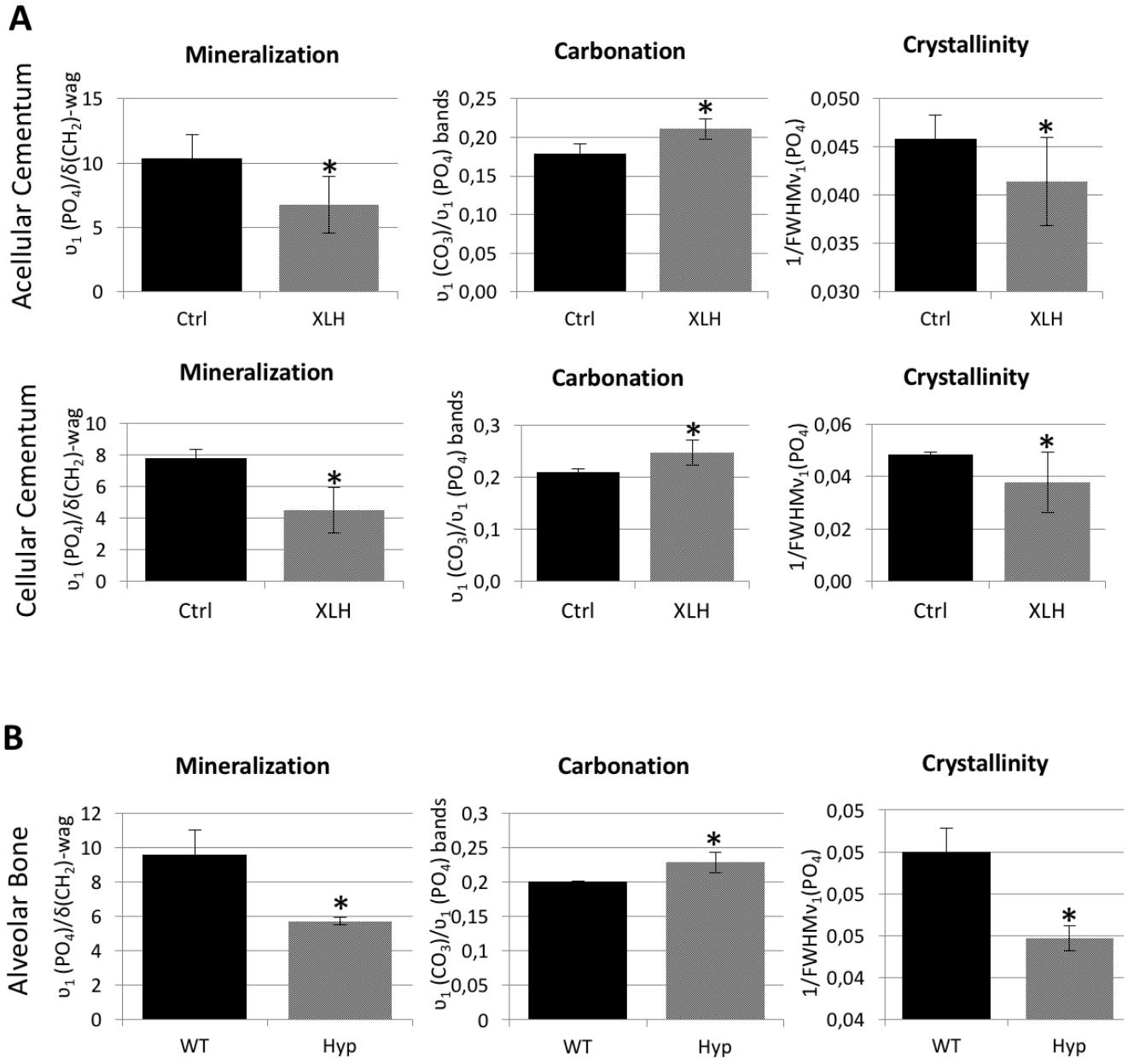
A
Acellular Cementum
Mineralization
$\upsilon_1(PO_4)/\delta(CH_2)$-wag
15
10
5
0
Ctrl
XLH
Carbonation
$\upsilon_1(CO_3)/\upsilon_1(PO_4)$ bands
0,25
0,20
0,15
0,10
0,05
0,00
Crystallinity
1/FWHM$\nu_1(PO_4)$
0,050
0,045
0,040
0,035
0,030
Cellular Cementum
10
8
6
4
2
0
0,3
0,2
0,1
0,0
0,06
0,04
0,02
0,00
B
Alveolar Bone
12
10
8
6
4
2
0
WT
Hyp
0,3
0,25
0,2
0,15
0,1
0,05
0,05
0,05
0,05
0,04
0,04

Fig. 5

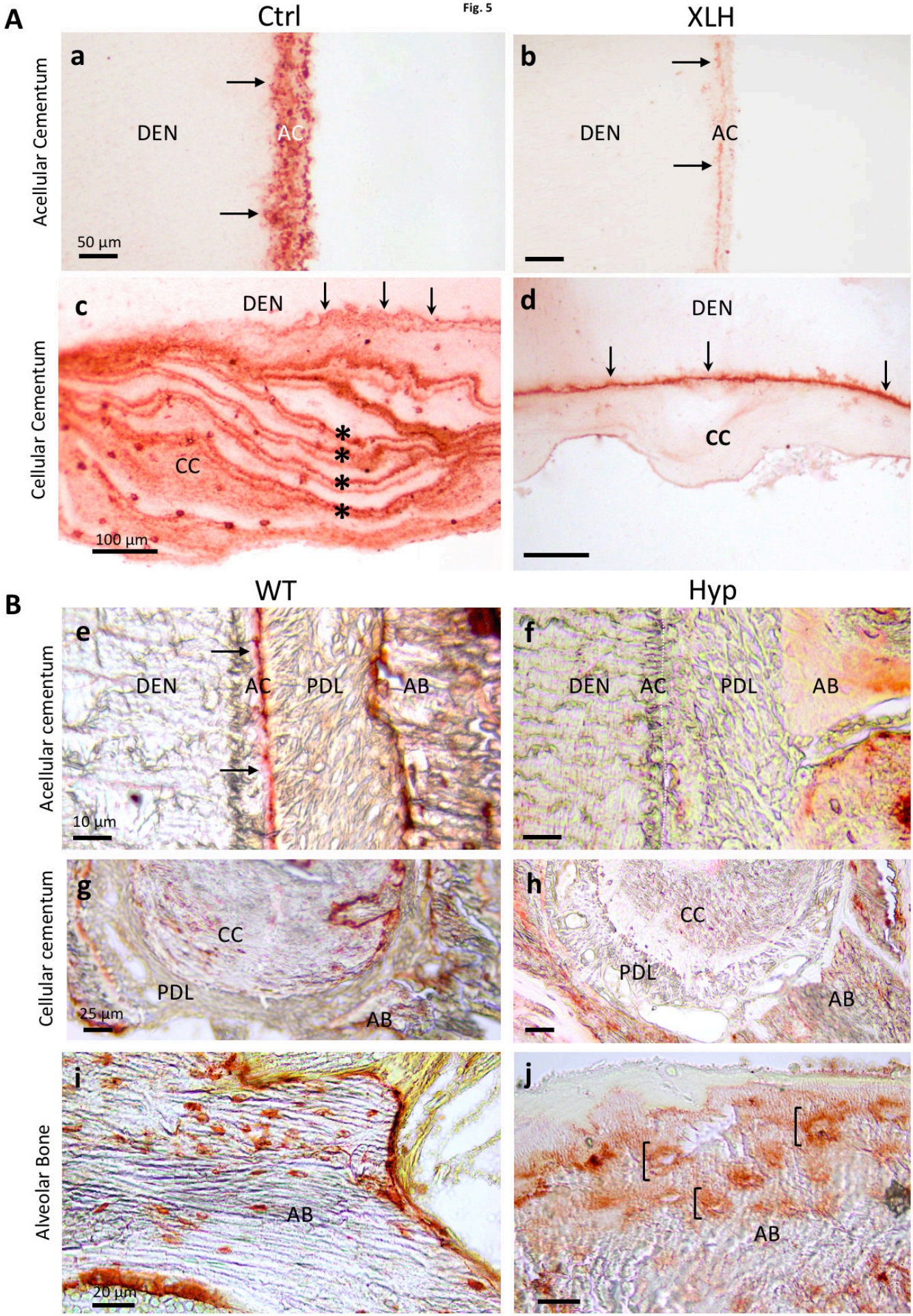
A
Ctrl
XLH
Acellular Cementum
a
DEN
AC
50 µm
b
DEN
AC
Cellular Cementum
c
DEN
CC
100 µm
d
DEN
cc
B
WT
Hyp
Acellular cementum
e
DEN
AC
PDL
AB
10 µm
f
DEN
AC
PDL
AB
Cellular cementum
g
CC
PDL
AB
25 µm
h
CC
PDL
AB
Alveolar Bone
i
AB
20 µm
j
AB

Fig. 6

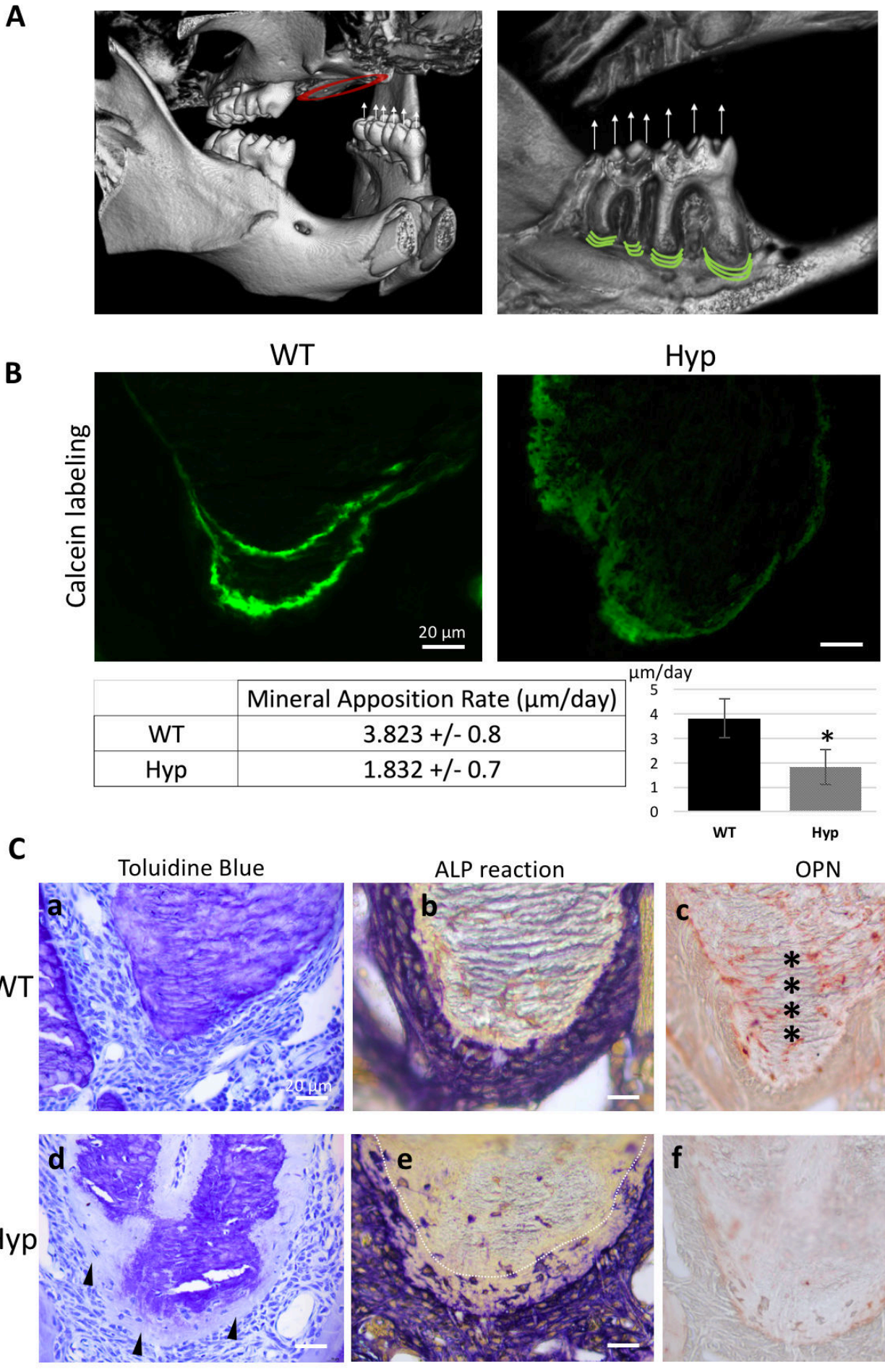

	Mineral Apposition Rate (µm/day)
WT	3.823 +/- 0.8
Hyp	1.832 +/- 0.7

Fig. 7

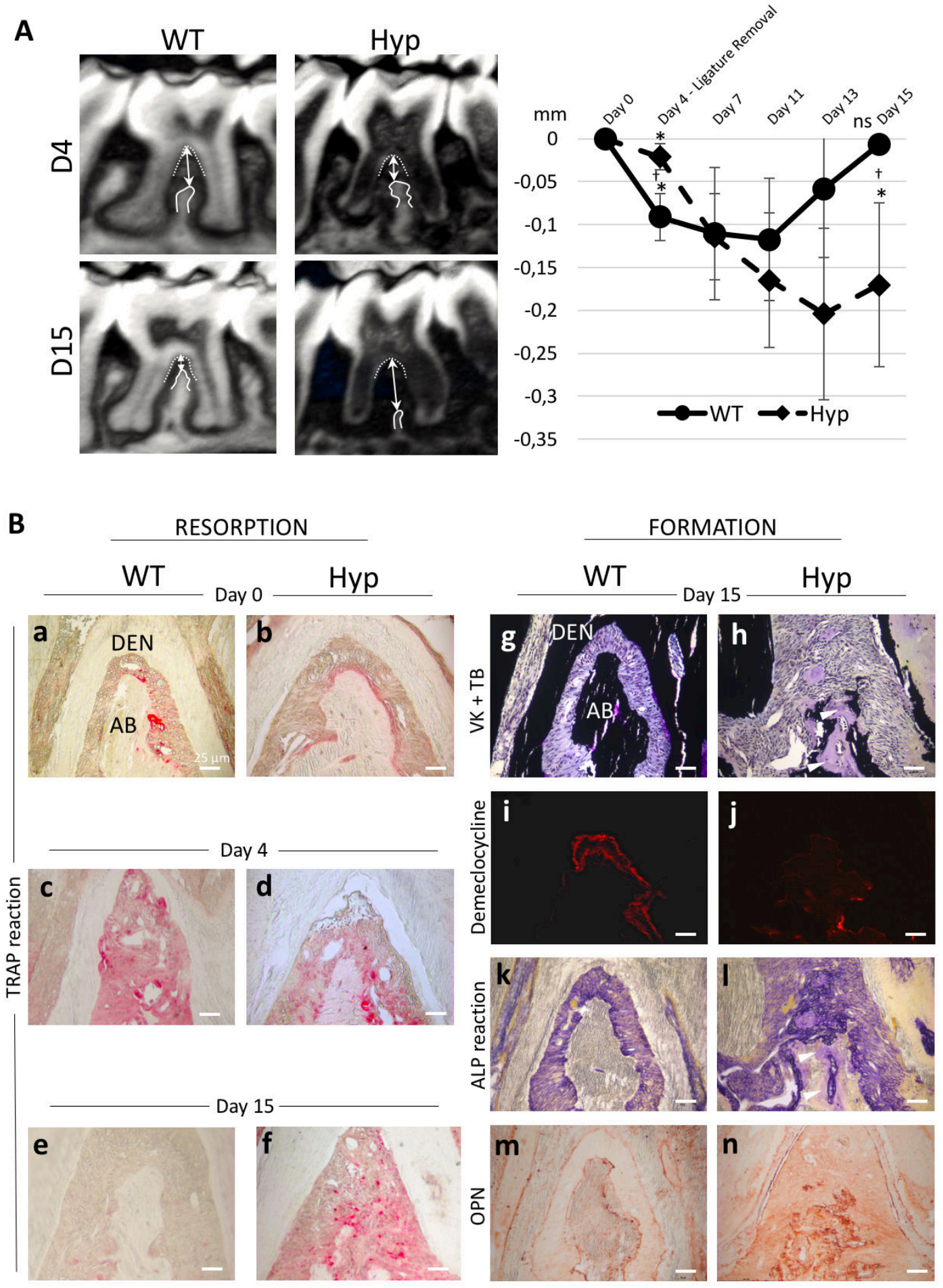
A
WT
Hyp
D4
D15
mm
0
-0,05
-0,1
-0,15
-0,2
-0,25
-0,3
-0,35
Day 0
Day 4 - Ligature Removal
Day 7
Day 11
Day 13
ns Day 15
WT
Hyp
B
RESORPTION
FORMATION
WT
Hyp
Day 0
Day 15
Day 4
Day 15
TRAP reaction
VK + TB
Demeclocycline
ALP reaction
OPN
DEN
AB
25 µm
a
b
c
d
e
f
g
h
i
j
k
l
m
n

Appendix 1

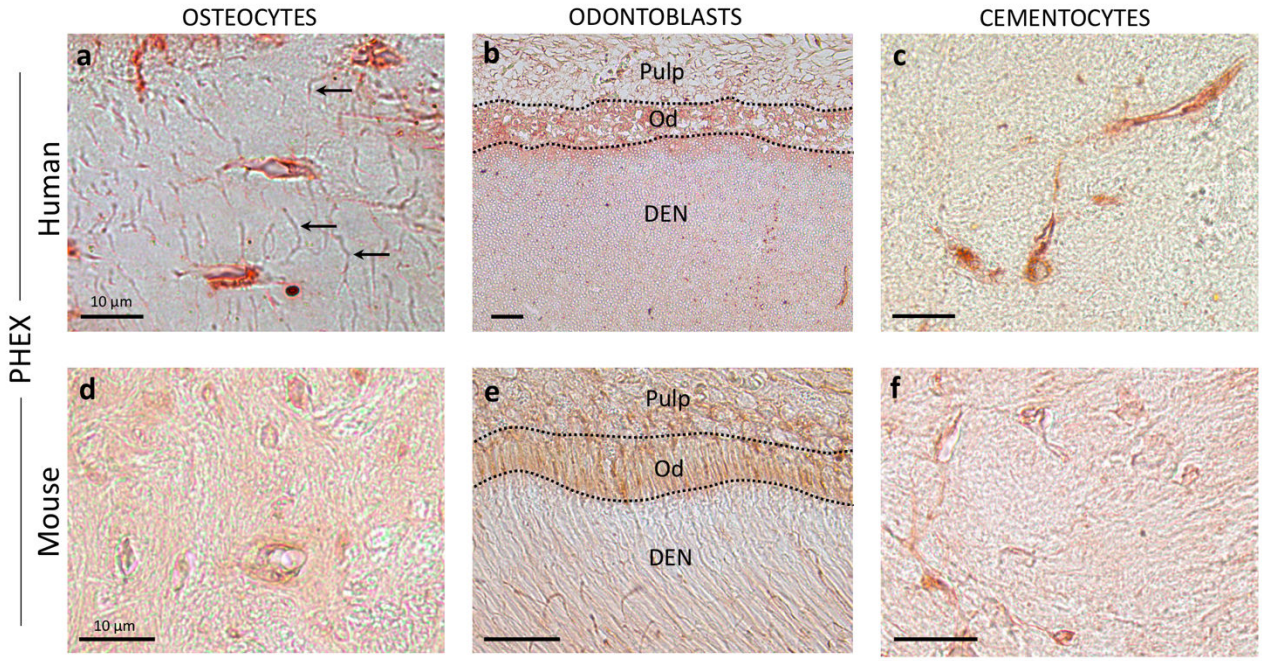

Dento-osseous immunohistochemical localization of PHEX protein. Immunohistochemical localization of PHEX (red) in paraffin sections of control individuals (upper panel) and WT mouse (lower panel). PHEX is expressed in osteocytes (**a, d**) particularly in the dendritic processes extending in bone canaliculi (a, black arrows). PHEX is expressed in odontoblasts (**b, e**) and in cementocytes of cellular cementum (**c, f**). Od, odontoblasts; DEN, dentin. (scale bars, 10 µm)

Appendix 2

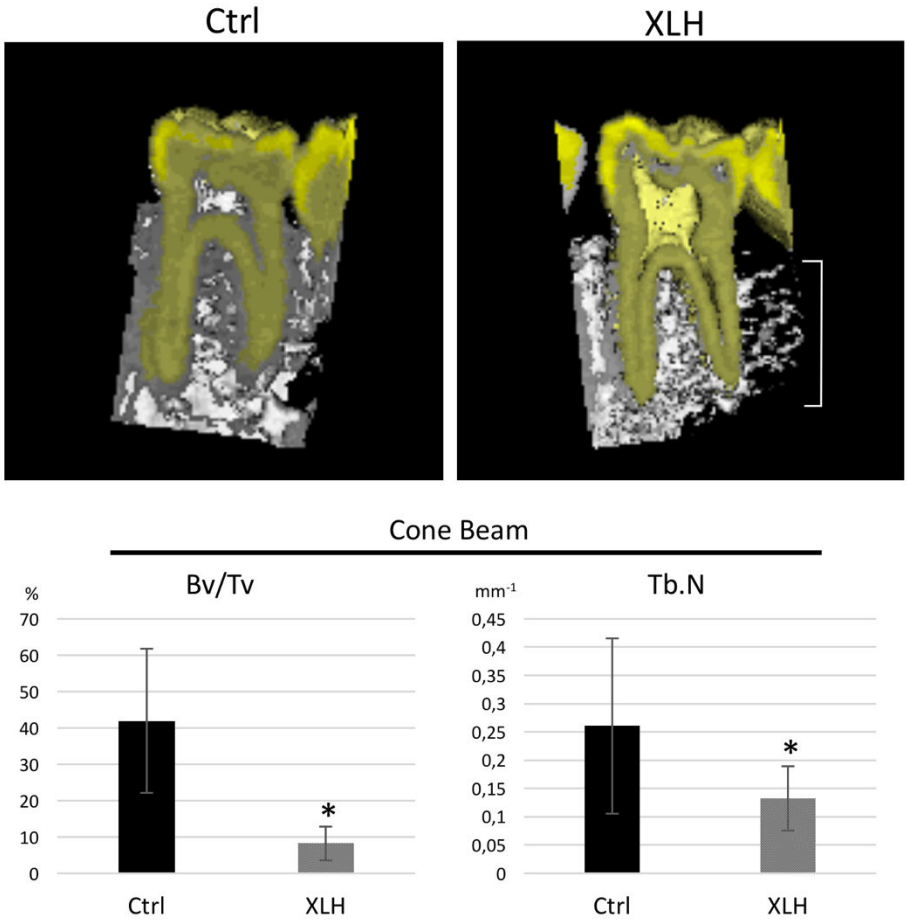

Trabecular bone microarchitecture indices of the alveolar bone of Ctrl individuals and XLH patients. Three-dimensional reconstructions (upper images) created from Cone Beam Computed Tomography sections of mandibular first molars of 15-year-old Crtl (left) and XLH (right) patients. Note the lower density of mineralized bone tissue (white bracket) in the XLH patient. Significant reduced bone volume fraction (Bv/Tv) and trabecular number (Tb.N) were found in the XLH alveolar bone (each bar is the mean ± SD of 3 different individuals in each Ctrl and XLH group, $p<0.05$).

Appendix 3

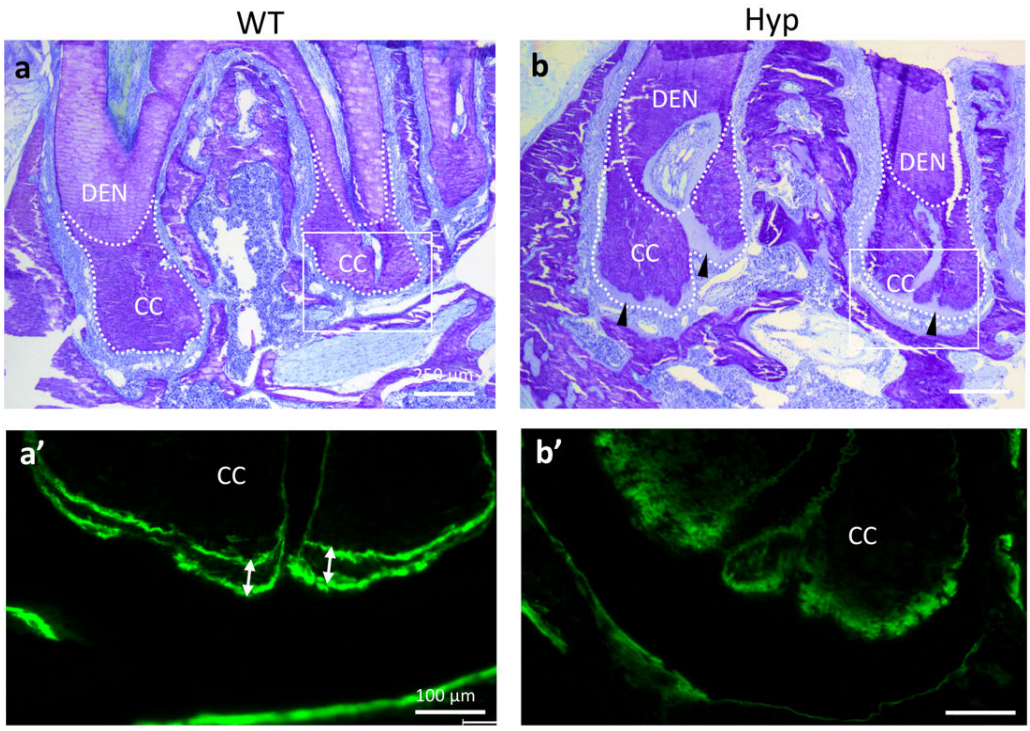

Hyp cellular cementum formation is delayed in a model of tooth overeruption. (**a-b**) Toluidine blue staining of WT (a) and Hyp (b) mouse second lower molars. Note the irregular margin and large cementoid layer in light blue (black arrowheads). DEN, dentin; CC, cellular cementum. (scale bars, 250 µm). (**a'-b'**) Magnification of A and B observed under ultraviolet light for calcein labeling visualization. Note the two distinct lines of cellular cementum formation at different time points of calcein incorporation in WT mouse (**a'**), whereas Hyp mouse cellular cementum formation appears as relatively blurred lines (**b'**). (scale bars, 100 µm)

Appendix 4

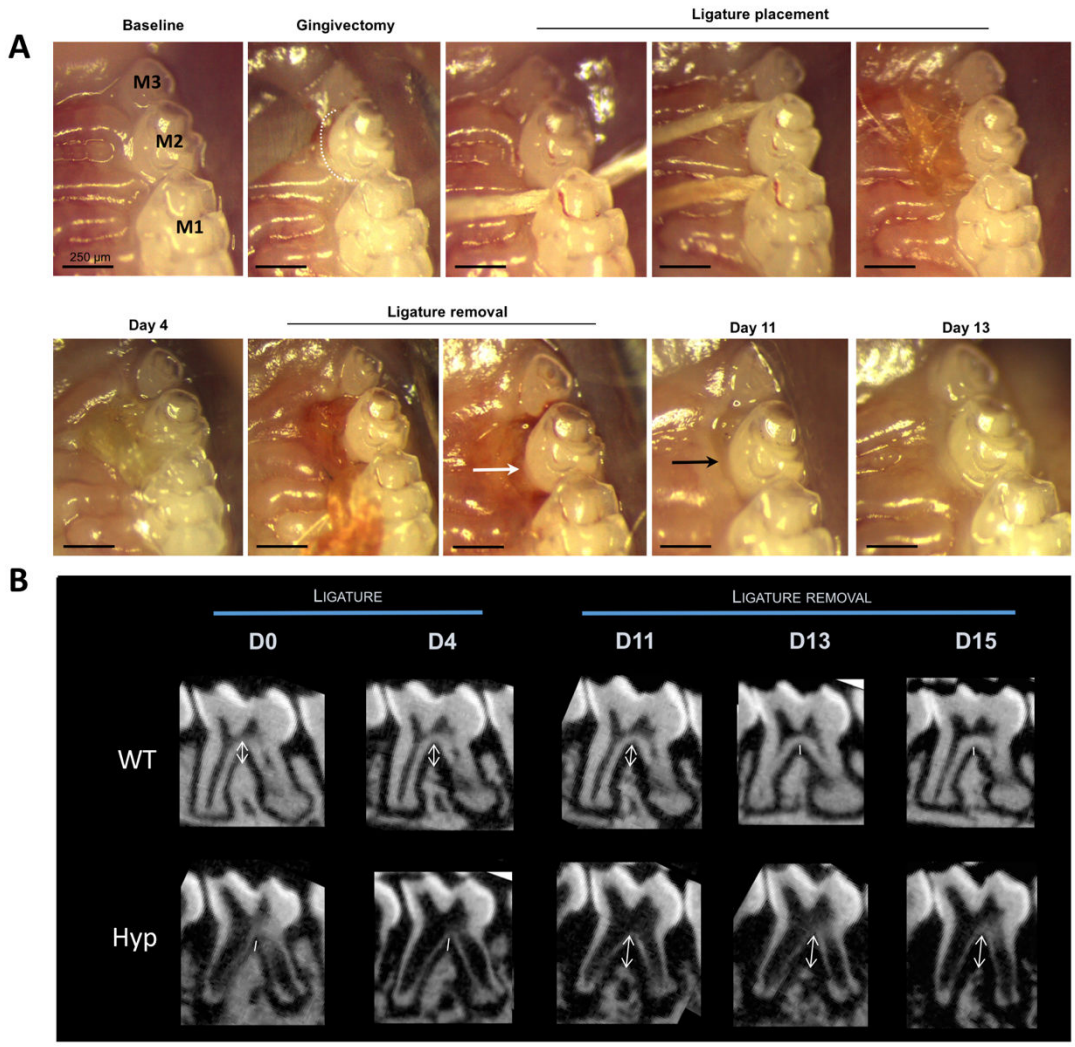

A: Murine model of ligature-induced periodontitis and alveolar bone repair. A gingivectomy is performed at the palato-cervical aspect of tooth #M2, followed by the insertion of a 5:0 suture through both contact points and a triple knot. After 4 days, the knot is untied and the suture is removed, leaving a gingival recession (white arrow). At Day 11, an ulceration remains (black arrow) that is clinically healed at day 13. (scale bars, 250 µm). **B:** The longitudinal micro-computed tomography follow-up of WT and Hyp mouse bone level is measured as the distance between the roof of the furcation and the top of the inter-radicular septum. Double-headed arrows show a delayed resorption and reconstruction of Hyp alveolar bone in the furcation area compared with WT alveolar periodontium.

7 Paper 3: Impaired intrinsic mineralization by X-linked hypophosphatemic pulp cells

Impaired intrinsic mineralization by X-linked hypophosphatemic pulp cells

Short title: **Collagen scaffold mineralization by XLH pulp cells**

Benjamin R. Coyac[1,2,3], Guillaume Falgayrac[4], Betty Hoac[3], Lotfi Slimani[1], Guillaume Penel[4], Agnès Linglart[5,6], Marc D. McKee[3], Catherine Chaussain[1,5,7*] & Claire Bardet[1*]

[1]: EA2496, Faculty of Dentistry, Paris Descartes University, Montrouge, France

[2]: Department of Periodontics and Implant Dentistry, Rothschild Hospital, AP-HP, Paris, France

[3]: Faculties of Dentistry and Medicine, Department of Anatomy and Cell Biology, McGill University, Montreal, Canada

[4]: Univ. Lille, Univ. Littoral Côte d'Opale, EA 4490 - PMOI – Physiopathologie des Maladies Osseuses Inflammatoires, F-59000 Lille, France

[5]: APHP, Reference Center for rare disorders of the Calcium and Phosphate Metabolism, filière OSCAR and Plateforme d'Expertise Maladies Rares Paris-Sud, Hôpital Bicêtre Paris Sud, Le Kremlin Bicêtre, France

[6]: INSERM U1169, Hôpital Bicêtre, Le Kremlin Bicêtre, and Université Paris-Saclay, France.

[7]: Department of Odontology, Bretonneau Hospital PNVS, AP-HP, Paris, France

*: Co-last authors

Key Words: PHEX, local mineralization, dental pulp cells, osteopontin, X-linked hypophosphatemia, collagen hydrogels

ACKNOWLEDGMENTS

This work was supported by grants from Paris Descartes University, *Fondation pour la Recherche Médicale* for *Plateforme d'imagerie du Vivant Paris Descartes* (FRM DGE20111123012), and the *Agence Nationale de la Recherche* (ANR-10-IAHU-01). BRC was supported by *Fondation pour la Recherche Médicale* (PhD grant FDM20140731354) (France). The authors thank Dimitra Athanasiadou, Lydia Malynowsky, Brigitte Baroukh and Annie Llorens for their help with the microscopy methods. MDM is a member of the FRQ-S Network for Oral and Bone Health Research, and the McGill Centre for Bone and Periodontal Research.

Contributors: BRC, CC and CB designed the study. BRC and GF performed the Raman spectroscopy experiments. BRC and LS performed the micro-CT analysis. BRC performed other experiments of the study. BRC, MDM, CC and CB contributed to the analysis of the data and the drafting of the manuscript. All authors approved the final version of the manuscript. CC and CB take responsibility for the integrity of the data analysis.

ABSTRACT

X-linked hypophosphatemia (XLH) is a rare skeletal disease caused by inactivating mutations of the *PHEX* gene. The impairment of PHEX protein leads to systemic decreased serum phosphate level resulting in defects of mineralized tissues (rickets/osteomalacia and growth impairment). It is not yet clear if the pathologic manifestations of bones and teeth are caused by the insufficient phosphate input to the mineralized tissue only or also by direct consequences of the absence of the PHEX enzyme. The aim of our study was to evaluate the local role of PHEX in a model of extracellular matrix mineralization. Dense collagen hydrogels were seeded with human dental pulp cells from patients with *PHEX* mutations and sex- and age-matched healthy controls and cultured up to 24 days under standard phosphate concentrations. Calcium quantification, microcomputed tomography, von Kossa staining and Raman spectroscopy showed a significantly lower mineral phase formation in XLH cell-seeded scaffolds. Scanning electron microscopy, energy-dispersive X-ray and Raman spectroscopy showed apatitic crystals organized along collagen fibrils in both groups. However, *PHEX*-mutated cells-seeded scaffolds presented an impaired mineral quality, with less carbonate substitution and lower crystallinity. Western blots, immunohistochemistry and immunogold labeling for osteopontin showed an accumulation of this mineralization inhibitor in the extracellular matrix of XLH scaffolds with an impaired processing of OPN fragments. Contrary to control scaffolds, ALP was strongly expressed by XLH cells as shown by enzymohistochemistry. Our results suggest that PHEX deficiency is directly involved in all pathologic features of bone and dentin attributed to hypophosphatemia in XLH and needs to be addressed in future treatment goals that currently mainly aim at improving systemic phosphate concentrations.

INTRODUCTION

X-linked hypophosphatemia (XLH) is a genetic dominant disorder characterized by hypophosphatemia, growth retardation and rickets/osteomalacia (Carpenter 2012). The genetic defects underlying XLH are loss-of-function mutations in the PHEX gene (Phosphate-regulating gene with homologies to endopeptidases on the X chromosome) (The HYP consortium). Mineralization defects (e.g. rickets and osteomalacia) observed with PHEX impairment are primarily caused by renal phosphate wasting following an increase in FGF23, a phosphaturic hormone expressed by osteocytes, osteoblasts and odontoblasts (Bonewald and Wacker 2013; Quarles 2003; Yoshiko et al. 2007b). Current and novel treatment strategies for XLH consist in supplementation in phosphate and vitamin D and monoclonal antibody raised against FGF23, respectively. In both cases, treatments for XLH aim at improving serum phosphate level (Carpenter et al. 2011; Linglart et al. 2014). However, accumulating evidence also point to a direct role of PHEX in the regulation of mineralization of calcified tissues where it is expressed (i.e. bone, dentin, cementum). Recently, *in vitro* and *in vivo* data using recombinant proteins or human XLH tissues or the *Hyp* mouse, a murine homolog of XLH, have shown the capacity of PHEX in binding and proteolytic processing the proteins and peptides regulating mineralization (Barros et al. 2013). Particularly, a SIBLING protein (Small Integrin-Binding-Ligand-N-linked Glycoprotein), osteopontin (OPN), was proposed to be substrate for PHEX enzyme that could accumulate in bone and dentin in XLH and contribute to the defective tissue mineralization (Boukpessi et al. 2016; McKee et al. 2013). However, *in vivo* studies cannot conclude on a direct role of PHEX in the regulation of mineralization homeostasis, as FGF23-related hypophosphatemia also leads to hypomineralization. In the field of tissue engineering, disease-modeling approach (so called “disease-in-a-dish”) has been extensively used to isolate pathologic mechanisms (Grskovic et

al. 2011). In this study, we used an *in vitro* model of human biomineralization, consisting in seeding dental pulp cells from patients with XLH and from control individuals into plastically compressed collagenous hydrogels (Coyac et al. 2013). We tested the hypothesis that local function of PHEX in extracellular matrices is physiologically critical and independent of circulating phosphate serum levels during development of mineralized tissues. By controlling surrounding phosphate levels in an *in vitro* model, we explored for the first time the human intrinsic cellular-mediated mineralization defects associated with PHEX deficiency.

MATERIALS AND METHODS

Patient information and Human teeth

XLH was diagnosed at the collaborating institutions based on the disorder's characteristic findings and a pattern of X-linked dominant disease transmission and positive *PHEX* mutation analysis. Teeth were obtained from the Dental Department of Academic Hospitals Paris Nord Val de Seine, AP-HP, France. Deciduous and permanent teeth were extracted for orthodontic reasons from three XLH patients and 3 sex- and age-matched healthy young individuals (11 and 15 years of age) with informed and oral consent from the patients and the parents according to ethical guidelines set by the French law (agreement IRB 00006477 n°DC-2009-927, *Cellule Bioéthique* DGRI/A5).

Cell Culture

Normal and XLH exfoliated human deciduous teeth and dental pulp stem cells were collected from 3 Control individuals and 3 XLH patients aged 11 and 15 yrs with the informed consent of the patients and their parents, and the approval from the Institutional Review Board (6477, subject N°16-024) of HUPNVS, AP-HP, France. Cells were isolated and expanded following an established protocol (Gronthos et al. 2011; Miura et al. 2003). For all experiments, pulp cells were used at passage 3.

Preparation of dense collagen hydrogels and mineralization assay

Sterile, rat-tail tendon-derived type I collagen (2.10 mg/mL of protein in 0.1% acetic acid) was used as starting materials and developed as previously described (appendix 1)(Coyac et al. 2013). Briefly, 3.6 mL of sterile rat-tail collagen type I at a protein concentration of 2.01 mg/mL in 0.1% acetic acid was mixed with 0.9 mL of ×10 DMEM (Dulbecco's Modified Eagle

Medium) and neutralized by drop-wise addition of 5 M NaOH to ~pH 7.4. After neutralization, dental pulp cells, either from control individuals or XLH patients were seeded within the hydrogels at a density of 150×10^3 cells/mL of collagen solution, immediately prior to gel polymerization. Cellularized collagen solutions were poured in four-well plates (0.9 mL/well of 4.5 mm height×16 mm diameter) to produce dense planar discs. Gelation was achieved by allowing the solutions to set at 37°C in a 5% CO_2 incubator for 30 min. Highly hydrated hydrogels (with < 0.5 weight % fibrillar collagen density) were removed from the molds and dense gels were produced by plastic compression (PC) as previously reported (Brown et al. 2005; Coyac et al. 2013). Briefly, highly hydrated gels were placed on a stack of blotting paper, nylon mesh, and metal mesh, and subjected to PC using an unconfined compressive stress of 0.5 kPa for 5 min, to remove the excess casting fluid. After compression, dense discs (16 mm diameter) were transferred to 12-well plates and cultured under static conditions for 24 days. Ctrl and XLH cellularized scaffolds were cultured in osteogenic medium (DMEM media supplemented with 300 µM L-ascorbic acid sodium salt, 10 nM dexamethasone, 4% fetal bovine serum, and 1% penicillin/streptomycin) either supplemented with 10 mM β-glycerophosphate (+P) or no β-glycerophosphate supplementation (-P) (Appendix 1). A same batch of FBS was used for all experiments.

Microscopy Analyses of Scaffolds and Cells

After 24 days of culture, scaffolds were rinsed in PBS (-Ca, -P) and fixed in 70% ethanol at 4°C and dehydrated in a graded ethanol series. Undecalcified samples were embedded in methyl methacrylate (Merck, Rahway, NJ). Serial sections, 4µm thick were cut on a microtome (Polycut E microtome, Leica, Wetzlar, Germany). Series of consecutive sections were stained respectively with toluidine blue (pH 3.8), with von Kossa reagent (5% silver nitrate solution,

Sigma-Aldrich). Light microscopy (LEITZ DM-RBE microscope, Leica, Germany, equipped with a Sony DXC-950 CCD camera) was used to examine Ctrl and XLH dental pulp cells-seeded scaffolds. For scanning electron microscopy (SEM) and transmission electron microscopy (TEM), scaffolds were rinsed in PBS and fixed in 1% glutaraldehyde (Electron Microscopy Sciences, Hatfield, PA, USA) and 2% paraformaldehyde in PBS for 1 hour at room temperature and then overnight at 4°C, and then dehydrated through a graded ethanol series. SEM and TEM were performed to analyze scaffold microstructure as well as cellular morphology and mineralization. Energy-dispersive X-ray spectroscopy (EDS) was performed for elemental analysis of mineral, and crystalline structure of the mineral was assessed by Raman spectroscopy.

Enzymohistochemistry

Alkaline phosphatase (ALP) was used to reveal the layer of osteogenic cells by incubating the sections with naphthol ASTR phosphate (Sigma-Aldrich, St Louis, MO) and diazonium fast blue RR salt (Sigma-Aldrich, St Louis, MO) for 30min at 37°C (pH 9) in the presence of $MgCl_2$.

Immunohistochemistry

Sections were deplastified. After rehydration in a graded ethanol series to pure distilled water, sections were blocked using 5% Normal Horse Serum/PBS-T. Sections were incubated for 12 hours at 4°C with goat anti-human OPN antibody (R&D Systems, Minneapolis, MN, USA) diluted 1:20 in 2.5% Normal Horse Serum/PBS-T. Sections were washed and then incubated with peroxidase-conjugated anti-IgG diluted 1:1000 in the same buffer. Peroxidase activity was detected using a diaminobenzadine substrate kit from Abcam (Cambridge, MA, USA) following the manufacturer's instructions. Control incubations to assess nonspecific staining consisted of the same procedure except the primary antibody

was substituted by non-immune serum (these control incubations resulted in nonspecific staining, data not shown). For electron microscopy, grid-mounted sections (80 nm) cut on an ultramicrotome were incubated with goat anti-human OPN antibody, followed by rabbit anti-goat secondary antibody and then protein A-colloidal gold (14 nm) conjugate (Dr. G. Posthuma, University of Utrecht, Utrecht, The Netherlands), and then conventional staining with uranyl acetate and lead citrate. Sections were viewed in a FEI Technai 12 transmission electron microscope (FEI, Hillsboro, OR, USA) operating at 120 kV and equipped with a 792 Bioscan 1k x_1k wide-angle multiscan CCD camera (Bioscan, Pleasanton, CA, USA). Control incubations to assess nonspecific binding of gold particles consisted of the same procedure except the primary antibody was omitted or substituted by non-immune serum (these control incubations resulted in no specific labeling, data not shown).

Western Blotting

Flash-frozen cell-seeded scaffolds were crushed in liquid nitrogen and solubilized in 10 V of lysis buffer containing 8 M Urea, 2 M Thiourea, 4% CHAPS, 50 mM DTE. After centrifugation (100 000 × *g* for 45 min at 6 °C), the supernatants were collected and, in order to remove DTT, all samples were treated with 2D Clean-Up kit (GE healthcare) according to the manufacturer's instructions. The resultant dry pellets were suspended into lysis buffer without DTT, and the pH was set to 8.5 with 1.5 M Tris-base. Protein concentration of samples was estimated according to the manufacturer's instructions using a commercial Bradford reagent (Quick Start Bradford protein assay, Bio-Rad) and samples were stored at −80°C until use. A 15-µg quantity of total protein extracts of each sample was separated by SDS-PAGE on a gradient gel (Biorad stain free anyKd), and transferred to a polyvinylidene difluoride membrane. The membrane was probed with goat anti-human OPN antibody diluted 1:1000 (AF 1433, R&D Systems, Minneapolis, MN, USA). Membrane was then

incubated with horseradish peroxidase-conjugated anti-goat secondary antibody and visualized with ECL Select^{TM} Prime Western Blotting Detection Reagent (GE Healthcare, Buckinghamshire, UK). Quantitation of digitized images of immunoblots was done using ImageJ software. The intensity of immunoreactive bands was normalized. Data are expressed as means ± SD.

Micro-computed Tomography Dataset Acquisition

Scaffolds were scanned using a high-resolution X-ray micro-CT device (Quantum FX Caliper, Life Sciences, Perkin Elmer, Waltham, MA, United States). Three-dimensional acquisitions were performed using an isotropic voxel size of 40x40x40 μm^3 (90 kV, 160 microA, 180 s). Morphometric measurements were performed using Skyscan software (v1.13.5.1, Kontich, Belgium). Measurements were performed at Days 24 on 12 scaffolds in each group (Ctrl +P, -P and XLH +P, -P).

Raman Microspectroscopy

Scaffolds were fixed in 70% ethanol solution and air-dried at room temperature. Raman analyses were carried out on a Labram HR800 microspectrometer (Horiba Gr, Jobin Yvon, Lille, France). The spectrometer was equipped with a diode laser (λ= 785nm), an air-cooled CDD (1024×256 pixels) and a ×100 objective (NA= 0.90, Olympus, France). The illumination spot size was ~1µm. Spectral acquisitions were done in the 300-1700cm^{-1} range. The total acquisition time for each spectrum was 1 min with an integration time of 30 s and 2 accumulations. Each spectrum was treated with smoothing filtering (filter width: 3; and polynomial order: 2) with Labspec software (Horiba GR, Jobin Yvon, Lille, France). A total of 30 spectra were obtained per scaffold. Physico-chemical variables were recorded as previously described (Colard et al. 2016; Mandair and Morris 2015). Briefly, mineralization

was evaluated as the mineral-to-organic ratio (υ_1 (PO_4)/$\delta(CH_2)$-wag), carbonatation was evaluated as Type-B carbonate substitution (υ_1 (CO_3)/υ_1 (PO_4) bands) and crystallinity was the inverse of the full width at half maximum intensity (FWHM) of the ν_1PO_4 band (1/FWHM de υ_1 (PO_4)). All data analyses were performed using Matlab R2010a (Mathworks, Inc., Natick, MA, USA).

Statistical Analysis

Experiments were performed in triplicate for each time-point and each condition. Data were compared by non-parametric tests (Mann-Whitney *U*-test for group comparisons). Differences were considered significant at $p<.05$. Data are expressed as mean ± SD.

RESULTS

Defective mineralization in XLH cells-seeded scaffolds

After 24 days of culture in osteogenic medium with standard concentrations of phosphate (+P: 4% FBS, 10 mM β-glycerophosphate), XLH dental pulp cells-seeded scaffolds showed a significant reduction of mineral formation measured by micro-CT, von Kossa reaction (Figure 1A) compared with control cells-seeded scaffolds. These observations were further supported by biochemical calcium quantification and Raman microspectroscopy (Figure 1B). When cultured under low phosphate concentration (osteogenic medium -P: 4% FBS), both Ctrl and XLH cell-seeded scaffolds presented a reduced mineral phase accumulation compared to regular phosphate concentration, but the quantity of mineral remained significantly lower in XLH scaffolds (Appendix 2). In both cell populations, the mineral phase was associated to the collagenous extracellular matrix and presented calcium and phosphate molecular components evidenced by energy-dispersive X-ray and Raman spectroscopy, consistent with an apatitic mineral (Figure 2A-C). However, XLH cells-seeded scaffolds Raman spectra showed an immature mineral formation with a recurrent absence of peaks for carbonate substitution (CO_3^{2-}: 1070 cm^{-1}) and a lower crystallinity (figure 2D, E).

PHEX deficiency directly impacts the expression of ALP and OPN

We then sought to analyze the expression of the molecular matrix components involved in the mineralization process and frequently investigated in the pathobiology of XLH (Boukpessi et al. 2016; Gaucher et al. 2009a; Martin et al. 2008). Increased ALP activity was observed in XLH cells-seeded scaffolds compared with Ctrl scaffolds as evidenced by the increased number of ALP-positive cells in XLH scaffolds (Figure 3). Whereas ALP – a mineralization

promoter – was strongly expressed by XLH cells, OPN – a mineralization inhibitor – accumulated in the extracellular matrix, more specifically into the forming mineral phase of XLH scaffolds (Figure 4 A-D). In addition, immunoblotting of total protein extract showed full length OPN as a ~50 kDa bands for both Ctrl and XLH cells-seeded scaffolds and revealed several OPN fragments at ~60 kDa, ~75 kDa, and ~37 kDa that were not detected in the control scaffolds (Figure 4E). Quantitative analysis showed that the amount of OPN was significantly higher in XLH compared with control cells-seeded scaffolds (Figure 4F).

DISCUSSION

In this study, using an *in vitro* osteogenic model with human dental pulp cells obtained from XLH patients and sex- and aged-matched control individuals, we showed a local cell-autonomous defective mineralization independent of hypophosphatemia in XLH.

In Humans, similar phenotypes result from various endocrine conditions characterized by mishandling of phosphate metabolism, such as XLH (loss of PHEX) and Autosomal Recessive Hypophosphatemic Rickets (loss of DMP1). This observation suggests that the pathologic phenotypes may have a stronger association with noted high levels of FGF23, and may not result from direct effects of the loss of PHEX or DMP1. Hence, current and novel treatment strategies for XLH only target systemic hypophosphatemia, either by supplementing in phosphate and vitamin D, or by inactivating FGF23 hormone through monoclonal antibodies.

However, intrinsic mineralization defects have been proposed in XLH tissues since classical 2D mineralization assay of osteoblasts derived from the *Hyp* mouse, the murine model of XLH, were associated to impaired mineralization, with diminished calcium accumulation when compared with wild type (WT) (Xiao et al. 1998). *In vivo*, *Hyp* osteoblasts transplanted into WT mice were also associated with mineralization defects (Ecarot et al. 1992). In addition, *Hyp/Fgf23* KO cross compound mice had a resolution of rickets, but not osteomalacia, revealing that although much of the phenotype in the *Hyp* mouse is due to the *FGF23* over-expression, yet local defects unrelated to FGF23 or hypophosphatemia led to osteomalacia (Liu et al. 2006; Sitara et al. 2004). This differential role played by PHEX and FGF23 in the *Hyp* mouse pathogenesis was further experimented by the transgenic expression of *Phex* in the *Hyp* mouse that restored the bone phenotype without improving phosphate metabolism deficiencies (Erben et al. 2005b; Zelenchuk et al. 2014a). Here, we

show abnormal mineralization associated with XLH cells cultured under regular phosphate conditions, using an efficient model to study the quality and quantity of biomineralization (Coyac et al. 2013).

Like in human appendicular bone tissues, where hypophosphatemia is believed to cause osteomalacia and impaired quality of the mineral phase (appendix 3), we observed the same defects in the mineral phase obtained by XLH cells cultured under standard phosphate concentrations. It has been previously shown that PHEX completely degrades full-length inhibitory OPN and promotes mineralization, but in the absence of PHEX activity, an OPN protein fragment accumulates in *Hyp* mouse bone (Barros et al. 2013) and in XLH human bone (Boukpessi et al. 2016) (Appendix 3G,H). Here, we show that XLH pulp cells also accumulate OPN fragments. Thus, these "soft bones" characteristics related to hypophosphatemia are worsened locally by PHEX deficiency, suggesting that the accumulation of OPN fragments *in vivo* is directly related to the absence of PHEX locally.

Altogether, our data show that hypophosphatemia alone does not explain the pathologic phenotype observed in XLH. Loss of PHEX independently impacts local extracellular matrix mineral formation and quality, possibly through the accumulation and impaired cleavage of OPN. The local function of PHEX, although less physiologically critical than FGF23 circulating serum levels, leads to defects in terms of mineral quantity and quality during formation of mineralized tissues, that need to be addressed in novel treatment goals.

REFERENCES

Barros NM, Hoac B, Neves RL, Addison WN, Assis DM, Murshed M, Carmona AK, McKee MD. 2013. Proteolytic processing of osteopontin by phex and accumulation of osteopontin fragments in hyp mouse bone, the murine model of x-linked hypophosphatemia. Journal of bone and mineral research : the official journal of the American Society for Bone and Mineral Research. 28(3):688-699.

Bonewald LF, Wacker MJ. 2013. Fgf23 production by osteocytes. Pediatric nephrology (Berlin, Germany). 28(4):563-568.

Boukpessi T, Hoac B, Coyac BR, Leger T, Garcia C, Wicart P, Whyte MP, Glorieux FH, Linglart A, Chaussain C et al. 2016. Osteopontin and the dento-osseous pathobiology of x-linked hypophosphatemia. Bone.

Brown RA, Wiseman M, Chuo CB, Cheema U, Nazhat SN. 2005. Ultrarapid engineering of biomimetic materials and tissues: Fabrication of nano- and microstructures by plastic compression. Advanced Functional Materials. 15(11):1762-1770.

Carpenter TO. 2012. The expanding family of hypophosphatemic syndromes. Journal of bone and mineral metabolism. 30(1):1-9.

Carpenter TO, Imel EA, Holm IA, Jan de Beur SM, Insogna KL. 2011. A clinician's guide to x-linked hypophosphatemia. Journal of bone and mineral research : the official journal of the American Society for Bone and Mineral Research. 26(7):1381-1388.

Colard T, Falgayrac G, Bertrand B, Naji S, Devos O, Balsack C, Delannoy Y, Penel G. 2016. New insights on the composition and the structure of the acellular extrinsic fiber cementum by raman analysis. PloS one. 11(12):e0167316.

Coyac BR, Chicatun F, Hoac B, Nelea V, Chaussain C, Nazhat SN, McKee MD. 2013. Mineralization of dense collagen hydrogel scaffolds by human pulp cells. Journal of dental research. 92(7):648-654.

Ecarot B, Glorieux FH, Desbarats M, Travers R, Labelle L. 1992. Defective bone formation by hyp mouse bone cells transplanted into normal mice: Evidence in favor of an intrinsic osteoblast defect. Journal of bone and mineral research : the official journal of the American Society for Bone and Mineral Research. 7(2):215-220.

Erben RG, Mayer D, Weber K, Jonsson K, Jüppner H, Lanske B. 2005. Overexpression of human phex under the human β-actin promoter does not fully rescue the hyp mouse phenotype. Journal of Bone and Mineral Research. 20(7):1149-1160.

Gaucher C, Boukpessi T, Septier D, Jehan F, Rowe PS, Garabedian M, Goldberg M, Chaussain-Miller C. 2009. Dentin noncollagenous matrix proteins in familial hypophosphatemic rickets. Cells, tissues, organs. 189(1-4):219-223.

A gene (pex) with homologies to endopeptidases is mutated in patients with x-linked hypophosphatemic rickets. The hyp consortium. 1995. Nature genetics. 11(2):130-136.

Gronthos S, Arthur A, Bartold PM, Shi S. 2011. A method to isolate and culture expand human dental pulp stem cells. Methods in molecular biology (Clifton, NJ). 698:107-121.

Grskovic M, Javaherian A, Strulovici B, Daley GQ. 2011. Induced pluripotent stem cells—opportunities for disease modelling and drug discovery. Nature reviews Drug discovery. 10(12):915-929.

Linglart A, Biosse-Duplan M, Briot K, Chaussain C, Esterle L, Guillaume-Czitrom S, Kamenicky P, Nevoux J, Prie D, Rothenbuhler A et al. 2014. Therapeutic management of hypophosphatemic rickets from infancy to adulthood. Endocrine connections. 3(1):R13-30.

Liu S, Zhou J, Tang W, Jiang X, Rowe DW, Quarles LD. 2006. Pathogenic role of fgf23 in hyp mice. American journal of physiology Endocrinology and metabolism. 291(1):E38-49.

Mandair GS, Morris MD. 2015. Contributions of raman spectroscopy to the understanding of bone strength. BoneKEy reports. 4:620.

Martin A, David V, Laurence JS, Schwarz PM, Lafer EM, Hedge AM, Rowe PS. 2008. Degradation of mepe, dmp1, and release of sibling asarm-peptides (minhibins): Asarm-peptide(s) are directly responsible for defective mineralization in hyp. Endocrinology. 149(4):1757-1772.

McKee MD, Hoac B, Addison WN, Barros NM, Millan JL, Chaussain C. 2013. Extracellular matrix mineralization in periodontal tissues: Noncollagenous matrix proteins, enzymes, and relationship to hypophosphatasia and x-linked hypophosphatemia. Periodontology 2000. 63(1):102-122.

Miura M, Gronthos S, Zhao M, Lu B, Fisher LW, Robey PG, Shi S. 2003. Shed: Stem cells from human exfoliated deciduous teeth. Proceedings of the National Academy of Sciences of the United States of America. 100(10):5807-5812.

Quarles LD. 2003. Fgf23, phex, and mepe regulation of phosphate homeostasis and skeletal mineralization. American journal of physiology Endocrinology and metabolism. 285(1):E1-9.

Sitara D, Razzaque MS, Hesse M, Yoganathan S, Taguchi T, Erben RG, Juppner H, Lanske B. 2004. Homozygous ablation of fibroblast growth factor-23 results in hyperphosphatemia and impaired skeletogenesis, and reverses hypophosphatemia in phex-deficient mice. Matrix biology : journal of the International Society for Matrix Biology. 23(7):421-432.

Xiao ZS, Crenshaw M, Guo R, Nesbitt T, Drezner MK, Quarles LD. 1998. Intrinsic mineralization defect in hyp mouse osteoblasts. The American journal of physiology. 275(4 Pt 1):E700-708.

Yoshiko Y, Wang H, Minamizaki T, Ijuin C, Yamamoto R, Suemune S, Kozai K, Tanne K, Aubin JE, Maeda N. 2007. Mineralized tissue cells are a principal source of fgf23. Bone. 40(6):1565-1573.

Zelenchuk LV, Hedge A-M, Rowe PS. 2014. Phex mimetic (spr4-peptide) corrects and improves hyp and wild type mice energy-metabolism. PloS one. 9(5):e97326.

FIGURES LEGENDS

Figure 1: Decreased mineralization in XLH cells-seeded scaffolds. (Panel A) Micro-computed tomography 3D reconstructions of control (A) and XLH (B) pulp cells-seeded scaffolds at Day 24 treated with the same osteogenic conditions: 300 µM L-ascorbic acid sodium salt, 10 nM dexamethasone, 4% fetal bovine serum, and 1% penicillin/streptomycin supplemented with 10 mM β-glycerophosphate. Note the white mineral phases spread inside the green collagenous scaffolds. Scale bars, 1 mm. **(C, D)** Light micrographs of Ctrl and XLH scaffolds stained with von Kossa for mineral (black staining). Scale bars, 100 µm. Mineral phase quantity assessed by micro-CT and von Kossa reaction. (Panel B) Calcium quantification and Raman spectroscopy measurements of the mineral phase (XLH, grey bars). Data are means ± SD, n=9 per group, $p<.05$.

Figure 2: Impaired mineral quality of XLH cell-seeded scaffolds. **(A, B)** At the ultrastructural level, SEM observations show mineral-encrusted collagen fibrils (arrowheads). Scale bars, 20 µm. Insets display Energy-dispersive X-ray (EDS) microanalysis of mineralized areas in Ctrl and XLH scaffolds with major spectral peaks for calcium (Ca), phosphorus (P) consistent with the mineral phase being hydroxyapatite. **(C)** Raman spectra of Ctrl and XLH pulp cells-seeded scaffolds at Day 24 treated with the same osteogenic conditions showing characteristic peaks for phosphate. Compared with Ctrl scaffolds, no carbonate band **(D)** and a decrease of the relative value of crystallinity ratio **(E)** are found in XLH scaffolds. Data are means ± SD, n=9 per group, $p<.05$.

Figure 3: Increased ALP enzyme activity in XLH pulp cells-seeded scaffolds. **(A, B)** ALP activity (blue staining) is strong in XLH compared with Ctrl cells in 3D scaffolds. **(C)** The number of ALP positive cells is higher in XLH cells-seeded scaffolds than in Ctrl. Scale bars, 25 µm, insets, 10 µm. Data are means ± SD, n=15 per group, $p<.05$.

Figure 4: (A, B) OPN immunohistochemistry (red). Whereas a faint immunostaining for OPN in controls occurs in pulp cells, in XLH scaffolds, OPN prominently localizes to the mineral phase in the extracellular matrix (brackets). Scale bars, 10 µm. **(C, D)** Ultrastructural immunogold labeling for OPN visualized by transmission electron microscopy in control and XLH scaffolds confirm higher levels of OPN in the mineral structures of PHEX-deficient cell-seeded scaffolds (XLH, arrowheads). Scale bars, 1 µm. **(E)** Western blotting for OPN of scaffolds total extracts reveals full-length OPN as a typical broad band and multiple OPN bands with ~50; 60; 75 kDa fragments in XLH that are not present in control scaffolds samples. In all cases, OPN levels were greatly increased in XLH scaffolds as compared to controls. **(F)** Quantitative analysis confirms a higher level of OPN in XLH scaffold samples compared to control scaffold samples, with a ratio of 5.67 in XLH patients.

Figure 1

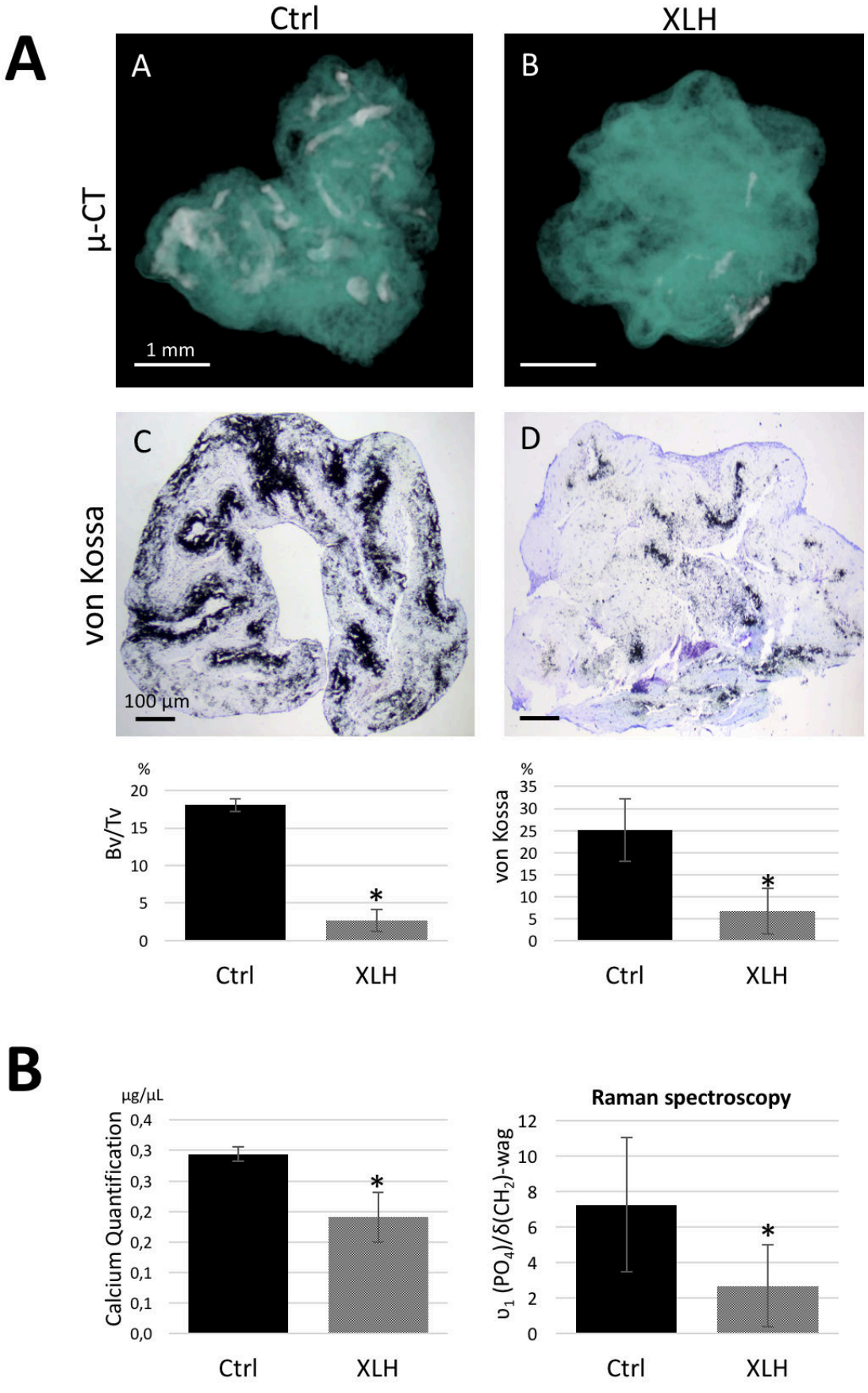
A
Ctrl
XLH
µ-CT
A
B
1 mm
von Kossa
C
D
100 µm
%
Bv/Tv
20
15
10
5
0
*
Ctrl
XLH
%
von Kossa
35
30
25
20
15
10
5
0
*
Ctrl
XLH
B
µg/µL
Calcium Quantification
0,4
0,3
0,3
0,2
0,2
0,1
0,1
0,0
*
Ctrl
XLH
Raman spectroscopy
υ1 (PO4)/δ(CH2)-wag
12
10
8
6
4
2
0
*
Ctrl
XLH

Figure 2

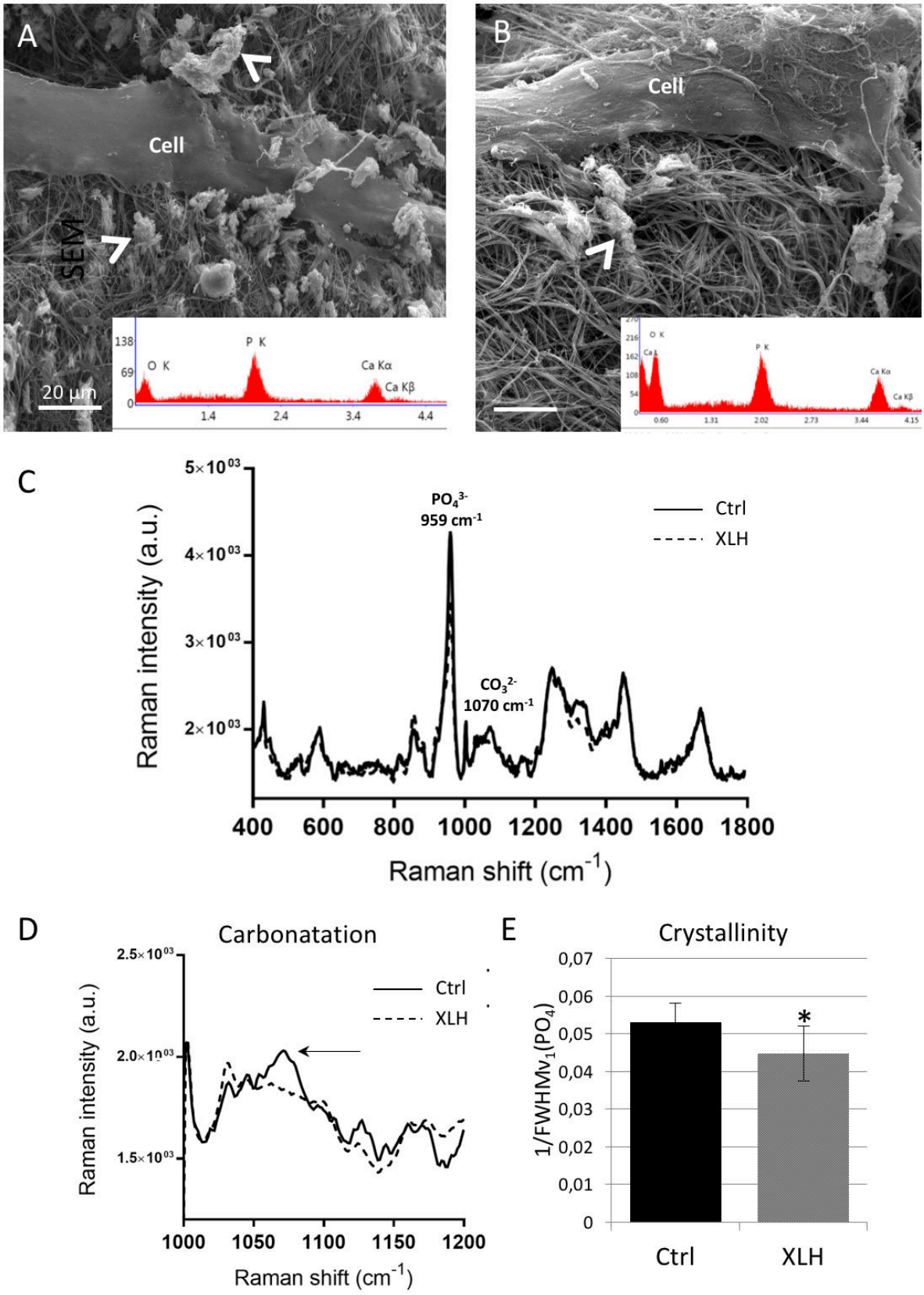
A
Cell
SEM
20 µm
O K
P K
Ca Kα
Ca Kβ
B
Cell
C
Raman intensity (a.u.)
Raman shift (cm-1)
PO4 3-
959 cm-1
CO3 2-
1070 cm-1
Ctrl
XLH
D
Carbonatation
Raman intensity (a.u.)
Raman shift (cm-1)
Ctrl
XLH
E
Crystallinity
1/FWHMν1(PO4)
Ctrl
XLH
*

Figure 3

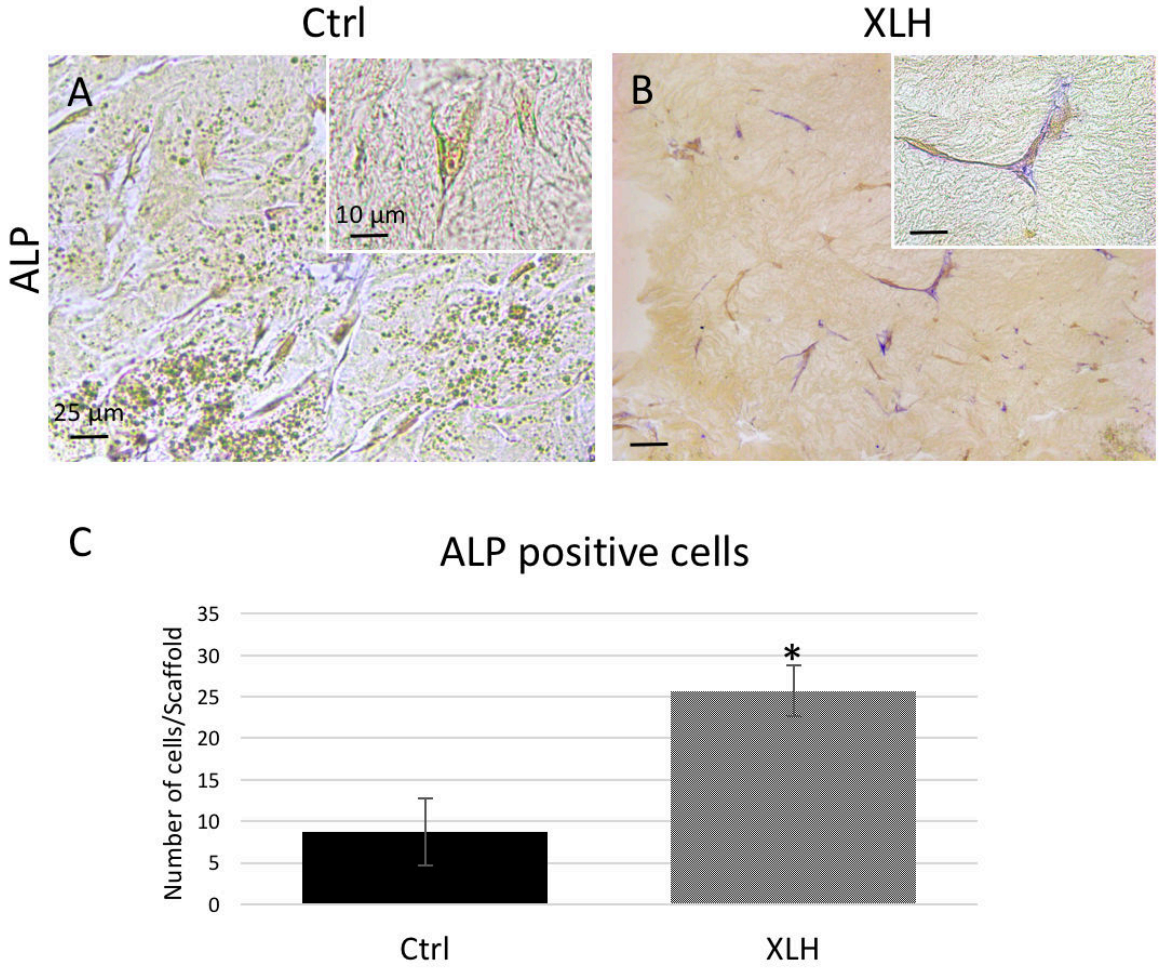
Ctrl
XLH
ALP
A
B
10 µm
25 µm
C
ALP positive cells
Number of cells/Scaffold
35
30
25
20
15
10
5
0
*
Ctrl
XLH

Figure 4

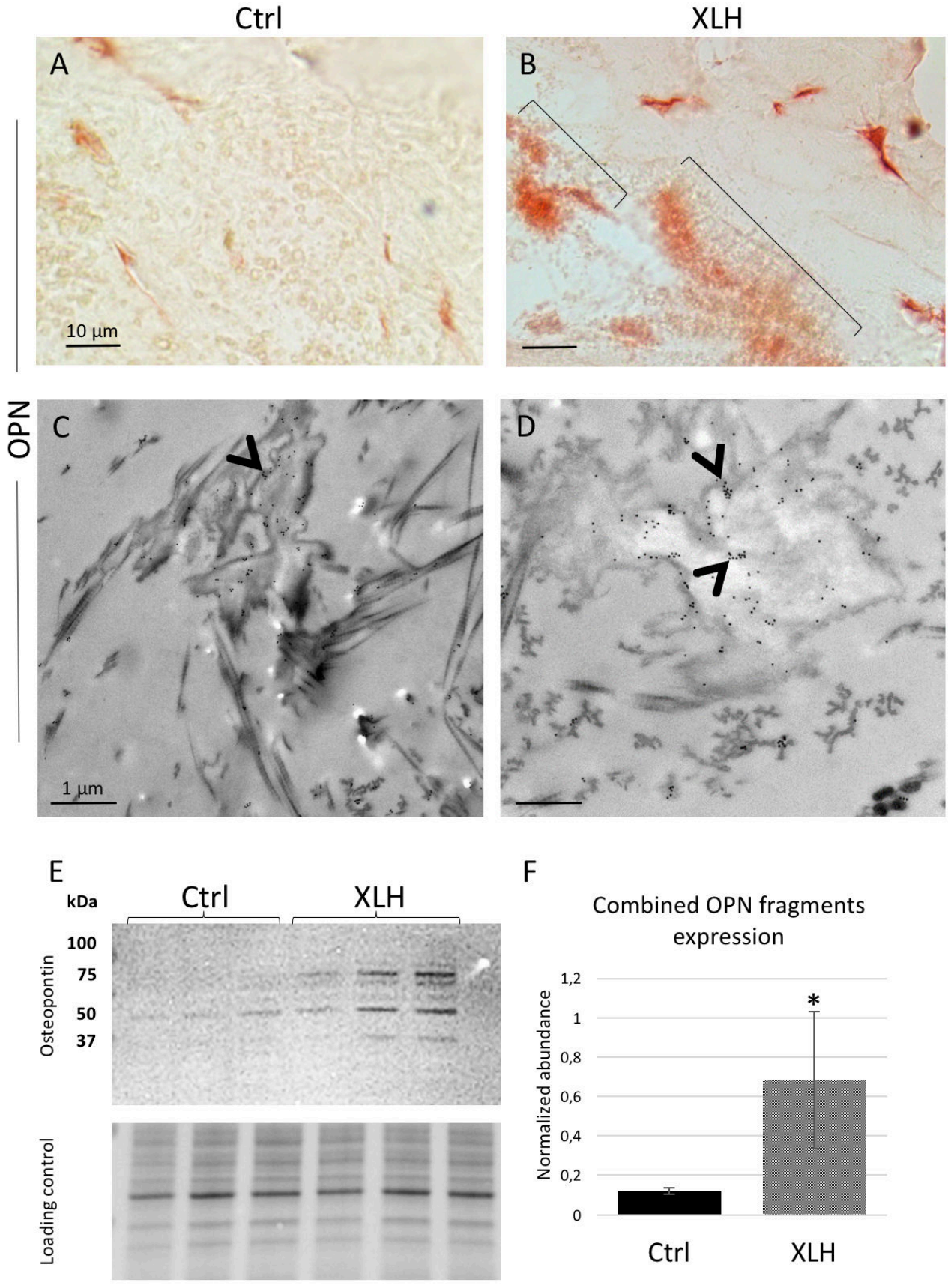
Ctrl
XLH
A
B
10 µm
OPN
C
D
1 µm
E
kDa
Ctrl
XLH
100
75
50
37
Osteopontin
Loading control
F
Combined OPN fragments expression
Normalized abundance
1,2
1
0,8
0,6
0,4
0,2
0
*
Ctrl
XLH

Appendix 1

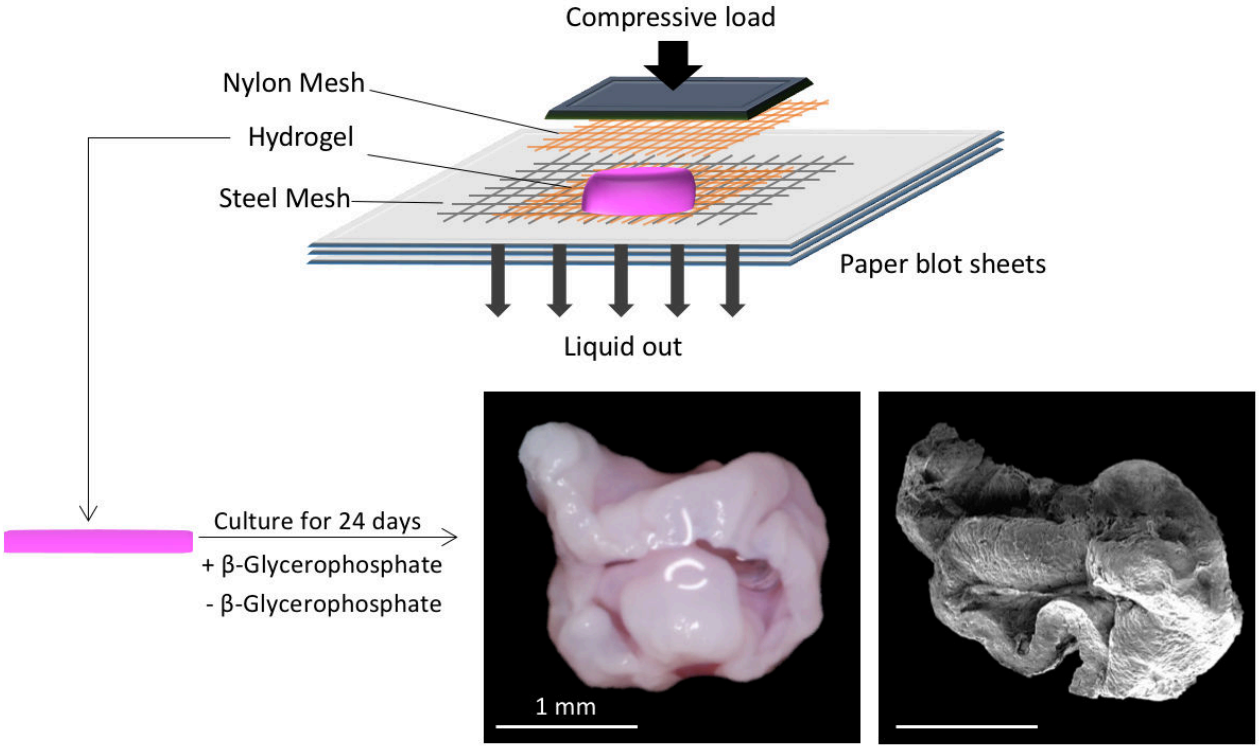

Appendix 1: Plastic compression of Highly hydrated hydrogels. Gel are placed on a stack of blotting paper, nylon mesh, and metal mesh, and subjected to plastic compression using an unconfined compressive stress of 0.5 kPa for 5 min to remove the excess casting fluid. After compression, dense Ctrl and XLH cellularized discs (16 mm diameter) are cultured for 24 days in osteogenic medium (DMEM media supplemented with 300 µM L-ascorbic acid sodium salt, 10 nM dexamethasone, 4% fetal bovine serum, and 1% penicillin/streptomycin) either supplemented with 10 mM β-glycerophosphate (+P) or no β-glycerophosphate supplementation (-P).

Appendix 2

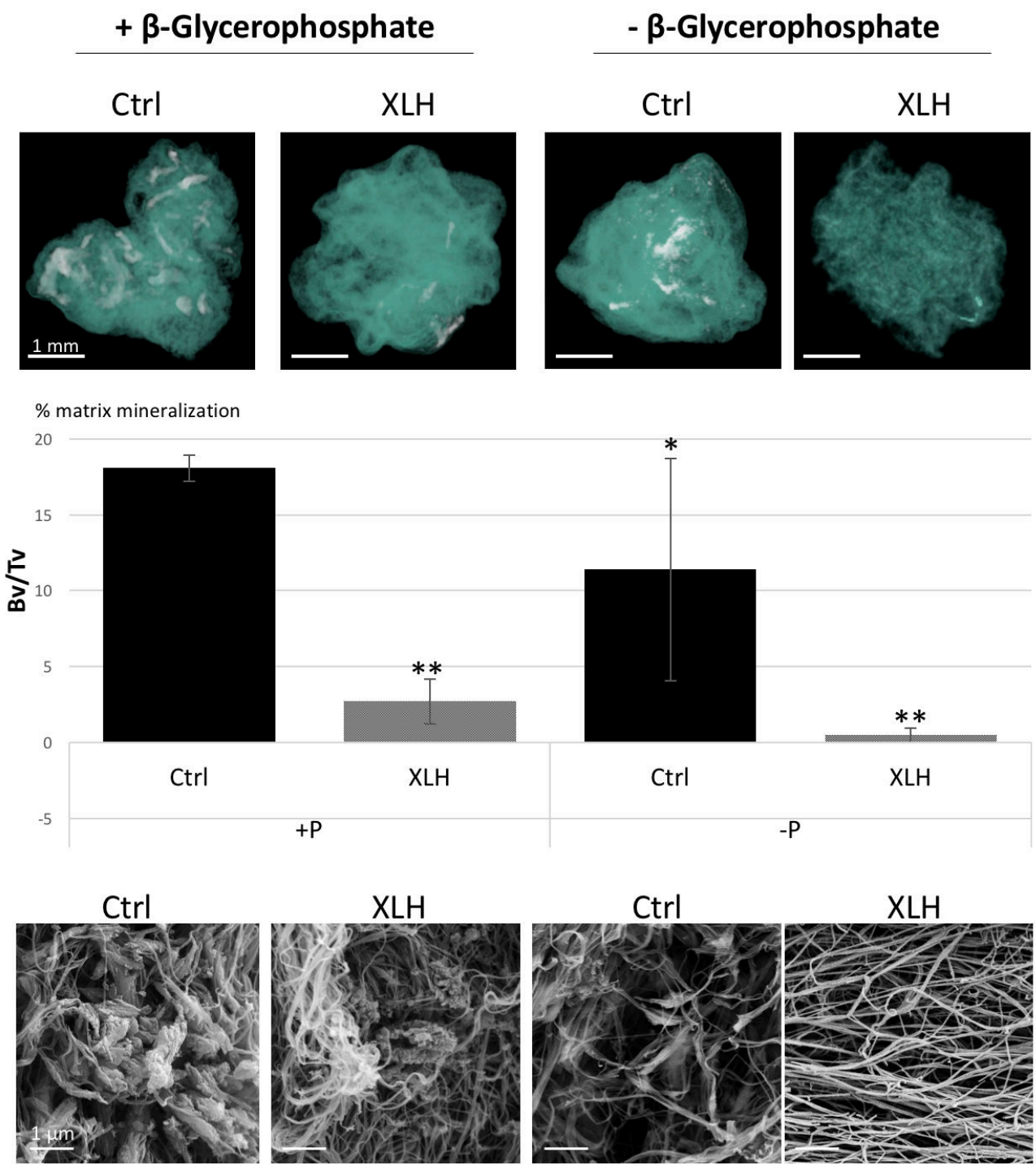

Appendix 2: Micro-CT 3D reconstruction of Ctrl and XLH cells-seeded scaffolds cultured in +P and -P media with a measurement of mineral phases in each condition Data are means ± SD, n=9 per group, p<.05. Ultrastructural scanning electron microscopy image of each condition.

Appendix 3

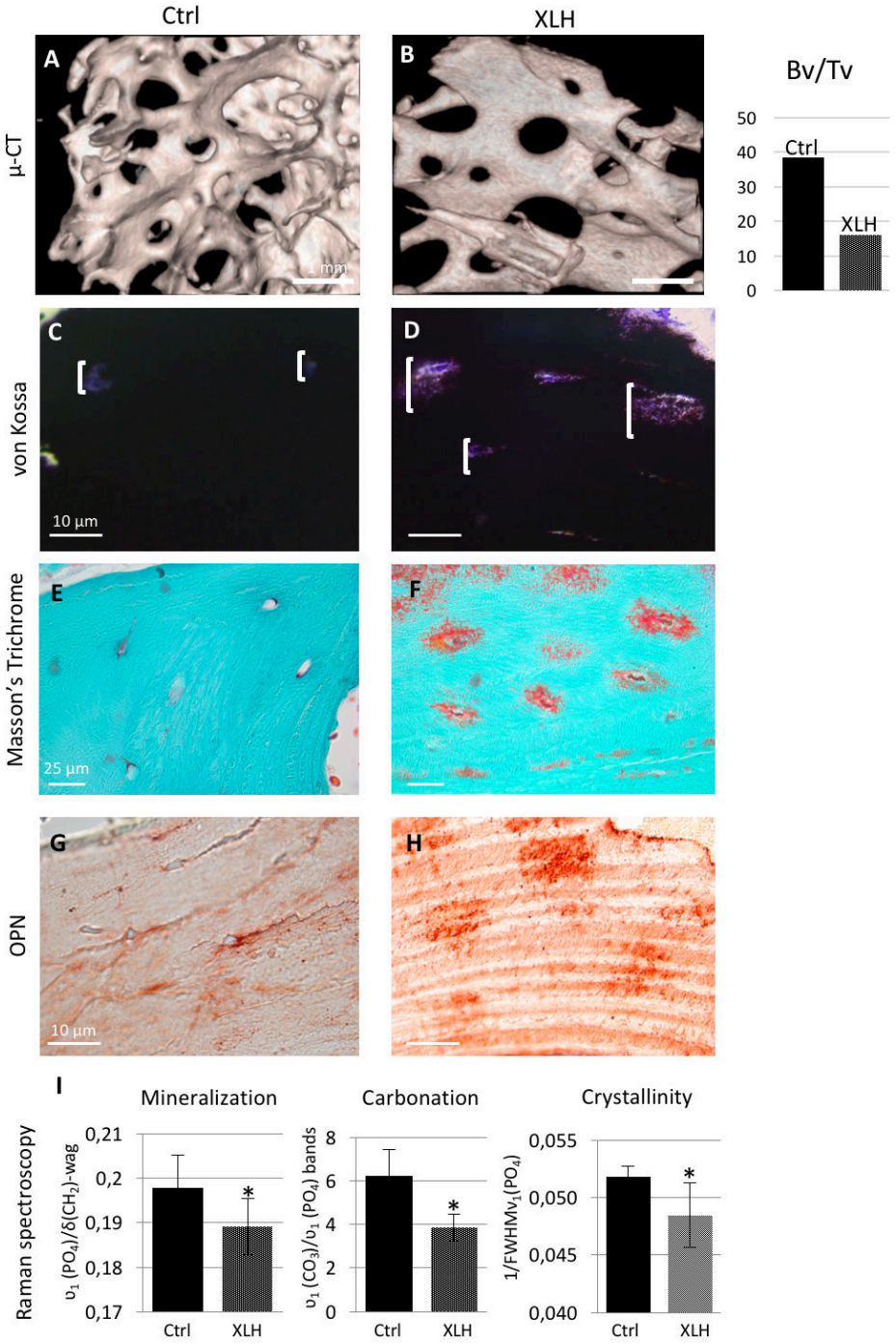

Appendix 3: Human appendicular bone tissue. (A, B) Micro-CT 3D reconstruction of Ctrl and XLH tibia samples with a measurement bone volume over total volume measurements. **(C-F)** von Kossa + toluidine blue and Masson's trichrome stainings revealing ostomalacia in XLH appendicular bone tissue. **(G, H)** OPN accumulation in periosteocytic lesions of XLH bone. **(I)** Raman spectroscopy analysis showing impaired mineralization and mineral quality in XLH bone. Data are means ± SD, p<.05.

8 General discussion, conclusion and future perspectives

8.1 XLH periodontium and local cell-mediated mineralization

Disorders in mineral metabolism can lead to skeletal alterations, including osteomalacia and diffuse ectopic precipitation of calcium and phosphate in soft tissues, leading to widespread organ dysfunction and damage. Investigation on the pathogenesis of inherited genetic disorders affecting the mineral metabolism, such as hypophosphatasia, permitted to unravel molecular pathways affecting bone and other organs. X-linked hypophosphatemia (XLH) is a genetic disorder (1:20,000 live births) of phosphate metabolism caused to *PHEX* mutations, resulting in severe skeletal and dental defects. Periodontitis is an inflammatory widespread disease affecting nearly 50% of the US adult population that leads to multiple tooth loss in its most severe form (8.5% of the adult population). Case series studies have recently proposed a higher susceptibility of XLH patients to developing periodontitis.

The aim of this dissertation was to investigate the impact of X-linked hypophosphatemia upon the periodontium and local cell-mediated mineralization. This study has shown that XLH/*Hyp* periodontium was dramatically affected, displaying cementum hypoplasia, “cementomalacia”, a lack of ligament anchorage and osteomalacia, with reduced mineral quality resulting in decreased adaptive capacities to tooth movement and to alveolar bone repair with an impaired formation of cellular cementum and bone. In addition, this study has demonstrated in human cells that PHEX deficiency locally affects the mineral phase formation and quality, independently of the phosphate concentration.

8.2 OPN and mineralization defects in XLH

OPN is a potent inhibitor of mineralization, it has been shown to be a substrate for PHEX, and its processing is impaired both *in vivo* in human and murine bone (Barros et al. 2013; Boukpessi et al. 2016) and *in vitro* where it is accumulated as several fragments, as we found in this study. Our results showing a tissue-specific expression/accumulation of OPN in bone whereas every mineralized tissue (i.e. bone, acellular and cellular cementum) was similarly

affected in XLH/*Hyp* suggest that contrary to previous reports (Barros et al. 2013; Boukpessi et al. 2016; Salmon et al. 2014), OPN is not the only etiologic factor in the hampered formation and impaired quality of XLH mineralized tissues. The bone accumulation of OPN in XLH is also found *in vitro*, in phosphate-normalized conditions of 3D scaffolds seeded with dental pulp cells, and so OPN is not either reflecting the involvement of bone to remodeling or P_i homeostasis. The weak signal of OPN in mineralized tissues other than bone and dentin suggests that OPN processing and accumulation are tissue-specific factors that contribute to the impaired mineralization in XLH, but other factors – such as other SIBLINGs – might play the same role in cementum. The specific pathologic role played by OPN in XLH could be further investigated by the generation of *Hyp/opn* KO cross compound mice to test the possible resolution of bone defects. Further investigations are needed to identify the inhibitors of cementum mineralization/formation in XLH.

8.3 XLH and periodontitis

Our observation that XLH patients are more prone to develop periodontitis extends the clinical dental scope of XLH (Foster et al. 2014b; Opsahl Vital et al. 2012), that was mainly described for its endodontic lesions with the so-called “spontaneous dental abscesses” (Chaussain-Miller et al. 2007; Chaussain-Miller et al. 2003). Our results in XLH/*Hyp* periodontium are broadly consistent with the literature in the *Phex*-mutated *Hyp* mouse reporting acellular cementum hypoplasia and alveolar bone osteoidosis (Fong et al. 2009; Koehne et al. 2013). These findings concur with a DMP1-deficient mouse model of hypophosphatemia (Ye et al. 2008), where alveolar bone and cementum defects were also reported. In hypophosphatasia, where TNAP is deficient, severe constitutional defects in bone and acellular cementum also result in a dramatic lack of ligament anchorage, leading to the exfoliation of rooted deciduous teeth (Chapple 1993; Foster et al. 2012; Linglart and Biosse-Duplan 2016; McKee et al. 2013). In hypophosphatemia, no spontaneous rooted tooth exfoliation has been reported in the literature and in our observations. Compared with other systemic conditions that represent a risk factor to periodontitis, such as uncontrolled diabetes (Kinane et al. 2006), the mean periodontal loss of attachment in XLH patients with erratic treatment during childhood is clinically mild. The most likely explanation of the

differential consequence on the periodontium resulting from TNAP and PHEX or DMP1 deficiencies is that systemic phosphate level/PHEX regulation (and likely DMP1 regulation) is less critical to maintain a functional periodontium than local phosphate:pyrophosphate ratio/ALP regulation (Foster et al. 2012). However, in X-linked hypophosphatemia, every mineralized periodontal tissue was affected, including cellular cementum, which is unaffected in hypophosphatasia (Foster et al. 2015). Our data support the inclusion of XLH besides HPP among the AAP classification of periodontal conditions associated with genetic disorders (Armitage 1999).

IV. Periodontitis as a Manifestation of Systemic Diseases
A. Associated with hematological disorders
1. Acquired neutropenia
2. Leukemias
3. Other
B. Associated with genetic disorders
1. Familial and cyclic neutropenia
2 Down syndrome
3. Leukocyte adhesion deficiency syndromes
4. Papillon-Lefèvre syndrome
5. Chediak-Higashi syndrome
6. Histiocytosis syndromes
7. Glycogen storage disease
8. Infantile genetic agranulocytosis
9. Cohen syndrome
10. Ehlers-Danlos syndrome (Types IV and VIII)
11. Hypophosphatasia
12. Other

Table 3 Classification of Periodontal Diseases and Conditions

Extract from the classification accepted by the American Academy of Periodontology

from Armitage, 1999, Annals of Periodontology

8.4 Tooth movement adaptation in the *Hyp* mouse

When challenged to functional solicitations, *Hyp* periodontium presented defective adaptive faculties. The experimental model of tooth movement was adapted from a rat model (Tran Van and Mailland 1981) where it was shown that unloaded teeth over-erupted/egressed following the extraction of antagonist teeth. Remodeling/modeling in the alveolar bone and cellular cementum, respectively, was shown to adapt the tooth to its migration. This model

has recently been adapted to the murine model (Salmon et al. 2016). In this research dissertation, we showed an impacted formation of cellular cementum in the *Hyp* mouse, and so an impaired adaptive capacity to tooth movement, with clinical consequences in terms of trauma response and orthodontic treatments.

8.5 Alveolar bone healing in the *Hyp* mouse

Our other experimental model investigated alveolar bone repair in a modified model of ligature-induced periodontitis. The fact that periodontitis is not uniquely a human disease (Page and Schroeder 1982) and involves common pathogenic mechanisms among different species validates the use of animal models to study periodontal pathobiology. Several other species than mice have been tested to mimic periodontitis, each with specific limitations and advantages, and a variety of different animals such as rats, dogs, and non-human primates have been used in periodontal wound healing research (Pellegrini et al. 2009). In our study, the murine model was the only choice of interest because of the availability of the *Hyp* mouse natural mutant (The HYP consortium). Ligature-induced periodontitis has extensively been described (Abe and Hajishengallis 2013; de Molon et al. 2014; Emerton et al. 2011; Kimura et al. 2000; Li and Amar 2007; Saadi-Thiers et al. 2013). This model presents major limitations, as it mimics an acute inflammation assessed by alveolar bone level changes contrary to periodontitis which is rather chronic and assessed by pocket formation and apical migration of the gingival junctional epithelium (Lang and Lindhe 2015). The placement of silk ligatures around posterior teeth facilitates local accumulation of indigenous bacteria and enhances bacteria-mediated gingival inflammation and bone loss. On the contrary, in other models of periodontitis induction, such as oral gavage model, gingival inflammation and bone loss are slowly induced following oral inoculation with bacteria associated with human periodontitis. Periodontitis-associated microbiotas in mice and humans differ, but this is not a prohibitive factor since periodontitis is a dysbiotic inflammatory disease (Hajishengallis 2014) and dysbiosis is dependent on any altered microbial community (Knights et al. 2013).

Defect type	Animal model	Advantages	Disadvantages
Furcation/infrabony periodontal defect	Dog and monkey	Surgical acute/chronic • short time to be created – less expensive • standardized morphological characteristics • does not regenerate spontaneously (chronic) • Class II–III furcation • bilateral similar defect • horizontal defect allows an estimation of the origin of the newly formed tissue • solid database describing healing (dog) • minimal palatal recession (monkey)	Surgical acute • does not reproduce inflammatory/ infective conditions • spontaneous partial regeneration (monkey) Surgical chronic • soft tissues compromised • variable amount of connective tissue regeneration
		Ligature induced • microbiological features similar to those of humans • morphological features similar to those of humans • does not regenerate spontaneously • can make similar lesions as control in contralateral defects	Ligature induced • nonpredictable disease development • nonstandardized defect morphology (dog) • requires time to be created and is expensive
Alveolar socket	Dog and monkey	Easy and fast to perform Reproduces well the events occurring in bone healing	Rapid bone repair compared with that for human (dog)
Infrabony peri-implant defect	Dog and monkey	Surgically created • short time needed to generate the defect • standard morphology-dimension Ligature induced • morphological and microbiological similarities with humans	Surgically created • spontaneous regeneration Ligature induced • spontaneous partial regeneration • long time required to generate the defect
Supra-alveolar peri-implant defect	Dog	Limited spontaneous regeneration Reproducibly created	Requires space-providing devices

Table 4 Commonly used periodontal models for reconstructive therapies

from Pellegrini et al. 2009, reprinted from Sculean et al., 2015, with permission from Wiley & Sons

In the limits of our ligature-induced alveolar bone breakdown and repair murine model, we investigated a specific hypothesis to test a discrete aspect of *Hyp* pathogenesis (Graves et al. 2008): alveolar bone repair following periodontal destruction is impaired. Indeed, after ligature-induced alveolar bone loss, the removal of ligatures and demeclocycline injections enabled a complete WT bone healing, that was dramatically impaired in *Hyp* mice. On the other hand, our clinical data showed that XLH patients with late or erratic treatments during childhood presented more frequent and more severe periodontitis, with more intrabony defects, that could be prevented with current treatment strategies. It is not known how new monoclonal antibody raised against human FGF23 (KRN23) that are tested in a phase 3 clinical trial in adult patients will impact the periodontium and periodontal condition (Imel et al. 2015).

8.6 PHEX deficiency impacts cell-autonomous mineralization

Local defects caused by PHEX deficiency in XLH have long been alleged because of the accumulating evidence from murine and *in vitro* studies showing an intrinsic *Hyp* osteoblasts-mediated impaired mineralization (Ecarot et al. 1992; Xiao et al. 1998), and showing that substrates for PHEX were among the SIBLING proteins (MEPE, DMP1, OPN) (Rowe 2015) located in mineralized tissues extracellular matrices.

Although *Hyp/Fgf23* knockout cross compound mice have a resolution of rickets, they still present osteomalacia (Liu et al. 2006; Sitara et al. 2004); on the other hand, transgenic expression of *Phex* in the *Hyp* mouse restores the bone phenotype without restoring P_i metabolism deficiencies (Erben et al. 2005b; Zelenchuk et al. 2014a). These studies revealed the presence of local defects unrelated to FGF23/hypophosphatemia in the *Hyp* mouse.

However, in humans with scarcer forms of hypophosphatemic rickets unrelated to PHEX, such as *FGF23* mutations (ADHR, autosomal dominant), *DMP1* mutations (ARHR, autosomal recessive) or tumor-induced osteomalacia (TIO), the pathologic phenotype seems clinically similar to XLH (Carpenter 2012), minoring the local direct role of PHEX in the pathobiology of XLH. The main pathologic feature causing rickets being hypophosphatemia, treatment strategies have focused on approaching the lower limit of physiologic plasma P_i level, thus restoring a proper skeletal and dental mineralization (Carpenter et al. 2011; Linglart et al. 2014). Here, we performed the first study that addressed local mineralization defects from human primary cells. The use of dental pulp cells was justified by their availability in routine extraction procedures following, or prior to orthodontic therapy, compared with primary osteoblastic cells, and by their capacity to differentiate *in vitro* into osteoblast-like cells with no secretion of dentin sialophosphoprotein (Coyac et al. 2013; Pedraza et al. 2010). We showed that in regular phosphate concentration, PHEX-deficient cells resulted in a reduced quantity of mineral with an impaired quality, displaying lower carbonation and lower crystallinity measured by Raman microspectroscopy. These results are consistent with the pathologic features observed in XLH appendicular bone and might partly explain its lower mineral quality. Whereas FGF23-mediated hypophosphatemia is the main pathologic aspect

of XLH, there also exists a PHEX deficiency-mediated impaired mineralization that current treatments neglect to target.

The exact role played by local defects resulting from PHEX deficiency in XLH pathogenesis might be further assessed by comparing cell-autonomous mineralization obtained from primary cultures of osteogenic cells obtained from ADHR, ARHR and XLH patients in addition to a comparison of the mineral phase in mineralized tissue samples from patients of each condition.

8.7 Conclusion and perspectives

In conclusion, XLH/*Hyp* displays an impacted periodontium, less prone to alveolar bone repair, tooth movement adaptation and trauma. Although patients present a higher susceptibility to periodontitis, it remains mild and improves with current systemic treatments. The difference with the periodontal condition of odonto/hypophosphatasia, another mineral homeostasis disorder, is that in XLH, every mineralized periodontal tissue is affected, with other consequences than the exfoliation of rooted teeth. The clinical implications of our findings consist in adapting elective procedures such as periodontal bone surgery and orthodontic therapy to the specific risks that XLH patients encounter as it relates to the hampered alveolar bone and cellular cementum formation. Osteopontin plays a role in the impaired mineralization of bone and dentin but does not seem to be involved in the defective XLH cementum. Overall, PHEX independently regulates mineralization at the local level and its loss of function impairs XLH extracellular matrix mineralization. Further complete treatment for XLH will need to address the local mineralization defects.

9 References

Abe T, Hajishengallis G. 2013. Optimization of the ligature-induced periodontitis model in mice. Journal of immunological methods. 394(1-2):49-54.

Addison WN, Azari F, Sorensen ES, Kaartinen MT, McKee MD. 2007. Pyrophosphate inhibits mineralization of osteoblast cultures by binding to mineral, up-regulating osteopontin, and inhibiting alkaline phosphatase activity. The Journal of biological chemistry. 282(21):15872-15883.

Addison WN, Masica DL, Gray JJ, McKee MD. 2010. Phosphorylation-dependent inhibition of mineralization by osteopontin asarm peptides is regulated by phex cleavage. Journal of bone and mineral research : the official journal of the American Society for Bone and Mineral Research. 25(4):695-705.

Addison WN, McKee MD. 2010. Asarm mineralization hypothesis: A bridge to progress. Journal of bone and mineral research : the official journal of the American Society for Bone and Mineral Research. 25(5):1191-1192.

Addison WN, Nakano Y, Loisel T, Crine P, McKee MD. 2008. Mepe-asarm peptides control extracellular matrix mineralization by binding to hydroxyapatite: An inhibition regulated by phex cleavage of asarm. Journal of bone and mineral research : the official journal of the American Society for Bone and Mineral Research. 23(10):1638-1649.

Albandar JM, Brunelle JA, Kingman A. 1999. Destructive periodontal disease in adults 30 years of age and older in the united states, 1988-1994. Journal of periodontology. 70(1):13-29.

Albright F, Butler AM, Bloomberg E. 1937. Rickets resistant to vitamin d therapy. American Journal of Diseases of Children. 54(3):529-547.

Alford AI, Hankenson KD. 2006. Matricellular proteins: Extracellular modulators of bone development, remodeling, and regeneration. Bone. 38(6):749-757.

Anderson PH, Lam NN, Turner AG, Davey RA, Kogawa M, Atkins GJ, Morris HA. 2013. The pleiotropic effects of vitamin d in bone. The Journal of steroid biochemistry and molecular biology. 136:190-194.

Aono Y, Yamazaki Y, Yasutake J, Kawata T, Hasegawa H, Urakawa I, Fujita T, Wada M, Yamashita T, Fukumoto S et al. 2009. Therapeutic effects of anti-fgf23 antibodies in hypophosphatemic rickets/osteomalacia. Journal of bone and mineral research : the official journal of the American Society for Bone and Mineral Research. 24(11):1879-1888.

Argiro L, Desbarats M, Glorieux FH, Ecarot B. 2001. Mepe, the gene encoding a tumor-secreted protein in oncogenic hypophosphatemic osteomalacia, is expressed in bone. Genomics. 74(3):342-351.

Armitage GC. 1999. Development of a classification system for periodontal diseases and conditions. Annals of periodontology / the American Academy of Periodontology. 4(1):1-6.

Atkins GJ, Rowe PS, Lim HP, Welldon KJ, Ormsby R, Wijenayaka AR, Zelenchuk L, Evdokiou A, Findlay DM. 2011. Sclerostin is a locally acting regulator of late-osteoblast/preosteocyte differentiation and regulates mineralization through a mepe-asarm-dependent mechanism. Journal of bone and mineral research : the

official journal of the American Society for Bone and Mineral Research. 26(7):1425-1436.

Autosomal dominant hypophosphataemic rickets is associated with mutations in fgf23. 2000. Nature genetics. 26(3):345-348.

Avery JK. 2011. Oral development and histology. Thieme.

Bai L, Collins JF, Ghishan FK. 2000. Cloning and characterization of a type iii na-dependent phosphate cotransporter from mouse intestine. American journal of physiology Cell physiology. 279(4):C1135-1143.

Bardet C, Delgado S, Sire JY. 2010. Mepe evolution in mammals reveals regions and residues of prime functional importance. Cellular and molecular life sciences : CMLS. 67(2):305-320.

Baron R. 2000. Anatomy and ultrastructure of bone - histogenesis, growth and remodeling. In: De Groot LJ, Beck-Peccoz P, Chrousos G, Dungan K, Grossman A, Hershman JM, Koch C, McLachlan R, New M, Rebar R et al., editors. Endotext. South Dartmouth (MA): MDText.com, Inc.

Baron R, Saito H, Gori F. 2012. Bone cells crosstalk: Noncanonical roring in the wnt. Cell metabolism. 15(4):415-417.

Barros NM, Hoac B, Neves RL, Addison WN, Assis DM, Murshed M, Carmona AK, McKee MD. 2013. Proteolytic processing of osteopontin by phex and accumulation of osteopontin fragments in hyp mouse bone, the murine model of x-linked hypophosphatemia. Journal of bone and mineral research : the official journal of the American Society for Bone and Mineral Research. 28(3):688-699.

Barthel TK, Mathern DR, Whitfield GK, Haussler CA, Hopper HA, Hsieh J-C, Slater SA, Hsieh G, Kaczmarska M, Jurutka PW. 2007. 1, 25-dihydroxyvitamin d 3/vdr-mediated induction of fgf23 as well as transcriptional control of other bone anabolic and catabolic genes that orchestrate the regulation of phosphate and calcium mineral metabolism. The Journal of steroid biochemistry and molecular biology. 103(3):381-388.

Bartold PM, Van Dyke TE. 2013. Periodontitis: A host-mediated disruption of microbial homeostasis. Unlearning learned concepts. Periodontology 2000. 62(1):203-217.

Beck GR, Jr., Sullivan EC, Moran E, Zerler B. 1998a. Relationship between alkaline phosphatase levels, osteopontin expression, and mineralization in differentiating mc3t3-e1 osteoblasts. Journal of cellular biochemistry. 68(2):269-280.

Beck GR, Jr., Zerler B, Moran E. 2000. Phosphate is a specific signal for induction of osteopontin gene expression. Proceedings of the National Academy of Sciences of the United States of America. 97(15):8352-8357.

Beck L, Karaplis AC, Amizuka N, Hewson AS, Ozawa H, Tenenhouse HS. 1998b. Targeted inactivation of npt2 in mice leads to severe renal phosphate wasting, hypercalciuria, and skeletal abnormalities. Proceedings of the National Academy of Sciences of the United States of America. 95(9):5372-5377.

Beck L, Leroy C, Beck-Cormier S, Forand A, Salaun C, Paris N, Bernier A, Urena-Torres P, Prie D, Ollero M et al. 2010. The phosphate transporter pit1 (slc20a1) revealed as a new essential gene for mouse liver development. PloS one. 5(2):e9148.

Beck L, Leroy C, Salaun C, Margall-Ducos G, Desdouets C, Friedlander G. 2009. Identification of a novel function of pit1 critical for cell proliferation and independent of its phosphate transport activity. The Journal of biological chemistry. 284(45):31363-31374.

Beck L, Soumounou Y, Martel J, Krishnamurthy G, Gauthier C, Goodyer CG, Tenenhouse HS. 1997. Pex/pex tissue distribution and evidence for a deletion in the 3' region of the pex gene in x-linked hypophosphatemic mice. The Journal of clinical investigation. 99(6):1200-1209.

Beertsen W, VandenBos T, Everts V. 1999. Root development in mice lacking functional tissue non-specific alkaline phosphatase gene: Inhibition of acellular cementum formation. Journal of dental research. 78(6):1221-1229.

Bellows CG, Heersche JN, Aubin JE. 1992. Inorganic phosphate added exogenously or released from beta-glycerophosphate initiates mineralization of osteoid nodules in vitro. Bone and mineral. 17(1):15-29.

Bergwitz C, Roslin NM, Tieder M, Loredo-Osti JC, Bastepe M, Abu-Zahra H, Frappier D, Burkett K, Carpenter TO, Anderson D et al. 2006. Slc34a3 mutations in patients with hereditary hypophosphatemic rickets with hypercalciuria predict a key role for the sodium-phosphate cotransporter napi-iic in maintaining phosphate homeostasis. American journal of human genetics. 78(2):179-192.

Berndt T, Craig TA, Bowe AE, Vassiliadis J, Reczek D, Finnegan R, Jan De Beur SM, Schiavi SC, Kumar R. 2003. Secreted frizzled-related protein 4 is a potent tumor-derived phosphaturic agent. The Journal of clinical investigation. 112(5):785-794.

Berndt T, Kumar R. 2009. Novel mechanisms in the regulation of phosphorus homeostasis. Physiology (Bethesda, Md). 24:17-25.

Berndt TJ, Bielesz B, Craig TA, Tebben PJ, Bacic D, Wagner CA, O'Brien S, Schiavi S, Biber J, Murer H et al. 2006. Secreted frizzled-related protein-4 reduces sodium-phosphate co-transporter abundance and activity in proximal tubule cells. Pflugers Archiv : European journal of physiology. 451(4):579-587.

Berndt TJ, Schiavi S, Kumar R. 2005. "Phosphatonins" and the regulation of phosphorus homeostasis. American journal of physiology Renal physiology. 289(6):F1170-1182.

Biosse Duplan M, Coyac BR, Bardet C, Zadikian C, Rothenbuhler A, Kamenicky P, Briot K, Linglart A, Chaussain C. 2016. Phosphate and vitamin d prevent periodontitis in x-linked hypophosphatemia. Journal of dental research.

Bloch L, Sineshchekova O, Reichenbach D, Reiss K, Saftig P, Kuro-o M, Kaether C. 2009. Klotho is a substrate for alpha-, beta- and gamma-secretase. FEBS letters. 583(19):3221-3224.

Bloch-Zupan A. 2016. Hypophosphatasia: Diagnosis and clinical signs - a dental surgeon perspective. International journal of paediatric dentistry. 26(6):426-438.

Bonewald LF. 2011. The amazing osteocyte. Journal of Bone and Mineral Research. 26(2):229-238.

Bonewald LF. 2012. Cell biology of craniofacial bone: Osteocytes. Mineralized Tissues in Oral and Craniofacial Science: Biological Principles and Clinical Correlates.63.

Bonewald LF, Wacker MJ. 2013. Fgf23 production by osteocytes. Pediatric nephrology (Berlin, Germany). 28(4):563-568.

Boskey AL, Coleman R. 2010. Aging and bone. Journal of dental research. 89(12):1333-1348.

Bosshardt DD, Selvig KA. 1997. Dental cementum: The dynamic tissue covering of the root. Periodontology 2000. 13:41-75.

Bouchard P, Carra MC, Boillot A, Mora F, Range H. 2016. Risk factors in periodontology: A conceptual framework. Journal of clinical periodontology.

Boukpessi T, Gaucher C, Leger T, Salmon B, Le Faouder J, Willig C, Rowe PS, Garabedian M, Meilhac O, Chaussain C. 2010. Abnormal presence of the matrix extracellular

phosphoglycoprotein-derived acidic serine- and aspartate-rich motif peptide in human hypophosphatemic dentin. The American journal of pathology. 177(2):803-812.

Boukpessi T, Hoac B, Coyac BR, Leger T, Garcia C, Wicart P, Whyte MP, Glorieux FH, Linglart A, Chaussain C et al. 2016. Osteopontin and the dento-osseous pathobiology of x-linked hypophosphatemia. Bone.

Boukpessi T, Septier D, Bagga S, Garabedian M, Goldberg M, Chaussain-Miller C. 2006. Dentin alteration of deciduous teeth in human hypophosphatemic rickets. Calcified tissue international. 79(5):294-300.

Bourgeois DM, Doury J, Hescot P. 1999. Periodontal conditions in 65-74 year old adults in france, 1995. International dental journal. 49(3):182-186.

Bouxsein ML, Boyd SK, Christiansen BA, Guldberg RE, Jepsen KJ, Muller R. 2010. Guidelines for assessment of bone microstructure in rodents using micro-computed tomography. Journal of bone and mineral research : the official journal of the American Society for Bone and Mineral Research. 25(7):1468-1486.

Brandi ML. 2009. Microarchitecture, the key to bone quality. Rheumatology (Oxford, England). 48 Suppl 4:iv3-8.

Bresler D, Bruder J, Mohnike K, Fraser WD, Rowe PS. 2004. Serum mepe-asarm-peptides are elevated in x-linked rickets (hyp): Implications for phosphaturia and rickets. The Journal of endocrinology. 183(3):R1-9.

Breusegem SY, Takahashi H, Giral-Arnal H, Wang X, Jiang T, Verlander JW, Wilson P, Miyazaki-Anzai S, Sutherland E, Caldas Y et al. 2009. Differential regulation of the renal sodium-phosphate cotransporters napi-iia, napi-iic, and pit-2 in dietary potassium deficiency. American journal of physiology Renal physiology. 297(2):F350-361.

Brockmann H. 1936. Die isolierung des antirachitischen vitamins aus thunfischleberöl. Hoppe-Seyler´ s Zeitschrift für physiologische Chemie. 241(1-3):104-115.

Brown A, Zhong M, Finch J, Ritter C, Slatopolsky E. 1995. The roles of calcium and 1, 25-dihydroxyvitamin d3 in the regulation of vitamin d receptor expression by rat parathyroid glands. Endocrinology. 136(4):1419-1425.

Brown RA, Wiseman M, Chuo CB, Cheema U, Nazhat SN. 2005. Ultrarapid engineering of biomimetic materials and tissues: Fabrication of nano- and microstructures by plastic compression. Advanced Functional Materials. 15(11):1762-1770.

Brownstein CA, Adler F, Nelson-Williams C, Iijima J, Li P, Imura A, Nabeshima Y, Reyes-Mugica M, Carpenter TO, Lifton RP. 2008. A translocation causing increased alpha-klotho level results in hypophosphatemic rickets and hyperparathyroidism. Proceedings of the National Academy of Sciences of the United States of America. 105(9):3455-3460.

Bruckner RJ, Rickles NH, Porter DR. 1962. Hypophosphatasia with premature shedding of teeth and aplasia of cementum. Oral surgery, oral medicine, and oral pathology. 15:1351-1369.

Capuano P, Radanovic T, Wagner CA, Bacic D, Kato S, Uchiyama Y, Arnoud RS-, Murer H, Biber J. 2005. Intestinal and renal adaptation to a low-pi diet of type ii napi cotransporters in vitamin d receptor-and 1αohase-deficient mice. American Journal of Physiology-Cell Physiology. 288(2):C429-C434.

Carpenter TO. 1997. New perspectives on the biology and treatment of x-linked hypophosphatemic rickets. Pediatric clinics of North America. 44(2):443-466.

Carpenter TO. 2012. The expanding family of hypophosphatemic syndromes. Journal of bone and mineral metabolism. 30(1):1-9.

Carpenter TO, Ellis BK, Insogna KL, Philbrick WM, Sterpka J, Shimkets R. 2005. Fibroblast growth factor 7: An inhibitor of phosphate transport derived from oncogenic osteomalacia-causing tumors. The Journal of clinical endocrinology and metabolism. 90(2):1012-1020.

Carpenter TO, Imel EA, Holm IA, Jan de Beur SM, Insogna KL. 2011. A clinician's guide to x-linked hypophosphatemia. Journal of bone and mineral research : the official journal of the American Society for Bone and Mineral Research. 26(7):1381-1388.

Cazalbou S, Combes C, Eichert D, Rey C, Glimcher MJ. 2004. Poorly crystalline apatites: Evolution and maturation in vitro and in vivo. Journal of bone and mineral metabolism. 22(4):310-317.

Chapple IL. 1993. Hypophosphatasia: Dental aspects and mode of inheritance. Journal of clinical periodontology. 20(9):615-622.

Chaussain-Miller C, Sinding C, Septier D, Wolikow M, Goldberg M, Garabedian M. 2007. Dentin structure in familial hypophosphatemic rickets: Benefits of vitamin d and phosphate treatment. Oral diseases. 13(5):482-489.

Chaussain-Miller C, Sinding C, Wolikow M, Lasfargues JJ, Godeau G, Garabedian M. 2003. Dental abnormalities in patients with familial hypophosphatemic vitamin d-resistant rickets: Prevention by early treatment with 1-hydroxyvitamin d. The Journal of pediatrics. 142(3):324-331.

Cheng PT, Pritzker KP. 1983. Pyrophosphate, phosphate ion interaction: Effects on calcium pyrophosphate and calcium hydroxyapatite crystal formation in aqueous solutions. The Journal of rheumatology. 10(5):769-777.

Christov M, Koren S, Yuan Q, Baron R, Lanske B. 2011. Genetic ablation of sfrp4 in mice does not affect serum phosphate homeostasis. Endocrinology. 152(5):2031-2036.

Cochran DL. 2008. Inflammation and bone loss in periodontal disease. Journal of periodontology. 79(8 Suppl):1569-1576.

Colard T, Falgayrac G, Bertrand B, Naji S, Devos O, Balsack C, Delannoy Y, Penel G. 2016. New insights on the composition and the structure of the acellular extrinsic fiber cementum by raman analysis. PloS one. 11(12):e0167316.

Collins JF, Bai L, Ghishan FK. 2004. The slc20 family of proteins: Dual functions as sodium-phosphate cotransporters and viral receptors. Pflugers Archiv : European journal of physiology. 447(5):647-652.

Coyac BR, Chicatun F, Hoac B, Nelea V, Chaussain C, Nazhat SN, McKee MD. 2013. Mineralization of dense collagen hydrogel scaffolds by human pulp cells. Journal of dental research. 92(7):648-654.

Cullinan MP, Westerman B, Hamlet SM, Palmer JE, Faddy MJ, Lang NP, Seymour GJ. 2001. A longitudinal study of interleukin-1 gene polymorphisms and periodontal disease in a general adult population. Journal of clinical periodontology. 28(12):1137-1144.

Cvek M, Mejare I, Andreasen JO. 2004. Conservative endodontic treatment of teeth fractured in the middle or apical part of the root. Dental traumatology : official publication of International Association for Dental Traumatology. 20(5):261-269.

D'Errico JA, MacNeil RL, Takata T, Berry J, Strayhorn C, Somerman MJ. 1997. Expression of bone associated markers by tooth root lining cells, in situ and in vitro. Bone. 20(2):117-126.

Dallas SL, Prideaux M, Bonewald LF. 2013. The osteocyte: An endocrine cell… and more. Endocrine reviews. 34(5):658-690.

Davey RA, Findlay DM. 2013. Calcitonin: Physiology or fantasy? Journal of bone and mineral research : the official journal of the American Society for Bone and Mineral Research. 28(5):973-979.

de Molon RS, de Avila ED, Boas Nogueira AV, Chaves de Souza JA, Avila-Campos MJ, de Andrade CR, Cirelli JA. 2014. Evaluation of the host response in various models of induced periodontal disease in mice. Journal of periodontology. 85(3):465-477.

Del Fattore A, Teti A, Rucci N. 2008. Osteoclast receptors and signaling. Archives of biochemistry and biophysics. 473(2):147-160.

Douyere D, Joseph C, Gaucher C, Chaussain C, Courson F. 2009. Familial hypophosphatemic vitamin d-resistant rickets--prevention of spontaneous dental abscesses on primary teeth: A case report. Oral surgery, oral medicine, oral pathology, oral radiology, and endodontics. 107(4):525-530.

Drezner MK. 2013. Chapter 32 - heritable renal phosphate wasting disorders a2 - thakker, rajesh v. In: Whyte MP, Eisman JA, Igarashi T, editors. Genetics of bone biology and skeletal disease. San Diego: Academic Press. p. 517-536.

Ebersole JL, Dawson DR, Morford LA, Peyyala R, Miller CS, Gonzaléz OA. 2013. Periodontal disease immunology: 'Double indemnity' in protecting the host. Periodontology 2000. 62(1):163-202.

Ecarot B, Glorieux FH, Desbarats M, Travers R, Labelle L. 1992. Defective bone formation by hyp mouse bone cells transplanted into normal mice: Evidence in favor of an intrinsic osteoblast defect. Journal of bone and mineral research : the official journal of the American Society for Bone and Mineral Research. 7(2):215-220.

Econs MJ, Drezner MK. 1994. Tumor-induced osteomalacia--unveiling a new hormone. The New England journal of medicine. 330(23):1679-1681.

Eicher EM, Southard JL, Scriver CR, Glorieux FH. 1976. Hypophosphatemia: Mouse model for human familial hypophosphatemic (vitamin d-resistant) rickets. Proceedings of the National Academy of Sciences of the United States of America. 73(12):4667-4671.

Ek-Rylander B, Andersson G. 2010. Osteoclast migration on phosphorylated osteopontin is regulated by endogenous tartrate-resistant acid phosphatase. Experimental cell research. 316(3):443-451.

Ek-Rylander B, Flores M, Wendel M, Heinegard D, Andersson G. 1994. Dephosphorylation of osteopontin and bone sialoprotein by osteoclastic tartrate-resistant acid phosphatase. Modulation of osteoclast adhesion in vitro. The Journal of biological chemistry. 269(21):14853-14856.

Eke PI, Dye BA, Wei L, Slade GD, Thornton-Evans GO, Borgnakke WS, Taylor GW, Page RC, Beck JD, Genco RJ. 2015. Update on prevalence of periodontitis in adults in the united states: Nhanes 2009 to 2012. Journal of periodontology. 86(5):611-622.

Eke PI, Dye BA, Wei L, Thornton-Evans GO, Genco RJ. 2012. Prevalence of periodontitis in adults in the united states: 2009 and 2010. Journal of dental research. 91(10):914-920.

el-Labban NG, Lee KW, Rule D. 1991. Permanent teeth in hypophosphatasia: Light and electron microscopic study. Journal of oral pathology & medicine : official publication of the International Association of Oral Pathologists and the American Academy of Oral Pathology. 20(7):352-360.

Emerton KB, Drapeau SJ, Prasad H, Rohrer M, Roffe P, Hopper K, Schoolfield J, Jones A, Cochran DL. 2011. Regeneration of periodontal tissues in non-human primates with rhgdf-5 and beta-tricalcium phosphate. Journal of dental research. 90(12):1416-1421.

Erben RG, Mayer D, Weber K, Jonsson K, Juppner H, Lanske B. 2005a. Overexpression of human phex under the human beta-actin promoter does not fully rescue the hyp mouse phenotype. Journal of bone and mineral research : the official journal of the American Society for Bone and Mineral Research. 20(7):1149-1160.

Erben RG, Mayer D, Weber K, Jonsson K, Jüppner H, Lanske B. 2005b. Overexpression of human phex under the human β-actin promoter does not fully rescue the hyp mouse phenotype. Journal of Bone and Mineral Research. 20(7):1149-1160.

Farr JN, Khosla S. 2015. Skeletal changes through the lifespan--from growth to senescence. Nature reviews Endocrinology. 11(9):513-521.

Farrow EG, Davis SI, Ward LM, White KE. 2007. The role of dmp1 in autosomal recessive hypophosphatemic rickets. Journal of musculoskeletal & neuronal interactions. 7(4):310-312.

Farrow EG, White KE. 2010. Recent advances in renal phosphate handling. Nature reviews Nephrology. 6(4):207-217.

Feng JQ, Ward LM, Liu S, Lu Y, Xie Y, Yuan B, Yu X, Rauch F, Davis SI, Zhang S et al. 2006. Loss of dmp1 causes rickets and osteomalacia and identifies a role for osteocytes in mineral metabolism. Nature genetics. 38(11):1310-1315.

Festing MH, Speer MY, Yang HY, Giachelli CM. 2009. Generation of mouse conditional and null alleles of the type iii sodium-dependent phosphate cotransporter pit-1. Genesis (New York, NY : 2000). 47(12):858-863.

Fisher LW, Fedarko NS. 2003. Six genes expressed in bones and teeth encode the current members of the sibling family of proteins. Connective tissue research. 44 Suppl 1:33-40.

Fleisch H, Bisaz S. 1962. Mechanism of calcification: Inhibitory role of pyrophosphate. Nature. 195:911.

Fleisch H, Straumann F, Schenk R, Bisaz S, Allgower M. 1966. Effect of condensed phosphates on calcification of chick embryo femurs in tissue culture. The American journal of physiology. 211(3):821-825.

Fong H, Chu EY, Tompkins KA, Foster BL, Sitara D, Lanske B, Somerman MJ. 2009. Aberrant cementum phenotype associated with the hypophosphatemic hyp mouse. Journal of periodontology. 80(8):1348-1354.

Forster I, Hernando N, Sorribas V, Werner A. 2011. Phosphate transporters in renal, gastrointestinal, and other tissues. Advances in chronic kidney disease. 18(2):63-76.

Foster BL, Nagatomo KJ, Nociti FH, Jr., Fong H, Dunn D, Tran AB, Wang W, Narisawa S, Millan JL, Somerman MJ. 2012. Central role of pyrophosphate in acellular cementum formation. PloS one. 7(6):e38393.

Foster BL, Nagatomo KJ, Tso HW, Tran AB, Nociti FH, Jr., Narisawa S, Yadav MC, McKee MD, Millan JI, Somerman MJ. 2013. Tooth root dentin mineralization defects in a mouse model of hypophosphatasia. Journal of bone and mineral research : the official journal of the American Society for Bone and Mineral Research. 28(2):271-282.

Foster BL, Nociti FH, Jr., Somerman MJ. 2014a. The rachitic tooth. Endocrine reviews. 35(1):1-34.

Foster BL, Popowics TE, Fong HK, Somerman MJ. 2007. Advances in defining regulators of cementum development and periodontal regeneration. Current topics in developmental biology. 78:47-126.

Foster BL, Ramnitz MS, Gafni RI, Burke AB, Boyce AM, Lee JS, Wright JT, Akintoye SO, Somerman MJ, Collins MT. 2014b. Rare bone diseases and their dental, oral, and craniofacial manifestations. Journal of dental research.

Foster BL, Sheen CR, Hatch NE, Liu J, Cory E, Narisawa S, Kiffer-Moreira T, Sah RL, Whyte MP, Somerman MJ et al. 2015. Periodontal defects in the a116t knock-in murine model of odontohypophosphatasia. Journal of dental research. 94(5):706-714.

Foster BL, Somerman MJ. 2012. Cementum. Mineralized tissues in oral and craniofacial science.169-181.

Foster BL, Tompkins KA, Rutherford RB, Zhang H, Chu EY, Fong H, Somerman MJ. 2008. Phosphate: Known and potential roles during development and regeneration of teeth and supporting structures. Birth defects research Part C, Embryo today : reviews. 84(4):281-314.

Francis F, Strom TM, Hennig S, Boddrich A, Lorenz B, Brandau O, Mohnike KL, Cagnoli M, Steffens C, Klages S et al. 1997. Genomic organization of the human pex gene mutated in x-linked dominant hypophosphatemic rickets. Genome research. 7(6):573-585.

Fraser D. 1957. Hypophosphatasia. The American journal of medicine. 22(5):730-746.

Fretz JA, Zella LA, Kim S, Shevde NK, Pike JW. 2007. 1, 25-dihydroxyvitamin d 3 induces expression of the wnt signaling co-regulator lrp5 via regulatory elements located significantly downstream of the gene's transcriptional start site. The Journal of steroid biochemistry and molecular biology. 103(3):440-445.

Fu Q, Jilka RL, Manolagas SC, O'Brien CA. 2002. Parathyroid hormone stimulates receptor activator of nfκb ligand and inhibits osteoprotegerin expression via protein kinase a activation of camp-response element-binding protein. Journal of Biological Chemistry. 277(50):48868-48875.

Fudge NJ, Kovacs CS. 2004. Physiological studies in heterozygous calcium sensing receptor (casr) gene-ablated mice confirm that the casr regulates calcitonin release in vivo. BMC physiology. 4(1):1.

Galliot B, Crescenzi M, Jacinto A, Tajbakhsh S. 2017. Trends in tissue repair and regeneration. Development (Cambridge, England). 144(3):357-364.

Gaucher C, Boukpessi T, Septier D, Jehan F, Rowe PS, Garabedian M, Goldberg M, Chaussain-Miller C. 2009a. Dentin noncollagenous matrix proteins in familial hypophosphatemic rickets. Cells, tissues, organs. 189(1-4):219-223.

Gaucher C, Walrant-Debray O, Nguyen TM, Esterle L, Garabedian M, Jehan F. 2009b. Phex analysis in 118 pedigrees reveals new genetic clues in hypophosphatemic rickets. Human genetics. 125(4):401-411.

Gemmell E, Marshall RI, Seymour GJ. 1997. Cytokines and prostaglandins in immune homeostasis and tissue destruction in periodontal disease. Periodontology 2000. 14:112-143.

Genco RJ, Borgnakke WS. 2013. Risk factors for periodontal disease. Periodontology 2000. 62(1):59-94.

A gene (pex) with homologies to endopeptidases is mutated in patients with x-linked hypophosphatemic rickets. The hyp consortium. 1995. Nature genetics. 11(2):130-136.

George A, Gui J, Jenkins NA, Gilbert DJ, Copeland NG, Veis A. 1994. In situ localization and chromosomal mapping of the ag1 (dmp1) gene. The journal of histochemistry and cytochemistry : official journal of the Histochemistry Society. 42(12):1527-1531.

George A, Veis A. 2008. Phosphorylated proteins and control over apatite nucleation, crystal growth, and inhibition. Chemical reviews. 108(11):4670-4693.

Giachelli CM, Steitz S. 2000. Osteopontin: A versatile regulator of inflammation and biomineralization. Matrix biology : journal of the International Society for Matrix Biology. 19(7):615-622.

Giral H, Caldas Y, Sutherland E, Wilson P, Breusegem S, Barry N, Blaine J, Jiang T, Wang XX, Levi M. 2009. Regulation of rat intestinal na-dependent phosphate transporters by dietary phosphate. American journal of physiology Renal physiology. 297(5):F1466-1475.

Glimcher MJ. 2006. Bone: Nature of the calcium phosphate crystals and cellular, structural, and physical chemical mechanisms in their formation. Reviews in mineralogy and geochemistry. 64(1):223-282.

Goetz R, Nakada Y, Hu MC, Kurosu H, Wang L, Nakatani T, Shi M, Eliseenkova AV, Razzaque MS, Moe OW et al. 2010. Isolated c-terminal tail of fgf23 alleviates hypophosphatemia by inhibiting fgf23-fgfr-klotho complex formation. Proceedings of the National Academy of Sciences of the United States of America. 107(1):407-412.

Goldblatt H, Soames KM. 1923. A study of rats on a normal diet irradiated daily by the mercury vapour quartz lamp or kept in darkness. Biochemical Journal. 17(2):294.

Graves DT, Fine D, Teng YT, Van Dyke TE, Hajishengallis G. 2008. The use of rodent models to investigate host-bacteria interactions related to periodontal diseases. Journal of clinical periodontology. 35(2):89-105.

Groeneveld MC, Everts V, Beertsen W. 1993. A quantitative enzyme histochemical analysis of the distribution of alkaline phosphatase activity in the periodontal ligament of the rat incisor. Journal of dental research. 72(9):1344-1350.

Groeneveld MC, Everts V, Beertsen W. 1995. Alkaline phosphatase activity in the periodontal ligament and gingiva of the rat molar: Its relation to cementum formation. Journal of dental research. 74(7):1374-1381.

Gronthos S, Arthur A, Bartold PM, Shi S. 2011. A method to isolate and culture expand human dental pulp stem cells. Methods in molecular biology (Clifton, NJ). 698:107-121.

Grskovic M, Javaherian A, Strulovici B, Daley GQ. 2011. Induced pluripotent stem cells—opportunities for disease modelling and drug discovery. Nature reviews Drug discovery. 10(12):915-929.

Gurley KA, Reimer RJ, Kingsley DM. 2006. Biochemical and genetic analysis of ank in arthritis and bone disease. American journal of human genetics. 79(6):1017-1029.

Hadjidakis DJ, Androulakis, II. 2006. Bone remodeling. Annals of the New York Academy of Sciences. 1092:385-396.

Haffajee AD, Socransky SS. 1994. Microbial etiological agents of destructive periodontal diseases. Periodontology 2000. 5:78-111.

Hajishengallis G. 2014. Immunomicrobial pathogenesis of periodontitis: Keystones, pathobionts, and host response. Trends in immunology. 35(1):3-11.

Hajishengallis G, Lamont RJ, Graves DT. 2015. The enduring importance of animal models in understanding periodontal disease. Virulence. 6(3):229-235.

Hansen NM, Felix R, Bisaz S, Fleisch H. 1976. Aggregation of hydroxyapatite crystals. Biochimica et biophysica acta. 451(2):549-559.

Harmey D, Hessle L, Narisawa S, Johnson KA, Terkeltaub R, Millan JL. 2004. Concerted regulation of inorganic pyrophosphate and osteopontin by akp2, enpp1, and ank: An integrated model of the pathogenesis of mineralization disorders. The American journal of pathology. 164(4):1199-1209.

Harmey D, Johnson KA, Zelken J, Camacho NP, Hoylaerts MF, Noda M, Terkeltaub R, Millan JL. 2006. Elevated skeletal osteopontin levels contribute to the hypophosphatasia phenotype in akp2(-/-) mice. Journal of bone and mineral research : the official journal of the American Society for Bone and Mineral Research. 21(9):1377-1386.

Hayashibara T, Hiraga T, Sugita A, Wang L, Hata K, Ooshima T, Yoneda T. 2007. Regulation of osteoclast differentiation and function by phosphate: Potential role of osteoclasts in the skeletal abnormalities in hypophosphatemic conditions. Journal of bone and mineral research : the official journal of the American Society for Bone and Mineral Research. 22(11):1743-1751.

He G, Dahl T, Veis A, George A. 2003. Dentin matrix protein 1 initiates hydroxyapatite formation in vitro. Connective tissue research. 44 Suppl 1:240-245.

He G, Gajjeraman S, Schultz D, Cookson D, Qin C, Butler WT, Hao J, George A. 2005. Spatially and temporally controlled biomineralization is facilitated by interaction between self-assembled dentin matrix protein 1 and calcium phosphate nuclei in solution. Biochemistry. 44(49):16140-16148.

Heitz-Mayfield LJ, Lang NP. 2013. Surgical and nonsurgical periodontal therapy. Learned and unlearned concepts. Periodontology 2000. 62(1):218-231.

Henry HL, Norman AW. 1974. Studies on calciferol metabolism ix. Renal 25-hydroxy-vitamin d3-1-hydroxylase. Involvement of cytochrome p-450 and other properties. Journal of Biological Chemistry. 249(23):7529-7535.

Hessle L, Johnson KA, Anderson HC, Narisawa S, Sali A, Goding JW, Terkeltaub R, Millan JL. 2002. Tissue-nonspecific alkaline phosphatase and plasma cell membrane glycoprotein-1 are central antagonistic regulators of bone mineralization. Proceedings of the National Academy of Sciences of the United States of America. 99(14):9445-9449.

Hienz SA, Paliwal S, Ivanovski S. 2015. Mechanisms of bone resorption in periodontitis. Journal of immunology research. 2015:615486.

Hilfiker H, Hattenhauer O, Traebert M, Forster I, Murer H, Biber J. 1998. Characterization of a murine type ii sodium-phosphate cotransporter expressed in mammalian small intestine. Proceedings of the National Academy of Sciences of the United States of America. 95(24):14564-14569.

Ho AM, Johnson MD, Kingsley DM. 2000. Role of the mouse ank gene in control of tissue calcification and arthritis. Science (New York, NY). 289(5477):265-270.

Hoac B, Kiffer-Moreira T, Millan JL, McKee MD. 2013. Polyphosphates inhibit extracellular matrix mineralization in mc3t3-e1 osteoblast cultures. Bone. 53(2):478-486.

Hoenderop JG, Nilius B, Bindels RJ. 2005. Calcium absorption across epithelia. Physiological reviews. 85(1):373-422.

Hu JC, Plaetke R, Mornet E, Zhang C, Sun X, Thomas HF, Simmer JP. 2000. Characterization of a family with dominant hypophosphatasia. European journal of oral sciences. 108(3):189-194.

Hu MC, Shi M, Zhang J, Pastor J, Nakatani T, Lanske B, Razzaque MS, Rosenblatt KP, Baum MG, Kuro-o M et al. 2010. Klotho: A novel phosphaturic substance acting as an autocrine enzyme in the renal proximal tubule. FASEB journal : official publication of the Federation of American Societies for Experimental Biology. 24(9):3438-3450.

Huang L, Salmon B, Yin X, Helms JA. 2016. From restoration to regeneration: Periodontal aging and opportunities for therapeutic intervention. Periodontology 2000. 72(1):19-29.

Ichikawa S, Imel EA, Kreiter ML, Yu X, Mackenzie DS, Sorenson AH, Goetz R, Mohammadi M, White KE, Econs MJ. 2007. A homozygous missense mutation in human klotho causes severe tumoral calcinosis. The Journal of clinical investigation. 117(9):2684-2691.

Imel EA, Econs MJ. 2005. Fibroblast growth factor 23: Roles in health and disease. Journal of the American Society of Nephrology : JASN. 16(9):2565-2575.

Imel EA, Zhang X, Ruppe MD, Weber TJ, Klausner MA, Ito T, Vergeire M, Humphrey JS, Glorieux FH, Portale AA et al. 2015. Prolonged correction of serum phosphorus in adults with x-linked hypophosphatemia using monthly doses of krn23. The Journal of clinical endocrinology and metabolism. 100(7):2565-2573.

Johnson K, Goding J, Van Etten D, Sali A, Hu SI, Farley D, Krug H, Hessle L, Millan JL, Terkeltaub R. 2003. Linked deficiencies in extracellular pp(i) and osteopontin mediate pathologic calcification associated with defective pc-1 and ank expression. Journal of bone and mineral research : the official journal of the American Society for Bone and Mineral Research. 18(6):994-1004.

Johnson K, Moffa A, Chen Y, Pritzker K, Goding J, Terkeltaub R. 1999. Matrix vesicle plasma cell membrane glycoprotein-1 regulates mineralization by murine osteoblastic mc3t3 cells. Journal of bone and mineral research : the official journal of the American Society for Bone and Mineral Research. 14(6):883-892.

Johnson K, Pritzker K, Goding J, Terkeltaub R. 2001. The nucleoside triphosphate pyrophosphohydrolase isozyme pc-1 directly promotes cartilage calcification through chondrocyte apoptosis and increased calcium precipitation by mineralizing vesicles. The Journal of rheumatology. 28(12):2681-2691.

Johnson KA, Hessle L, Vaingankar S, Wennberg C, Mauro S, Narisawa S, Goding JW, Sano K, Millan JL, Terkeltaub R. 2000. Osteoblast tissue-nonspecific alkaline phosphatase antagonizes and regulates pc-1. American journal of physiology Regulatory, integrative and comparative physiology. 279(4):R1365-1377.

Kaartinen MT, El-Maadawy S, Rasanen NH, McKee MD. 2002. Tissue transglutaminase and its substrates in bone. Journal of bone and mineral research : the official journal of the American Society for Bone and Mineral Research. 17(12):2161-2173.

Kaartinen MT, Murshed M, Karsenty G, McKee MD. 2007. Osteopontin upregulation and polymerization by transglutaminase 2 in calcified arteries of matrix gla protein-deficient mice. The journal of histochemistry and cytochemistry : official journal of the Histochemistry Society. 55(4):375-386.

Kaartinen MT, Sun W, Kaipatur N, McKee MD. 2005. Transglutaminase crosslinking of sibling proteins in teeth. Journal of dental research. 84(7):607-612.

Kantarci A, Hasturk H, Van Dyke TE. 2015. Animal models for periodontal regeneration and peri-implant responses. Periodontology 2000. 68(1):66-82.

Karring T, Isidor F, Nyman S, Lindhe J. 1985. New attachment formation on teeth with a reduced but healthy periodontal ligament. Journal of clinical periodontology. 12(1):51-60.

Kavanaugh MP, Kabat D. 1996. Identification and characterization of a widely expressed phosphate transporter/retrovirus receptor family. Kidney international. 49(4):959-963.

Kawakami M, Takano-Yamamoto T. 1997. Orthodontic treatment of a patient with hypophosphatemic vitamin d-resistant rickets. ASDC journal of dentistry for children. 64(6):395-399.

Kawasaki K, Weiss KM. 2006. Evolutionary genetics of vertebrate tissue mineralization: The origin and evolution of the secretory calcium-binding phosphoprotein family. Journal of experimental zoology Part B, Molecular and developmental evolution. 306(3):295-316.

Khoshniat S, Bourgine A, Julien M, Weiss P, Guicheux J, Beck L. 2011. The emergence of phosphate as a specific signaling molecule in bone and other cell types in mammals. Cellular and molecular life sciences : CMLS. 68(2):205-218.

Kido S, Kaneko I, Tatsumi S, Segawa H, Miyamoto K. 2013. Vitamin d and type ii sodium-dependent phosphate cotransporters. Contributions to nephrology. 180:86-97.

Kimura S, Nagai A, Onitsuka T, Koga T, Fujiwara T, Kaya H, Hamada S. 2000. Induction of experimental periodontitis in mice with porphyromonas gingivalis-adhered ligatures. Journal of periodontology. 71(7):1167-1173.

Kinane DF, Peterson M, Stathopoulou PG. 2006. Environmental and other modifying factors of the periodontal diseases. Periodontology 2000. 40:107-119.

Knights D, Lassen KG, Xavier RJ. 2013. Advances in inflammatory bowel disease pathogenesis: Linking host genetics and the microbiome. Gut. 62(10):1505-1510.

Koehne T, Marshall RP, Jeschke A, Kahl-Nieke B, Schinke T, Amling M. 2013. Osteopetrosis, osteopetrorickets and hypophosphatemic rickets differentially affect dentin and enamel mineralization. Bone. 53(1):25-33.

Kondo H, Guo J, Bringhurst FR. 2002. Cyclic adenosine monophosphate/protein kinase a mediates parathyroid hormone/parathyroid hormone-related protein receptor regulation of osteoclastogenesis and expression of rankl and osteoprotegerin mrnas by marrow stromal cells. Journal of Bone and Mineral Research. 17(9):1667-1679.

Koyama Y, Rittling SR, Tsuji K, Hino K, Salincarnboriboon R, Yano T, Taketani Y, Nifuji A, Denhardt DT, Noda M. 2006. Osteopontin deficiency suppresses high phosphate load-induced bone loss via specific modulation of osteoclasts. Endocrinology. 147(6):3040-3049.

Krebsbach PH, Gu K, Franceschi RT, Rutherford RB. 2000. Gene therapy-directed osteogenesis: Bmp-7-transduced human fibroblasts form bone in vivo. Human gene therapy. 11(8):1201-1210.

Kumar R, Riggs B. 1980. Pathologic bone physiology. Fundamental and clinical bone physiology Lippincott, Philadelphia.394-406.

Kuro OM, Moe OW. 2016. Fgf23-alphaklotho as a paradigm for a kidney-bone network. Bone.

Kuro-o M, Matsumura Y, Aizawa H, Kawaguchi H, Suga T, Utsugi T, Ohyama Y, Kurabayashi M, Kaname T, Kume E. 1997. Mutation of the mouse klotho gene leads to a syndrome resembling ageing. Nature. 390(6655):45-51.

Kurosu H, Ogawa Y, Miyoshi M, Yamamoto M, Nandi A, Rosenblatt KP, Baum MG, Schiavi S, Hu M-C, Moe OW. 2006. Regulation of fibroblast growth factor-23 signaling by klotho. Journal of Biological Chemistry. 281(10):6120-6123.

Landis WJ, Hodgens KJ, Arena J, Song MJ, McEwen BF. 1996a. Structural relations between collagen and mineral in bone as determined by high voltage electron microscopic tomography. Microscopy research and technique. 33(2):192-202.

Landis WJ, Hodgens KJ, Song MJ, Arena J, Kiyonaga S, Marko M, Owen C, McEwen BF. 1996b. Mineralization of collagen may occur on fibril surfaces: Evidence from conventional and high-voltage electron microscopy and three-dimensional imaging. Journal of structural biology. 117(1):24-35.

Landis WJ, Jacquet R. 2013. Association of calcium and phosphate ions with collagen in the mineralization of vertebrate tissues. Calcified tissue international. 93(4):329-337.

Lang NP, Lindhe J. 2015. Clinical periodontology and implant dentistry, 2 volume set. John Wiley & Sons.

Lau WL, Festing MH, Giachelli CM. 2010. Phosphate and vascular calcification: Emerging role of the sodium-dependent phosphate co-transporter pit-1. Thrombosis and haemostasis. 104(3):464-470.

Levi M, Lotscher M, Sorribas V, Custer M, Arar M, Kaissling B, Murer H, Biber J. 1994. Cellular mechanisms of acute and chronic adaptation of rat renal p(i) transporter to alterations in dietary p(i). The American journal of physiology. 267(5 Pt 2):F900-908.

Levy-Litan V, Hershkovitz E, Avizov L, Leventhal N, Bercovich D, Chalifa-Caspi V, Manor E, Buriakovsky S, Hadad Y, Goding J et al. 2010. Autosomal-recessive hypophosphatemic rickets is associated with an inactivation mutation in the enpp1 gene. American journal of human genetics. 86(2):273-278.

Li CH, Amar S. 2007. Morphometric, histomorphometric, and microcomputed tomographic analysis of periodontal inflammatory lesions in a murine model. Journal of periodontology. 78(6):1120-1128.

Li H, Martin A, David V, Quarles LD. 2011. Compound deletion of fgfr3 and fgfr4 partially rescues the hyp mouse phenotype. American journal of physiology Endocrinology and metabolism. 300(3):E508-517.

Li X, Giachelli CM. 2007. Sodium-dependent phosphate cotransporters and vascular calcification. Current opinion in nephrology and hypertension. 16(4):325-328.

Li X, Yang HY, Giachelli CM. 2006. Role of the sodium-dependent phosphate cotransporter, pit-1, in vascular smooth muscle cell calcification. Circulation research. 98(7):905-912.

Liang G, Katz LD, Insogna KL, Carpenter TO, Macica CM. 2009. Survey of the enthesopathy of x-linked hypophosphatemia and its characterization in hyp mice. Calcified tissue international. 85(3):235-246.

Ling Y, Rios HF, Myers ER, Lu Y, Feng JQ, Boskey AL. 2005. Dmp1 depletion decreases bone mineralization in vivo: An ftir imaging analysis. Journal of bone and mineral research : the official journal of the American Society for Bone and Mineral Research. 20(12):2169-2177.

Linglart A, Biosse-Duplan M. 2016. Hypophosphatasia. Current osteoporosis reports. 14(3):95-105.

Linglart A, Biosse-Duplan M, Briot K, Chaussain C, Esterle L, Guillaume-Czitrom S, Kamenicky P, Nevoux J, Prie D, Rothenbuhler A et al. 2014. Therapeutic management of hypophosphatemic rickets from infancy to adulthood. Endocrine connections. 3(1):R13-30.

Liu ES, Martins JS, Raimann A, Chae BT, Brooks DJ, Jorgetti V, Bouxsein ML, Demay MB. 2016. 1,25-dihydroxyvitamin d alone improves skeletal growth, microarchitecture, and

strength in a murine model of xlh, despite enhanced fgf23 expression. Journal of bone and mineral research : the official journal of the American Society for Bone and Mineral Research. 31(5):929-939.

Liu S, Brown TA, Zhou J, Xiao ZS, Awad H, Guilak F, Quarles LD. 2005. Role of matrix extracellular phosphoglycoprotein in the pathogenesis of x-linked hypophosphatemia. Journal of the American Society of Nephrology : JASN. 16(6):1645-1653.

Liu S, Rowe PS, Vierthaler L, Zhou J, Quarles LD. 2007. Phosphorylated acidic serine-aspartate-rich mepe-associated motif peptide from matrix extracellular phosphoglycoprotein inhibits phosphate regulating gene with homologies to endopeptidases on the x-chromosome enzyme activity. The Journal of endocrinology. 192(1):261-267.

Liu S, Zhou J, Tang W, Jiang X, Rowe DW, Quarles LD. 2006. Pathogenic role of fgf23 in hyp mice. American journal of physiology Endocrinology and metabolism. 291(1):E38-49.

Lorenz-Depiereux B, Bastepe M, Benet-Pages A, Amyere M, Wagenstaller J, Muller-Barth U, Badenhoop K, Kaiser SM, Rittmaster RS, Shlossberg AH et al. 2006a. Dmp1 mutations in autosomal recessive hypophosphatemia implicate a bone matrix protein in the regulation of phosphate homeostasis. Nature genetics. 38(11):1248-1250.

Lorenz-Depiereux B, Benet-Pages A, Eckstein G, Tenenbaum-Rakover Y, Wagenstaller J, Tiosano D, Gershoni-Baruch R, Albers N, Lichtner P, Schnabel D et al. 2006b. Hereditary hypophosphatemic rickets with hypercalciuria is caused by mutations in the sodium-phosphate cotransporter gene slc34a3. American journal of human genetics. 78(2):193-201.

Lorenz-Depiereux B, Schnabel D, Tiosano D, Hausler G, Strom TM. 2010. Loss-of-function enpp1 mutations cause both generalized arterial calcification of infancy and autosomal-recessive hypophosphatemic rickets. American journal of human genetics. 86(2):267-272.

Lundgren T, Stenport V, Wetter A, Linde A. 1998. Parathyroid hormone (1-34) receptor-binding and second-messenger response in rat incisor odontoblasts. Calcified tissue international. 62(3):255-259.

MacDougall M, Simmons D, Gu TT, Dong J. 2002. Mepe/of45, a new dentin/bone matrix protein and candidate gene for dentin diseases mapping to chromosome 4q21. Connective tissue research. 43(2-3):320-330.

Macica CM, King HE, Wang M, McEachon CL, Skinner CW, Tommasini SM. 2016. Novel anatomic adaptation of cortical bone to meet increased mineral demands of reproduction. Bone. 85:59-69.

Mackler BF, Frostad KB, Robertson PB, Levy BM. 1977. Immunoglobulin bearing lymphocytes and plasma cells in human periodontal disease. Journal of periodontal research. 12(1):37-45.

Makitie O, Doria A, Kooh SW, Cole WG, Daneman A, Sochett E. 2003. Early treatment improves growth and biochemical and radiographic outcome in x-linked hypophosphatemic rickets. The Journal of clinical endocrinology and metabolism. 88(8):3591-3597.

Mandair GS, Morris MD. 2015. Contributions of raman spectroscopy to the understanding of bone strength. BoneKEy reports. 4:620.

Marie PJ. 2008. Transcription factors controlling osteoblastogenesis. Archives of biochemistry and biophysics. 473(2):98-105.

Marie PJ, Glorieux FH. 1983. Relation between hypomineralized periosteocytic lesions and bone mineralization in vitamin d-resistant rickets. Calcified tissue international. 35(4-5):443-448.

Martin A, David V, Laurence JS, Schwarz PM, Lafer EM, Hedge AM, Rowe PS. 2008. Degradation of mepe, dmp1, and release of sibling asarm-peptides (minhibins): Asarm-peptide(s) are directly responsible for defective mineralization in hyp. Endocrinology. 149(4):1757-1772.

Martin A, Liu S, David V, Li H, Karydis A, Feng JQ, Quarles LD. 2011. Bone proteins phex and dmp1 regulate fibroblastic growth factor fgf23 expression in osteocytes through a common pathway involving fgf receptor (fgfr) signaling. FASEB journal : official publication of the Federation of American Societies for Experimental Biology. 25(8):2551-2562.

Matsumura Y, Aizawa H, Shiraki-Iida T, Nagai R, Kuro-o M, Nabeshima Y. 1998. Identification of the human klotho gene and its two transcripts encoding membrane and secreted klotho protein. Biochemical and biophysical research communications. 242(3):626-630.

McCauley LK, Somerman MJ. 2012. Mineralized tissues in oral and craniofacial science: Biological principles and clinical correlates. John Wiley & Sons.

McCulloch CA, Lekic P, McKee MD. 2000. Role of physical forces in regulating the form and function of the periodontal ligament. Periodontology 2000. 24:56-72.

McKee MD, Addison WN, Kaartinen MT. 2005. Hierarchies of extracellular matrix and mineral organization in bone of the craniofacial complex and skeleton. Cells, tissues, organs. 181(3-4):176-188.

McKee MD, Hoac B, Addison WN, Barros NM, Millan JL, Chaussain C. 2013. Extracellular matrix mineralization in periodontal tissues: Noncollagenous matrix proteins, enzymes, and relationship to hypophosphatasia and x-linked hypophosphatemia. Periodontology 2000. 63(1):102-122.

McKee MD, Murshed M, Kaartinen MT. 2012. Extracellular matrix and mineralization of craniofacial bone. Mineralized Tissues in Oral and Craniofacial Science: Biological Principles and Clinical Correlates.99.

McKee MD, Nakano Y, Masica DL, Gray JJ, Lemire I, Heft R, Whyte MP, Crine P, Millan JL. 2011a. Enzyme replacement therapy prevents dental defects in a model of hypophosphatasia. Journal of dental research. 90(4):470-476.

McKee MD, Nanci A. 1995. Postembedding colloidal-gold immunocytochemistry of noncollagenous extracellular matrix proteins in mineralized tissues. Microscopy research and technique. 31(1):44-62.

McKee MD, Pedraza CE, Kaartinen MT. 2011b. Osteopontin and wound healing in bone. Cells, tissues, organs. 194(2-4):313-319.

McNally EA, Schwarcz HP, Botton GA, Arsenault AL. 2012. A model for the ultrastructure of bone based on electron microscopy of ion-milled sections. PloS one. 7(1):e29258.

Melcher AH. 1976. On the repair potential of periodontal tissues. Journal of periodontology. 47(5):256-260.

Mellanby E. 1921. Experimental rickets. HM Stationery Office.

Meyer JL. 1984. Can biological calcification occur in the presence of pyrophosphate? Archives of biochemistry and biophysics. 231(1):1-8.

Meyle J, Chapple I. 2015. Molecular aspects of the pathogenesis of periodontitis. Periodontology 2000. 69(1):7-17.

Millán JL. 2006. Introduction. Mammalian alkaline phosphatases. Wiley-VCH Verlag GmbH & Co. KGaA. p. 1-2.

Millan JL, Narisawa S, Lemire I, Loisel TP, Boileau G, Leonard P, Gramatikova S, Terkeltaub R, Camacho NP, McKee MD et al. 2008. Enzyme replacement therapy for murine hypophosphatasia. Journal of bone and mineral research : the official journal of the American Society for Bone and Mineral Research. 23(6):777-787.

Miura M, Gronthos S, Zhao M, Lu B, Fisher LW, Robey PG, Shi S. 2003. Shed: Stem cells from human exfoliated deciduous teeth. Proceedings of the National Academy of Sciences of the United States of America. 100(10):5807-5812.

Miyamoto K, Haito-Sugino S, Kuwahara S, Ohi A, Nomura K, Ito M, Kuwahata M, Kido S, Tatsumi S, Kaneko I et al. 2011. Sodium-dependent phosphate cotransporters: Lessons from gene knockout and mutation studies. Journal of pharmaceutical sciences. 100(9):3719-3730.

Mozar A, Haren N, Chasseraud M, Louvet L, Maziere C, Wattel A, Mentaverri R, Morliere P, Kamel S, Brazier M et al. 2008. High extracellular inorganic phosphate concentration inhibits rank-rankl signaling in osteoclast-like cells. Journal of cellular physiology. 215(1):47-54.

Murayama T, Iwatsubo R, Akiyama S, Amano A, Morisaki I. 2000. Familial hypophosphatemic vitamin d-resistant rickets: Dental findings and histologic study of teeth. Oral surgery, oral medicine, oral pathology, oral radiology, and endodontics. 90(3):310-316.

Murer H, Forster I, Hernando N, Lambert G, Traebert M, Biber J. 1999. Posttranscriptional regulation of the proximal tubule napi-ii transporter in response to pth and dietary p(i). The American journal of physiology. 277(5 Pt 2):F676-684.

Murer H, Forster I, Hilfiker H, Pfister M, Kaissling B, Lotscher M, Biber J. 1998. Cellular/molecular control of renal na/pi-cotransport. Kidney international Supplement. 65:S2-10.

Murer H, Hernando N, Forster I, Biber J. 2000. Proximal tubular phosphate reabsorption: Molecular mechanisms. Physiol Rev. 80(4):1373-1409.

Murer H, Hernando N, Forster I, Biber J. 2003. Regulation of na/pi transporter in the proximal tubule. Annual review of physiology. 65:531-542.

Murshed M, Harmey D, Millan JL, McKee MD, Karsenty G. 2005. Unique coexpression in osteoblasts of broadly expressed genes accounts for the spatial restriction of ecm mineralization to bone. Genes & development. 19(9):1093-1104.

Nagao M, Feinstein TN, Ezura Y, Hayata T, Notomi T, Saita Y, Hanyu R, Hemmi H, Izu Y, Takeda S et al. 2011. Sympathetic control of bone mass regulated by osteopontin. Proceedings of the National Academy of Sciences of the United States of America. 108(43):17767-17772.

Nagpal S, Na S, Rathnachalam R. 2005. Noncalcemic actions of vitamin d receptor ligands. Endocrine reviews. 26(5):662-687.

Nakano Y, Kawamoto T, Oda K, Takano Y. 2003. Alkaline and acid phosphatases in bone cells serve as phosphohydrolases at physiological ph in vivo: A histochemical implication. Connective tissue research. 44 Suppl 1:219-222.

Nanci A. 2012. Ten cate's oral histology, development, structure, and function. (8th Edition).

Nanci A, Bosshardt DD. 2006. Structure of periodontal tissues in health and disease. Periodontology 2000. 40:11-28.

Narayanan K, Ramachandran A, Hao J, He G, Park KW, Cho M, George A. 2003. Dual functional roles of dentin matrix protein 1. Implications in biomineralization and gene

transcription by activation of intracellular ca2+ store. The Journal of biological chemistry. 278(19):17500-17508.

Narayanan K, Srinivas R, Ramachandran A, Hao J, Quinn B, George A. 2001. Differentiation of embryonic mesenchymal cells to odontoblast-like cells by overexpression of dentin matrix protein 1. Proceedings of the National Academy of Sciences of the United States of America. 98(8):4516-4521.

Nashiki K, Taketani Y, Takeichi T, Sawada N, Yamamoto H, Ichikawa M, Arai H, Miyamoto K, Takeda E. 2005a. Role of membrane microdomains in pth-mediated down-regulation of napi-iia in opossum kidney cells. Kidney international. 68(3):1137-1147.

Nashiki K, Taketani Y, Takeichi T, Sawada N, Yamamoto H, Ichikawa M, Arai H, Miyamoto K-I, Takeda E. 2005b. Role of membrane microdomains in pth-mediated down-regulation of napi-iia in opossum kidney cells. Kidney international. 68(3):1137-1147.

Naveh GR, Brumfeld V, Shahar R, Weiner S. 2013. Tooth periodontal ligament: Direct 3d microct visualization of the collagen network and how the network changes when the tooth is loaded. Journal of structural biology. 181(2):108-115.

Naveh GR, Lev-Tov Chattah N, Zaslansky P, Shahar R, Weiner S. 2012a. Tooth-pdl-bone complex: Response to compressive loads encountered during mastication - a review. Archives of oral biology. 57(12):1575-1584.

Naveh GR, Shahar R, Brumfeld V, Weiner S. 2012b. Tooth movements are guided by specific contact areas between the tooth root and the jaw bone: A dynamic 3d microct study of the rat molar. Journal of structural biology. 177(2):477-483.

Netter P, Bardin T, Bianchi A, Richette P, Loeuille D. 2004. The ankh gene and familial calcium pyrophosphate dihydrate deposition disease. Joint, bone, spine : revue du rhumatisme. 71(5):365-368.

Niall H, Keutmann H, Sauer R, Hogan M, Dawson B, Aurbach G, Potts Jr J. 1970. The amino acid sequence of bovine parathyroid hormone i. Hoppe-Seyler's Zeitschrift fur Physiologische Chemie. 351(12):1586-1588.

Nishimura M, Naito S. 2008. Tissue-specific mrna expression profiles of human solute carrier transporter superfamilies. Drug metabolism and pharmacokinetics. 23(1):22-44.

Nociti FH, Jr., Berry JE, Foster BL, Gurley KA, Kingsley DM, Takata T, Miyauchi M, Somerman MJ. 2002. Cementum: A phosphate-sensitive tissue. Journal of dental research. 81(12):817-821.

Nudelman F, Lausch AJ, Sommerdijk NA, Sone ED. 2013. In vitro models of collagen biomineralization. Journal of structural biology. 183(2):258-269.

Nurnberg P, Thiele H, Chandler D, Hohne W, Cunningham ML, Ritter H, Leschik G, Uhlmann K, Mischung C, Harrop K et al. 2001. Heterozygous mutations in ankh, the human ortholog of the mouse progressive ankylosis gene, result in craniometaphyseal dysplasia. Nature genetics. 28(1):37-41.

Oftebro H, Saarem K, Bjorkhem I, Pedersen JI. 1981. Side chain hydroxylation of c27-steroids and vitamin d3 by a cytochrome p-450 enzyme system isolated from human liver mitochondria. Journal of lipid research. 22(8):1254-1264.

Omelon S, Georgiou J, Henneman ZJ, Wise LM, Sukhu B, Hunt T, Wynnyckyj C, Holmyard D, Bielecki R, Grynpas MD. 2009. Control of vertebrate skeletal mineralization by polyphosphates. PloS one. 4(5):e5634.

Onishi T, Okawa R, Ogawa T, Shintani S, Ooshima T. 2007. Phex mutation causes the reduction of npt2b mrna in teeth. Journal of dental research. 86(2):158-162.

Opsahl Vital S, Gaucher C, Bardet C, Rowe PS, George A, Linglart A, Chaussain C. 2012. Tooth dentin defects reflect genetic disorders affecting bone mineralization. Bone. 50(4):989-997.

Ornitz DM, Xu J, Colvin JS, McEwen DG, MacArthur CA, Coulier F, Gao G, Goldfarb M. 1996. Receptor specificity of the fibroblast growth factor family. The Journal of biological chemistry. 271(25):15292-15297.

Page RC, Schroeder HE. 1976. Pathogenesis of inflammatory periodontal disease. A summary of current work. Laboratory investigation; a journal of technical methods and pathology. 34(3):235-249.

Page RC, Schroeder HE. 1982. Periodontitis in man and other animals. A comparative review. S. karger.

Pagni G, Kaigler D, Rasperini G, Avila-Ortiz G, Bartel R, Giannobile W. 2012. Bone repair cells for craniofacial regeneration. Advanced drug delivery reviews. 64(12):1310-1319.

Panda DK, Miao D, Tremblay ML, Sirois J, Farookhi R, Hendy GN, Goltzman D. 2001. Targeted ablation of the 25-hydroxyvitamin d 1α-hydroxylase enzyme: Evidence for skeletal, reproductive, and immune dysfunction. Proceedings of the National Academy of Sciences. 98(13):7498-7503.

Panmekiate S, Ngonphloy N, Charoenkarn T, Faruangsaeng T, Pauwels R. 2015. Comparison of mandibular bone microarchitecture between micro-ct and cbct images. Dento maxillo facial radiology. 44(5):20140322.

Pedraza CE, Marelli B, Chicatun F, McKee MD, Nazhat SN. 2010. An in vitro assessment of a cell-containing collagenous extracellular matrix-like scaffold for bone tissue engineering. Tissue engineering Part A. 16(3):781-793.

Pedraza CE, Nikolcheva LG, Kaartinen MT, Barralet JE, McKee MD. 2008. Osteopontin functions as an opsonin and facilitates phagocytosis by macrophages of hydroxyapatite-coated microspheres: Implications for bone wound healing. Bone. 43(4):708-716.

Pellegrini G, Seol YJ, Gruber R, Giannobile WV. 2009. Pre-clinical models for oral and periodontal reconstructive therapies. Journal of dental research. 88(12):1065-1076.

Peng J-B, Chen X-Z, Berger UV, Vassilev PM, Tsukaguchi H, Brown EM, Hediger MA. 1999. Molecular cloning and characterization of a channel-like transporter mediating intestinal calcium absorption. Journal of Biological Chemistry. 274(32):22739-22746.

Picard N, Capuano P, Stange G, Mihailova M, Kaissling B, Murer H, Biber J, Wagner CA. 2010. Acute parathyroid hormone differentially regulates renal brush border membrane phosphate cotransporters. Pflugers Archiv : European journal of physiology. 460(3):677-687.

Prie D, Urena Torres P, Friedlander G. 2009. Latest findings in phosphate homeostasis. Kidney international. 75(9):882-889.

Prüfer K, Racz A, Lin GC, Barsony J. 2000. Dimerization with retinoid x receptors promotes nuclear localization and subnuclear targeting of vitamin d receptors. Journal of Biological Chemistry. 275(52):41114-41123.

Qin C, Baba O, Butler WT. 2004. Post-translational modifications of sibling proteins and their roles in osteogenesis and dentinogenesis. Critical reviews in oral biology and medicine : an official publication of the American Association of Oral Biologists. 15(3):126-136.

Qin C, Brunn JC, Cook RG, Orkiszewski RS, Malone JP, Veis A, Butler WT. 2003. Evidence for the proteolytic processing of dentin matrix protein 1. Identification and

characterization of processed fragments and cleavage sites. The Journal of biological chemistry. 278(36):34700-34708.

Quarles LD. 2003. Fgf23, phex, and mepe regulation of phosphate homeostasis and skeletal mineralization. American journal of physiology Endocrinology and metabolism. 285(1):E1-9.

Rasmussen H, Tenenhouse H. 1995. Mendelian hypophosphatemias. The metabolic and molecular bases of inherited disease. 3:3717-3745.

Ravera S, Virkki LV, Murer H, Forster IC. 2007. Deciphering pit transport kinetics and substrate specificity using electrophysiology and flux measurements. American journal of physiology Cell physiology. 293(2):C606-620.

Reibel A, Maniere MC, Clauss F, Droz D, Alembik Y, Mornet E, Bloch-Zupan A. 2009. Orodental phenotype and genotype findings in all subtypes of hypophosphatasia. Orphanet journal of rare diseases. 4:6.

Reichenberger E, Tiziani V, Watanabe S, Park L, Ueki Y, Santanna C, Baur ST, Shiang R, Grange DK, Beighton P et al. 2001. Autosomal dominant craniometaphyseal dysplasia is caused by mutations in the transmembrane protein ank. American journal of human genetics. 68(6):1321-1326.

Rey C, Combes C, Drouet C, Glimcher MJ. 2009. Bone mineral: Update on chemical composition and structure. Osteoporosis international : a journal established as result of cooperation between the European Foundation for Osteoporosis and the National Osteoporosis Foundation of the USA. 20(6):1013-1021.

Reynolds JJ, Meikle MC. 1997. Mechanisms of connective tissue matrix destruction in periodontitis. Periodontology 2000. 14:144-157.

Riccardi D, Park J, Lee W-S, Gamba G, Brown EM, Hebert SC. 1995. Cloning and functional expression of a rat kidney extracellular calcium/polyvalent cation-sensing receptor. Proceedings of the National Academy of Sciences. 92(1):131-135.

Riminucci M, Collins MT, Fedarko NS, Cherman N, Corsi A, White KE, Waguespack S, Gupta A, Hannon T, Econs MJ et al. 2003. Fgf-23 in fibrous dysplasia of bone and its relationship to renal phosphate wasting. The Journal of clinical investigation. 112(5):683-692.

Roach HI. 1999. Association of matrix acid and alkaline phosphatases with mineralization of cartilage and endochondral bone. The Histochemical journal. 31(1):53-61.

Roberts S, Narisawa S, Harmey D, Millan JL, Farquharson C. 2007. Functional involvement of phospho1 in matrix vesicle-mediated skeletal mineralization. Journal of bone and mineral research : the official journal of the American Society for Bone and Mineral Research. 22(4):617-627.

Roberts SJ, Stewart AJ, Sadler PJ, Farquharson C. 2004. Human phospho1 exhibits high specific phosphoethanolamine and phosphocholine phosphatase activities. The Biochemical journal. 382(Pt 1):59-65.

Rodrigues TL, Foster BL, Silverio KG, Martins L, Casati MZ, Sallum EA, Somerman MJ, Nociti FH, Jr. 2012. Correction of hypophosphatasia-associated mineralization deficiencies in vitro by phosphate/pyrophosphate modulation in periodontal ligament cells. Journal of periodontology. 83(5):653-663.

Rodriguez DE, Thula-Mata T, Toro EJ, Yeh YW, Holt C, Holliday LS, Gower LB. 2014. Multifunctional role of osteopontin in directing intrafibrillar mineralization of collagen and activation of osteoclasts. Acta biomaterialia. 10(1):494-507.

Rosenblatt M, SEGRE GV, TREGEAR GW, SHEPARD GL, TYLER GA, POTTS Jr JT. 1978. Human parathyroid hormone: Synthesis and chemical, biological, and immunological evaluation of the carboxyl-terminal region*. Endocrinology. 103(3):978-984.

Rowe PS. 1997. The pex gene: Its role in x-linked rickets, osteomalacia, and bone mineral metabolism. Experimental nephrology. 5(5):355-363.

Rowe PS. 2012. The chicken or the egg: Phex, fgf23 and siblings unscrambled. Cell biochemistry and function. 30(5):355-375.

Rowe PS. 2015. A unified model for bone-renal mineral and energy metabolism. Current opinion in pharmacology. 22:64-71.

Rowe PS, de Zoysa PA, Dong R, Wang HR, White KE, Econs MJ, Oudet CL. 2000. Mepe, a new gene expressed in bone marrow and tumors causing osteomalacia. Genomics. 67(1):54-68.

Rowe PS, Garrett IR, Schwarz PM, Carnes DL, Lafer EM, Mundy GR, Gutierrez GE. 2005. Surface plasmon resonance (spr) confirms that mepe binds to phex via the mepe-asarm motif: A model for impaired mineralization in x-linked rickets (hyp). Bone. 36(1):33-46.

Roy S, Martel J, Ma S, Tenenhouse HS. 1994. Increased renal 25-hydroxyvitamin d3-24-hydroxylase messenger ribonucleic acid and immunoreactive protein in phosphate-deprived hyp mice: A mechanism for accelerated 1,25-dihydroxyvitamin d3 catabolism in x-linked hypophosphatemic rickets. Endocrinology. 134(4):1761-1767.

Ruchon AF, Marcinkiewicz M, Siegfried G, Tenenhouse HS, DesGroseillers L, Crine P, Boileau G. 1998. Pex mrna is localized in developing mouse osteoblasts and odontoblasts. The journal of histochemistry and cytochemistry : official journal of the Histochemistry Society. 46(4):459-468.

Ruchon AF, Tenenhouse HS, Marcinkiewicz M, Siegfried G, Aubin JE, DesGroseillers L, Crine P, Boileau G. 2000. Developmental expression and tissue distribution of phex protein: Effect of the hyp mutation and relationship to bone markers. Journal of bone and mineral research : the official journal of the American Society for Bone and Mineral Research. 15(8):1440-1450.

Russell J, Bar A, Sherwood LM, Hurwitz S. 1993. Interaction between calcium and 1, 25-dihydroxyvitamin d3 in the regulation of preproparathyroid hormone and vitamin d receptor messenger ribonucleic acid in avian parathyroids. Endocrinology. 132(6):2639-2644.

Rutsch F, Terkeltaub R. 2005. Deficiencies of physiologic calcification inhibitors and low-grade inflammation in arterial calcification: Lessons for cartilage calcification. Joint, bone, spine : revue du rhumatisme. 72(2):110-118.

Ryan LM. 2001. The ank gene story. Arthritis research. 3(2):77-79.

Saadi-Thiers K, Huck O, Simonis P, Tilly P, Fabre JE, Tenenbaum H, Davideau JL. 2013. Periodontal and systemic responses in various mice models of experimental periodontitis: Respective roles of inflammation duration and porphyromonas gingivalis infection. Journal of periodontology. 84(3):396-406.

Sabbagh Y, O'Brien SP, Song W, Boulanger JH, Stockmann A, Arbeeny C, Schiavi SC. 2009. Intestinal npt2b plays a major role in phosphate absorption and homeostasis. Journal of the American Society of Nephrology : JASN. 20(11):2348-2358.

Saffar JL, Lasfargues JJ, Cherruau M. 1997. Alveolar bone and the alveolar process: The socket that is never stable. Periodontology 2000. 13:76-90.

Salmon B. 2012. Asarm et biominéralisation de progéniteurs pulpaires : Asarm and dental pulp stem cells mineralization. Chaussain-Miller, Catherine (thesis director).

Salmon B, Bardet C, Coyac BR, Baroukh B, Naji J, Rowe PS, Opsahl Vital S, Linglart A, McKee MD, Chaussain C. 2014. Abnormal osteopontin and matrix extracellular phosphoglycoprotein localization, and odontoblast differentiation, in x-linked hypophosphatemic teeth. Connective tissue research. 55 Suppl 1:79-82.

Salmon B, Bardet C, Khaddam M, Naji J, Coyac BR, Baroukh B, Letourneur F, Lesieur J, Decup F, Le Denmat D et al. 2013. Mepe-derived asarm peptide inhibits odontogenic differentiation of dental pulp stem cells and impairs mineralization in tooth models of x-linked hypophosphatemia. PloS one. 8(2):e56749.

Salmon CR, Giorgetti AP, Paes Leme AF, Domingues RR, Sallum EA, Alves MC, Kolli TN, Foster BL, Nociti FH, Jr. 2016. Global proteome profiling of dental cementum under experimentally-induced apposition. Journal of proteomics. 141:12-23.

Sauer GR, Wuthier RE. 1988. Fourier transform infrared characterization of mineral phases formed during induction of mineralization by collagenase-released matrix vesicles in vitro. The Journal of biological chemistry. 263(27):13718-13724.

Schwartz S, Scriver CR, Reade TM, Shields ED. 1988. Oral findings in patients with autosomal dominant hypophosphatemic bone disease and x-linked hypophosphatemia: Further evidence that they are different diseases. Oral surgery, oral medicine, and oral pathology. 66(3):310-314.

Segawa H, Kawakami E, Kaneko I, Kuwahata M, Ito M, Kusano K, Saito H, Fukushima N, Miyamoto K. 2003. Effect of hydrolysis-resistant fgf23-r179q on dietary phosphate regulation of the renal type-ii na/pi transporter. Pflugers Archiv : European journal of physiology. 446(5):585-592.

Segawa H, Onitsuka A, Furutani J, Kaneko I, Aranami F, Matsumoto N, Tomoe Y, Kuwahata M, Ito M, Matsumoto M et al. 2009a. Npt2a and npt2c in mice play distinct and synergistic roles in inorganic phosphate metabolism and skeletal development. American journal of physiology Renal physiology. 297(3):F671-678.

Segawa H, Onitsuka A, Kuwahata M, Hanabusa E, Furutani J, Kaneko I, Tomoe Y, Aranami F, Matsumoto N, Ito M et al. 2009b. Type iic sodium-dependent phosphate transporter regulates calcium metabolism. Journal of the American Society of Nephrology : JASN. 20(1):104-113.

Seow WK, Brown JP, Tudehope DA, O'Callaghan M. 1984. Dental defects in the deciduous dentition of premature infants with low birth weight and neonatal rickets. Pediatric dentistry. 6(2):88-92.

Sexton PM, Findlay DM, Martin TJ. 1999. Calcitonin. Current medicinal chemistry. 6(11):1067-1093.

Seymour GJ, Greenspan JS. 1979. The phenotypic characterization of lymphocyte subpopulations in established human periodontal disease. Journal of periodontal research. 14(1):39-46.

Seymour GJ, Taylor JJ. 2004. Shouts and whispers: An introduction to immunoregulation in periodontal disease. Periodontology 2000. 35:9-13.

Shanahan CM, Crouthamel MH, Kapustin A, Giachelli CM. 2011. Arterial calcification in chronic kidney disease: Key roles for calcium and phosphate. Circulation research. 109(6):697-711.

Sheen CR, Pilarowski GO, Wang W, Millan JL. 2012. Molecular characterisation of the hyp deletion and an improved assay for its detection. Bone. 50(3):592-595.

Shimada T, Hasegawa H, Yamazaki Y, Muto T, Hino R, Takeuchi Y, Fujita T, Nakahara K, Fukumoto S, Yamashita T. 2004a. Fgf-23 is a potent regulator of vitamin d metabolism and phosphate homeostasis. Journal of bone and mineral research : the official journal of the American Society for Bone and Mineral Research. 19(3):429-435.

Shimada T, Kakitani M, Yamazaki Y, Hasegawa H, Takeuchi Y, Fujita T, Fukumoto S, Tomizuka K, Yamashita T. 2004b. Targeted ablation of fgf23 demonstrates an essential physiological role of fgf23 in phosphate and vitamin d metabolism. The Journal of clinical investigation. 113(4):561-568.

Shinki T, Ueno Y, DeLuca HF, Suda T. 1999. Calcitonin is a major regulator for the expression of renal 25-hydroxyvitamin d3-1alpha-hydroxylase gene in normocalcemic rats. Proceedings of the National Academy of Sciences of the United States of America. 96(14):8253-8258.

Silver FH, Landis WJ. 2011. Deposition of apatite in mineralizing vertebrate extracellular matrices: A model of possible nucleation sites on type i collagen. Connective tissue research. 52(3):242-254.

Sitara D, Razzaque MS, Hesse M, Yoganathan S, Taguchi T, Erben RG, Juppner H, Lanske B. 2004. Homozygous ablation of fibroblast growth factor-23 results in hyperphosphatemia and impaired skeletogenesis, and reverses hypophosphatemia in phex-deficient mice. Matrix biology : journal of the International Society for Matrix Biology. 23(7):421-432.

Socransky SS, Haffajee AD, Cugini MA, Smith C, Kent RL, Jr. 1998. Microbial complexes in subgingival plaque. Journal of clinical periodontology. 25(2):134-144.

Suda T, Takahashi N, Udagawa N, Jimi E, Gillespie MT, Martin TJ. 1999. Modulation of osteoclast differentiation and function by the new members of the tumor necrosis factor receptor and ligand families. Endocrine reviews. 20(3):345-357.

Sullivan W, Carpenter T, Glorieux F, Travers R, Insogna K. 1992. A prospective trial of phosphate and 1,25-dihydroxyvitamin d3 therapy in symptomatic adults with x-linked hypophosphatemic rickets. The Journal of clinical endocrinology and metabolism. 75(3):879-885.

Sykaras N, Opperman LA. 2003. Bone morphogenetic proteins (bmps): How do they function and what can they offer the clinician? Journal of oral science. 45(2):57-73.

Tatsumi S, Segawa H, Morita K, Haga H, Kouda T, Yamamoto H, Inoue Y, Nii T, Katai K, Taketani Y et al. 1998. Molecular cloning and hormonal regulation of pit-1, a sodium-dependent phosphate cotransporter from rat parathyroid glands. Endocrinology. 139(4):1692-1699.

Tenenhouse HS. 1999. X-linked hypophosphataemia: A homologous disorder in humans and mice. Nephrology, dialysis, transplantation : official publication of the European Dialysis and Transplant Association - European Renal Association. 14(2):333-341.

Tenorio D, Hughes F. 1996. An immunohistochemical investigation of the expression of parathyroid hormone receptors in rat cementoblasts. Archives of oral biology. 41(3):299-305.

Terkeltaub RA. 2001. Inorganic pyrophosphate generation and disposition in pathophysiology. American journal of physiology Cell physiology. 281(1):C1-c11.

Termine JD, Peckauskas RA, Posner AS. 1970. Calcium phosphate formation in vitro. Ii. Effects of environment on amorphous-crystalline transformation. Archives of biochemistry and biophysics. 140(2):318-325.

Toroian D, Lim JE, Price PA. 2007. The size exclusion characteristics of type i collagen: Implications for the role of noncollagenous bone constituents in mineralization. The Journal of biological chemistry. 282(31):22437-22447.

Toyosawa S, Okabayashi K, Komori T, Ijuhin N. 2004. Mrna expression and protein localization of dentin matrix protein 1 during dental root formation. Bone. 34(1):124-133.

Toyosawa S, Shintani S, Fujiwara T, Ooshima T, Sato A, Ijuhin N, Komori T. 2001. Dentin matrix protein 1 is predominantly expressed in chicken and rat osteocytes but not in osteoblasts. Journal of bone and mineral research : the official journal of the American Society for Bone and Mineral Research. 16(11):2017-2026.

Tran Van P, Mailland ML. 1981. Short - term effects of occlusal hypofunction following antagonist tooth extraction upon periodontal tissues in the rat. Journal de biologie buccale. 9(4):385-400.

Traub W, Arad T, Weiner S. 1992. Origin of mineral crystal growth in collagen fibrils. Matrix (Stuttgart, Germany). 12(4):251-255.

Tregear GW, RIETSCHOTEN JV, GREENE E, KEUTMANN HT, NIALL HD, REIT B, PARSONS JA, POTTS JR JT. 1973. Bovine parathyroid hormone: Minimum chain length of synthetic peptide required for biological activity. Endocrinology. 93(6):1349-1353.

Tricker N, Garetto L. 1997. Cortical bone turnover and mineral apposition in dentate dog mandible. Journal of dental research. 76:1503-1503.

Udagawa N, Takahashi N, Akatsu T, Tanaka H, Sasaki T, Nishihara T, Koga T, Martin TJ, Suda T. 1990. Origin of osteoclasts: Mature monocytes and macrophages are capable of differentiating into osteoclasts under a suitable microenvironment prepared by bone marrow-derived stromal cells. Proceedings of the national academy of sciences. 87(18):7260-7264.

Urakawa I, Yamazaki Y, Shimada T, Iijima K, Hasegawa H, Okawa K, Fujita T, Fukumoto S, Yamashita T. 2006. Klotho converts canonical fgf receptor into a specific receptor for fgf23. Nature. 444(7120):770-774.

Vaes BL, Dechering KJ, van Someren EP, Hendriks JM, van de Ven CJ, Feijen A, Mummery CL, Reinders MJ, Olijve W, van Zoelen EJ et al. 2005. Microarray analysis reveals expression regulation of wnt antagonists in differentiating osteoblasts. Bone. 36(5):803-811.

Vaingankar SM, Fitzpatrick TA, Johnson K, Goding JW, Maurice M, Terkeltaub R. 2004. Subcellular targeting and function of osteoblast nucleotide pyrophosphatase phosphodiesterase 1. American journal of physiology Cell physiology. 286(5):C1177-1187.

van den Bos T, Handoko G, Niehof A, Ryan LM, Coburn SP, Whyte MP, Beertsen W. 2005. Cementum and dentin in hypophosphatasia. Journal of dental research. 84(11):1021-1025.

Van der Velden U, Abbas F, Armand S, Loos BG, Timmerman MF, Van der Weijden GA, Van Winkelhoff AJ, Winkel EG. 2006. Java project on periodontal diseases. The natural development of periodontitis: Risk factors, risk predictors and risk determinants. Journal of clinical periodontology. 33(8):540-548.

Verge CF, Lam A, Simpson JM, Cowell CT, Howard NJ, Silink M. 1991. Effects of therapy in x-linked hypophosphatemic rickets. The New England journal of medicine. 325(26):1843-1848.

Vignery A, Baron R. 1980. Dynamic histomorphometry of alveolar bone remodeling in the adult rat. The Anatomical record. 196(2):191-200.

Villa-Bellosta R, Ravera S, Sorribas V, Stange G, Levi M, Murer H, Biber J, Forster IC. 2009. The na+-pi cotransporter pit-2 (slc20a2) is expressed in the apical membrane of rat renal proximal tubules and regulated by dietary pi. American journal of physiology Renal physiology. 296(4):F691-699.

Villa-Bellosta R, Sorribas V. 2010. Compensatory regulation of the sodium/phosphate cotransporters napi-iic (scl34a3) and pit-2 (slc20a2) during pi deprivation and acidosis. Pflugers Archiv : European journal of physiology. 459(3):499-508.

Wang C, Li Y, Shi L, Ren J, Patti M, Wang T, de Oliveira JR, Sobrido MJ, Quintans B, Baquero M et al. 2012. Mutations in slc20a2 link familial idiopathic basal ganglia calcification with phosphate homeostasis. Nature genetics. 44(3):254-256.

Weninger M, Stinson RA, Plenk H, Jr., Bock P, Pollak A. 1989. Biochemical and morphological effects of human hepatic alkaline phosphatase in a neonate with hypophosphatasia. Acta paediatrica Scandinavica Supplement. 360:154-160.

Werner A, Kinne RK. 2001. Evolution of the na-p(i) cotransport systems. American journal of physiology Regulatory, integrative and comparative physiology. 280(2):R301-312.

Werner S, Duan DS, de Vries C, Peters KG, Johnson DE, Williams LT. 1992. Differential splicing in the extracellular region of fibroblast growth factor receptor 1 generates receptor variants with different ligand-binding specificities. Molecular and cellular biology. 12(1):82-88.

Weyant RJ, Tracy SL, Anselmo TT, Beltran-Aguilar ED, Donly KJ, Frese WA, Hujoel PP, Iafolla T, Kohn W, Kumar J et al. 2013. Topical fluoride for caries prevention: Executive summary of the updated clinical recommendations and supporting systematic review. Journal of the American Dental Association (1939). 144(11):1279-1291.

White KE, Larsson TE, Econs MJ. 2006. The roles of specific genes implicated as circulating factors involved in normal and disordered phosphate homeostasis: Frizzled related protein-4, matrix extracellular phosphoglycoprotein, and fibroblast growth factor 23. Endocrine reviews. 27(3):221-241.

Whyte MP. 1994. Hypophosphatasia and the role of alkaline phosphatase in skeletal mineralization. Endocrine reviews. 15(4):439-461.

Whyte MP. 2008. Hypophosphatasia: Nature's window on alkaline phosphatase function in humans. Principles of bone biology. 1:1573-1598.

Whyte MP. 2010. Physiological role of alkaline phosphatase explored in hypophosphatasia. Annals of the New York Academy of Sciences. 1192(1):190-200.

Whyte MP. 2017. Hypophosphatasia: Enzyme replacement therapy brings new opportunities and new challenges. Journal of bone and mineral research : the official journal of the American Society for Bone and Mineral Research.

Whyte MP, McAlister WH, Patton LS, Magill HL, Fallon MD, Lorentz WB, Jr., Herrod HG. 1984. Enzyme replacement therapy for infantile hypophosphatasia attempted by intravenous infusions of alkaline phosphatase-rich paget plasma: Results in three additional patients. The Journal of pediatrics. 105(6):926-933.

Winters RW, Graham JB, Williams TF, McFalls VW, Burnett CH. 1991. A genetic study of familial hypophosphatemia and vitamin d resistant rickets with a review of the literature. 1958. Medicine. 70(3):215-217.

Xiao ZS, Crenshaw M, Guo R, Nesbitt T, Drezner MK, Quarles LD. 1998. Intrinsic mineralization defect in hyp mouse osteoblasts. The American journal of physiology. 275(4 Pt 1):E700-708.

Yadav MC, Simao AM, Narisawa S, Huesa C, McKee MD, Farquharson C, Millan JL. 2011. Loss of skeletal mineralization by the simultaneous ablation of phospho1 and alkaline phosphatase function: A unified model of the mechanisms of initiation of skeletal calcification. Journal of bone and mineral research : the official journal of the American Society for Bone and Mineral Research. 26(2):286-297.

Yamashita T, Yoshioka M, Itoh N. 2000. Identification of a novel fibroblast growth factor, fgf-23, preferentially expressed in the ventrolateral thalamic nucleus of the brain. Biochemical and biophysical research communications. 277(2):494-498.

Yamazaki Y, Tamada T, Kasai N, Urakawa I, Aono Y, Hasegawa H, Fujita T, Kuroki R, Yamashita T, Fukumoto S et al. 2008. Anti-fgf23 neutralizing antibodies show the physiological role and structural features of fgf23. Journal of bone and mineral research : the official journal of the American Society for Bone and Mineral Research. 23(9):1509-1518.

Ye L, Liu R, White N, Alon US, Cobb CM. 2011. Periodontal status of patients with hypophosphatemic rickets: A case series. Journal of periodontology. 82(11):1530-1535.

Ye L, MacDougall M, Zhang S, Xie Y, Zhang J, Li Z, Lu Y, Mishina Y, Feng JQ. 2004. Deletion of dentin matrix protein-1 leads to a partial failure of maturation of predentin into dentin, hypomineralization, and expanded cavities of pulp and root canal during postnatal tooth development. The Journal of biological chemistry. 279(18):19141-19148.

Ye L, Mishina Y, Chen D, Huang H, Dallas SL, Dallas MR, Sivakumar P, Kunieda T, Tsutsui TW, Boskey A et al. 2005. Dmp1-deficient mice display severe defects in cartilage formation responsible for a chondrodysplasia-like phenotype. The Journal of biological chemistry. 280(7):6197-6203.

Ye L, Zhang S, Ke H, Bonewald LF, Feng JQ. 2008. Periodontal breakdown in the dmp1 null mouse model of hypophosphatemic rickets. Journal of dental research. 87(7):624-629.

Yoshiko Y, Candeliere GA, Maeda N, Aubin JE. 2007a. Osteoblast autonomous pi regulation via pit1 plays a role in bone mineralization. Molecular and cellular biology. 27(12):4465-4474.

Yoshiko Y, Wang H, Minamizaki T, Ijuin C, Yamamoto R, Suemune S, Kozai K, Tanne K, Aubin JE, Maeda N. 2007b. Mineralized tissue cells are a principal source of fgf23. Bone. 40(6):1565-1573.

Zelenchuk LV, Hedge A-M, Rowe PS. 2014a. Phex mimetic (spr4-peptide) corrects and improves hyp and wild type mice energy-metabolism. PloS one. 9(5):e97326.

Zelenchuk LV, Hedge AM, Rowe PS. 2014b. Phex mimetic (spr4-peptide) corrects and improves hyp and wild type mice energy-metabolism. PloS one. 9(5):e97326.

Zhan Y, Holtfreter B, Meisel P, Hoffmann T, Micheelis W, Dietrich T, Kocher T. 2014. Prediction of periodontal disease: Modelling and validation in different general german populations. Journal of clinical periodontology. 41(3):224-231.

Zhong Y, Armbrecht HJ, Christakos S. 2009. Calcitonin, a regulator of the 25-hydroxyvitamin d3 1alpha-hydroxylase gene. The Journal of biological chemistry. 284(17):11059-11069.

Zoidis E, Ghirlanda-Keller C, Gosteli-Peter M, Zapf J, Schmid C. 2004. Regulation of phosphate (pi) transport and napi-iii transporter (pit-1) mrna in rat osteoblasts. The Journal of endocrinology. 181(3):531-540.

10 Appendix

10.1 Appendix 1: *In Vitro* Model of Human Biomineralization

RESEARCH REPORTS
Biomaterials & Bioengineering

B.R. Coyac[1,2,4,5], F. Chicatun[3], B. Hoac[1], V. Nelea[1], C. Chaussain[4,5], S.N. Nazhat[3], and M.D. McKee[1]*[,2]

[1]Faculty of Dentistry, McGill University, Montreal, QC, Canada; [2]Department of Anatomy and Cell Biology, McGill University, Montreal, QC, Canada; [3]Department of Mining and Materials Engineering, McGill University, Montreal, QC, Canada; [4]EA 2496, Pathologies, Imaging and Biotherapies of the Tooth, Faculty of Dentistry, University Paris Descartes PRES Sorbonne Paris Cité, Montrouge, France; and [5]AP-HP Odontology Department, Bretonneau Hôpitaux Universitaires PNVS and Centre de Référence des Maladies Rares du Métabolisme du Calcium et du Phosphore, AP-HP, Kremlin-Bicêtre, France; *corresponding author, marc.mckee@mcgill.ca

J Dent Res 92(7):648-654, 2013

Mineralization of Dense Collagen Hydrogel Scaffolds by Human Pulp Cells

ABSTRACT

While advances in biomineralization have been made in recent years, unanswered questions persist on bone- and tooth-cell differentiation, on outside-in signaling from the extracellular matrix, and on the link between protein expression and mineral deposition. In the present study, we validate the use of a bioengineered three-dimensional (3D) dense collagen hydrogel scaffold as a cell-culture model to explore these questions. Dental pulp progenitor/stem cells from human exfoliated deciduous teeth (SHEDs) were seeded into an extracellular matrix-like collagen gel whose fibrillar density was increased through plastic compression. SHED viability, morphology, and metabolic activity, as well as scaffold mineralization, were investigated over 24 days in culture. Additionally, measurements of alkaline phosphatase enzymatic activity, together with immunoblotting for mineralized tissue cell markers ALPL (tissue-non-specific alkaline phosphatase), DMP1 (dentin matrix protein 1), and OPN (osteopontin), demonstrated osteo/odontogenic cell differentiation in the dense collagen scaffolds coincident with mineralization. Analyses of the mineral phase by electron microscopy, including electron diffraction and energy-dispersive x-ray spectroscopy, combined with Fourier-transform infrared spectroscopy and biochemical analyses, were consistent with the formation of apatitic mineral that was frequently aligned along collagen fibrils. In conclusion, use of a 3D dense collagen scaffold promoted SHED osteo/odontogenic cell differentiation and mineralization.

KEY WORDS: dental pulp stem cells, deciduous teeth, dense collagen hydrogels, plastic compression, cell differentiation, tissue engineering, bioengineering.

DOI: 10.1177/0022034513488599

Received January 11, 2013; Last revision April 4, 2013; Accepted April 9, 2013

A supplemental appendix to this article is published electronically only at http://jdr.sagepub.com/supplemental.

INTRODUCTION

Characteristic of mineralized tissues is a fibrillar collagenous extracellular matrix infiltrated with additional non-collagenous proteins and proteoglycans thought to guide the mineralization process (McKee *et al*., 2012). Conditions for matrix mineralization require macromolecular assembly and maturation, which involve enzymatic processing of matrix components (Kaartinen *et al*., 2002, 2005; Barros *et al*., 2012). As a result, in bone, dentin, and cementum, there is a lag time before mineralization occurs, resulting in an unmineralized layer of osteoid, predentin, and cementoid, respectively. Such a three-dimensional (3D) extracellular matrix scaffolding appears to be essential for eliciting differentiation responses from resident cells to create a molecular environment receptive to mineralization.

Currently, there is a lack of cell-culture models for mineralized tissues capable of reproducing, in particular, the 3D matrix environment essential for the study of cell differentiation as it relates to matrix mineralization. While primary cell cultures that produce mineralizing extracellular matrix nodules are useful for some purposes, most commonly used cell-culture lines produce very little extracellular matrix and are largely two-dimensional (2D) systems on plastic dish surfaces, thus calling into question their physiologic relevance. From a handful of cell lines that are often used to study mineralization, only the MC3T3-E1 (subclones 4/14) mouse osteoblast cell line has highly reproducible osteoblastic differentiation, abundant extracellular matrix production/accumulation, assembly and maturation, and mineralization (Wang *et al*., 1999). Thus, available culture systems for bone, cartilage, and tooth cells remain far from replicating *in vivo* conditions, and thus the use of 3D collagen hydrogel scaffolds is currently being explored to mimic natural osteoid, predentin, and cartilage (Wallace and Rosenblatt, 2003; Geckil *et al*., 2010; Salmon *et al*., 2013). Dense collagen 3D scaffolds likely better reflect the natural matrix environment in terms of guiding cell differentiation (and mineralization) relevant to tooth and bone biology (Bitar *et al*., 2008; Buxton *et al*., 2008; Pedraza *et al*., 2010; Chicatun *et al*., 2011) compared with the highly hydrated collagen hydrogels used previously (Wiesmann *et al*., 2003; Takitoh *et al*., 2010).

Plastic compression of *in vitro* reconstituted collagen type I hydrogels is a rapid and reproducible technique for the production of scaffolds with physiologically relevant increased collagen fibrillar density (*i.e*., greater than 10%

by weight) (Brown *et al*., 2005). This compression method results in scaffolds with increased mechanical properties and extracellular matrix-like mesoscale characteristics, while including the option of having viable cell seeding as part of the processing route (Abou Neel *et al*., 2006; Pedraza *et al*., 2010; Chicatun *et al*., 2011; Ghezzi *et al*., 2011); as such, they show great promise for tissue-engineering applications.

While some cell-culture models exist that mimic certain aspects of tooth development and matrix mineralization, the quantity of *in vitro* experimental data available for tooth cells has generally not kept pace with that obtained for osteoblasts and chondroblasts/cytes, and mineralized tissue craniofacial biology research as a whole has suffered from this lack of information. However, there have been recent improvements in methodologies for obtaining and cultivating stem cells from teeth (Gronthos *et al*., 2000; Shi and Gronthos, 2003). Promising new approaches can now be applied to dental ectomesenchymal progenitor cells (stem cells) obtained from human exfoliated deciduous teeth (SHEDs) that are readily available through routine tooth extraction and natural tooth exfoliation (Miura *et al*., 2003; Kerkis and Caplan, 2012). Combined use of SHEDs with 3D dense collagen hydrogel scaffolds would thus appear to be promising for promoting cell differentiation toward the odontoblastic and osteoblastic phenotypes in a way that would not only allow for a better understanding of tooth and bone cell biology, but which could also be useful for dental and craniofacial reconstructions and other bioengineering purposes (Huang *et al.*, 2009; Kim *et al.*, 2012). Having previously reported on SHED differentiation in 2D conventional cell cultures (Salmon *et al*., 2013), and with the objective of describing their behavior in the 3D environment of plastically compressed, dense collagen scaffolds, here we report that, in these 3D scaffolds, SHEDs are a highly proliferative population of cells that differentiate toward an odontoblastic/osteoblastic phenotype with concomitant mineralization of the surrounding collagen.

MATERIALS & METHODS

Cell Source and Culture

Normal exfoliated human deciduous teeth were collected from children aged 3 to 7 yrs with the informed consent of the patients and their parents, according to ethical guidelines set by French bioethics law. SHEDs were isolated and expanded following an established protocol (Gronthos *et al*., 2000; Miura *et al*., 2003). For all experiments, SHEDs were used between passages 4 and 7.

Scaffold Preparation

Plastically compressed collagen gels were used as 3D scaffolds and were prepared as previously described (Brown *et al*., 2005; Abou Neel *et al*., 2006). Briefly, 3.6 mL of sterile rat-tail collagen type I (First Link Ltd., Wolverhampton, UK) at a protein concentration of 2.01 mg/mL in 0.6% acetic acid was mixed with 0.9 mL of ×10 DMEM (Dulbecco's Modified Eagle Medium) and neutralized by drop-wise addition of 5 M NaOH to ~pH 7.4. After neutralization, SHEDs were incorporated into the collagen solution at a cell density of 150,000 cells/mL, and then a quantity of 0.9 mL/well was pipetted into a 4-well plate, followed by 30 min of incubation at 37°C.

After polymerization, highly hydrated hydrogels (with < 0.5 weight % fibrillar collagen density) were placed on a stack of blotting paper, nylon, and stainless mesh, and dense collagen scaffolds (with > 10 weight % fibrillar collagen density) were produced by the application of an unconfined compressive stress of 1 kPa for 5 min to remove excess casting fluid (Fig. 1A) (Brown *et al*., 2005).

Osteo/Odontogenic Cell Differentiation

Scaffolds were cultured in 6-well plates with osteogenic medium (DMEM media supplemented with 300 μM L-ascorbic acid sodium salt, 10 nM dexamethasone, 10 mM β-glycerophosphate, 10% fetal bovine serum, and 1% penicillin/streptomycin). Acellular gels cultured in this osteogenic medium served as control scaffolds.

Assessment of Cell Viability within the Scaffold

Cell viability and distribution among the dense collagen scaffolds were assessed using the Live/Dead® cell viability-cytotoxicity assay (Invitrogen, Carlsbad, CA, USA) at days 0, 8, and 16 as viewed with a confocal laser scanning microscope (CLSM, Carl Zeiss, LSM5 Exciter, Toronto, ON, Canada).

Microscopy Analyses of Scaffolds and Cells

Light microscopy was used to examine SHED-seeded scaffolds after 16 days in culture. Scanning electron microscopy (SEM) and transmission electron microscopy (TEM) were performed to analyze scaffold microstructure as well as cellular morphology and mineralization. Energy-dispersive x-ray spectroscopy (EDS) was performed for elemental analysis of mineral, and crystalline structure of the mineral was assessed by electron diffraction.

Attenuated Total Reflectance Fourier-transform Infrared Spectroscopy (ATR-FTIR)

Structural characterization of mineralized scaffolds was performed by ATR-FTIR. Spectra were baseline-corrected and normalized at absorbance 1.5 on the amide I peak for comparison purposes (Spectrum software, Perkin-Elmer, Waltham, MA, USA).

Phosphate and Calcium Quantification

To assess phosphate levels, we incubated samples at days 0, 8, 16, and 24 in 15% trichloroacetic acid for 1 hr. After centrifugation, the supernatant was assayed by the addition of 50% acetone, 2.5 M sulfuric acid, and 2.5 mM ammonium molybdate (Sigma, St. Louis, MO, USA). Color development was stopped by the addition of 1 M citric acid, and absorbance was measured at a wavelength of 355 nm. Calcium levels in the supernatant were spectrophotometrically measured at wavelength 595 nm by means of a calcium assay kit (Genzyme Diagnostics, Mount Laurel, NJ, USA).

Alkaline Phosphatase (ALP) Activity Measurement

Cultured scaffolds were solubilized, and after sonication and centrifugation, supernatant ALP activity at each time-point was

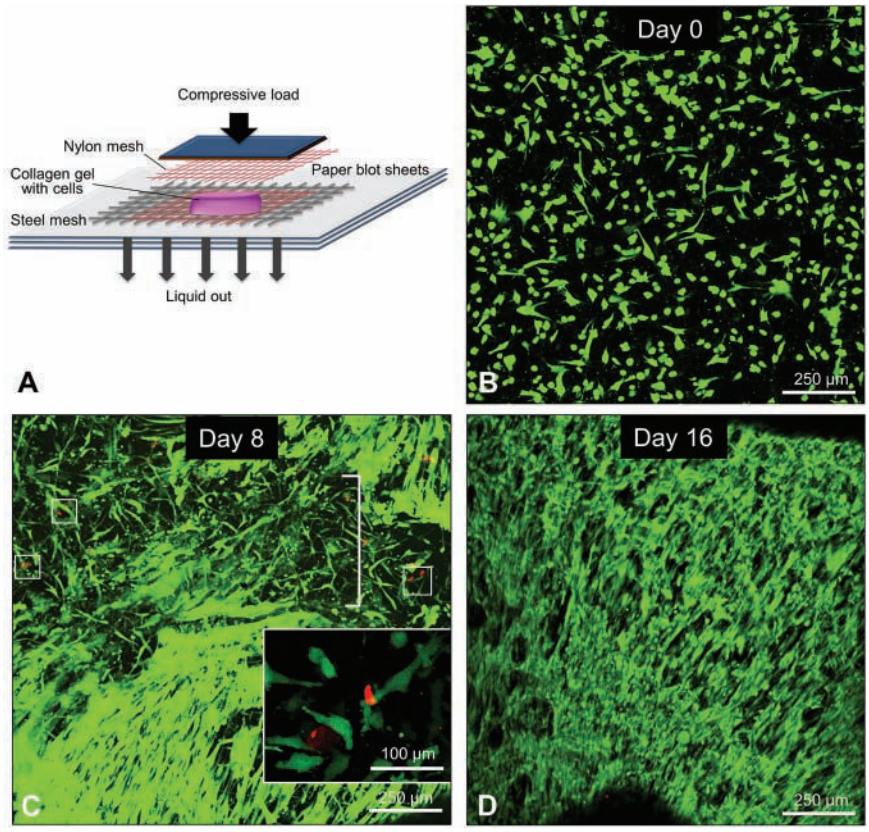

Figure 1. 3D scaffolds made by plastic compression of collagen gels and SHED-seeded viability and morphology. (**A**) Diagram showing the layered elements used to form dense collagen scaffolds by plastic compression of pre-formed, highly hydrated collagen gels. Polymerized gels are compressed between a stack of blotting paper, nylon mesh, and stainless steel mesh (schema adapted from Brown *et al.*, 2005). (**B-D**) Live/Dead® cell staining at different time-points after culture of cells seeded within dense collagen under osteogenic conditions. Green-labeled cells represent viable cells with no membrane disruption, while the nucleus of dead cells stains red (boxed regions). At day 0, immediately after plastic compression, all cells are observed to be viable (green) and well-dispersed throughout the entire scaffold. At days 8 and 16, a high density of viable cells is observed with a limited number of dead cells (red, in boxes in panel C and inset). Two cell populations are observed: a population of finer, more stellar-shaped cells abundant in the core of the scaffold (bracket) and another cell population located more toward the edges of the scaffold presenting an aligned, spindle-shaped morphology. Scale bar equals 250 µm.

determined colorimetrically with a substrate solution (SIGMA *FAST*™ p-nitrophenyl phosphate and Tris buffer tablets, Sigma). Absorbance reading was taken at 405 nm. Calf intestinal ALP (Sigma) was used as a standard.

Western Blotting

A 20-µg quantity of total protein extracts of each sample was separated by SDS-PAGE on a 10% gel, transferred to a polyvinylidene difluoride membrane, and blocked in 5% bovine serum albumin (BSA) in Tris-buffered saline/Tween 20 (TBS-T). The membranes were probed with the following antibodies: goat anti-human osteopontin (OPN) antibody (AF 808, R&D Systems, Minneapolis, MN, USA), mouse anti-human DMP1 (LF-148), mouse anti-human ALP (B4-78 supernatant; Jerry A. Katzmann, Developmental Studies Hybridoma Bank, Mayo Clinic, Rochester, NY, USA), and rabbit anti-mouse actin (Sigma) in 5% BSA/TBS-T. Membranes were then incubated with horseradish peroxidase-conjugated anti-goat, -mouse, or -rabbit secondary antibody and visualized with Amersham™ ECL™ Prime Western Blotting Detection Reagent (GE Healthcare, Buckinghamshire, UK).

Statistical Analysis

Experiments were performed in triplicate for each time-point and each condition. Data were compared with baseline values (day 0) by non-parametric tests (Kruskal-Wallis test followed, if significant, by group comparisons with the Mann-Whitney *U*-test). Differences were considered significant at $p < .05$. Data are expressed as mean ± SD. [Additional experimental details are available online in the Appendix.]

RESULTS

SHED Viability, Distribution, and Morphology within Dense Collagen Gels

After plastic compression of SHED-seeded collagen gels (Fig. 1A), Live/Dead® staining showed that cells were viable and well-distributed throughout the scaffold immediately after compression (Fig. 1B). At days 8 (Fig. 1C) and 16 (Fig. 1D) in culture, cells maintained their viability throughout the full thickness of the scaffold (Figs. 1B-1D), but displayed 2 distinct morphologies depending on their location. Centrally located cells appeared more stellar-shaped (bracket in Fig. 1C), while cells toward the edges of the scaffold were more spindle-shaped and aligned. SEM and TEM of acellular (Figs. 2A, 2B) and cell-seeded (Figs. 2C-2F) scaffolds revealed a fine meshwork of collagen fibrils constituting the scaffold and well-integrated cells dispersed throughout, with close approximations between cells and collagen fibrils (Figs. 2E, 2F).

Detection of Osteo/Odontogenic Cell Differentiation

Immunoblotting for mineralization-associated marker proteins ALPL, DMP1, and OPN produced under osteogenic conditions by the SHEDs in the scaffolds revealed osteo/odontogenic cell differentiation over time (Fig. 2G). ALP enzyme activity within the cultures increased initially, and then decreased, with time (Fig. 2H).

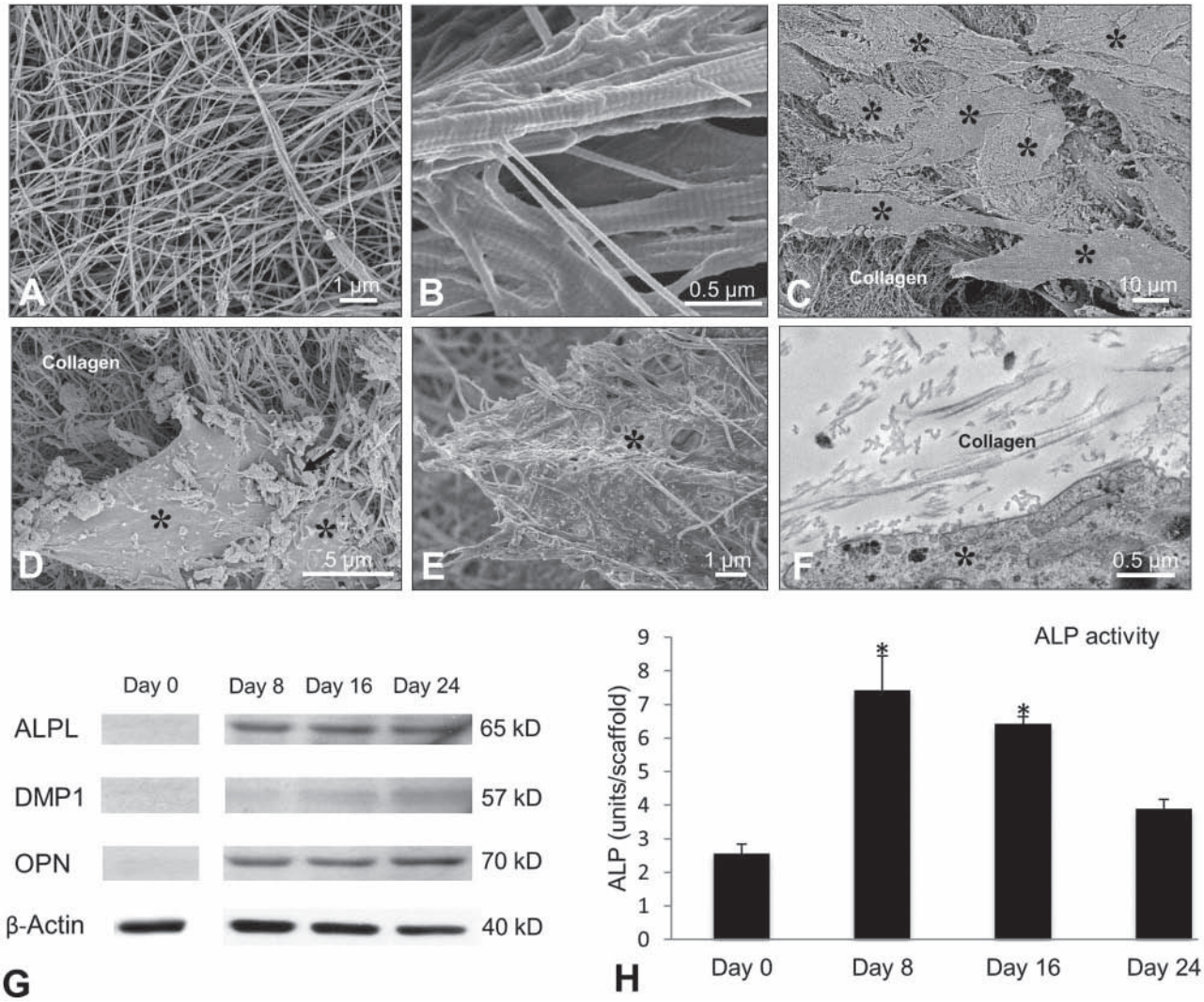

Figure 2. Microscopic analysis of SHEDs in dense collagen gels and enzyme activity and marker protein immunoblotting. (**A,B**) Scanning electron microscopy (SEM) of control acellular dense collagen scaffolds incubated at 37°C in osteogenic medium. The collagen fibrillar meshwork is clearly visible, as is the fibril banding pattern, and there is no evidence of mineralization. (**C**) SEM micrograph of a cell-seeded 16-day scaffold incubated with osteogenic medium. SHEDs (asterisks) appear in close proximity to one another within the collagen scaffold. (**D,E**) Higher magnification SEM micrographs of single cells (asterisks) embedded within the collagen (day 16 with osteogenic medium), showing some mineral-encrusted collagen fibrils (arrow) at some sites (D), and the close proximity of collagen fibrils to the cell surface at other sites (E). (**F**) Transmission electron microscopy (TEM) of the outer portion of a cell (asterisk) showing the close proximity of the cell membrane with collagen fibrils. (**G**) Western blotting of mineralization-associated proteins ALPL, DMP1, and OPN produced by SHEDs (whole-cell lysates) at the indicated time-points after incubation in osteogenic medium. Actin was used as a loading control. (**H**) Alkaline phosphatase enzymatic activity at the indicated time-points after incubation in osteogenic medium (n = 3). * indicates $p < .05$ relative to day 0. Values are expressed as mean (± SD).

Mineralization of SHED-seeded Collagen Scaffolds

Under osteogenic conditions, calcium and phosphate concentrations within the scaffolds increased over time in the cell-seeded scaffolds compared with acellular scaffolds (Figs. 3A, 3B), and evidence obtained by FTIR revealed a phosphate peak suggesting the presence of carbonato-apatite (Fig. 3C). Mid-infrared ATR-FTIR spectra of the mineralized scaffolds at day 16 revealed characteristic peaks for collagen (amide I band at 1653 cm^{-1}, with additional amide bands II and III). The shape and the value of PO_4^{3-} band at 1028 cm^{-1} and the presence of the absorbance peak at 882 cm^{-1}, which is attributed to the stretching mode of CO_3^{2-}, suggested that the mineral phase was carbonated apatite.

With microscopic approaches to the analysis of sections of cell-seeded scaffolds under osteogenic conditions, von Kossa staining revealed mineral deposition within the collagenous scaffold (Figs. 4A, 4B), but not in acellular control scaffolds (data not shown). SEM and TEM confirmed the extracellular location of the mineral along collagen fibrils (Figs. 4C-4F), and x-ray microanalysis and electron diffraction identified the mineral as apatite (Fig. 4G). Occasionally, spherulitic mineral deposits were observed in the scaffolds (Figs. 4H-4J), presumably resulting from radial expansion of originally smaller mineralization foci whose origin is unknown.

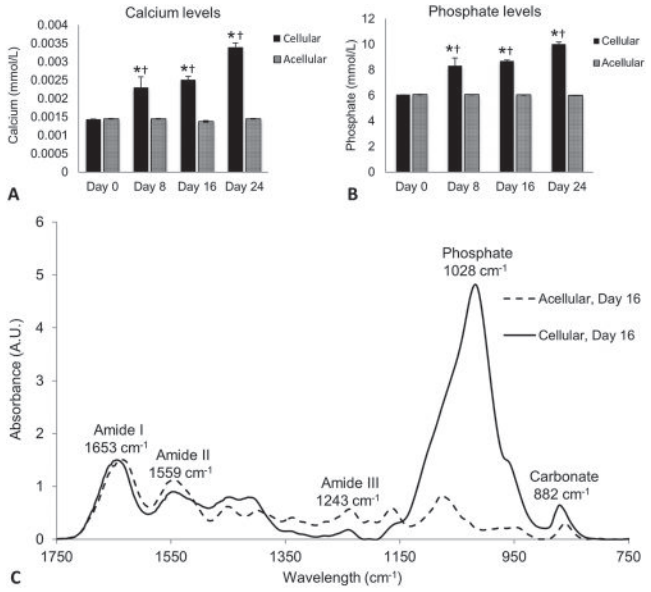

Figure 3. Biochemical and FTIR analyses of mineralization of SHED-seeded dense collagen scaffolds under osteogenic conditions. Calcium (**A**) and phosphate (**B**) levels in cellular and acellular scaffolds incubated in osteogenic medium up to 24 days (n = 3). * indicates p < .05 relative to day 0. † indicates p < .05 relative to acellular scaffold alone incubated in osteogenic medium at the same time-point. Values are expressed as mean (± SD). (**C**) ATR-FTIR spectra of cellular and acellular scaffolds at day 16 in culture in osteogenic medium (n = 3). Spectra were obtained in transmittance mode at 4 cm^{-1} resolution (64 scans) over a range of 4,000-650 cm^{-1}. Spectra were baseline-corrected and normalized to absorbance 1.5 of the amide I peak for comparison purposes.

DISCUSSION

In the present study, our objective was to determine whether a 3D fibrillar collagen gel scaffold with a density approaching that of native extracellular matrix as found in osteoid and predentin could sustain cell viability and induce odonto/osteoblastic differentiation from human exfoliated tooth pulp-derived stem cells (SHEDs). Furthermore, the production of odonto/osteoblastic marker proteins over time coincided with collagen scaffold mineralization. Importantly, and unlike what so often occurs dystrophically in other mineralizing cell-culture models (other than when the MC3T3-E1 cell line is used), mineralization occurred appropriately along collagen fibrils in a manner described previously for the potential of collagen fibrils to mineralize (Silver and Landis, 2011), and the calcium-phosphate mineral phase was apatitic as is found in bones and teeth.

In the cultures, alkaline phosphatase activity − a commonly used measure for mineralized tissue cell lineage progression at early culture time-points − steadily increased until day 16 and then decreased, an observation consistent with previous reports for a variety of cell types (Bitar *et al*., 2008; Pedraza *et al*., 2010; Chicatun *et al*., 2011). DMP1 and OPN were also detected early in the cell cultures, starting from day 8. Analysis of the considerable quantity of recent data indicates that DMP1 promotes mineralization (Gajjeraman *et al*., 2007), while phosphorylated OPN and its peptides are generally thought to regulate crystal growth by direct binding and inhibition at formed crystallographic surfaces (Boskey *et al*., 2002; Gericke *et al*., 2005; Hunter *et al.*, 2010). Indeed, the presence of these secreted marker proteins, and their correlation with the appearance of mineralization in the cultures, attests to the matrix-inducible, cell-mediated deposition and regulation of the mineral phase, which is a critical end-point hallmark feature when odonto/osteoblastic differentiation is being considered. Likewise, the ultrastructural localization of the mineral phase along the dense collagen fibrils constituting the scaffold, together with identifying characteristic mineral properties, further attests to the fact that this 3D cell-culture system mimics, in some key ways, the conditions permissive to physiologic mineralization as seen *in vivo* in bones and teeth. Indeed, the finding of a carbonate peak by FTIR from the mineral phase is consistent with the known carbonate content (carbonate-substituted apatite, or carbonatoapatite) of tooth and bone mineral (Pedraza *et al*., 2010; Chicatun *et al*., 2011). Furthermore, the electron diffraction pattern showing poorly crystallized apatite is consistent with biologic hydroxyapatite (Lee *et al*., 1986).

We have previously reported that plastic compression of osteoprogenitor (MC3T3-E1 cells)-seeded collagen gels resulted in osteoblast marker gene expression and scaffold mineralization (Pedraza *et al.*, 2010). In that study, the differentiated osteoblasts produced nascent collagen fibrils that assembled extracellularly and contributed to the scaffold environment. In the present study, there was little evidence of this collagen production. For SHEDs as used in this system, the collagen scaffold provided to the cells appeared to be sufficient (not requiring additional nascent collagen secretion) to provide outside-in signaling, leading to cell differentiation and to the secretion of other, mineralization-regulating proteins (shown here for ALPL, DMP1, and OPN) concomitant with the observed scaffold mineralization. Somewhat different from our previous osteoblast study, where scaffold mineralization generally occurred in peripheral regions of the scaffold and in close proximity to the cells (Pedraza *et al.*, 2010), here we observed a fairly evenly dispersed mineralization pattern throughout all regions of the scaffold. On occasion, slightly increased mineralization was seen in the more central regions, perhaps reflecting a slight cell preference for hypoxic conditions, as has been proposed to increase cell-mediated mineralization (Li *et al*., 2011).

In conclusion, the current results indicate that SHEDs may behave similarly to rodent cell lines used previously showing cell differentiation, but with the important additional feature of now allowing for the consideration of potentially using patient cells for clinical repair of osseous and dental defects. Bioengineered mineralized tissue repair strategies might also benefit from this work, as might patients having genetic disorders detrimentally affecting bone and dentin mineralization.

ACKNOWLEDGMENTS

This study was supported by CIHR and NSERC (Canada), McGill University Faculty of Engineering Gerald Hatch Faculty Fellowship (for SNN) and McGill Engineering Doctoral Awards, the Vasdaz and Hatch Fellowships (for FC), and, from France, by the Fondation de l'Avenir, the Fondation des Gueules Cassées, and the Conseil National de l'Ordre des Chirurgiens-

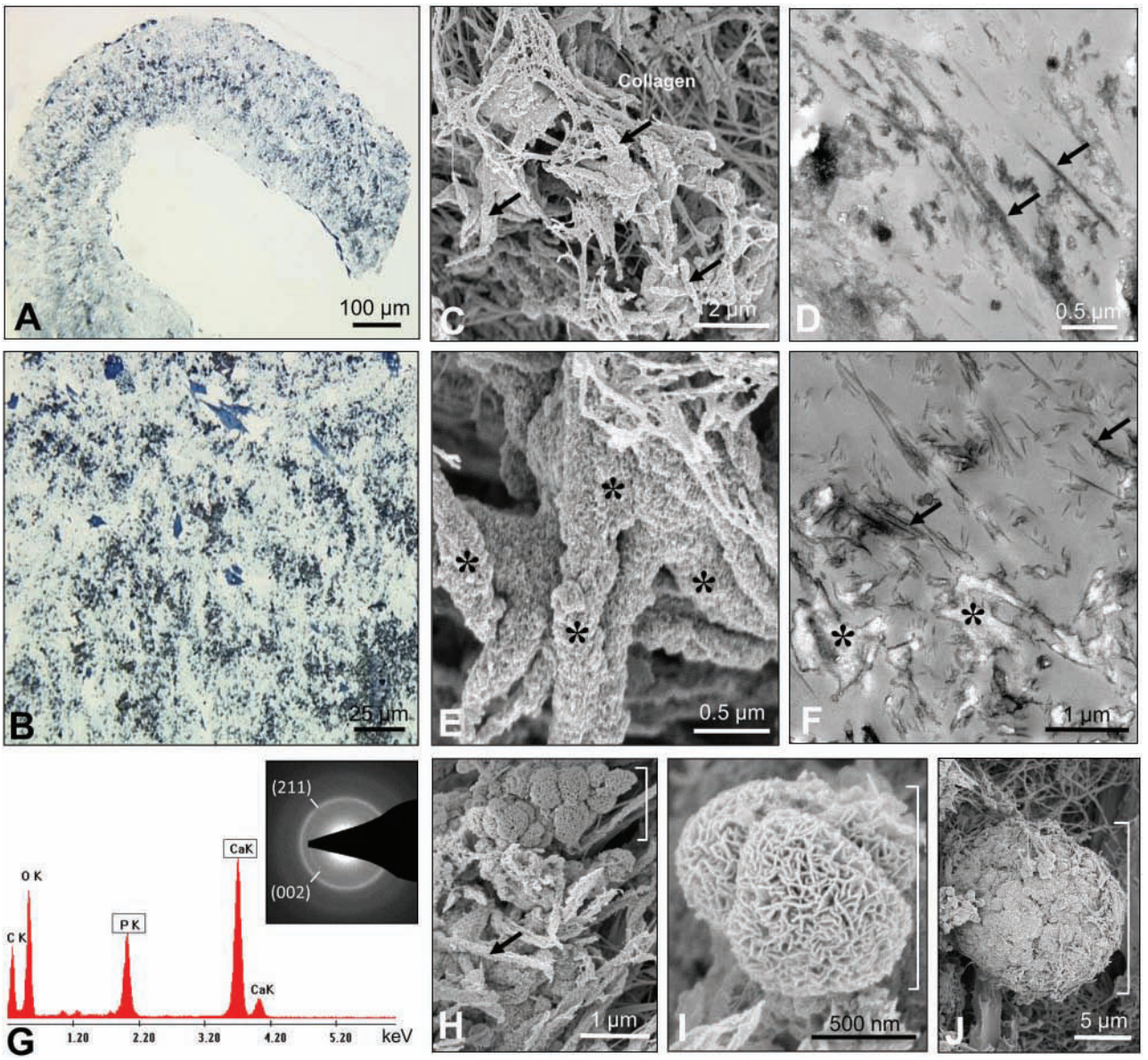

Figure 4. Microscopy of mineralization of SHED-seeded dense collagen scaffolds under osteogenic conditions at 16 days of culture. (**A,B**) Light micrographs of a sectioned cell-seeded scaffold stained for mineral (von Kossa staining, black) and counterstained with toluidine blue. Cells and mineral are found throughout the scaffold, with some slight concentration of mineral toward the core of the scaffold. (**C-F**) At the ultrastructural level, SEM (C,E) and TEM (D,F) observations show mineral-encrusted collagen fibrils of small (arrows) and larger (asterisks) diameter. (**G**) Energy-dispersive x-ray (EDS) spectroscopy of mineralized collagen shows major spectral peaks for calcium (Ca) and phosphorus (P), and electron diffraction shows diffraction maxima characteristic of apatite (inset). (**H-J**) Occasionally, spherulitic mineral deposits (brackets) were observed among mineralized collagen fibrils (arrow).

Dentistes (for BRC). We thank Lydia Malynowsky for assistance with microscopy and Dr. Louis Lassalle for assistance with the statistics. The authors declare no potential conflicts of interest with respect to the authorship and/or publication of this article.

REFERENCES

Abou Neel EA, Cheema U, Knowles JC, Brown RA, Nazhat SN (2006). Use of multiple unconfined compression for control of collagen gel scaffold density and mechanical properties. *Soft Matter* 2:986-992.

Barros NMT, Hoac B, Neves RL, Addison WN, Assis DM, Murshed M, *et al.* (2013). Proteolytic processing of osteopontin by PHEX and accumulation of osteopontin fragments in Hyp mouse bone, the murine model of X-linked hypophosphatemia. *J Bone Miner Res* 28:688-699.

Bitar M, Brown RA, Salih V, Kidane AG, Knowles JC, Nazhat SN (2008). Effect of cell density on osteoblastic differentiation and matrix degradation of biomimetic dense collagen scaffolds. *Biomacromolecules* 9:129-135.

Boskey AL, Spevak L, Paschalis E, Doty SB, McKee MD (2002). Osteopontin deficiency increases mineral content and mineral crystallinity in mouse bone. *Calcif Tissue Int* 71:145-154.

Brown RA, Wiseman M, Chuo CB, Cheema U, Nazhat SN (2005). Ultrarapid engineering of biomimetic materials and tissues: fabrication

of nano- and microstructures by plastic compression. *Advanced Functional Mater* 15:1762-1770.

Buxton PG, Bitar M, Gellynck K, Parkar M, Brown RA, Young AM, *et al*. (2008). Dense collagen matrix accelerates osteogenic differentiation and rescues the apoptotic response to MMP inhibition. *Bone* 43:377-385.

Chicatun F, Pedraza CE, Ghezzi CE, Marelli B, Kaartinen MT, McKee MD, *et al*. (2011). Osteoid-mimicking dense collagen/chitosan hybrid gels. *Biomacromolecules* 12:2946-2956.

Gajjeraman S, Narayanan K, Hao J, Qin C, George A (2007). Matrix macromolecules in hard tissues control the nucleation and hierarchical assembly of hydroxyapatite. *J Biol Chem* 282:1193-1204.

Geckil H, Xu F, Zhang X, Moon S, Demirci U (2010). Engineering hydrogels as extracellular matrix mimics. *Nanomedicine* 5:469-484.

Gericke A, Qin C, Spevak L, Fujimoto Y, Butler WT, Sorensen ES, *et al*. (2005). Importance of phosphorylation for osteopontin regulation of biomineralization. *Calcif Tissue Int* 77:45-54.

Ghezzi CE, Marelli B, Muja N, Hirota N, Martin JG, Barralet JE, *et al*. (2011). Mesenchymal stem cell-seeded multilayered dense collagen-silk fibroin hybrid for tissue engineering applications. *Biotechnol J* 6:1198-1207.

Gronthos S, Mankani M, Brahim J, Robey PG, Shi S (2000). Postnatal human dental pulp stem cells (DPSCs) in vitro and in vivo. *Proc Natl Acad Sci USA* 97:13625-13630.

Huang GTJ, Gronthos S, Shi S (2009). Mesenchymal stem cells derived from dental tissues *vs*. those from other sources: their biology and role in regenerative medicine. *J Dent Res* 88:792-806.

Hunter GK, O'Young J, Grohe B, Karttunen M, Goldberg HA (2010). The flexible polyelectrolyte hypothesis of protein-biomineral interaction. *Langmuir* 26:18639-18646.

Kaartinen MT, El-Maadawy S, Rasanen NH, McKee MD (2002). Tissue transglutaminase and its substrates in bone. *J Bone Miner Res* 17:2161-2173.

Kaartinen MT, Sun W, Kaipatur N, McKee MD (2005). Transglutaminase crosslinking of SIBLING proteins in teeth. *J Dent Res* 84:607-612.

Kerkis I, Caplan AI (2012). Stem cells in dental pulp of deciduous teeth. *Tissue Eng Part B Rev* 18:129-138.

Kim BC, Bae H, Kwon IK, Lee EJ, Park JH, Khademhosseini A, *et al*. (2012). Osteoblastic/cementoblastic and neural differentiation of dental stem cells and their applications to tissue engineering and regenerative medicine. *Tissue Eng Part B Rev* 18(3):235-244.

Lee DD, Landis WJ, Glimcher MJ (1986). The solid, calcium-phosphate mineral phases in embryonic chick bone characterized by high-voltage electron diffraction. *J Bone Miner Res* 1:425-432.

Li L, Zhu YQ, Jiang L, Peng W, Ritchie HH (2011). Hypoxia promotes mineralization of human dental pulp cells. *J Endod* 37:799-802.

McKee MD, Murshed M, Kaartinen MT (2012). Extracellular matrix and mineralization of craniofacial bone. In: Mineralized tissues in oral and craniofacial science: biological principles and clinical correlates. McCauley LK, Somerman MJ, editors. USA: Wiley-Blackwell, pp. 99-109.

Miura M, Gronthos S, Zhao MR, Lu B, Fisher LW, Robey PG, *et al*. (2003). SHED: stem cells from human exfoliated deciduous teeth. *Proc Natl Acad Sci USA* 100:5807-5812.

Pedraza CE, Marelli B, Chicatun F, McKee MD, Nazhat SN (2010). An in vitro assessment of a cell-containing collagenous extracellular matrix-like scaffold for bone tissue engineering. *Tissue Eng Part A* 16:781-793.

Salmon B, Bardet C, Khaddam M, Naji J, Coyac BR, Baroukh B, *et al* (2013). MEPE-derived ASARM peptide inhibits odontogenic differentiation of dental pulp stem cells and impairs mineralization in tooth models of X-linked hypophosphatemia *PLOS ONE* 8:e56749.

Shi S, Gronthos S (2003). Perivascular niche of postnatal mesenchymal stem cells in human bone marrow and dental pulp. *J Bone Miner Res* 18:696-704.

Silver FH, Landis WJ (2011). Deposition of apatite in mineralizing vertebrate extracellular matrices: a model of possible nucleation sites on type I collagen. *Connect Tissue Res* 52:242-254.

Takitoh T, Kato Y, Nakasu A, Tadokoro M, Bessho M, Hirose M, *et al*. (2010). In vitro osteogenic differentiation of HOS cells on two types of collagen gels. *J Biosci Bioeng* 110:471-478.

Wallace DG, Rosenblatt J (2003) Collagen gel systems for sustained delivery and tissue engineering. *Adv Drug Deliv Rev* 55:1631-1649.

Wang D, Christensen K, Chawla K, Xiao GZ, Krebsbach PH, Franceschi RT (1999). Isolation and characterization of MC3T3-E1 preosteoblast subclones with distinct in vitro and in vivo differentiation mineralization potential. *J Bone Miner Res* 14:893-903.

Wiesmann HP, Nazer N, Klatt C, Szuwart T, Meyer U (2003). Bone tissue engineering by primary osteoblast-like cells in a monolayer system and 3-dimensional collagen gel. *J Oral Maxillofac Surg* 61:1455-1462.

10.2 Appendix 2: Osteopontin and the Pathobiology of XLH Appendicular Bone

Bone 95 (2017) 151–161

Contents lists available at ScienceDirect

Bone

journal homepage: www.elsevier.com/locate/bone

Full Length Article

Osteopontin and the dento-osseous pathobiology of X-linked hypophosphatemia☆

Tchilalo Boukpessi [a,b,c,*], Betty Hoac [a], Benjamin R. Coyac [a,b], Thibaut Leger [d], Camille Garcia [d], Philippe Wicart [e], Michael P. Whyte [f], Francis H. Glorieux [g], Agnès Linglart [h], Catherine Chaussain [b,c,1], Marc D. McKee [a,i,**,1]

[a] Faculty of Dentistry, McGill University, Montreal, QC, Canada
[b] EA 2496, Laboratory of Orofacial Pathologies, Imaging and Biotherapies, School of Dentistry University Paris Descartes Sorbonne Paris Cité, Paris, France
[c] AP-HP Department of Odontology, Charles Foix and Bretonneau Hospitals, Reference Center for Rare Diseases of Calcium and Phosphorus Metabolism, Paris, France
[d] Jacques Monod Institute, Proteomic Facility, University Paris Diderot Sorbonne Paris Cité, Paris, France
[e] AP-HP Department of Pediatric Orthopedics, Necker Hospital, School of Medicine University Paris Descartes Sorbonne Paris Cité, Reference Center for Rare Diseases of Calcium and Phosphorus Metabolism, Paris, France
[f] Center for Metabolic Bone Disease and Molecular Research, Shriners Hospital for Children, Division of Bone and Mineral Diseases, Department of Internal Medicine, Washington University School of Medicine at Barnes-Jewish Hospital, St. Louis, MO, USA
[g] Shriners Hospital for Children, McGill University, Montreal, QC, Canada
[h] AP-HP Department of Pediatric Endocrinology, Kremlin Bicêtre Hospital, School of Medicine University Paris Sud, Reference Center for Rare Diseases of Calcium and Phosphorus Metabolism, Paris, France
[i] Department of Anatomy and Cell Biology, Faculty of Medicine, McGill University, Montreal, QC, Canada

ARTICLE INFO

Article history:
Received 18 October 2016
Revised 11 November 2016
Accepted 19 November 2016
Available online 21 November 2016

Keywords:
PHEX
Mineralization
Rickets
Bone
Dentin
Osteocytic halos
Osteomalacia

ABSTRACT

Seven young patients with X-linked hypophosphatemia (XLH, having inactivating *PHEX* mutations) were discovered to accumulate osteopontin (OPN) at the sites of defective bone mineralization near osteocytes — the so-called hallmark periosteocytic (lacunar) "halos" of XLH. OPN was also localized in the pericanalicular matrix extending beyond the osteocyte lacunae, as well as in the hypomineralized matrix of tooth dentin. OPN, a potent inhibitor of mineralization normally degraded by *PHEX*, is a member of a family of acidic, phosphorylated, calcium-binding, extracellular matrix proteins known to regulate dental, skeletal, and pathologic mineralization. Associated with the increased amount of OPN (along with inhibitory OPN peptide fragments) in XLH bone matrix, we found an enlarged, hypomineralized, lacuno-canalicular network – a defective pattern of skeletal mineralization that decreases stiffness locally at: *i*) the cell-matrix interface in the pericellular environment of the mechanosensing osteocyte, and *ii*) the osteocyte's dendritic network of cell processes extending throughout the bone. Our findings of an excess of inhibitory OPN near osteocytes and their cell processes, and in dentin, spatially correlates with the defective mineralization observed at these sites in the skeleton and teeth of XLH patients. These changes likely contribute to the dento-osseous pathobiology of XLH, and participate in the aberrant bone adaptation and remodeling seen in XLH.

1. Introduction

X-linked hypophosphatemia (XLH) is the most prevalent heritable rickets/osteomalacia, and typically also manifests dental disease [1,2]. XLH is caused by inactivating mutations in the *PHEX* gene (phosphate-regulating gene with homologies to endopeptidases on the X chromosome) which encodes a zinc metallo-endopeptidase (The HYP Consortium) [3–5]. *PHEX* is predominantly expressed by the resident cells of bone matrix and tooth dentin [6]. In XLH, absent or decreased *PHEX* activity causes (among other changes) an increase in the circulating levels of the phosphatonin fibroblast growth factor 23 (FGF23), which leads to the renal phosphate wasting generally considered to be the primary pathophysiological disturbance responsible for the defective mineralization that manifests as skeletal osteomalacia and tooth dentinomalacia [2,7,8]. In most XLH patients, hypophosphatemia is diagnosed during early childhood as assessed by delayed walking, leg bowing, and growth failure. Patients frequently experience spontaneous dental abscesses both in the primary and permanent dentition, with infection and tissue damage extending beyond the tooth into the surrounding alveolar bone

☆ Was presented in part as an oral presentation at the annual meeting of the American Society for Bone and Mineral Research, September 16–19, 2016, Atlanta, GA, USA.

* Correspondence to: T. Boukpessi, EA 2496, Dental School University Paris Descartes Sorbonne Paris Cité, 1 rue Maurice Arnoux, 92120 Montrouge, France.
** Correspondence to: M.D. McKee, Faculty of Dentistry, Department of Anatomy and Cell Biology, McGill University, Montreal, QC H3A 0C7, Canada.
E-mail addresses: Tchilalo.boukpessi@parisdescartes.fr (T. Boukpessi), marc.mckee@mcgill.ca (M.D. McKee).
[1] Co-last authors.

http://dx.doi.org/10.1016/j.bone.2016.11.019
8756-3282/

[9,10]. Within XLH bone, a histopathologic hallmark is localized hypomineralization in the perilacunar matrix surrounding osteocytes. These focal mineralization defects are commonly referred to as osteocyte "halos" (or osteocytic lesions) based on their radiolucent appearance in thin, bone-section contact microradiographs, and their lack of mineralization in undecalcified bone histology [11]. A link between hypophosphatemia and these specific halos is uncertain, as is any common relationship to the milder halos seen in autosomal recessive hypophosphatemic rickets (ARHR) [12] and to the iron-dependent halos observed in the murine model of autosomal dominant hypophosphatemic rickets (ADHR) [13]; indeed, it is likely that multiple factors are involved in creating such a hypomineralized region in the bone extracellular matrix.

Osteopontin (OPN) is secreted by bone and tooth cells as a highly acidic, calcium-binding, extracellular matrix phosphoprotein that binds to mineral in bones and teeth (to inhibit crystal growth), and to pathologically deposited mineral when calcification occurs ectopically (*e.g.* cardiovascular calcification, nephrolithiasis) [14]. OPN is a member of the SCPP (secreted calcium-binding phosphoprotein) family of proteins that more specifically includes the SIBLING proteins (*S*mall *I*ntegrin-*B*inding *LI*gand, *N*-linked *G*lycoproteins) abundant in the extracellular matrix of mineralizing tissues (bones and teeth) [15]. SIBLING proteins are highly phosphorylated – a post-translational modification that imparts additional negative charge for binding to mineral at the exposed surface crystal lattice calcium having positive charge [16]. The SIBLING proteins are substantially processed extracellularly by enzymes, including degradation into active peptide fragments [17–23]. One of the major common characteristics of all SIBLING proteins is that they contain at least one highly acidic and phosphorylated motif called ASARM (*A*cidic *S*erine and *A*spartate-*R*ich *M*otif) [24] – an amino acid sequence with potent mineralization-regulating properties that persists within SIBLING protein fragments [25] and as an isolated peptide when cleaved from the C-terminal of matrix extracellular phosphoglycoprotein (MEPE) [21,24]. While the ASARM amino acid sequence is slightly variable among SIBLING proteins and among different species, this sequence (particularly when maximally phosphorylated) generally constitutes the most negatively charged modular domain of SIBLING proteins, and thus binds electrostatically very strongly to ionic calcium and positively charged mineral lattice calcium to act as a mineralization inhibitor [20]. While present in all SIBLING proteins, the best-characterized ASARM peptides are those of MEPE and OPN, both of which can be cleaved by *PHEX* at multiple sites to inactivate their mineralization-inhibiting potential [19,20].

To date, OPN remains the most studied of the SIBLING proteins, with a remarkable array of functions in different tissues [26–28]. For biomineralization, extensive *in vitro* and *in vivo* data indicate that OPN and its proteolytic fragments are extremely potent inhibitors of mineralization [29–32]. *In vitro*, native full-length OPN (particularly the phosphorylated forms) and its ASARM-containing peptides potently inhibit MC3T3-E1 osteoblast culture mineralization by binding to hydroxyapatite crystals in the extracellular matrix [19,20,32]. *In vivo*, OPN localizes to essentially all sites of mineralization observed in tissues, both normal and pathologic. Various transgenic mouse models support its inhibitory role in mineralization [33–37].

Of note, mineralization-inhibiting full-length OPN and OPN fragments (including the SIBLING protein ASARM peptide) accumulate in the hypomineralized bone matrix of Hyp mouse bone [23], the murine model of XLH carrying an inactivating *PHEX* mutation [38], and in hypomineralized human tooth dentin [21]. Among the enzymes that process SIBLING proteins and unlike most which target a single (or several) cleavage sites, *PHEX* uniquely and extensively degrades both full-length OPN protein and its peptides at dozens of sites, rendering them essentially inactive for inhibition of mineralization [39–41]. Hence, we investigated whether inhibitory OPN and OPN-ASARM-containing peptides accumulate in bone and tooth dentin of XLH patients. Our findings describing OPN accumulation in XLH provide a possible explanation for the osteocytic halos, and suggest a novel mechanism involving OPN in the defective mineralization of this disease. These findings are important to consider for the development of future therapies for XLH targeting specifically the mineralization defect; the current (1 alpha hydroxylated vitamin D analogs and phosphate supplementation) [10,42], or the latest-generation XLH treatments (antibody against FGF23) [43], mainly focus on correcting phosphate wasting.

2. Materials and methods

2.1. Patient information

XLH had been diagnosed at the collaborating institutions based on the disorder's characteristic findings and, when available, a pattern of X-linked dominant disease transmission and positive *PHEX* mutation analysis. Informed written consistent for the research procedures was obtained from the institutional ethics committees from all clinical sites (Paris, France; St. Louis, USA; Montreal, Canada). Bone and tooth samples were obtained with informed consent from the parents and patients, and with the approval of the local ethics committee (no. DC-2009-927, Cellule Bioéthique DGRI/A5, Paris, France, and the Human Research Protection Office, Washington University School of Medicine, St. Louis, MO, USA).

The clinical and biological characteristics of seven patients having familial hypophosphatemic rickets with identified *PHEX* mutations (XLH) are summarized in Table 1. Ten deciduous teeth were collected from Patients 1–4 having at least 2.5 years of medical therapy, consisting of conventional phosphate and 1-hydroxyvitamin D3 treatment [10,18,44]. Three of these teeth were extracted because of spontaneous tooth necrosis (Patient 2). The other teeth were vital at the time of tooth extraction; from these, two were extracted because of retarded exfoliation (Patient 1), and five were collected immediately after natural exfoliation (Patients 3 and 4). Two permanent teeth were collected from Patient 5 after extraction for reasons of infection. None of the collected teeth (deciduous and permanent) had an active carious lesion. The control group was constituted by sound deciduous and permanent teeth ($n = 4$ per group), obtained from healthy age-matched patients extracted for orthodontic reasons (or naturally exfoliated for deciduous teeth). Immediately after extraction, teeth were gently cleaned with tap water and stored at −80 °C prior to protein extraction.

Bone samples from three XLH patients (Patients 1, 6, and 7) were also collected during surgical correction of lower limb deformities. Sound, age-matched bone samples were collected from control patients having non-XLH-related surgical procedures. These bone samples were either fixed in 4% paraformaldehyde for histology and electron microscopy procedures, or were stored at −80 °C until processing for protein extraction.

2.2. Clinical and radiographic examination of XLH patients

Oral examination was performed by a senior dental practitioner at the National Reference Centre for Rare Disease (Kremlin Bicêtre Hospital, France) followed by taking of intraoral radiographs and an orthopantomogram. Also, tooth periapical inflammatory lesions were detected on panoramic radiographs and further characterized by 3D examination (cone-beam computerized tomography).

2.3. Protein extraction

XLH and control teeth and bone were prepared for protein extraction by thawing the samples and then trimming away excess tissue to exclusively have pure bone and dentin. To obtain protein extracts from these tissues, a 2-step sequential protein extraction scheme was used to first release protein from the unmineralized portion of the sample (cells and unmineralized matrix) termed the first guanidine extract (G1-extract), followed by a second step using EDTA to dissolve the

Table 1
Clinical and biological findings in 7 patients with *PHEX* mutations.
*At the time of tooth or bone sample collection. ΔFor Patient 1, deciduous teeth were collected during the childhood and bone at the end of growth when the leg surgery was indicated.
**DMFT for "Decayed, Missing, Filled permanent tooth and dft for "decayed, filled primary tooth". NA "non- applicable".

Patient	1Δ	2	3	4	5	1Δ	6	7
Gender	M	M	F	F	M	M	F	M
PHEX mutation	ex5 c.538 del T	Del ex 7–8	ex6 c.732 + 1 del GT	ex13 c.1471 del G	ex4 c.413 T > C	ex5 c.538 del T		ex17 c.1735 G > A
Age (years)*	6	7.5	5	9.5	16	13.5	18	17
Height (cm)*	97.0/−3.7	121.5/−0.2	108.3/0.5	127.5/−0.9	ND	136.0/−2.6	134.0/−6.8	152.5/−3.6
Weight (kg)*	16.0/−1.7	27.5/1.4	22.0/3.7	39/3.7	ND	44.5/0.0	52.0/−0.2	55.0/0.3
Signs of rickets								
Leg bowing*	++	+	+	+	+++	+++	+++	+++
Leg surgery	NA	NA	NA	NA	NA	Yes	Yes	Yes
Serum phosphate *(mM) NR: 1.2–1.6	0.74	0.61	1.02	0.63	0.72	0.68	0.84	0.54
Calcemia* (total, mM) NR: 2.25–2.65	2.38	2.36	2.58	2.28	2.25	2.45	2.15	2.26
Phosphaturia* (mM)	45	53.9	91.7	60	46.53	73.34	28.8	64.3
Treatment								
Medical treatment*	+	+	+	+	+	+	−	+
Compliance*	Good	Good	Good	Good	Bad	Bad	NA	Bad
Age at onset of treatment	1	0.5	2.5	3	0.75	1	−	3.75
1 alpha hydroxylated vitamin D analogs (μg/day)	1.5	1.2	2.25	0.3	3.5	2.5	−	3
Phosphates (mg/kg/day)	80	53	74.4	112	40	148.8	−	158.1
Dental status								
DMFT or dft index**	1	2	0	1	8	−	−	−
History of dental abscesses	Yes	Yes	Yes	No	Yes	Yes	−	Yes
Type of tooth collected	Deciduous	Deciduous	Deciduous	Deciduous	Permanent	NA	NA	NA
Bone collected	No	No	No	No	No	Yes	Yes	Yes
Teeth collected	Yes	Yes	Yes	Yes	Yes	No	No	No

inorganic phase of the sample and release mineral-bound proteins (the demineralized E1-extract); this procedure has been detailed previously [45]. Briefly, bone and dentin blocks were ground to a fine powder using a manual biopulverizer cooled in liquid nitrogen. To remove as much as possible the unmineralized portions of the tissue, powdered samples were initially extracted with 4 M guanidium-HCl in 50 mM Tris-HCl, pH 7.4, containing 0.1 mM phenylmethylsulfonyl fluoride (PMSF), 100 mg/mL of benzamidine and 5 mg/mL leupeptin, for two cycles of 24 h at 4 °C (G1-extract). This was followed by preparation of an EDTA-based demineralization extract (E-extract) using two repetitive cycles of 0.5 M EDTA exposure, in 50 mM Tris-HCl at pH 7.4, along with addition of 0.1 mM PMSF, 100 mg/mL benzamidine, and 5 mg/mL leupeptin, for 24 h at 4 °C.

2.4. Immunoblotting

Protein quantification of the bone and dentin extracts was initially performed using the bicinchoninic acid (BCA) protein assay (Pierce, Rockford, IL, USA). For immunoblotting of the protein extracts, for each sample, 3 μg of total protein extract was separated by SDS-PAGE on a 4% to 20% gradient gel, transferred to a PVDF membrane which was blocked in 5% bovine serum albumin (BSA) in Tris-buffered saline/Tween 20 (TBS-T), followed by probing of the membrane using goat anti-human OPN antibody (Cat. No. AF1433, R&D Systems, Minneapolis, USA) in 5% BSA/TBS-T and the visualization reagent (Pierce™ ECL Western Blotting Substrate, Rockford, USA). For immunoblotting with rabbit anti-phosphoserine antibody (Cat. No. 618100, Invitrogen, Camarillo, USA), the blocking solution used was 5% BSA with 0.1% gelatin in Tris-buffered saline/Tween 20 (TBS-T). Immunoblotted membranes were exposed to Carestream® Kodak® BioMax® light film (Sigma-Aldrich, St. Louis, USA) and developed films were scanned using an HP Scanjet G3110 scanner (Hewlett-Packard, Palo Alto, USA). Equal amounts of protein loading into gel lanes was verified by silver staining (data not shown).

2.5. Quantitation of OPN in XLH bone and dentin protein extracts

Protein extracts from two controls and two patients were processed for SDS-PAGE as above, and protein bands were excised from the gels for in-gel digestion overnight at 37 °C using sequencing-grade trypsin (12.5 μg/m; Promega, Madison, WI, USA) in 20 μL of 25 mmol/L NH_4HCO_3. Mass spectrometry (LC-MS/MS) data acquisition was performed with an Orbitrap Fusion Tribrid coupled to a Nano-LC Proxeon 1000 equipped with an easy-spray ion source (all from Thermo Scientific). Peptides were separated by Pepmap-RSLC Proxeon C_{18} column (50 cm, 75 μm i.d., 2 μm, 100 Å) with a 2-hour gradient. MS/MS data were processed using an in-house Mascot search engine (Matrix Science, Boston, MA; version 2.4.1). MS/MS data were searched against the Swissprot database with the *Homo sapiens* taxonomy. We searched for variable modifications: oxidation (M), carbamidomethylation (C) phosphorylation (S, T, Y), acetylation (K, N-term), deamidation (N, Q). Between-subject analyses for label-free quantification were carried out on the various datasets using Progenesis-QI software 2.0 (Nonlinear Dynamics Ltd., Newcastle, U.K.) according to the following procedure: *i*) chromatogram alignment, *ii*) peptide abundance normalization (total ion current), *iii*) statistical analyses of features, and *iv*) peptide identification using the Mascot server search. Peptides with a Mascot score under 15 were rejected for identification and quantification. Protein abundances are represented using the arc sinus hyperbolic function ($y = \ln(x + \sqrt{(1 + x^2)})$) for better representation of variation in abundance; Anova *p*-values were calculated to justify abundance variation.

2.6. Microscopy and immunostaining of human bone and dentin sections for OPN

Aldehyde-fixed bone and dentin samples used for histology, electron microscopy and immunostaining were either left undemineralized, or demineralized in 10% EDTA with 0.1% glutaraldehyde for 2 weeks at 4 °C before embedding in paraffin, LR White acrylic resin, or methyl methacrylate resin.

For light microscopy-level immunostaining for OPN, paraffin sections (10 μm) were dewaxed in xylene, hydrated in a graded ethanol series to pure distilled water, blocked using 5% BSA/TBS-T, and incubated for 1 h at room temperature with goat anti-human OPN antibody (R&D Systems, Minneapolis, MN, USA) diluted 1:200 in 5% BSA/TBS-T. Sections were washed and then incubated with peroxidase-conjugated anti-IgG diluted 1:1000 in the same buffer. Visualization of antibody staining was by peroxidase activity detection using a diaminobenzadine substrate kit from Abcam (Cambridge, MA, USA). Control incubations to assess nonspecific staining consisted of the same procedure except the primary antibody was omitted or substituted by non-immune serum (these control incubations resulted in no specific staining, data not shown).

For plastic/resin histology and transmission electron microscopy after immunogold labeling for OPN, bone samples were dehydrated and directly embedded in LR White acrylic resin (London Resin Company, Berkshire, UK), which was polymerized in block molds at 55 °C for 2 days. For electron microscopy, grid-mounted sections (80 nm) cut on an ultramicrotome were incubated with goat anti-human OPN antibody, followed by rabbit anti-goat secondary antibody and then protein A-colloidal gold (14 nm) conjugate (Dr. G. Posthuma, University of Utrecht, Utrecht, The Netherlands), and then conventional staining with uranyl acetate and lead citrate. Sections were viewed in a FEI Technai 12 transmission electron microscope (FEI, Hillsboro, OR, USA) operating at 120 kV and equipped with a 792 Bioscan 1k x_1k wide-angle multiscan CCD camera (Bioscan, Pleasanton, CA, USA). Control incubations to assess nonspecific binding of gold particles consisted of the same procedure except the primary antibody was omitted or substituted by non-immune serum (these control incubations resulted in no specific labeling, data not shown).

In some instances, bone samples in microtomed and/or polished block faces were imaged using scanning electron microscopy (Helios NanoLab 660 dual-beam microscope, FEI, Eindhoven, The Netherlands) operating in the backscattered electron imaging – a detection mode where the signal derives from atomic number in the specimen, thus discriminating mineralized from unmineralized tissue.

2.7. Contact radiography

Contact microradiography, which discriminates mineralized from unmineralized matrix, was performed using control and XLH bone samples as previously described after polishing (to 80-μm-thick) sections obtained using a circular saw [11]. X-ray microradiographs were obtained at 10 kV and 10 mA.

2.8. X-ray micro-computed tomography

Scanning of a dentin sample from Patient 5 was performed by micro-computed tomography (Bruker-MicroCT, model 1072, Kontich, Belgium) where the tomograph was equipped with a sealed, air-cooled microfocused X-ray source with a polychromatic beam derived from a tungsten target operating at 55 kV and 180 μA and using a 0.5 mm-thick aluminum filter. The sample was rotated 0.9°/step for 180°, while images were captured with an integrated, cooled CCD sensor (1024 × 1024 pixels) with fibre optic coupling to the scintillator. The resulting X-ray images were then reconstructed using NRecon (v. 1.6.1.3) and the image processing was performed using CT Analyzer (v. 1.10.0.2) which was also used to create a 3D-rendered reconstructed a slab of dentin from compiling multiple X-ray slices/images with a threshold setting chosen to highlight qualitatively the mineralization defects in XLH dentin.

3. Results

3.1. Bone and tooth characteristics of XLH

The seven XLH patients studied herein were receiving medical treatment with 1 alpha hydroxylated vitamin D analogs and phosphate supplementation (Table 1). All presented with leg deformities and three were scheduled for leg correction surgery (Fig. 1A). They underwent clinical and dental examinations, including radiographic studies. Despite medical therapy, their dental manifestations were characteristic of XLH [1], including: a normal (but slightly thinner) enamel layer, a radiolucent dentin layer with enlarged pulp chambers and prominent pulp horns, and a history of frequent spontaneous dental abscesses associated with severe bone resorption (Suppl. 1A,B and Suppl. 2) [46].

Three out of the seven patients (Patients 1, 6 and 7) had leg correction surgery and bone samples were collected during this procedure. Contact microradiographs of XLH cortical bone revealed the hallmark osteocyte “halos” appearing as enlarged radiolucent voids in osteons after contact radiography (Fig. 1B), and as hypomineralized matrix zones around osteocytes in conventional, plastic light microscopy sections of undemineralized samples after Goldner's Trichrome staining to discriminate mineralized (green) from unmineralized (magenta) bone (Fig. 1C). Widened and irregularly unmineralized osteoid seams characteristic of osteomalacia were evident in these samples. Higher-resolution imaging of the bone by scanning electron microscopy, using the backscattered electron signal deriving from the bone surface, revealed fine details of the hypomineralized halos compared to controls (Fig. 1D). In these samples, the hypomineralized perilacunar matrix surrounding osteocytes was readily observed, as was the delicate network of hypomineralized canaliculi emanating from the lacunae (collectively comprising the lacuno-canalicular system of bone), where canaliculi were more obvious and widened in diameter.

3.2. OPN accumulates in the abnormal osteocyte lacuno-canalicular system in XLH bone

To examine a potential cause for the hypomineralized osteocyte lacuna halo effect as well as the widening of the extended canalicular system, we studied this area for the distribution of OPN in the XLH patients as well as in controls. Immunohistochemistry for OPN at the light microscopic level, and immunogold labeling for OPN at the electron microscopic level, revealed an unusual abnormal distribution of OPN in the lacuno-canalicular system in XLH bone compared to control bone, and reproducible across samples. In control bone, OPN immunostaining was characteristically strongest at cement lines (corresponding to bone remodeling reversal sites), and only weakly associated with the lacuno-canalicular system (Fig. 2A, left panels) [47]. On the other hand, immunohistochemistry of XLH bone revealed intense OPN staining precisely located in the enlarged halo regions around osteocytes, and also in the canalicular network, a reaction not seen in control bone (Fig. 2A, right panels). At the ultrastructural level, using transmission electron microscopy after immunogold labeling for OPN to determine more precisely the localization of OPN at these specific sites, in control bone, accumulation of OPN at the lacuno-canalicular margins was restricted to a thin, well-defined *lamina limitans* [48] (Fig. 2B, left panels). In XLH bone, immunogold labeling for OPN was strong and diffuse at these sites in the lacuno-canalicular network, correlating with the discrete hypomineralized regions shown in Figs. 1B–D. Not all osteocytes in XLH have hypomineralized halos (Fig. 1C) [11], and the degree of osteocyte preservation state varies widely in human bone samples which are necessarily fixed by slowly penetrating aldehyde molecules in immersion fixation, but the immunolabeling observations were generally reproducible across osteocyte halos and patients.

We next performed sequential protein extractions from freshly collected XLH bone samples at the time of surgery to analyze their OPN content, and compare it to control bone. We first analyzed the

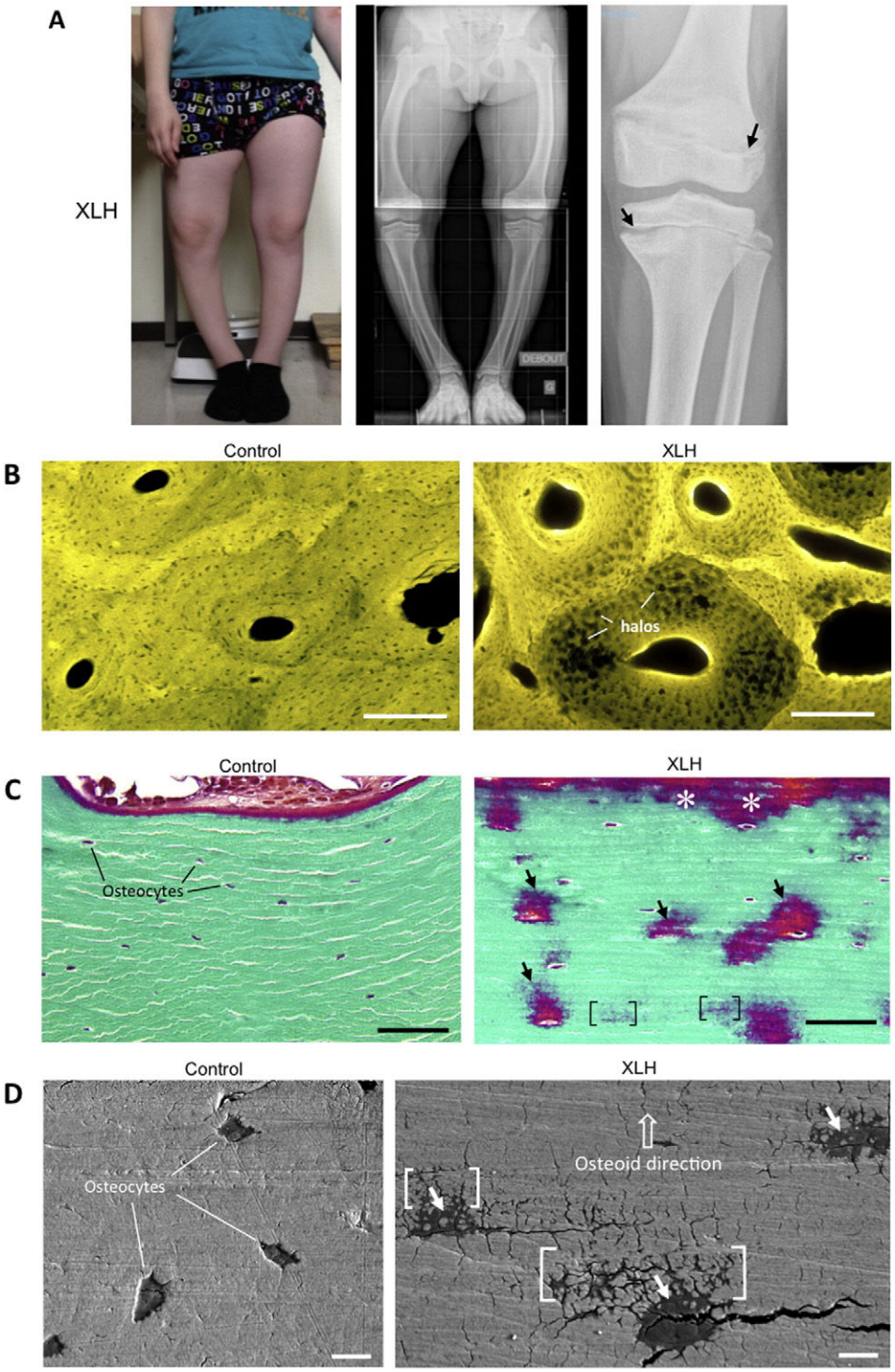

Fig. 1. A: Skeletal manifestations in a young patient with XLH. Photograph and antero-posterior radiographs of the lower extremities (standing) of a 13-year-old child (Patient 7) with XLH showing significant *genum varum* deformity. Antero-posterior radiograph of the knees demonstrates the physeal changes typical of untreated (or insufficiently-treated) XLH rickets. The physes are vertically widened and the growth plates have an irregular appearance (arrows). Some metaphyseal bowing of the femorae and tibiae is apparent. The patient (and parents) chose corrective leg surgery because of gait disturbance, activity limitations and leg pain. B, C, D: Microscopy of mineralization defects in XLH bone. B: Control and osteomalacic XLH patient bone (Patient 6) after contact microradiography of a thin femoral bone slice (scale bars, 200 μm). Hypomineralized "halos" around osteocytes are well-known, characteristic hallmark of this disease. C: Goldner's Trichrome staining of a sectioned (undecalcified) control and XLH bone (Patient 6) sample (scale bars, 50 μm). Osteoidosis (asterisks) and hypomineralized halos (arrows) appear as magenta-colored bone matrix (mineralized bone matrix is otherwise green), and on closer examination, even clusters of canaliculi (brackets) also show a fine, reticulated pattern of hypomineralization. D: Backscattered electron imaging in a dual-beam scanning electron microscope (scale bars, 10 μm). Whereas control bone is well mineralized both at the level of the osteoid with well-defined and clear, sharp-edged osteocyte lacunar margins, XLH bone (Patient 7) shows extensive periosteocytic "halos" (arrows) corresponding to hypomineralized bone matrix at these sites. Brackets indicate hypomineralized matrix surrounding canaliculi in XLH bone which results in the canaliculi being noticeably more prominent as they radiate away from osteocyte lacunae compared to control bone where their unmineralized diameters are less, and thus they are less visible.

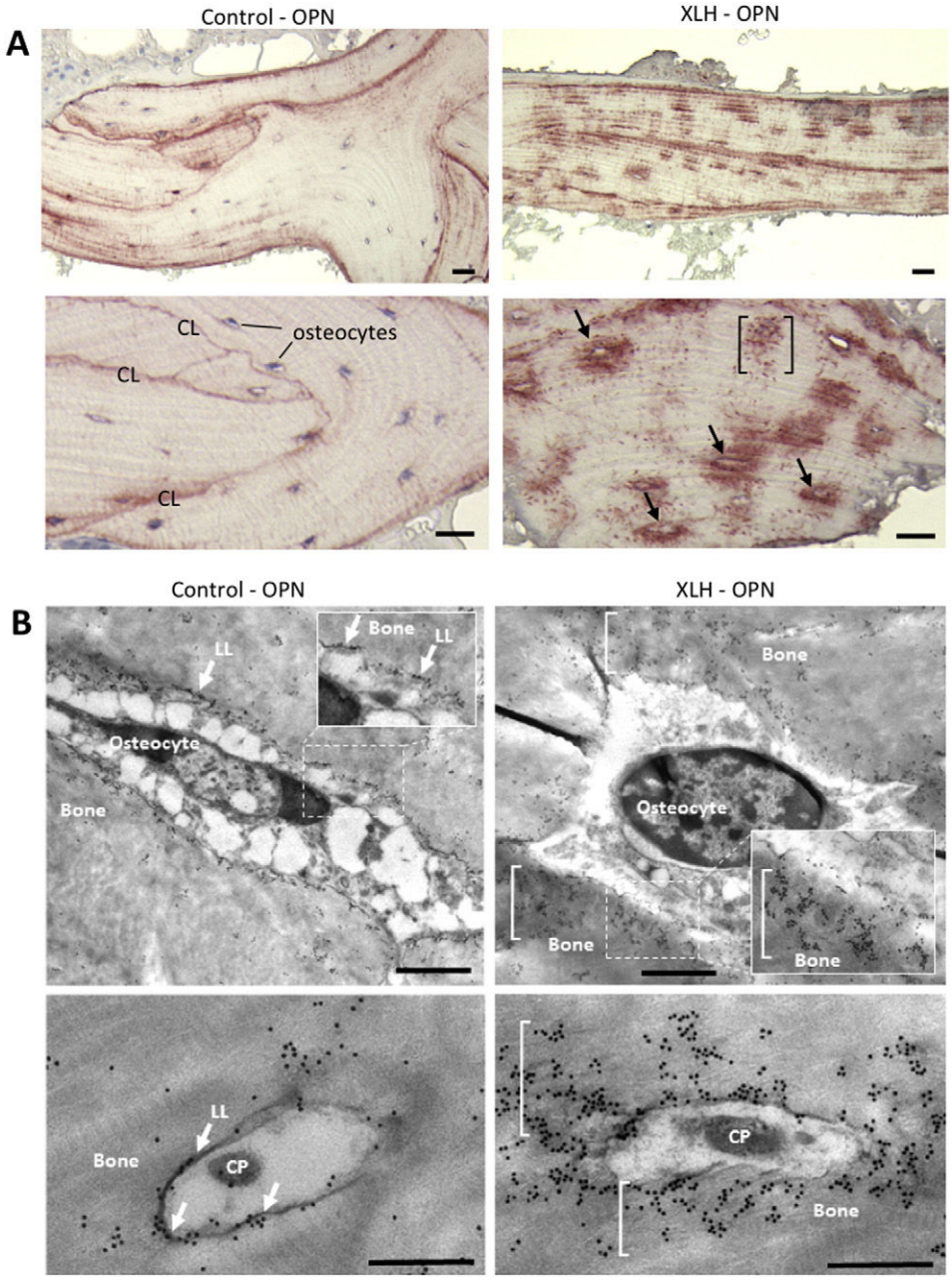

Fig. 2. Immunolocalization of OPN in bone in young patients with XLH. A: Immunohistochemical localization of OPN (red) in paraffin sections of control bone (left panels) and osteomalacic XLH bone (Patient 6, right panels), from demineralized samples to highlight the organic matrix. Whereas the strongest immunostaining for OPN in control bone occurs in cement lines (CL), in XLH bone, OPN prominently localizes to the pericellular hypomineralized halo area around osteocytes (arrows) and around their cell processes in canaliculi, which has a fine spotted appearance where canaliculi are cut in cross- or tangential-section (brackets). Scale bars, 50 μm. B: Ultrastructural immunogold labeling for OPN visualized by transmission electron microscopy in control and XLH bone (Patient 6) confirmed higher levels of OPN in a zone of perilacunar matrix surrounding osteocytes in XLH bone (upper panels), and surrounding osteocyte cell processes (CP) in the canalicular wall (brackets, lower panels); in control bone, the OPN labeling is restricted to a well-defined structure called the *lamina limitans* (LL). Upper panel scale bars, 1 μm; lower panel scale bars, 0.5 μm.

demineralization (by EDTA) extract fraction (E-extract) that corresponds to proteins bound to the mineral phase as released by the demineralization agent. Immunoblotting of bone E-extract showed full-length OPN as a typical broad smear (because of variable phosphorylation status and crosslinked polymers of OPN) between ~50 and 90 kDa and higher, along with a weakly stained OPN fragment band at ~27 kDa (Fig. 3A), both of which were weaker in the XLH bone samples (Patients 1, 6 and 7) compared to control bone. Quantitative analysis by mass spectrometry of mineral-binding proteins/peptides contained in these E-extracts showed slightly decreased amounts of OPN in XLH bone (Anova p-value = 0.12, fold = 2.95, for the full-length and Anova p-value = 0.54, fold = 1.30, for the ~27 kDa-fragment) (Fig. 3B).

Conversely, the same analysis performed on the first guanidine extract fraction (G1-extract) which contains the proteins found in the unmineralized bone matrix, and which would include proteins from any unmineralized/hypomineralized matrix in the lacuno-canalicular network, revealed a wide and prominent smeared band in the XLH bone samples (except for Patient 7) that was not detected in the control bone (Fig. 3C). More precisely, for Patients 1 and 6, several OPN fragments were detected at ~65 kDa, ~40 kDa, ~37 kDa, and ~25 kDa.

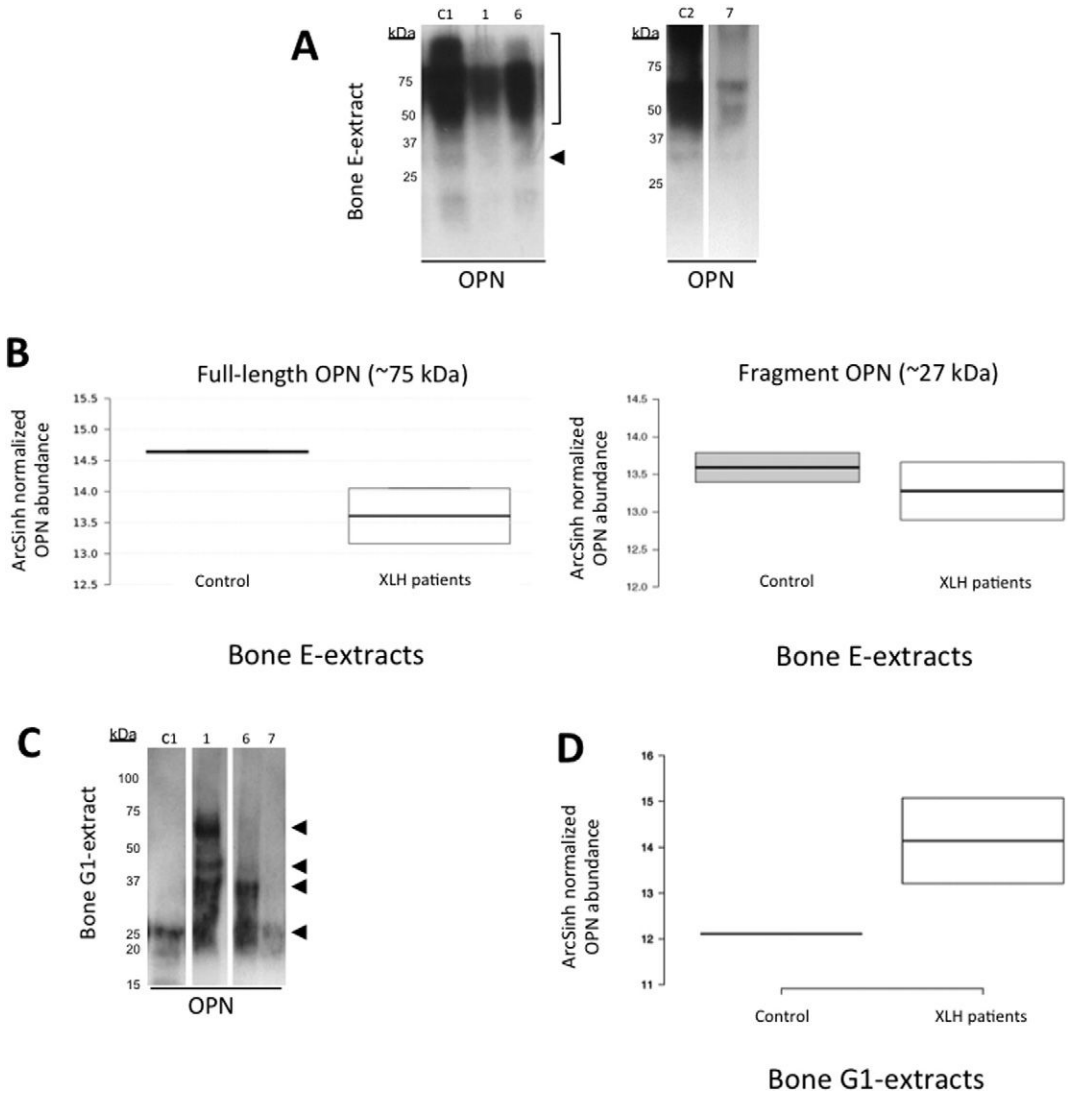

Fig. 3. Biochemical and proteomic analyses of bone in young patients with XLH. A: Biochemical investigation of OPN extracted from bone samples. Western blotting for OPN of bone E-extracts (the fraction of OPN bound to mineral and released by dissolution of mineral using EDTA) reveals full-length OPN as a typical broad band (smeared because of variable post-translational modification of this protein, predominantly phosphorylation) extending above ~50 kDa (bracket), and an additional ~27 kDa fragment (arrowhead), and some smaller fragments. In all cases, OPN levels were greatly diminished in Patients 1, 6 and 7 as compared to controls (C). B: Quantitative analysis by mass spectrometry of mineral-binding proteins/peptides contained in these E-extracts showed slightly decreased amounts of OPN in XLH bone with Anova p-value = 0.12, fold = 2.95, for the full-length OPN (left panel), and Anova p-value = 0.54, fold = 1.30, for the ~27 kDa-fragment (right panel). C: Western blotting for OPN of the initial bone G1-extracts (which contain proteins found in the unmineralized bone matrix) reveals multiple OPN bands in most of the XLH bone samples (Patients 1, 6 and 7) that are not present in control bone samples. D: Label-free quantification by mass spectrometry of proteins found in bone G1-extracts confirms a higher level of OPN in XLH bone samples compared to control bone samples, with a ratio of 11.19 in XLH patients (and a total Mascot score of 291.23).

Mass spectrometry, performed directly on the G1-extract solution, revealed increased amounts of OPN with a ratio of 11.19 in XLH patients (and a total Mascot score of 291.23) (Fig. 3D).

In parallel, we examined the phosphorylation status of the mineral-binding proteins in the XLH and control bone samples by immunoblotting using an antibody raised against phosphorylated serine residues (Suppl. 3A). Similar bands showing phosphorylation were detected in the E-extracts in both groups (but less phosphorylation was observed in the XLH bone), while essentially no reactive bands were detected in the G1-extracts, Suppl. 3B), indicating that only sufficiently phosphorylated proteins (including OPN) were incorporated into the mineralized (hypomineralized in XLH) bone matrix.

3.3. Full-length OPN and OPN fragments accumulate in XLH dentin

In our similar analysis of dentin samples collected from the XLH patients, immunohistochemistry for OPN in paraffin sections of decalcified teeth showed OPN accumulation near the dentino-enamel junction predominantly in the interglobular spaces of dentin between unmerged calcospherites (Fig. 4A). Similar protein extraction and analysis was carried out on dentin obtained from teeth collected from 5 out of 7 patients (Patients 1–5). When compared to control dentin, Western blot analysis for OPN of E-extracts of from XLH patient dentin revealed intensely stained bands corresponding to full-length OPN (Fig. 4B). More precisely, full-length OPN appeared as a broad smeared band located at ~60–90 kDa and higher for most XLH patients, but additional fragments were detected at ~30 kDa and ~22 kDa in Patients 1–4, and at ~37 kDa and ~22 kDa in Patient 5. Quantitative mass spectrometry of the dentin E-extracts showed that the amount of full-length OPN was significantly higher in XLH dentin compared with control dentin (Anova p-value < 0.02, fold = 10.3) (Fig. 4C), and confirmed the presence of additional OPN fragments in XLH around ~37 kDa (data not shown) and ~27 kDa (Anova p-value = 0.02, fold = 69.53). The sequence of full-length OPN showing fragment peptide sequences

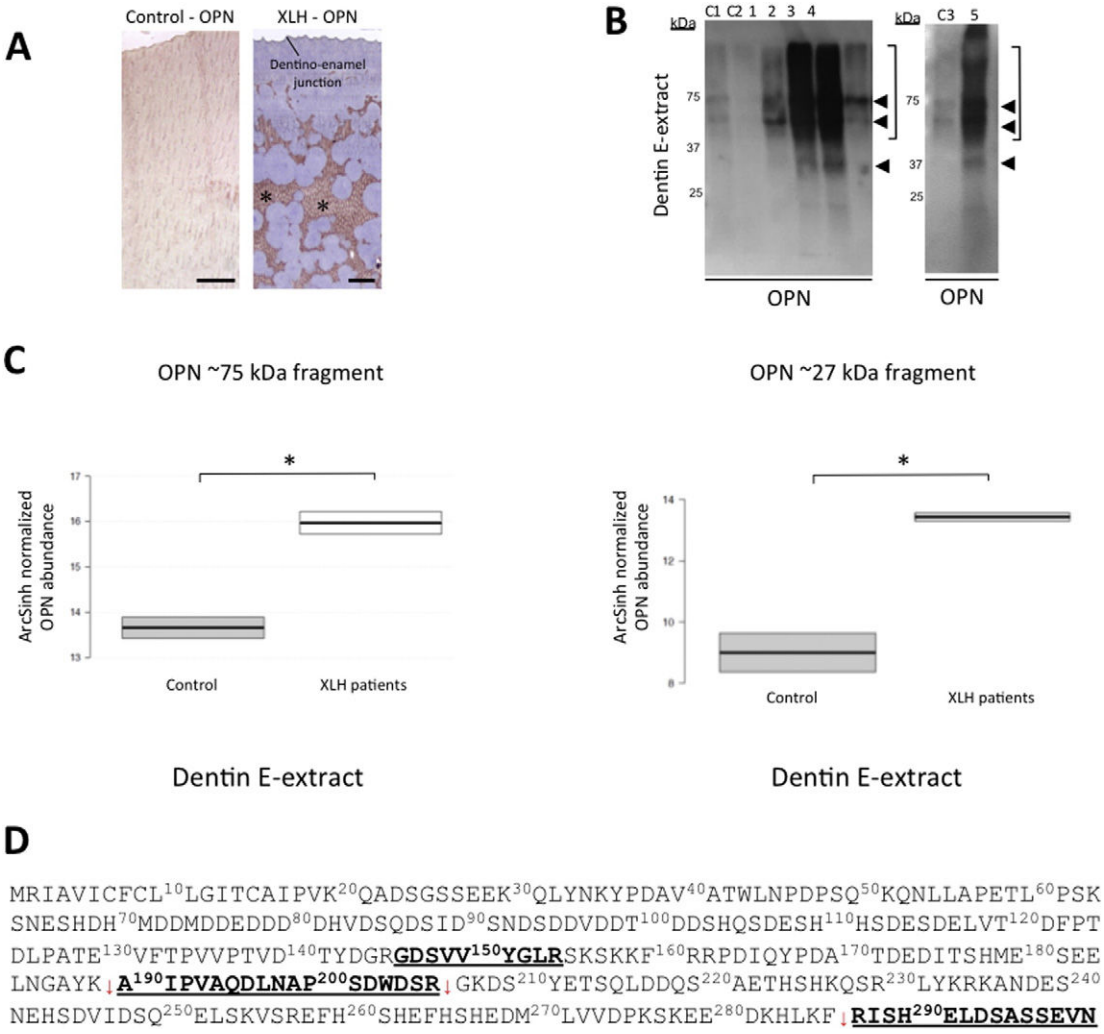

Fig. 4. Immunohistochemical, biochemical and proteomic analyses of tooth dentin in young patients with XLH. A: In paraffin sections of demineralized control and XLH teeth, immunohistochemistry for OPN (light brown) shows in XLH samples a prominent, patchy accumulation of OPN near the dentino-enamel junction predominantly in the interglobular spaces of dentin (between unmerged calculospherites, asterisks), whereas in control dentin, OPN staining is diffuse without prominent localization sites. Scale bar, 100 μm. B: Western blotting for OPN of dentin E-extracts reveals a strongly stained and smeared broad band extending above ~50 kDa (bracket) in some XLH patients (Patients 2, 3 and 5), while in others patients, multiple discrete OPN protein bands are readily apparent (Patients 1 and 4), with all patients showing staining for OPN far above that seen in control dentin samples (C1, C2 and C3). C: Quantitative mass spectrometry of dentin E-extracts shows that the amount of full-length OPN (~75 kDa) detected is significantly (asterisks *) increased in XLH dentin compared to control dentin ($p = 0.02$, fold = 10.3, 3 peptides) (left panel). The OPN fragment at ~27 kDa found in XLH dentin is significantly (asterisks *) higher ($p = 0.02$, fold = 69.53, 1 peptide) than in the control dentin (right panel). No significant difference exists between samples for the ~37 kDa OPN fragment (data not shown). D: Sequence of full-length human OPN showing fragment peptide sequences identified by mass spectrometry that accumulate in XLH dentin.

identified by mass spectrometry that accumulate in XLH dentin is shown in Fig. 4D. Western blot analysis for phosphoserine content revealed that proteins extracted from XLH dentin globally were more phosphorylated compared to controls (Suppl. 4).

4. Discussion

Until recently, little has been revealed concerning the physiologic role of *PHEX* [6]. Several recent studies, however, have suggested a role for *PHEX* in regulating the mineralization of the extracellular matrix at the local level in mineralized bone and dentin, and in maintaining mineralized matrix homeostasis through the cleavage of acidic, noncollagenous SIBLING proteins and peptides of the extracellular matrix [18,25,49]. In the present study — examining bone and dentin from seven patients with XLH — we show that mineralization-inhibiting OPN accumulation, resulting from deficiency in *PHEX* activity, potentially contributes to the pathobiology of this disease at specific sites in the extracellular matrix.

In XLH, diminished functional *PHEX* increases the circulating level of FGF23, which causes renal Pi wasting, considered to be the primary disturbance responsible for the characteristic rickets/osteomalacia [50]. Here, however, we explored whether a mineralization inhibitor explains another hallmark of XLH – the localized hypomineralization (halos) in the perilacunar matrix surrounding osteocytes [11]. Given our previous work demonstrating that the potent, mineralization-inhibiting bone matrix protein osteopontin (OPN) and its ASARM peptide are substrates for *PHEX* [23,51], and knowing that *PHEX* is highly expressed by osteocytes [52] and cleaves its substrates optimally at low pH [53] (as commonly occurs around osteocytes) [54], we examined the distribution of OPN in the osteocyte lacuno-canalicular network of XLH bone. We demonstrated the presence of high levels of OPN in the periosteocytic mineralization lesions in the XLH patient samples, and we also showed the mineralization defect extending into the canalicular network radiating from the osteocytes. To probe this region for mineralization-inhibiting OPN, light microscopy immunohistochemistry for OPN, as well as ultrastructural assessment by transmission electron microscopy after immunogold labeling for OPN, both

showed strikingly high levels of OPN at these mineralization-defect sites. Aligned with our previous work in the Hyp mouse (the murine model of XLH) [23], analysis of noncollagenous proteins obtained by biochemical extraction and then analyzed by SDS-PAGE immunoblotting and mass spectrometry confirmed high levels of OPN and OPN fragments in XLH bone. These findings suggest an inhibitory role for OPN in the defective mineralization of XLH, and provide a possible explanation for the osteocytic halos that are a hallmark of this disease. Such a scenario does not preclude other factors likewise contributing to creation of the halos, and consistent with this notion, a recent report showed that inhibitory pyrophosphate is also increased in Hyp mouse bone [55]. Related to this, and possibly also influencing extracellular OPN levels, is our observation that pyrophosphate upregulates OPN expression [32].

Previously we demonstrated, using biochemical approaches, that OPN is degraded in human XLH dentin as well as in Hyp mouse long bones [23,46]. Herein, combining microscopy (including ultrastructural analysis by electron microscopy) and biochemical assays and mass spectrometry, we found abnormal abundant localization of OPN in XLH bone and dentin. In XLH dentin, full-length OPN and OPN fragments were enriched in protein extracts obtained by demineralizing the samples (the E-extract), these being the abnormally high amounts predicted by diminished *PHEX* enzymatic activity in XLH that would otherwise normally act upon this substrate protein and its peptides. These data are consistent with reported findings showing accumulation of OPN (full-length and fragments) in demineralized protein extracts of Hyp mouse long bones [23] — teeth were not examined in this previous mouse study. Surprisingly to us, the demineralized protein extract (E-extract) of human XLH bone revealed slightly lower amounts of OPN as compared to control human bone. From this observation, we then reasoned that if OPN accumulated in the periosteocytic unmineralized matrix halos, we might extract it without the demineralization step, in the initial guanidine extract (G1-extract), where it might show greater abundance than in control bone. Indeed, this was the case. Our results, taken together, establish that in XLH bone, abundant OPN and OPN fragments reside in the unmineralized portions of the extracellular matrix. For XLH dentin, for reasons that are not clear to us at this time, most OPN in the protein extracts was associated with the mineralized E-extract (although immunohistochemistry for OPN showed some accumulation in the dentin extracellular matrix in mineralization defects near the dentino-enamel junction). This difference between bone and dentin may be a consequence of differences in mineral metabolism between these two tissues, where dentin is more static and the mineralized matrix does not remodel as it does in bone.

Efficient bone remodeling and adaptation improves skeletal performance and reduces the risk of fracture. The connected osteocyte network is central to this process [54]. In bone adaptation, osteocytes and their processes in the lacuno-canalicular network detect mechanical forces (as well as changes in mechanical forces) and signal for appropriate changes in bone architecture to meet loading requirements. Our microscopy and immunolocalization studies identified abundant OPN (also an integrin ligand) in the hypomineralized (or even completely unmineralized) pericellular matrix surrounding the lacuno-canalicular network. Although we did not do any mechanical testing of bone in this study, inhibition of mineralization at this important mechanosensory osteocyte-matrix interface [54] would likely greatly influence the stiffness (reduced) detected by the cells and their cell processes in this region. This would have important implications for transducing mechanical loading towards bone adaptation and remodeling.

Hypomineralization in the pericellular matrix surrounding the lacuno-canalicular network not only contributes to reduced overall mineralization of the skeleton partly engendered by the hypophosphatemia of XLH, but also to altered local cell-matrix interactions likely affecting the osteocyte mechanosensory response to loading. Hence, both disturbances would contribute to bone deformation in XLH. Dendritic osteocytes have long, connected cell processes ramifying throughout bone to form an extended network that plays a mechanosensory role in maintaining skeletal health [56]. Various degrees of mineralization in the pericellular matrix immediately surrounding osteocytes and their cell processes in canaliculi are present in healthy bone [11], but the variation is generally small. Broadening of the pliant hypomineralized perilacunar and pericanalicular matrix in XLH (forming widened, unmineralized regions around lacunae and canaliculi) possibly creates a "vicious cycle" where skeletal elements are overstimulated because of reduced mineralization [57], and simultaneously the strain-amplification feedback loop from the "soft" matrix to the mechanosensory osteocytes is disrupted. This reduced bone stiffness would not only cause deformity, but also failure in the fine-tuning of bone microstructure occurring at the cellular and lacuno-canalicular network level. These changes would lead to the bone deformations characteristic of load-bearing limbs in XLH, and the increased bone formation and bone mineral density measured in XLH patients by DXA and PqCT analyses [57]. In the XLH skeleton, increased proportions of osteoid occur in both trabecular and cortical bone [58], but less cortical bone and more trabecular bone is reported in these patients [57]. Perturbed osteocyte network mechanosensing in bone (as a consequence of the reduced stiffness in the lacuno-canalicular system caused by mineralization-inhibiting OPN accumulation) may overestimate the mechanical loads in XLH bone and, as a compensatory adaptation reaction, may change relative proportions of cortical *versus* trabecular bone [57].

Taken together, our results show that current therapies for XLH (and therapies in development) aimed at restoring circulating phosphate and 1,25-dihydroxyvitamin D levels (and modulating circulating FGF23 activity) may not fully rescue the OPN-induced lacuno-canalicular hypomineralization defect that resides locally within the bone extracellular matrix when *PHEX* activity is diminished. Future studies should consider whether both the systemic hypophosphatemia (FGF23-mediated) and the local hypomineralization defect in the lacuno-canalicular network (OPN-mediated) must be targeted.

Supplementary data to this article can be found online at http://dx.doi.org/10.1016/j.bone.2016.11.019.

Authors' roles

TB, BH, and MDM designed the study.
BRC performed the OPN immunohistochemistry.
TL and CG performed mass spectrometry experiments.
FHG performed contact microradiography experiments.
TB and BH performed other experiments of the study.
MPW, AL, PW, and CC followed the patients and collected the clinical data and bone and tooth specimens.
TB, CC and MDM drafted the initial version of the manuscript, and all authors subsequently participated in the manuscript writing and editing.
CC and MDM take responsibility for the integrity of the data analysis.

Conflict of interest statement

TB, BH, AL, TL, CG, PW, CC, MDM have declared that no conflict of interest exists.
MPW, FWG, AL: Research grant and/or consulting from Ultragenyx Pharmaceutical, Novato, CA.

Acknowledgments

This study was supported by the Canadian Institutes of Health Research (MOP-142330), and in part by the University Paris Descartes (France), and the Shriners of North America. TB was supported by a specific grant from "Assistance Publique Hôpitaux de Paris (AP-HP)" (France). The authors also thank Lydia Malynowsky, Line Mongeon, and Patrice Caron for their help with the microscopy methods, and Dr. Nilana M.T. Barros for many stimulating discussions about this work. MDM is a member of the FRQ-S Network for Oral and Bone Health Research, and the McGill Centre for Bone and Periodontal Research.

References

[1] S. Opsahl Vital, C. Gaucher, C. Bardet, P.S. Rowe, A. George, A. Linglart, C. Chaussain, Tooth dentin defects reflect genetic disorders affecting bone mineralization, Bone 50 (2012) 989–997.

[2] M.D. McKee, B. Hoac, W.N. Addison, N.M. Barros, J.L. Millan, C. Chaussain, Extracellular matrix mineralization in periodontal tissues: noncollagenous matrix proteins, enzymes, and relationship to hypophosphatasia and X-linked hypophosphatemia, Periodontol. 63 (2013) 102–122.

[3] P.S. Rowe, The PEX gene: its role in X-linked rickets, osteomalacia, and bone mineral metabolism, Exp. Nephrol. 5 (1997) 355–363.

[4] F. Francis, T.M. Strom, S. Hennig, A. Boddrich, B. Lorenz, O. Brandau, K.L. Mohnike, M. Cagnoli, C. Steffens, S. Klages, K. Borzym, T. Pohl, C. Oudet, M.J. Econs, P.S. Rowe, R. Reinhardt, T. Meitinger, H. Lehrach, Genomic organization of the human PEX gene mutated in X-linked dominant hypophosphatemic rickets, Genome Res. 7 (1997) 573–585.

[5] H.S. Tenenhouse, X-linked hypophosphataemia: a homologous disorder in humans and mice, Nephrol. Dial. Transplant. 14 (1999) 333–341.

[6] A.F. Ruchon, M. Marcinkiewicz, G. Siegfried, H.S. Tenenhouse, L. DesGroseillers, P. Crine, G. Boileau, Pex mRNA is localized in developing mouse osteoblasts and odontoblasts, J. Histochem. Cytochem. 46 (1998) 459–468.

[7] S. Liu, W. Tang, J. Fang, J. Ren, H. Li, Z. Xiao, L.D. Quarles, Novel regulators of Fgf23 expression and mineralization in Hyp bone, Mol. Endocrinol. 23 (2009) 1505–1518.

[8] T. Onishi, S. Umemura, S. Shintani, T. Ooshima, PHEX mutation causes overexpression of FGF23 in teeth, Arch. Oral Biol. 53 (2008) 99–104.

[9] C. Chaussain-Miller, C. Sinding, D. Septier, M. Wolikow, M. Goldberg, M. Garabedian, Dentin structure in familial hypophosphatemic rickets: benefits of vitamin D and phosphate treatment, Oral Dis. 13 (2007) 482–489.

[10] A. Linglart, M. Biosse-Duplan, K. Briot, C. Chaussain, L. Esterle, S. Guillaume-Czitrom, P. Kamenicky, J. Nevoux, D. Prie, A. Rothenbuhler, P. Wicart, P. Harvengt, Therapeutic management of hypophosphatemic rickets from infancy to adulthood, Endocr. Connect. 3 (2014) R13–R30.

[11] P.J. Marie, F.H. Glorieux, Relation between hypomineralized periosteocytic lesions and bone mineralization in vitamin D-resistant rickets, Calcif. Tissue Int. 35 (1983) 443–448.

[12] J.Q. Feng, L.M. Ward, S. Liu, Y. Lu, Y. Xie, B. Yuan, X. Yu, F. Rauch, S.I. Davis, S. Zhang, H. Rios, M.K. Drezner, L.D. Quarles, L.F. Bonewald, K.E. White, Loss of DMP1 causes rickets and osteomalacia and identifies a role for osteocytes in mineral metabolism, Nat. Genet. 38 (2006) 1310–1315.

[13] E.G. Farrow, X. Yu, L.J. Summers, S.I. Davis, J.C. Fleet, M.R. Allen, A.G. Robling, K.R. Stayrook, V. Jideonwo, M.J. Magers, H.J. Garringer, R. Vidal, R.J. Chan, C.B. Goodwin, S.L. Hui, M. Peacock, K.E. White, Iron deficiency drives an autosomal dominant hypophosphatemic rickets (ADHR) phenotype in fibroblast growth factor-23 (Fgf23) knock-in mice, Proc. Natl. Acad. Sci. U. S. A. 108 (2011) E1146–E1155.

[14] T. Wada, M.D. McKee, S. Steitz, C.M. Giachelli, Calcification of vascular smooth muscle cell cultures: inhibition by osteopontin, Circ. Res. 84 (1999) 166–178.

[15] L.W. Fisher, N.S. Fedarko, Six genes expressed in bones and teeth encode the current members of the SIBLING family of proteins, Connect. Tissue Res. 44 (Suppl. 1) (2003) 33–40.

[16] N.R. Kaipatur, M. Murshed, M.D. McKee, Matrix Gla protein inhibition of tooth mineralization, J. Dent. Res. 87 (2008) 839–844.

[17] Y. Sun, L. Chen, S. Ma, J. Zhou, H. Zhang, J.Q. Feng, C. Qin, Roles of DMP1 processing in osteogenesis, dentinogenesis and chondrogenesis, Cells Tissues Organs 194 (2011) 199–204.

[18] A. Martin, V. David, J.S. Laurence, P.M. Schwarz, E.M. Lafer, A.M. Hedge, P.S. Rowe, Degradation of MEPE, DMP1, and release of SIBLING ASARM-peptides (minhibins): ASARM-peptide(s) are directly responsible for defective mineralization in HYP, Endocrinology 149 (2008) 1757–1772.

[19] W.N. Addison, Y. Nakano, T. Loisel, P. Crine, M.D. McKee, MEPE-ASARM peptides control extracellular matrix mineralization by binding to hydroxyapatite: an inhibition regulated by PHEX cleavage of ASARM, J. Bone Miner. Res. 23 (2008) 1638–1649.

[20] W.N. Addison, D.L. Masica, J.J. Gray, M.D. McKee, Phosphorylation-dependent inhibition of mineralization by osteopontin ASARM peptides is regulated by PHEX cleavage, J. Bone Miner. Res. 25 (2010) 695–705.

[21] T. Boukpessi, C. Gaucher, T. Leger, B. Salmon, J. Le Faouder, C. Willig, P.S. Rowe, M. Garabedian, O. Meilhac, C. Chaussain, Abnormal presence of the matrix extracellular phosphoglycoprotein-derived acidic serine- and aspartate-rich motif peptide in human hypophosphatemic dentin, Am. J. Pathol. 177 (2010) 803–812.

[22] B. Salmon, C. Bardet, B.R. Coyac, B. Baroukh, J. Naji, P.S. Rowe, S. Opsahl Vital, A. Linglart, M.D. McKee, C. Chaussain, Abnormal osteopontin and matrix extracellular phosphoglycoprotein localization, and odontoblast differentiation, in X-linked hypophosphatemic teeth, Connect. Tissue Res. 55 (Suppl. 1) (2014) 79–82.

[23] N.M. Barros, B. Hoac, R.L. Neves, W.N. Addison, D.M. Assis, M. Murshed, A.K. Carmona, M.D. McKee, Proteolytic processing of osteopontin by PHEX and accumulation of osteopontin fragments in Hyp mouse bone, the murine model of X-linked hypophosphatemia, J. Bone Miner. Res. 28 (2013) 688–699.

[24] D. Bresler, J. Bruder, K. Mohnike, W.D. Fraser, P.S. Rowe, Serum MEPE-ASARM-peptides are elevated in X-linked rickets (HYP): implications for phosphaturia and rickets, J. Endocrinol. 183 (2004) R1–R9.

[25] P.S. Rowe, The chicken or the egg: PHEX, FGF23 and SIBLINGs unscrambled, Cell Biochem. Funct. 30 (2012) 355–375.

[26] V.N. Subramani, M. Narasimhan, M. Thiyagarajan, B.D. Munuswamy, L. Jayamani, Expression of osteopontin in oral squamous cell carcinoma and its surgical margins - an immunohistochemical study, J. Clin. Diagn. Res. 9 (2015) ZC66–ZC69.

[27] A.B. Tuck, B.E. Elliott, C. Hota, E. Tremblay, A.F. Chambers, Osteopontin-induced, integrin-dependent migration of human mammary epithelial cells involves activation of the hepatocyte growth factor receptor (Met), J. Cell. Biochem. 78 (2000) 465–475.

[28] L.F. Brown, B. Berse, L. Van de Water, A. Papadopoulos-Sergiou, C.A. Perruzzi, E.J. Manseau, H.F. Dvorak, D.R. Senger, Expression and distribution of osteopontin in human tissues: widespread association with luminal epithelial surfaces, Mol. Biol. Cell 3 (1992) 1169–1180.

[29] G.K. Hunter, C.L. Kyle, H.A. Goldberg, Modulation of crystal formation by bone phosphoproteins: structural specificity of the osteopontin-mediated inhibition of hydroxyapatite formation, Biochem. J. 300 (Pt 3) (1994) 723–728.

[30] A.L. Boskey, Osteopontin and related phosphorylated sialoproteins: effects on mineralization, Ann. N. Y. Acad. Sci. 760 (1995) 249–256.

[31] J.R. Hoyer, J.R. Asplin, L. Otvos, Phosphorylated osteopontin peptides suppress crystallization by inhibiting the growth of calcium oxalate crystals, Kidney Int. 60 (2001) 77–82.

[32] W.N. Addison, F. Azari, E.S. Sorensen, M.T. Kaartinen, M.D. McKee, Pyrophosphate inhibits mineralization of osteoblast cultures by binding to mineral, up-regulating osteopontin, and inhibiting alkaline phosphatase activity, J. Biol. Chem. 282 (2007) 15872–15883.

[33] M.C. Yadav, C. Huesa, S. Narisawa, M.F. Hoylaerts, A. Moreau, C. Farquharson, J.L. Millan, Ablation of osteopontin improves the skeletal phenotype of phospho1(−/−) mice, J. Bone Miner. Res. 29 (2014) 2369–2381.

[34] A.L. Boskey, L. Spevak, E. Paschalis, S.B. Doty, M.D. McKee, Osteopontin deficiency increases mineral content and mineral crystallinity in mouse bone, Calcif. Tissue Int. 71 (2002) 145–154.

[35] S.R. Rittling, H.N. Matsumoto, M.D. McKee, A. Nanci, X.R. An, K.E. Novick, A.J. Kowalski, M. Noda, D.T. Denhardt, Mice lacking osteopontin show normal development and bone structure but display altered osteoclast formation in vitro, J. Bone Miner. Res. 13 (1998) 1101–1111.

[36] M.Y. Speer, M.D. McKee, R.E. Guldberg, L. Liaw, H.Y. Yang, E. Tung, G. Karsenty, C.M. Giachelli, Inactivation of the osteopontin gene enhances vascular calcification of matrix Gla protein-deficient mice: evidence for osteopontin as an inducible inhibitor of vascular calcification in vivo, J. Exp. Med. 196 (2002) 1047–1055.

[37] S.A. Steitz, M.Y. Speer, M.D. McKee, L. Liaw, M. Almeida, H. Yang, C.M. Giachelli, Osteopontin inhibits mineral deposition and promotes regression of ectopic calcification, Am. J. Pathol. 161 (2002) 2035–2046.

[38] E.M. Eicher, J.L. Southard, C.R. Scriver, F.H. Glorieux, Hypophosphatemia: mouse model for human familial hypophosphatemic (vitamin D-resistant) rickets, Proc. Natl. Acad. Sci. U. S. A. 73 (1976) 4667–4671.

[39] J. Hou, A. Renigunta, A.S. Gomes, M. Hou, D.L. Paul, S. Waldegger, D.A. Goodenough, Claudin-16 and claudin-19 interaction is required for their assembly into tight junctions and for renal reabsorption of magnesium, Proc. Natl. Acad. Sci. U. S. A. 106 (2009) 15350–15355.

[40] G. Cazzolli, F. Wang, S. a Beccara, A. Gershenson, P. Faccioli, P.L. Wintrode, Serpin latency transition at atomic resolution, Proc. Natl. Acad. Sci. U. S. A. 111 (2014) 15414–15419.

[41] S. Zengin, A B, S. Karta, B. Can, M. Orkmez, A. Taskin, U. Lok, B. Gulen, C. Yildirim, S. Taysi, An assessment of antioxidant status in patients with carbon monoxide poisoning, World J. Emerg. Med. 5 (2014) 91–95.

[42] F.H. Glorieux, P.J. Marie, J.M. Pettifor, E.E. Delvin, Bone response to phosphate salts, ergocalciferol, and calcitriol in hypophosphatemic vitamin D-resistant rickets, N. Engl. J. Med. 303 (1980) 1023–1031.

[43] Carpenter TO, E.A. Imel, M.D. Ruppe, T.J. Weber, M.A. Klausner, M.M. Wooddell, T. Kawakami, T. Ito, X. Zhang, J. Humphrey, K.L. Insogna, M. Peacock, Randomized trial of the anti-FGF23 antibody KRN23 in X-linked hypophosphatemia, J. Clin. Invest. 124 (2014) 1587–1597.

[44] O. Makitie, A. Doria, S.W. Kooh, W.G. Cole, A. Daneman, E. Sochett, Early treatment improves growth and biochemical and radiographic outcome in X-linked hypophosphatemic rickets, J. Clin. Endocrinol. Metab. 88 (2003) 3591–3597.

[45] H.A. Goldberg, J. Sodek, Purification of mineralized tissue-associated osteopontin, Methods Cell Sci. 16 (1994) 211–215.

[46] T. Boukpessi, D. Septier, S. Bagga, M. Garabedian, M. Goldberg, C. Chaussain-Miller, Dentin alteration of deciduous teeth in human hypophosphatemic rickets, Calcif. Tissue Int. 79 (2006) 294–300.

[47] M.D. McKee, A. Nanci, Osteopontin and the bone remodeling sequence. Colloidal-gold immunocytochemistry of an interfacial extracellular matrix protein, Ann. N. Y. Acad. Sci. 760 (1995) 177–189.

[48] M.D. McKee, M.C. Farach-Carson, W.T. Butler, P.V. Hauschka, A. Nanci, Ultrastructural immunolocalization of noncollagenous (osteopontin and osteocalcin) and plasma (albumin and alpha 2HS-glycoprotein) proteins in rat bone, J. Bone Miner. Res. 8 (1993) 485–496.

[49] C. Qin, O. Baba, W.T. Butler, Post-translational modifications of sibling proteins and their roles in osteogenesis and dentinogenesis, Crit. Rev. Oral Biol. Med. 15 (2004) 126–136.

[50] Carpenter TO, E.A. Imel, I.A. Holm, S.M. Jan de Beur, K.L. Insogna, A clinician's guide to X-linked hypophosphatemia, J. Bone Miner. Res. 26 (2011) 1381–1388.

[51] P P, A. BA, P. DR, Sulfated exopolysaccharide produced by *Labrenzia* sp. PRIM-30, characterization and prospective applications, Int. J. Biol. Macromol. 69 (2014) 290–295.

[52] A.F. Ruchon, H.S. Tenenhouse, M. Marcinkiewicz, G. Siegfried, J.E. Aubin, L. DesGroseillers, P. Crine, G. Boileau, Developmental expression and tissue distribution of PHEX protein: effect of the Hyp mutation and relationship to bone markers, J. Bone Miner. Res. 15 (2000) 1440–1450.

[53] M. Campos, C. Couture, I.Y. Hirata, M.A. Juliano, T.P. Loisel, P. Crine, L. Juliano, G. Boileau, A.K. Carmona, Human recombinant endopeptidase PHEX has a strict S1' specificity for acidic residues and cleaves peptides derived from fibroblast growth factor-23 and matrix extracellular phosphoglycoprotein, Biochem. J. 373 (2003) 271–279.
[54] S.L. Dallas, M. Prideaux, L.F. Bonewald, The osteocyte: an endocrine cell … and more, Endocr. Rev. 34 (2013) 658–690.
[55] S.K. Murali, O. Andrukhova, E.L. Clinkenbeard, K.E. White, R.G. Erben, Excessive osteocytic Fgf23 secretion contributes to pyrophosphate accumulation and mineralization defect in Hyp mice, PLoS Biol. 14 (2016), e1002427.
[56] M.J. Alaia, O. Khatib, M. Shah, J. AB, L. MJ, E.J. Strauss, The utility of plain radiographs in the initial evaluation of knee pain amongst sports medicine patients, Knee Surg. Sports Traumatol. Arthrosc. 23 (2015) 2213–2217.
[57] F. Rauch, Material matters: a mechanostat-based perspective on bone development in osteogenesis imperfecta and hypophosphatemic rickets, J. Musculoskelet. Neuronal Interact. 6 (2006) 142–146.
[58] M. Cheung, P. Roschger, K. Klaushofer, L.N. Veilleux, P. Roughley, F.H. Glorieux, F. Rauch, Cortical and trabecular bone density in X-linked hypophosphatemic rickets, J. Clin. Endocrinol. Metab. 98 (2013) E954–E961.

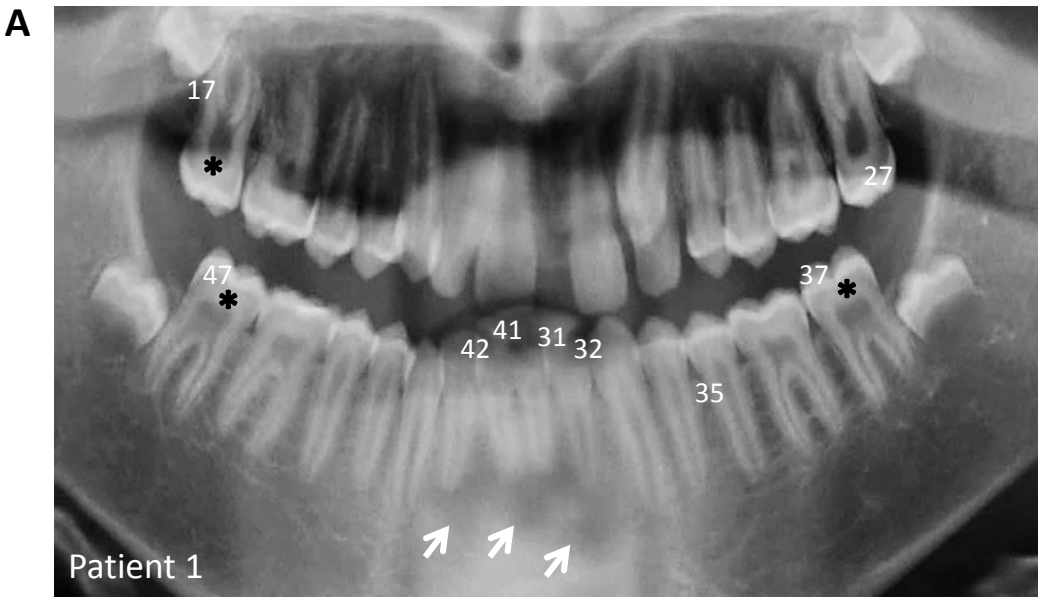

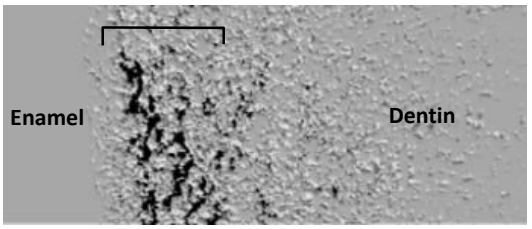

A: Orthopantomograph of Patient 1 showing characteristic dental manifestations of XLH, including a normal (but slightly thinner) enamel layer, a radiolucent dentin layer with enlarged pulp chambers (asterisks *) and prominent pulp horns, and apical periodontitis radiolucency associated with the mandibular incisors (arrows).

B: Cone-beam computerized tomography showing axial, sagittal and coronal acquisitions revealing in Patient 1 significant bone necrosis and apical periodontitis (arrows) related to several teeth (here, mandibular incisors). Note the enlarged pulp chambers, indicated by asterisks (*).

C: Micro-CT reconstruction of a tooth from Patient 5 showing highly abnormal crown dentin mineralization, with focal mineralization defects (black areas, bracketed zone) being most pronounced near the dentino-enamel junction. This defective mineralization pattern corresponds to interglobular spaces present between unmerged calculospherites characteristic of XLH dentin.

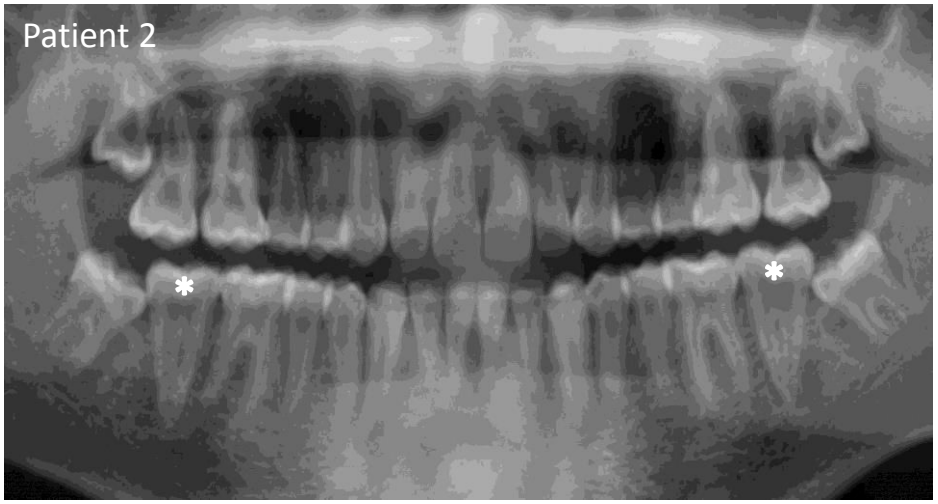

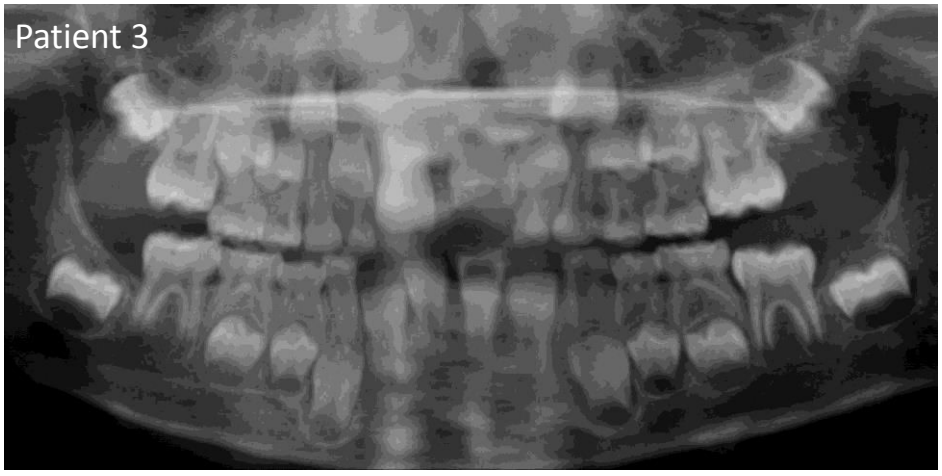

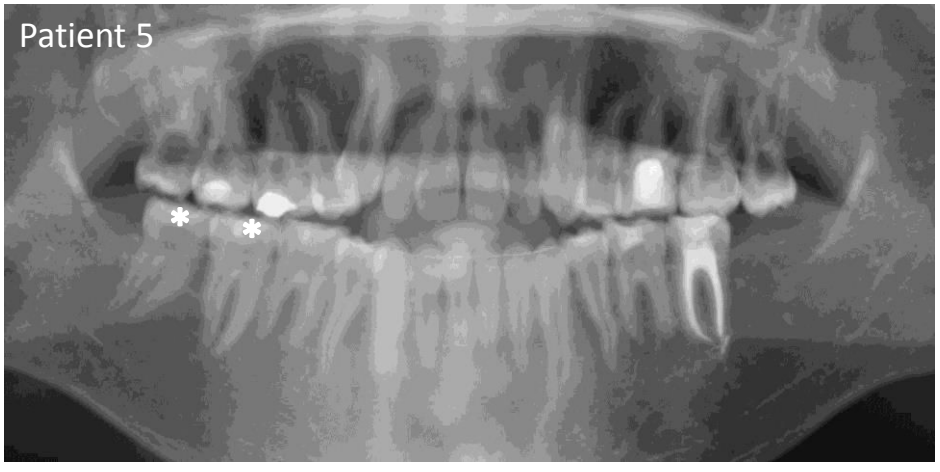

Orthopanthomograms of XLH patients: Patient 2 presented enlarged pulp chambers (asterisks *). Patient 3, who had a sporadic mutation, presented with a thin enamel layer, but the pulps seemed normal. For Patient 4, XLH dental characteristics are less obvious. Patient 5 presented many coronal restorations, peri-apical endodontic lesions on the first left mandibular molar, and a second left lower molar that was endodontically treated. Note the enlarged pulp chambers, indicated by asterisks (*).

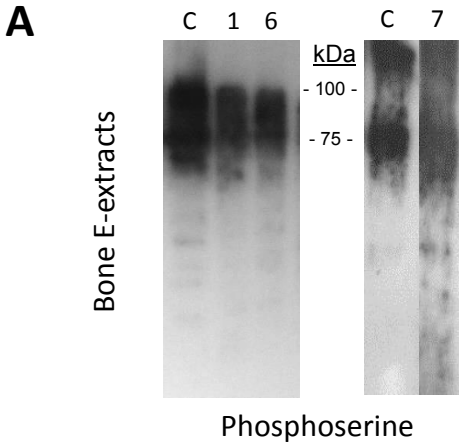

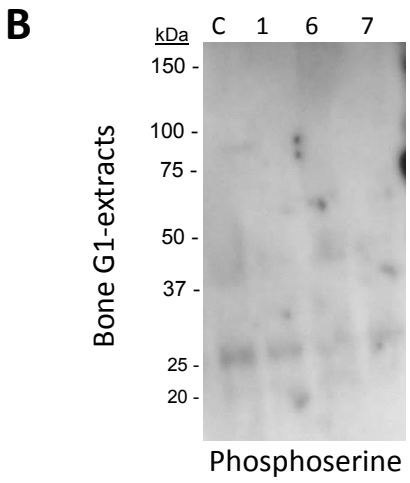

A: Western blotting for phosphoserine in bone E-extracts showed in controls (C) and XLH patients (1, 6, 7) similar bands (a smear between ~75 kDa and 100 kDa). No bands were detected in the G1-extract **(B).**

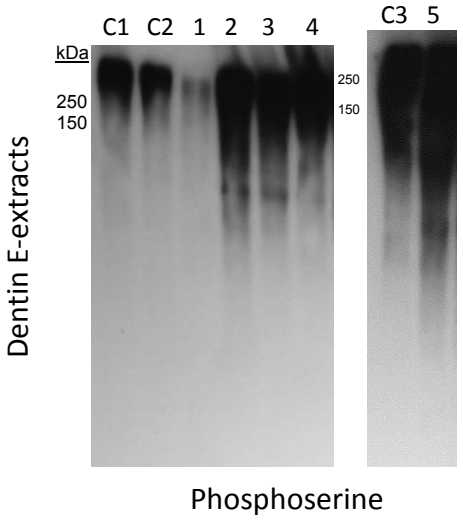

Western blot analysis for phosphoserine content revealed that proteins extracted from XLH dentin E-extracts were globally more phosphorylated than those from control dentin.

10.3 Appendix 3: Osteopontin and MEPE Accumulation in XLH Dentin

connective tissue research

http://informahealthcare.com/cts
ISSN: 0300-8207 (print), 1607-8438 (electronic)

Connect Tissue Res, 2014; 55(S1): 79–82
 DOI: 10.3109/03008207.2014.923864

informa healthcare

Abnormal osteopontin and matrix extracellular phosphoglycoprotein localization, and odontoblast differentiation, in X-linked hypophosphatemic teeth

B. Salmon[1,2]*, C. Bardet[1]*, B. R. Coyac[1,3], B. Baroukh[1], J. Naji[1], P. S. Rowe[4], S. Opsahl Vital[1,2], A. Linglart[5,6], M. D. Mckee[7], and C. Chaussain[1,2,5]

[1]EA 2496, Faculty of Dentistry, Paris Descartes University, France, [2]Bretonneau and Louis Mourier Odontology Department, HNPVS, AP-HP, Paris, France, [3]Department of Periodontology, Rothschild Hospital, AP-HP, Paris, France, [4]Kidney Institute, University of Kansas, USA, [5]Centre de référence des maladies rares du métabolisme du phosphore et du calcium, AP-HP le Kremlin Bicêtre, France, [6]Medical School Paris Sud University, Department of Pediatric Endocrinology, France, and [7]Faculty of Dentistry, Department of Anatomy and Cell Biology, McGill University, Canada

Abstract

Mutations in phosphate-regulating gene (*PHEX*) lead to X-linked hypophosphatemic rickets (XLH), a genetic disease characterized by impaired mineralization in bones and teeth. In human XLH tooth dentin, calcospherites that would normally merge as part of the mineralization process are separated by unmineralized interglobular spaces where fragments of matrix proteins accumulate. Here, we immunolocalized osteopontin (OPN) in human XLH teeth, in a three-dimensional XLH human dental pulp stem cell-collagen scaffold culture model and in a rat tooth injury repair model treated with acidic serine- and aspartate-rich motif peptides (ASARM). In parallel, matrix extracellular phosphoglycoprotein (MEPE) immunolocalization and alkaline phosphatase (ALP) activity were assessed in XLH teeth. OPN was expressed by odontoblasts in the XLH models, and localized to the abnormal calcospherites of XLH tooth dentin. In addition, ALP activity and MEPE localization were abnormal in human XLH teeth, with MEPE showing an accumulation in the unmineralized interglobular spaces in dentin. Furthermore, XLH odontoblasts failed to form a well-polarized odontoblast layer. These data suggest that both MEPE and OPN are involved in impaired tooth mineralization associated with XLH, possibly through different effects on the mineralization process.

Keywords

Alkaline phosphatase, acidic serine- and aspartate-rich motif (ASARM), dentin, matrix extracellular phosphoglycoprotein (MEPE), osteopontin, odontoblast, X-linked hypophosphatemia (XLH)

History

Received 7 November 2013
Revised 12 December 2013
Accepted 19 December 2013
Published online 11 August 2014

Introduction

Inactivating mutations in *PHEX* (phosphate-regulating gene with homologies to endopeptidases on the X-chromosome) cause X-linked hypophosphatemic rickets (XLH, comprising ~80% of patients with familial hypophosphatemic rickets) (1). XLH results in impaired skeleton mineralization (osteomalacia) leading to severe lower limb deformities (rickets) and oral manifestations, including spontaneous dental abscesses. Scanning electron microscopy and histological examination of XLH teeth have indicated abnormal dentin mineralization showing unmerged mineralization calcospherites, and enlarged pulp chambers with prominent pulp horns (2).

PHEX is a transmembrane endopeptidase expressed most prominently by osteoblasts, osteocytes, odontoblasts and cementoblasts. It is the only known enzyme capable of cleaving enzyme-resistant, small acidic serine- and aspartate-rich motif (ASARM) peptides found in bone and tooth extracellular matrix proteins, whose accumulation leads to inhibition of mineralization. PHEX also completely degrades the bone and dentin mineralization-inhibiting matrix protein osteopontin (OPN), including its ASARM peptide (3). The ASARM motif is shared by all SIBLING proteins (Small Integrin-Binding LIgand N-linked Glycoproteins), a family of noncollagenous phosphoproteins known to regulate mineralization (4). MEPE (Matrix Extracellular PhosphoglycoprotEin) – first identified in oncogenic hypophosphatemic osteomalacia (OHO) tumors – interacts with PHEX under normal conditions (5). We have previously demonstrated that MEPE-derived ASARM peptide accumulates in the dentin of XLH patients where it may impair dentinogenesis (6). Furthermore, the study of tooth models of XLH pathology has indicated that a phosphorylated synthetic MEPE-derived ASARM peptide (p-ASARM) inhibits odontoblastic differentiation and extracellular matrix (ECM) mineralization, and induces an increase in MEPE and tissue-nonspecific phosphatase alkaline (TNAP) expression (7). Notably, we have also identified degraded fragments of OPN in extracts from human XLH dentin and Hyp (mouse

*These authors contributed equally to this work.

Correspondence: Catherine Chaussain, Faculty of Dentistry – EA 2496, Paris Descartes University, 1, rue Maurice Arnoux, Montrouge, 92120, France. E-mail: catherine.chaussain@parisdescartes.fr

homolog) bones (2,3). These data suggest that along with MEPE fragments, the accumulation of OPN fragments in XLH dentin may also contribute to impairment of the mineralization process. To test this hypothesis, we examined OPN expression in a three-dimensional (3D) collagen scaffold) XLH culture model, in a rat tooth-wound repair model in the presence of p-ASARM, and in human teeth from a patient with XLH. In parallel, to confirm the abnormal MEPE expression and alkaline phosphatase (ALP) activity reported in our tooth models (7), we assessed the localization of these proteins in human XLH dentin.

Material and methods

Characterization of XLH human teeth

Human permanent third molars were collected in the context of an orthodontic treatment plan from a 15-year-old female XLH patient and from a gender- and age-matched control patient. Clinical characteristics of the XLH patient at the time of tooth extraction included alkaline phosphatase at 523 IU/l, serum phosphate at 0.58 mmol/l, −2.1 standard deviation of height, moderate leg bowing, and moderate compliancy of Unalfa® and phosphate treatment. Immediately after extraction, teeth were fixed for 7 d at 4 °C in 70% ethanol, embedded in methyl methacrylate (Merck, Darmstadt, Germany) without any demineralization process and sectioned. Toluidine blue staining and the ALP enzymatic reaction were performed as previously described (8). For immunohistochemistry, goat polyclonal OPN antibody (AF1433, R&D Systems, Minneapolis, MN) and rabbit polyclonal antibody for the mid-region of MEPE (7) were used with peroxidase staining, and sections were counterstained with hematoxylin.

XLH *in vitro* model: 3D SHED cultures in the presence of phosphorylated ASARM

3D culture of dental pulp stem cells from human exfoliated deciduous teeth (SHEDs) were established as previously reported (7,9). Briefly, to induce the odontoblastic differentiation pathway, cells seeded into a 3D collagen/tooth slice scaffold were cultured for up to 21 d at 37 °C with 5% CO_2, 10% FBS, and 100 U/ml penicillin and 100 µg/ml streptomycin in supplemented DMEM in the presence of 10 mM β-glycerophosphate, 50 µg/ml ascorbic acid, and 10^{-8} M dexamethasone with or without 20 µM of phosphorylated ASARM peptide (p-ASARM, having 3 phosphoserine residues synthesized according to the human MEPE-derived sequence RDDSSESSDSGS(PO_3H_2)SS(PO_3H_2)ES(PO_3H_2)DGD. For OPN immunohistochemistry, SHED-seeded 3D collagen/tooth slice scaffolds were embedded in methyl methacrylate and goat polyclonal OPN antibody was used at a 1/10 dilution with peroxidase staining and hematoxylin counterstaining.

XLH *in vivo* model: rat pulp/dentin injury repair in the presence of phosphorylated ASARM

Affi-Gel agarose beds (Bio-Rad Laboratories, Hercules, CA) soaked in a solution of PBS with or without p-ASARM (2 µg/µl) were implanted into the pulp of the upper first molar of nine rats (6-weeks-old, OFA/SD Charles River, Lyon, France) using a previously reported surgical procedure (7). Each animal received both treatments, with one each on the left and right first maxillary molars. The rats were sacrificed after 1 month and tissue demineralization was then performed in 4.13% EDTA for approximately 8 weeks followed by paraffin embedding. Sections were prepared for immunohistochemistry and incubated overnight at 4 °C with rabbit polyclonal antibody for OPN (LF175, generous gift from Dr Larry W. Fisher, NIH) at a 1/100 dilution with peroxidase staining and hematoxylin counterstaining.

Ethics statement

All teeth were collected with informed and oral consent in agreement with ethical guidelines set by French law (Loi Bioéthique n°2004-800, agreement n°DC-2009-927, Cellule Bioéthique DGRI/A5). Animal studies were conducted according to ARRIVE guidelines (agreement CEEA34.CC.016.11).

Results

Pulp–dentin complex in human XLH teeth

Compared to normal dentin (Figure 1A and B) and consistent with our previous observations (2), XLH dentin (Figure 1C and D) had an enlarged predentin layer and large interglobular spaces resulting from unmerged calcospherites (Figure 1D). In addition, XLH odontoblasts failed to form a well-polarized cell layer as compared to control pulp.

OPN localization in XLH models and in human XLH teeth

Immunostaining for OPN showed localization in odontoblasts, predentin and dentin in both control (Figure 1E and F) and XLH (Figure 1G and H) teeth, with the strongest OPN staining being associated with mineralized XLH dentin (Figure 1G and H).

In our 3D tooth culture model, OPN immunostaining was associated with dental pulp cells and mineralization nodules in the control group (Figure 1I), and only with dental pulp cells where mineralization was inhibited by p-ASARM (Figure 1J). In the rat pulp injury repair model, compared to dentin bridge formation observed after control-PBS bead treatment (Figure 1K), p-ASARM bead treatment impaired bridge formation and OPN labeling was observed in the heterogeneously mineralized and disorganized reparative dentin (Figure 1L).

MEPE expression and ALP activity in human XLH teeth

Odontoblasts in control (Figure 2A and B) and XLH (Figure 2C and D) dentin exhibited ALP activity. However, in XLH teeth, this activity appeared less prominent, heterogeneous and diffuse in the odontoblast layer when compared to the strong staining of control odontoblasts.

Compared to MEPE immunostaining of control teeth (Figure 2E and F), XLH teeth showed odontoblasts and dentin tubules having slightly stronger staining, and interglobular

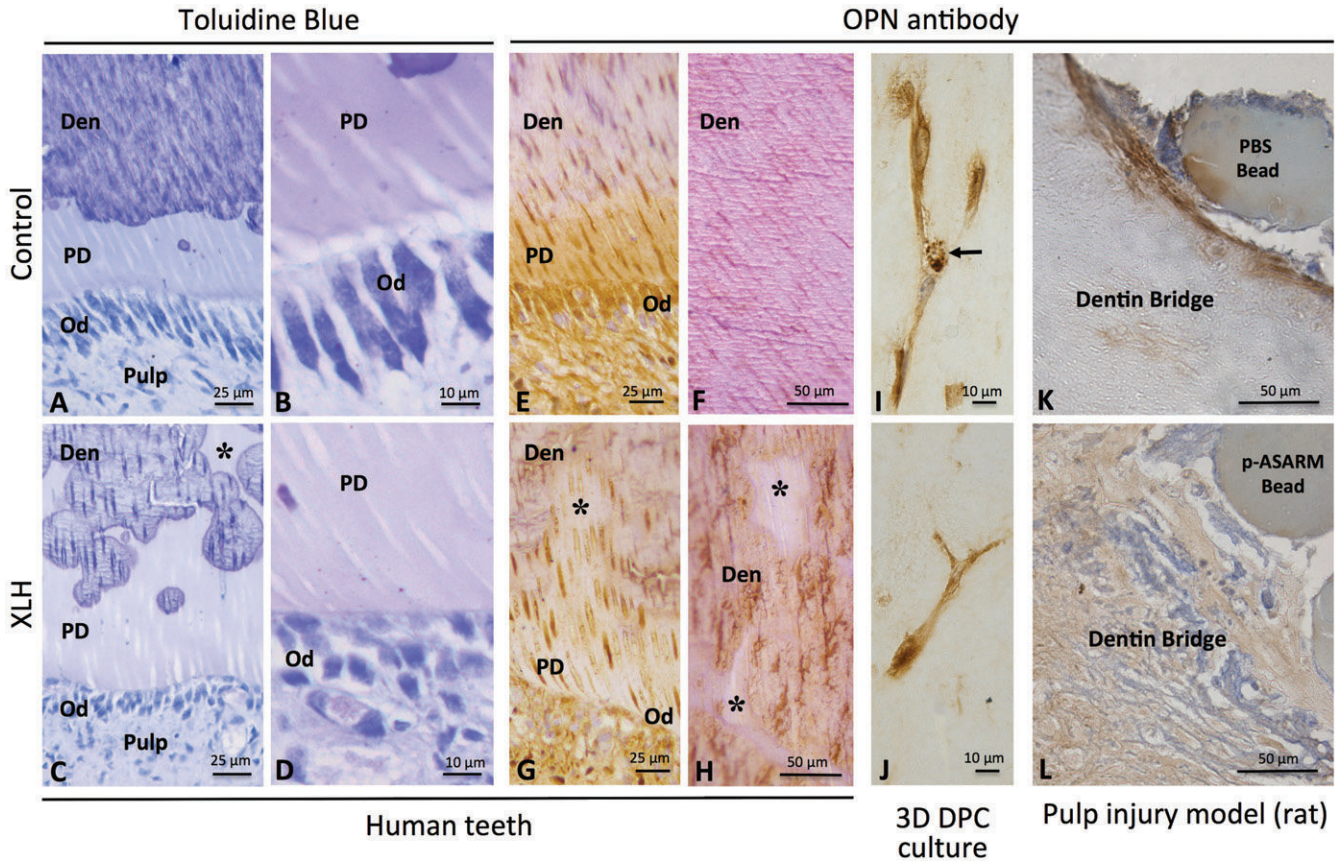

Figure 1. Histology and OPN immunostaining. (A–D) Toluidine blue staining of undemineralized human control and XLH teeth. Impaired polarization and organization of odontoblasts, and an enlarged predentin with fewer well-defined dentinal tubules and unmerged calcospherites creating interglobular spaces (asterisks) are observed in XLH teeth. (E–H) Immunostaining for OPN shows prominent localization in XLH mineralized dentin and along dentinal tubules. (I and J) In 3D dental pulp cell cultures, OPN immunostaining is strong in cells and mineralized nodules (arrow) in the control cultures, and in cells only after p-ASARM treatment. (K and L) In the rat pulp injury repair model, OPN staining is prominent throughout the irregular reparative dentin bridge induced by p-ASARM (L) versus control PBS-soaked beads (K). Den, dentin; PD, predentin; Od, odontoblast.

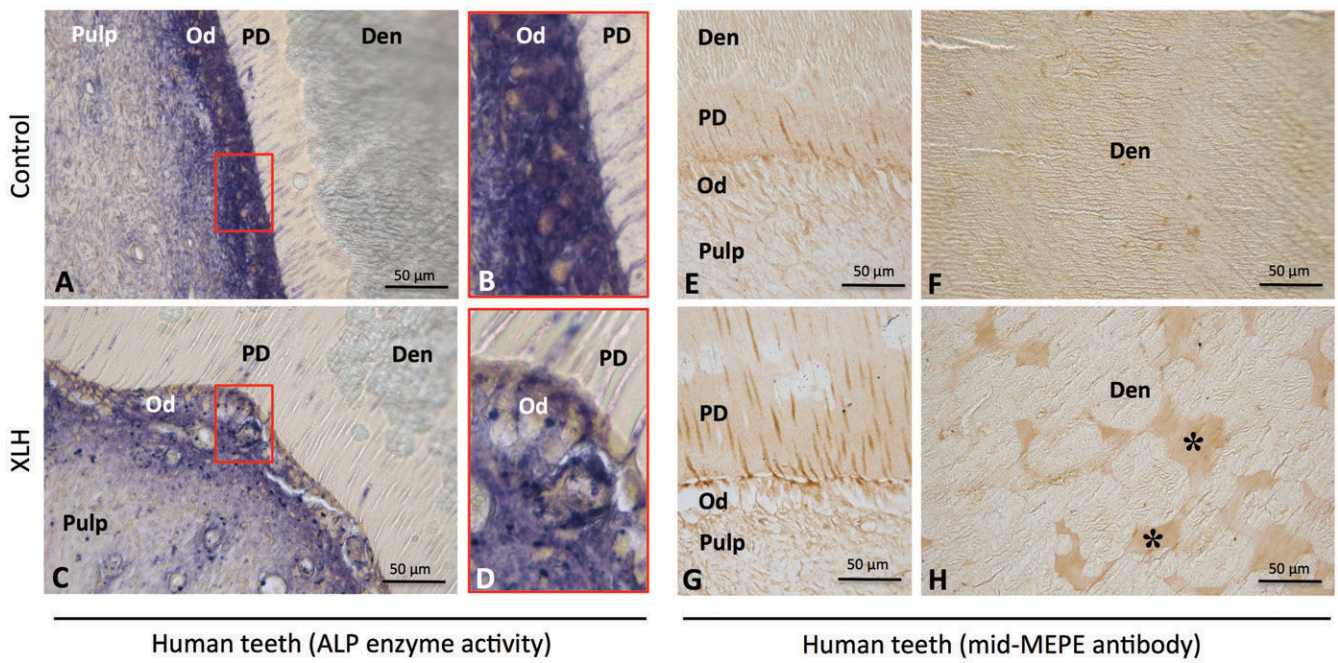

Figure 2. ALP enzymatic activity and MEPE immunostaining. (A–D) In undemineralized tooth samples, strong ALP activity is uniformly spread throughout the odontoblast layer of control teeth, whereas that in XLH teeth is less intense and patchy in appearance. (E–H) MEPE immunostaining is localized to odontoblasts and their cell processes, and to predentin and dentin in both groups, but is particularly concentrated in abnormal interglobular spaces (asterisks) in XLH dentin. Od, odontoblast; PD, predentin; Den, dentin.

spaces between calcospherites were stained for MEPE (Figure 2G and H), consistent with our previous findings (7).

Discussion

We have previously shown in animal and cell culture models of XLH that a MEPE-derived ASARM peptide inhibits ECM mineralization and odontoblast differentiation, while increasing MEPE and TNAP expression (7). Based on the analysis of dental tooth germs, our present study indicates that ALP activity and MEPE and OPN localization in odontoblasts and dentin from XLH teeth are abnormal and show an accumulation of MEPE in unmineralized interglobular spaces.

Interestingly, the pulp–dentin complex in XLH teeth is poorly organized and shows impaired odontoblast organization and polarization. This observation is consistent with an inhibition of odontoblastic differentiation, possibly resulting from the increased MEPE expression in XLH (7).

PHEX mutations lead to an accumulation of SIBLING protein fragments contributing to mineralization defects observed in pathologic bone and dentin (2,3). As reported for MEPE-derived ASARM peptides, full-length OPN and its derived-fragments (including OPN ASARM) have been shown to be physiologically relevant substrates for PHEX (3). Full-length phosphorylated OPN and phosphorylated OPN ASARM peptide are both strong mineralization inhibitors (10,11). In this present work, we show that OPN accumulates in the XLH tooth dentin, especially in the abnormal calcospherites. In addition, this protein is highly expressed by dental pulp cells treated with p-ASARM peptide in our 3D culture model and is associated with mineralization defects observed in the formation of an abnormal disorganized dentin bridge in the presence of p-ASARM. Taken together, our data suggest that both MEPE and OPN are involved in impaired tooth mineralization associated with XLH probably through different effects on mineralization and differentiation processes, with MEPE acting at the level of the unmineralized interglobular spaces and OPN acting within the mineralized calcospherites. In XLH teeth, elevated MEPE accumulating in the tubules and in the matrix may result in impaired odontoblast differentiation and in defective dentin mineralization.

Declaration of interest

This study was supported by University Paris Descartes, Fondation pour la Recherche Médicale (PhD program support for BS), Fondation de l'Avenir to EA2496, and the National Institutes of Health grant (5RO-1-AR51598-01 to PSR). The authors state no conflict of interest.

References

1. Gaucher C, Walrant-Debray O, Nguyen TM, Esterle L, Garabedian M, Jehan F, . PHEX analysis in 118 pedigrees reveals new genetic clues in hypophosphatemic rickets. Hum Genet 2009;125: 401–11.
2. Boukpessi T, Septier D, Bagga S, Garabedian M, Goldberg M, Chaussain-Miller C. Dentin alteration of deciduous teeth in human hypophosphatemic rickets. Calcif Tissue Int 2006;79: 294–300.
3. Barros NM, Hoac B, Neves RL, Addison WN, Assis DM, Murshed M, Carmona AK, McKee MD. Proteolytic processing of osteopontin by PHEX and accumulation of osteopontin fragments in Hyp mouse bone, the murine model of X-linked hypophosphatemia. J Bone Miner Res 2013;28:688–99.
4. Fisher LW, Fedarko NS. Six genes expressed in bones and teeth encode the current members of the SIBLING family of proteins. Connect Tissue Res 2003;44:33–40.
5. Rowe PS, de Zoysa PA, Dong R, Wang HR, White KE, Econs MJ, Oudet CL. MEPE, a new gene expressed in bone marrow and tumors causing osteomalacia. Genomics 2000;67: 54–68.
6. Boukpessi T, Gaucher C, Leger T, Salmon B, Le Faouder J, Willig C, Rowe PS, Garabedian M, Meilhac O, Chaussain C. Abnormal presence of the matrix extracellular phosphoglycoprotein-derived acidic serine- and aspartate-rich motif peptide in human hypophosphatemic dentin. Am J Pathol 2010;177: 803–12.
7. Salmon B, Bardet C, Khaddam M, Naji J, Coyac BR, Baroukh B, Letourneur F, Lesieur J, Decup F, Le Denmat D, Nicoletti A, Poliard A, Rowe PS, Huet E, Vital SO, Linglart A, McKee MD, Chaussain C. MEPE-derived ASARM peptide inhibits odontogenic differentiation of dental pulp stem cells and impairs mineralization in tooth models of X-linked hypophosphatemia. PLoS One 2013;8: e56749.
8. Baroukh B, Cherruau M, Dobigny C, Guez D, Saffar JL. Osteoclasts differentiate from resident precursors in an in vivo model of synchronized resorption: a temporal and spatial study in rats. Bone 2000;27:627–34.
9. Miura M, Gronthos S, Zhao M, Lu B, Fisher LW, Robey PG, Shi S. SHED: stem cells from human exfoliated deciduous teeth. Proc Natl Acad Sci USA 2003;100:5807–12.
10. Addison WN, Azari F, Sorensen ES, Kaartinen MT, McKee MD. Pyrophosphate inhibits mineralization of osteoblast cultures by binding to mineral, up-regulating osteopontin, and inhibiting alkaline phosphatase activity. J Biol Chem 2007;282: 15872–83.
11. Addison WN, Masica DL, Gray JJ, McKee MD. Phosphorylation-dependent inhibition of mineralization by osteopontin ASARM peptides is regulated by PHEX cleavage. J Bone Miner Res 2010; 25:695–705.

10.4 Appendix 4: ASARM Peptides Inhibit Odontogenic Differentiation

OPEN ACCESS Freely available online

PLOS ONE

MEPE-Derived ASARM Peptide Inhibits Odontogenic Differentiation of Dental Pulp Stem Cells and Impairs Mineralization in Tooth Models of X-Linked Hypophosphatemia

Benjamin Salmon[1,2,3☯], Claire Bardet[1☯], Mayssam Khaddam[1], Jiar Naji[1], Benjamin R. Coyac[1,2,10], Brigitte Baroukh[1], Franck Letourneur[4], Julie Lesieur[1], Franck Decup[1,6], Dominique Le Denmat[1], Antonino Nicoletti[11,12], Anne Poliard[1], Peter S. Rowe[5], Eric Huet[7], Sibylle Opsahl Vital[1,2,3], Agnès Linglart[3,8,9], Marc D. McKee[10], Catherine Chaussain[1,2,3]*

1 EA 2496, Pathologies, Imaging and Biotherapies of the Tooth, UFR Odontologie, University Paris Descartes PRES Sorbonne Paris Cité, Montrouge, France, **2** AP-HP Odontology Department Bretonneau – Louis Mourier, Hôpitaux Universitaires Paris Nord Val de Seine, Paris France, **3** Centre de Référence des Maladies Rares du Métabolisme du Phosphore et du Calcium, AP-HP, Kremlin Bicêtre, France, **4** Institut Cochin, University Paris Descartes PRES Sorbonne Paris Cité, Paris, France, **5** The Kidney Institute, University of Kansas Medical Center, Kansas City, Kansas, United States of America, **6** AP-HP Odontology Department Charles Foix, Ivry Sur Seine, France, **7** Université Paris-Est, Laboratoire CRRET, CNRS, Créteil, France, **8** APHP Endocrinology and Diabetology for Children, Bicêtre Paris Sud Hospital, Kremlin Bicêtre, France, **9** Université Paris-Sud, Kremlin Bicêtre, France, **10** Faculty of Dentistry, and Department of Anatomy and Cell Biology, McGill University, Montreal, Quebec, Canada, **11** Inserm UMRS698, Paris, France, **12** Denis Diderot University, UMRS698, Paris, France

Abstract

Mutations in *PHEX* (phosphate-regulating gene with homologies to endopeptidases on the X-chromosome) cause X-linked familial hypophosphatemic rickets (XLH), a disorder having severe bone and tooth dentin mineralization defects. The absence of functional PHEX leads to abnormal accumulation of ASARM (acidic serine- and aspartate-rich motif) peptide – a substrate for PHEX and a strong inhibitor of mineralization – derived from MEPE (matrix extracellular phosphoglycoprotein) and other matrix proteins. MEPE-derived ASARM peptide accumulates in tooth dentin of XLH patients where it may impair dentinogenesis. Here, we investigated the effects of ASARM peptides *in vitro* and *in vivo* on odontoblast differentiation and matrix mineralization. Dental pulp stem cells from human exfoliated deciduous teeth (SHEDs) were seeded into a 3D collagen scaffold, and induced towards odontogenic differentiation. Cultures were treated with synthetic ASARM peptides (phosphorylated and nonphosphorylated) derived from the human MEPE sequence. Phosphorylated ASARM peptide inhibited SHED differentiation *in vitro*, with no mineralized nodule formation, decreased odontoblast marker expression, and upregulated MEPE expression. Phosphorylated ASARM peptide implanted in a rat molar pulp injury model impaired reparative dentin formation and mineralization, with increased MEPE immunohistochemical staining. In conclusion, using complementary models to study tooth dentin defects observed in XLH, we demonstrate that the MEPE-derived ASARM peptide inhibits both odontogenic differentiation and matrix mineralization, while increasing MEPE expression. These results contribute to a partial mechanistic explanation of XLH pathogenesis: direct inhibition of mineralization by ASARM peptide leads to the mineralization defects in XLH teeth. This process appears to be positively reinforced by the increased MEPE expression induced by ASARM. The MEPE-ASARM system can therefore be considered as a potential therapeutic target.

Citation: Salmon B, Bardet C, Khaddam M, Naji J, Coyac BR, et al. (2013) MEPE-Derived ASARM Peptide Inhibits Odontogenic Differentiation of Dental Pulp Stem Cells and Impairs Mineralization in Tooth Models of X-Linked Hypophosphatemia. PLoS ONE 8(2): e56749. doi:10.1371/journal.pone.0056749

Editor: Irina Kerkis, Instituto Butantan, Brazil

Received November 8, 2012; **Accepted** January 13, 2013; **Published** February 22, 2013

Funding: This study was supported by grants from University Paris Descartes, Fondation pour la Recherche Médicale, Fondation de l'Avenir to EA2496, and by the National Institutes of Health grant (5RO-1-AR51598-01 to PSR). MDM is a member of the Fonds de Recherche Québec-Santé (FRQ-S) Réseau de Recherche en Santé Buccodentaire et Osseuse, the FRQ-S Groupe de Recherche Axé sur la Structure des Protéines, and the Jamson T.N. Wong Laboratories in Calcified Tissue Research of the McGill Centre for Bone and Periodontal Research. The Ph.D. program of BS was supported by the Fondation pour la Recherche Médicale and by the Société Française des Tissus Minéralisés. The funders had no role in study design, data collection and analysis, decision to publish, or preparation of the manuscript.

Competing Interests: MDM has received research contracts and consulting honoraria from Enobia Pharma (now Alexion Pharmaceuticals). The other authors state no conflict of interest. This does not alter the authors' adherence to all the PLOS ONE policies on sharing data and materials.

* E-mail: catherine.chaussain@parisdescartes.fr

☯ These authors contributed equally to this work.

Introduction

Mineralization is regulated by a number of determinants, including small molecules such as pyrophosphate, and proteins (including enzymes and hormones), that act either locally in the extracellular matrix and/or systemically to regulate calcium and phosphate metabolism. Currently, the complex links between these molecules are not well understood. Of note for tooth dentin

(unlike bone) is that dentin is not involved in the regulation of the calcium and phosphate metabolism, and dentin is not remodeled. Thus, it is a tissue showing a permanent chronological record of disease that may be useful in deciphering these complex molecular interactions and mechanisms of mineralization.

Skeletal mineralization is severely impaired in patients with mutations in the genes encoding mineralization-regulating proteins [1]. Genetic disorders, such as X-linked familial hypophosphatemic rickets (XLH), may affect both bone and tooth mineralization [2]. Mineralization defects in XLH appear in children as rickets with severe skeletal deformities and as osteomalacia and bone or join pain in adults. Patients with XLH frequently present spontaneous dental abscesses, without any history of tooth trauma or decay [3,4,5]. Despite the fact that teeth of patients with XLH seem visibly normal, radiography commonly reveals thin enamel and radiolucent dentin – the latter being associated with unusually large pulp chambers. In XLH, dentin mineralization is impaired [6,7,8], with the defect appearing as unmerged, persistent mineralization foci (calcospherites) surrounded by extensive interglobular regions of unmineralized dentin matrix [6]. These abnormalities may lead to rapid pulp necrosis associated with periapical bone infection. Within the pathologic, unmineralized interglobular dentin matrix, many of the extracellular matrix (ECM) components, including noncollagenous proteins (NCPs), are degraded [7,9,10,11]. Among them, degraded members of the SIBLING family (small integrin-binding ligand N-linked glycoproteins) have been identified in XLH dentin [12,13]. This family of proteins shares a common acidic serine- and aspartate-rich motif (ASARM), which has a key role in the mineralization process [14,15,16,17,18,19].

Among the SIBLING proteins, MEPE (matrix extracellular phosphoglycoprotein) has been shown to be involved in pathologic processes associated with hypophosphatemic rickets [16,20,21,22,23]. MEPE is expressed by both osteoblasts and odontoblasts and is normally protected from cleavage by a protein-protein interaction between its ASARM motif and PHEX (phosphate-regulating gene with homologies to endopeptidases on the X-chromosome) [24,25] − a transmembrane endopeptidase. More than 80% of patients with familial hypophosphatemic rickets carry a mutation in the *PHEX* gene [26,27,28,29]. In these patients, unprotected MEPE is exposed to pathologic cleavage by local proteinases such as cathepsin B, releasing ASARM peptides into the ECM and the circulation [24,30,31]. Moreover, since ASARM is normally a substrate for the enzymatic activity of PHEX [32,33], the lack of functional PHEX in XLH patients results in the accumulation of these proteinase-resistant peptides that are thought to lead to mineralization defects in bone and tooth ECM [12,14,23,34]. Other mineralization-regulating SIBLING proteins, such as OPN and DMP1 (dentin matrix protein 1), as well as the ASARM-containing peptides derived from their cleavage, may also be involved in the mineralization pathology [14,32,35,36]. Previous *in vitro* studies have shown that mouse-derived bone marrow stromal cells (BMSCs) and osteoblasts treated with phosphorylated MEPE-derived (and OPN-derived) ASARM synthetic peptides failed to properly mineralize their ECM [14,32,33,37,38].Since human teeth are severely affected by the disease [3,6], this study aimed to investigate *in vitro* and *in vivo* the effects of the MEPE-derived ASARM peptide on tooth dentin mineralization. We used pulp progenitor stem cells from human exfoliated deciduous teeth (SHEDs), as we and others have shown that deciduous teeth are mostly affected in patients with XLH [3,7,8,30]. These cells were induced toward an odontogenic differentiation program using a cell culture collagen/tooth slice 3D scaffold model. In parallel, we implanted MEPE-derived ASARM peptides into surgically injured pulp of rat molars [39], and their effects on reparative dentin formation were evaluated. From these *in vitro* and *in vivo* studies reported here, we demonstrate that phosphorylated MEPE-derived ASARM peptide inhibits dentin mineralization, disturbs odontoblast differentiation and dramatically upregulates MEPE expression. This ASARM peptide − previously identified and shown to accumulate in dentin from patients with XLH [12] − therefore appears to be a key molecule in the pathogenesis of tooth dentin abnormalities as observed in XLH patients.

Materials and Methods

Human Teeth

Teeth were obtained from the Dental Department of Hopitaux Universitaires Paris Nord Val de Seine, AP-HP, France. Deciduous teeth were collected after trauma or after exfoliation from three healthy young children (3–7 years of age). Permanent third molars were obtained after extraction according to an orthodontic treatment plan. All teeth were collected with informed and oral consent from the patients and the parents according to ethical guidelines set by the French law (Loi Bioéthique n°2004–800) and with a special authorization for our team (n°DC-2009–927, Cellule Bioéthique DGRI/A5, direction générale pour la recherche et l'innovation, Ministère de l'enseignement supérieur et de la recherche, Paris, France).

Synthetic ASARM Peptides

Phosphorylated ASARM (p-ASARM with 3 phosphoserine residues) and nonphosphorylated ASARM (np-ASARM) peptides were synthesized according to the human MEPE-derived sequence as previously reported [14], and were RDDSSESSDSG-S(PO_3H_2)SS(PO_3H_2)ES(PO_3H_2)DGD and RDDSSESSDSGSS-SESDGD, respectively.

Cell Culture

Culture of pulp stem cells from human exfoliated deciduous teeth (SHEDs) were established as previously reported [40]. Briefly, after decontamination with povidone-iodine solution (Betadine, Meda Pharma, France), teeth were sectioned longitudinally and exposed pulp tissues were collected and enzymatically digested with type I collagenase (3 mg/ml; Worthington Biochem, Freehold, NJ, USA) and dispase (4 mg/ml; Boehringer Mannheim, Germany). Single-cell suspensions were obtained by passing the digested tissues through a 70 µm cell strainer. Cells were then seeded at a density of $10^4/cm^2$, and the cultures were maintained with Dulbecco's Modified Eagle Medium 1 g/L D-Glucose (DMEM; Invitrogen, Grand island, NY, USA) supplemented with 10% fetal bovine serum (FBS; Invitrogen), 1% penicillin/streptomycin (PS; Invitrogen), at 37°C with 5% CO_2. The medium was refreshed the next day after initial cell attachment and then after at 3 times per week. Cells were detached by trypsinization at 70–80% confluence (0.25% trypsin EDTA solution Sigma-Aldrich, St. Louis, MO, USA) and either re-plated at the same density or frozen at −80°C. For all experiments, SHEDs were used between passages 2 and 4. Their SHED phenotype (CD90+, CD29+, CD44+, CD45−, CD73+, CD105+, CD146+, and 10% of STRO-1+) was confirmed by polychromatic flow cytometry analysis (LSRII, Becton Dickinson, NJ; antibodies from Biolegend, CA, BDBiosciences, NJ and eBioscience, CA) (Fig. S1).

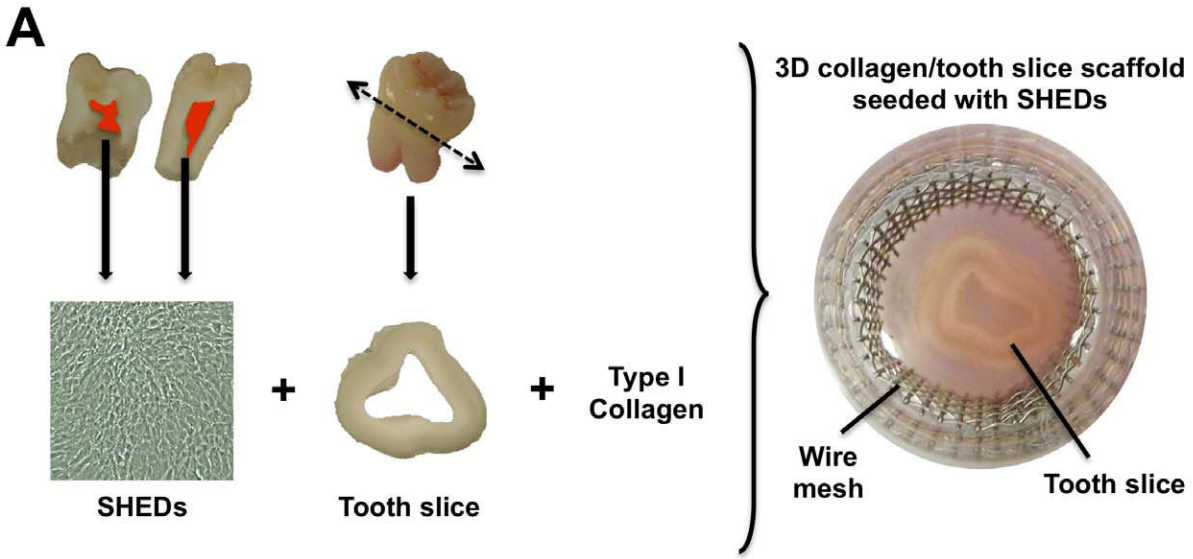
A
SHEDs
Tooth slice
Type I Collagen
3D collagen/tooth slice scaffold seeded with SHEDs
Wire mesh
Tooth slice

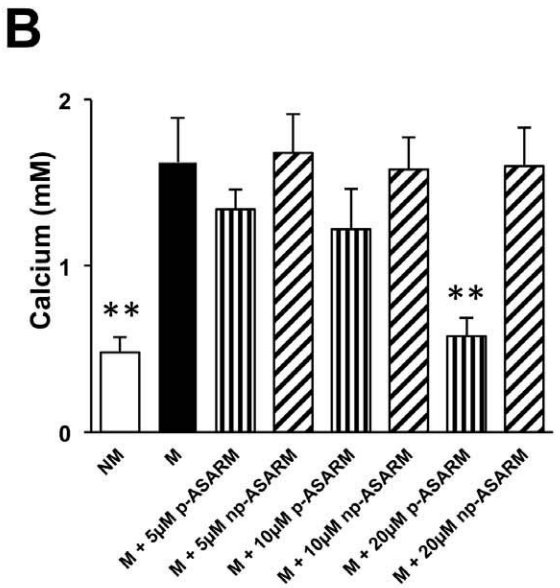
B
Calcium (mM)
NM
M
M + 5μM p-ASARM
M + 5μM np-ASARM
M + 10μM p-ASARM
M + 10μM np-ASARM
M + 20μM p-ASARM
M + 20μM np-ASARM

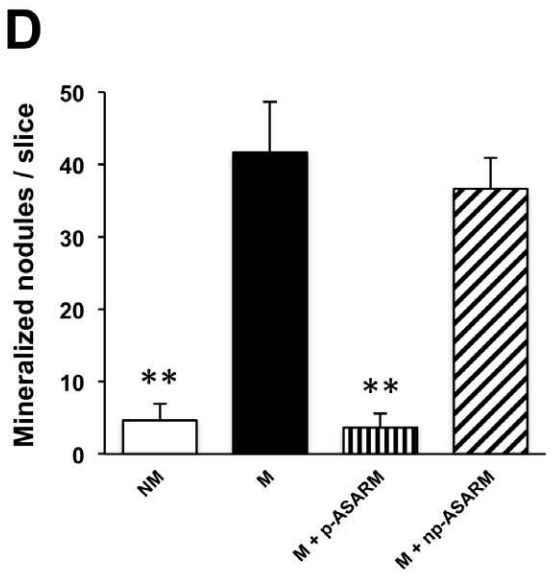
D
Mineralized nodules / slice
NM
M
M + p-ASARM
M + np-ASARM

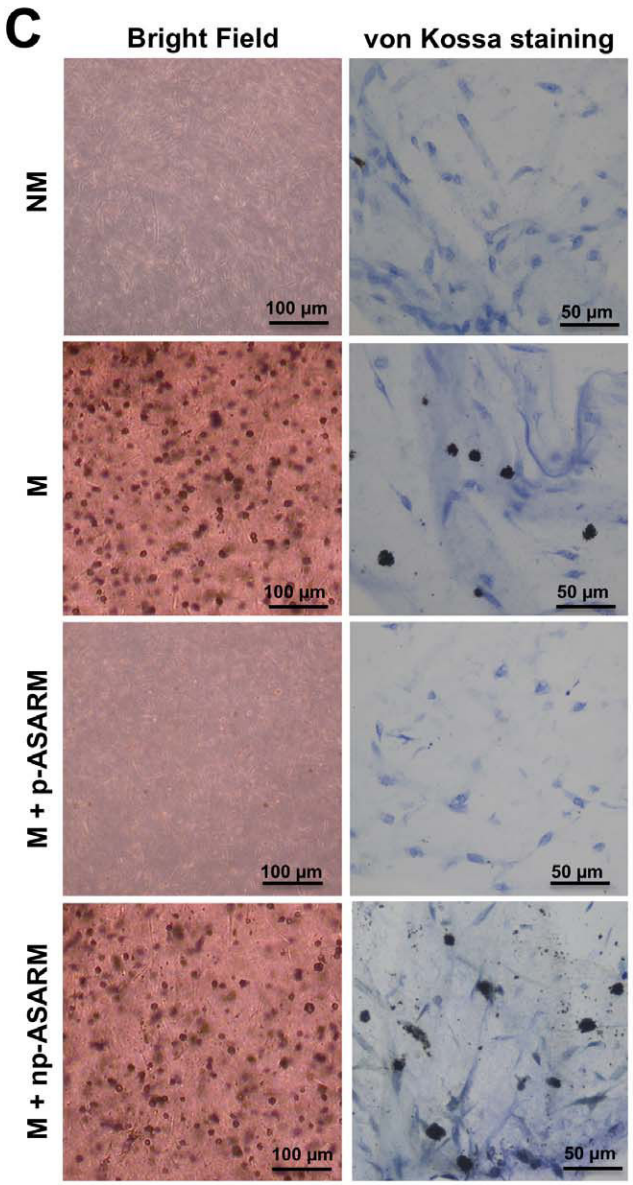
C
Bright Field
von Kossa staining
NM
M
M + p-ASARM
M + np-ASARM
100 μm
50 μm

Figure 1. Inhibition of mineralization by phosphorylated MEPE-ASARM peptide in a 3D collagen/tooth slice culture model. A: Schematic of the 3D culture model. Stem cells from human deciduous exfoliated teeth (SHEDs) were obtained for cell cultures studies from the pulp of caries-free human third molars. Passaged cells (10^6 SHEDs) seeded into a type I collagen gel scaffold were applied to a human tooth slice with a pulp chamber cavity to mimick the tooth/dentin environment, all of which were supported peripherally by a steel wire mesh to minimize collagen gel contraction. **B:** Calcium content in the cell/matrix layer determined by flame atomic absorption spectrometry of cultures maintained in NM or M conditions in the absence or presence of p-ASARM or np-ASARM at a concentration of 5, 10 or 20 μM for 21 days. Calcium content significantly decreased in the presence of 20 μM of p-ASARM while the nonphosphorylated form of the peptide had no effect on calcium content of the cultures. **C-D:** SHED cultures were maintained in nonmineralizing (NM) or mineralizing (M) conditions (see Materials and Methods) in the absence or presence of 20 μM phosphorylated (p-ASARM) or nonphosphorylated (np-ASARM) peptide for 21 days. Mineralized nodules in the extracellular matrix were clearly visible by light microscopy after von Kossa staining in the M and M+np-ASARM. Quantification of mineralized nodules (**D**) shows that they were essentially undetectable in presence of the p-ASARM peptide, whereas about 40 nodules were counted per slice in the M and M+np-ASARM samples. $n = 3$, error bars +/− SD, ** indicates significant difference ($p<0.01$) relative to mineralizing condition without peptide.
doi:10.1371/journal.pone.0056749.g001

Tooth Slice Preparation

Caries-free human third molars extracted for orthodontic treatment purposes were collected from healthy young adults (18–25 years of age) with informed and oral consent of the patient, according to ethical guidelines set by the French law (see above). One-mm-thick tooth slices were prepared as previously described [41]. After disinfection with 70% ethanol, teeth were transversely sectioned at the cervical region using a diamond saw blade under cooling with sterile phosphate-buffered saline (PBS, Invitrogen) to obtain 1-mm-thick dentin slices. The pulp tissue was completely removed and tooth slices were immersed in 0.05% sodium hypochlorite for 10 s, then washed with sterile 1× PBS.

3D Culture Model Seeded with SHEDs

Tooth slices (one slice per well) were placed into wells of a 24-well culture plate for the cell culture studies. To provide a 3-dimensional (3D) cell culture environment, the empty pulp chamber was filled with 1 ml of polymerizing collagen gel prepared by mixing 10% (v/v) of ice-cold 10× DMEM (Sigma-Aldrich), 10% (v/v) of $NaHCO_3$ (37 g/l), 50% (v/v) of type I collagen solution (2 mg/ml) and 30% (v/v) of SHEDs in suspension at 10^6 cells/ml. To avoid adhesion and migration of the cells from the scaffold to the bottom of a conventional cell culture plate, cell culture-suspension plates were used (Cellstar, Greiner bio-one, Basel, Switzerland). The type I collagen used was extracted from rat tail tendons as previously described [42]. A sterile, stainless steel grid (Weber Metaux, Paris, France) was placed along the edge of the well to prevent gel contraction.

Induction of the Odontoblast Differentiation Program

To induce the odontoblast differentiation program in the SHEDs, cells seeded into the 3D collagen/tooth slice scaffold (Fig. 1A) were cultured up to 21 days at 37°C with 5% CO_2, 10% FBS, and 1% penicillin/streptomycin in supplemented DMEM in the presence of 10 mM ß-glycerophosphate (a source of phosphate for mineralization), 50 μg/ml ascorbic acid (promotes collagen secretion and matrix assembly), and of 10^8 M dexamethasone (which induces expression of biomineralization markers) − this is termed the mineralization condition (M) in our study [43]. Using this mineralization condition, either p-ASARM or np-ASARM (at concentrations of 5, 10, 20 μM for both) were added to the cultures during media changes 3 times per week. The negative control, termed the nonmineralizing condition (NM), consisted of DMEM cultures supplemented with 10% FBS and 1% PS. In all cases, medium was changed 3 times a week. Samples were collected at days 7, 14 and 21. At each time point and for each condition, cell morphology was observed using an inverted microscope (Olympus CKX41, Tokyo, Japan). All experiments were repeated in triplicate with cells from the same donor.

Mineralization Assays

For assessing mineralized nodule formation after 3 weeks of culture, SHED-seeded 3D collagen/tooth slice scaffolds were fixed overnight at 4°C in 4% paraformaldehyde (PFA) solution and embedded in methyl methacrylate (Merck, Darmstadt, Germany) without any demineralization process [44]. Nine-micrometer-thick tissue sections were prepared, and mineralization in the ECM was revealed by von Kossa staining carried out by applying a 5% silver nitrate solution (Sigma) to the sections. Sections were then counterstained with toluidine blue. Mineralized nodules were counted in 30 randomly analyzed fields for each condition at 20× magnification and results are expressed as the number of nodules/tooth slice scaffold.

Table 1. Primer design for RT-PCR analysis.

	5′ –3′ Forward primer	5′ –3′ Reverse primer	Product
MEPE	GAGTTTTCTGTGTGGGACTACT	GCTTTGCTTAGTTTTCTCAGTC	86-bp
NM_020203.2			
DSPP	GAGGAGATGCTTCTTATAACTCTG	GTGCTATCACTGTCATCATCTT	91-bp
NM_014208.3			
Osteocalcin	GCACCCTTCTTTCCTCTT	GGAGTTTATTTGGGAGCAG	95-bp
NM_199173.3			
COL1	TGACTGGAAGAGTGGAGAGTA	TCTTGCTGATGTACCAGTTCT	149-bp
NM_000088.3			
ALPL	AACTGATGTGGAGTATGAGAGTG	GAAGTGGGAGTGCTTGTATCT	112-bp
NM_000478.4			

doi:10.1371/journal.pone.0056749.t001

Table 2. Clinical and biological characteristics of the patients with XLH at the time of tooth extraction.

Patients with XLH	**1**	**2**
Sex	M	F
Age (yr)	3	15
(at the time of tooth collection)		
Treatment	–	+
Age at onset (yr)	*not yet started at the time*	3.3
Duration (yr)	*of tooth collection*	10
Unalfa® (μg/day)	–	1.25
Phosphates (mg/day)	–	2100
Compliancy	–	moderate
Signs of rickets		
Leg bowing	+++	+
Height (SD)	−3	−2.1
Serum P (mmol/l)	0.63	0.58
Alkaline phosphatase (IU/L)*	498	523
Dental status	vital	vital
DMFT or dft**	7	2
Collected tooth	61,71	38, 48
Type	deciduous	permanent
Pulp status	vital	vital
Reason of extraction	(trauma)	(orthodontic treatment
		plan)

*(normal range is inferior to 300 IU/L).
**DMFT: Decayed Missing Filled permanent Teeth; dft: decayed filled deciduous teeth.
doi:10.1371/journal.pone.0056749.t002

Quantification of calcium content extracted from mineral deposits within the cell/matrix layer after 21 days of culture was also assessed. For this, the 3D collagen scaffolds seeded with the SHEDs were gently removed from the tooth slice, rinsed twice with PBS, and decalcified with 0.5 M HCl for 1 hr at room temperature under constant agitation. After centrifugation at 2.150 g for 10 min, the calcium content in the supernatant was determined by the flame atomic absorption spectrometry method (AAnalyst, Perkin Elmer, Waltham, MA, USA).

Immunohistochemistry

After 3 weeks of culture, SHED-seeded 3D collagen/slice scaffolds were fixed overnight at 4°C in 4% paraformaldehyde (PFA) solution, and embedded in methyl methacrylate (Merck, Darmstadt, Germany) without any demineralization process [44]. Nine-micrometre-thick tissue sections were prepared and endogenous peroxidases were blocked by incubation of the sections with 5 mM periodic acid at room temperature for 10 min. After extended rinsing in PBS, background activity was blocked at room temperature for 90 min using 1% bovine serum albumin (BSA) in PBS. Mouse monoclonal antibodies for osteocalcin (ab13420, Abcam, Cambridge, UK) and DSP (dentin sialoprotein, LFMb-21, Santa Cruz Biotechnology, CA, USA), and rabbit polyclonal antibodies for the MEPE mid-region and PHEX [14] were used all at a 1/200 dilution. Sections were treated in a moist chamber overnight at 4°C and further incubated for 90 min with a polyclonal goat anti-mouse immunoglobulin/HRP conjugate (Dako, Glostrup, Denmark) or with a polyclonal swine anti-rabbit immunoglobulin/HRP conjugate (Dako). Peroxidase visualization was obtained over 45 s in a dark chamber using 3.3′-diaminobenzidine tetrahydrochloride (Fast Dab, Sigma-Aldrich). The sections were counterstained with hematoxylin staining. Controls were carried out by omitting the primary antibody to exclude nonspecific binding. For PHEX, a goat anti-rabbit immunoglobulin-G Alexa Fluor 488 was used at a dilution of 1/200 (Sigma-Aldrich) in a dark-chamber, and nuclei were counterstained with dapi (Invitrogen). Microscopic images were merged using Image J software ver1.45p (public domain image processing and analysis software developed at the National Institutes of Health, Bethesda, MD, USA).

Scanning Electron Microscopy

After 3 weeks of culture, 3D collagen/tooth slice scaffolds were fixed overnight in 1% PBS-buffered glutaraldehyde at 4°C and processed for scanning electron microscopy (SEM). Samples were fractured in liquid nitrogen and carbon- or gold-sputtered surfaces were observed in a scanning electron microscope (Cambridge S260 SEM, UK) equipped with an Everhart-Tornley and back-scattered electron detector (BSE) and with an energy-dispersive X-ray spectrometer (EDX) for X-ray microanalysis (Bruker Axs, WI, USA) with Esprit2 software.

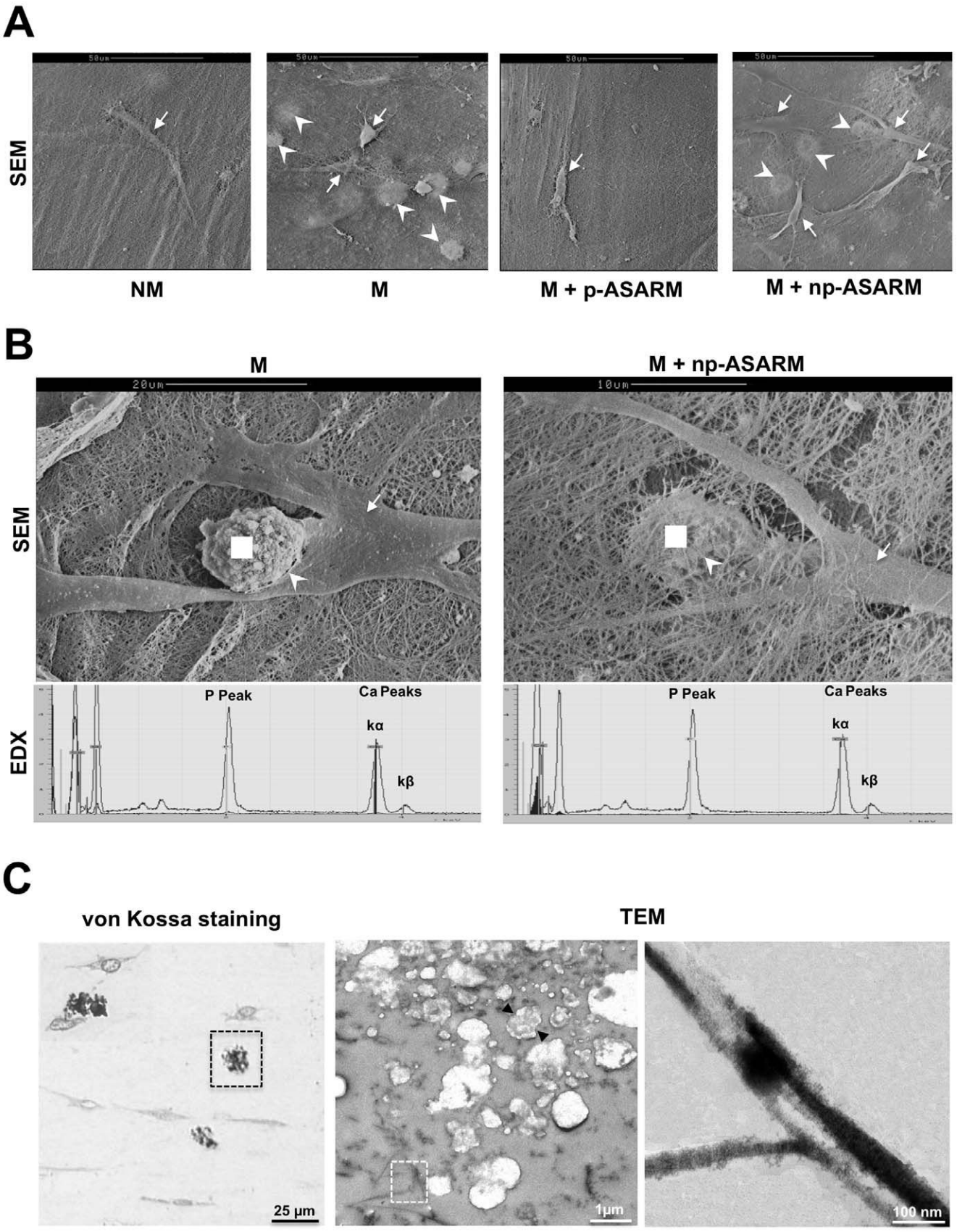

Figure 2. Light and electron microscopy of the cells, matrix and mineral in 3D SHED cell cultures. SHED cell cultures maintained in nonmineralizing (NM) or mineralizing (M) conditions in the absence or presence of 20 μM of either phosphorylated (p-ASARM) or nonphosphorylated

(np-ASARM) ASARM peptide for 21 days were visualized by light microscopy and by scanning (SEM) and transmission (TEM) electron microscopy. **A,B:** SEM reveals SHEDs (arrows) well integrated into the collagen scaffold. Mineralization of the cultures appears as nodules within the collagen scaffold (arrowheads) only in the M and the M+np-ASARM conditions. Energy-dispersive X-ray spectroscopy (EDX) for compositional microanalysis of the nodules (performed at the white square) shows major spectral peaks for calcium (Ca) and phosphorus (P) with an acquired Ca/P ratio of 1.67+/−0.05 in both mineralizing conditions where nodules appeared. **C:** Light microscopy (left panel) and TEM (center and right panel) of the mineralized cultures (M and M+np-ASARM). Mineralized nodules (black box, left panel) are often in close proximity to the SHED cells, and consist of aggregates of multiple, smaller mineralization nodules (arrowheads) and occasional mineralized collagen fibrils (white box center panel, and right panel).
doi:10.1371/journal.pone.0056749.g002

Light Microscopy and Transmission Electron Microscopy

Light microscopy and transmission electron microscopy (TEM) were used to analyze cells and mineralization of the 3D collagen/tooth slice scaffolds. Scaffolds were fixed overnight at 4°C in 4% paraformaldehyde and embedded in methyl methacrylate (Merck, Darmstadt, Germany). One-µm-thick survey sections were cut for light microscopy using a Reichert Ultracut S microtome, and sections were stained with von Kossa reagent (5% silver nitrate solution, Sigma) to reveal mineralization sites within the scaffold, and then counterstained with toluidine blue. Thin sections (90 nm) were cut and placed onto an electron microscopy grid followed by conventional staining with uranyl acetate and lead citrate at room temperature, and some sections were additionally subsequently stained with von Kossa reagent (5% silver nitrate solution, Sigma). Mineralized regions of the scaffolds were examined, and images recorded, using a Leitz DMRBE optical microscope equipped with a Sony DXC-950 CCD camera, and using a JEOL 1011 TEM operating at 80 kV and equipped with a GATAN Erlangshen camera 1000.

RT-PCR Analysis for Gene Expression

The mineralizing potential of the SHED cultures treated with the ASARM peptides was investigated by analyzing the expression of type I collagen α-chain (*COL1*), dentin sialophosphoprotein (*DSPP*), *MEPE*, *PHEX*, osteocalcin, and tissue-nonspecific alkaline phosphatase (*ALPL*) genes after extraction of total RNA from the cultures after 7, 14 and 21 days using RNeasy Mini kit (Qiagen, Hilden, Germany). 300 ng of total RNA was reverse-transcribed with Superscript II (Gibco, Invitrogen) using oligodT. cDNA was amplified with specific primers (Eurofins mwg operon, Ebersberg, Germany) in a SYBR® Green PCR Master Mix (Roche, Basel, Switzerland). Each primer pair was chosen for best efficiency and controlled for specificity (Table 1). Quantitative real-time PCR (qPCR) analysis was carried out using LigthCycler 480 [45]. The PCR cycles consisted of an initial pre-incubation step (95°C for 5 min), followed by 45 cycles of amplification (95°C for 5 s, 55°C for 5 s, 70°C for 10 s). Relative gene expression levels were estimated using the deltaCq method [46]. *GAPDH* and *ubiquitine C* (*UBC)* were determined using GeNorm software on a set of 5 standard housekeeping genes and were used as housekeeping genes for the rest of the study. Results were expressed as mean ± SD of relative mRNA level for each time point and for the different conditions.

Total Protein Extraction and Western Blot Analysis

At 7, 14 and 21 days, the collagen matrices seeded with SHEDs were gently removed from the tooth slices and processed for total protein extraction using ice-cold extraction buffer (each collagen scaffold was placed in 100 µl buffer: 50 mM Tris-HCl, pH 7.5, containing 5 mM EDTA, 150 mM NaCl and 0.2% Triton X-100), supplemented with 1/100 Protease Inhibitor Cocktail Set V EDTA free (Calbiochem, La Jolla, CA, USA). The resulting homogenates were briefly sonicated on ice, cleared by centrifugation at 10,000 g for 10 min at 4°C and stored at −80°C. Homogenates (10 µg) were subjected to 10% SDS-PAGE and transferred onto a nitrocellulose membrane (Bio-Rad). Membranes were incubated overnight at 4°C with monoclonal anti-DSP (1/2000; LFMB-21, Santa Cruz) and anti-osteocalcin (1/1000; ab13420, Abcam) antibodies, or polyclonal anti-MEPE mid-region and anti-PHEX antibodies at 1/2000 dilution [14]. Membranes were incubated with a peroxidase-linked swine anti-rabbit secondary antibody (1/10,000) for 2 hrs at room temperature, then rinsed and followed by enhanced chemiluminescence detection of bound primary antibodies (Roche Diagnostics, Meylan, France). As a control for protein loading, membranes were carefully washed in stripping buffer (Pierce Chemical, Rockford, IL, USA) and processed with a monoclonal mouse anti-α tubulin antibody (clone B-5-1-2, Sigma). Quantification was performed using Image J software.

Implantation of ASARM Peptides in a Rat Pulp/Dentin Injury Model

Affi-Gel agarose beds (Bio-Rad Laboratories) were soaked in a solution of p-ASARM or np-ASARM dissolved in PBS (2 µg/µl) for 2 hrs, and dried overnight at 37°C. Beads soaked with PBS were used as a control. The beads were implanted into the pulp of the upper first molar of 9 rats (6 week-old, OFA/SD Charles River, Lyon, France) using a surgical procedure previously described [47]; this study was designed according to the ARRIVE guidelines and approved by the Animal Care Committee of the University Paris Descartes (agreement CEEA34.CC.016.11, Comité d'éthique pour l'expérimentation animale n° 34, Paris, France). Each animal received two of the three compared treatments on the left and right first maxillary molars. Treatments were then analyzed between animals using the molar as the statistical unit. Briefly, after gingival electrosurgery, 18 half-moon-shaped class V 0.5 mm cavities were prepared on the mesial aspect of the first upper molar using a 0.2-mm-diameter round bur (E0123, Dentsply Maillefer, Ballaigues, Switzerland). Pulp exposure was accomplished with a root-canal-shaping rotary nickel-titanium file system (Protaper, Dentsply), after which 10 peptide-treated beads − either with buffer (n = 6), or p-ASARM (n = 6), or np-ASARM (n = 6) − were implanted into the pulp using a blunt steel probe. After bead placement, cavities were filled with Biodentine cement (Septodont, Saint-Maur des Fossés, France). The rats were sacrificed after one month and X-ray micro-computed tomography (micro-CT) analysis was performed on the treated molars (Skyscan Model 1172, Kontich, Belgium). Semi-automatic segmentation of X-ray serial images allows the calculation of the unmineralized pulp volume in order to indirectly quantify the mineralization of the reparative dentin within the teeth. After X-ray scanning, tissue demineralization was then performed in 4.13% EDTA for approximately 8 weeks. After tissue embedding in paraffin (Paraplast), 7-µm-thick sections were cut on a rotary microtome and either prepared for staining with hematoxylin-eosin stain, or prepared for immunohistochemistry. Sections were deparaffinized and rehydrated before blocking with 10% normal goat serum for 45 min at room temperature. Sections were incubated overnight at 4°C with primary antibody against

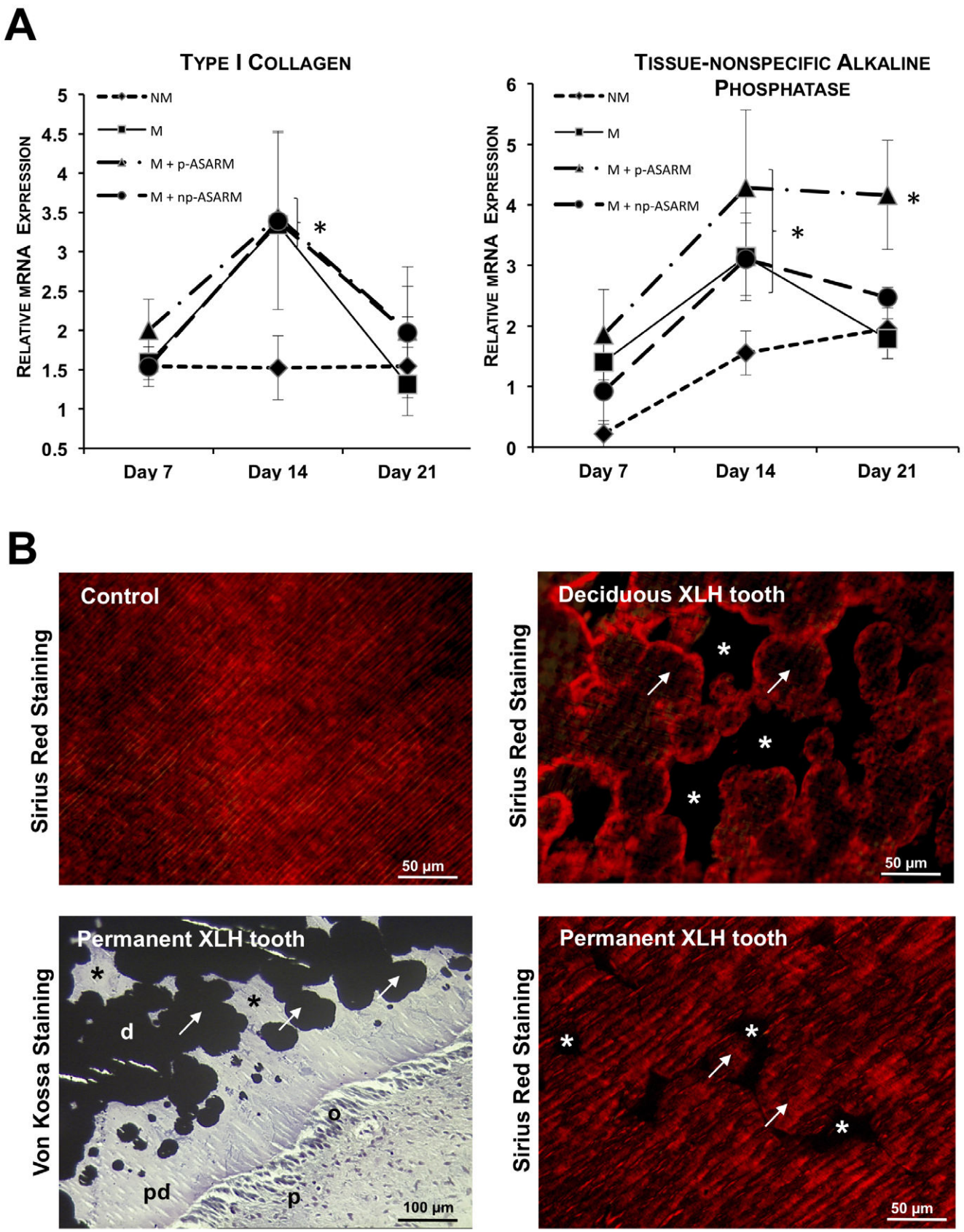

Figure 3. Effect of MEPE-ASARM peptides on type I collagen and tissue-nonspecific alkaline phosphatase expression. A: Quantitative real-time PCR (as described in Materials and Methods) for type I collagen and tissue-nonspecific alkaline phosphatase expression in 3D cultures of SHEDs maintained in nonmineralizing (NM) or mineralizing (M) conditions in the absence or presence of either 20 μM phosphorylated (p-ASARM) or

nonphosphorylated (np-ASARM) ASARM peptide for 21 days. mRNA expression levels were upregulated from day 7 to day 14 in M, M+p-ASARM and M+np-ASARM conditions and, at day 21, returned to a level comparable to that of the NM condition, except for alkaline phosphatase which remained high in the M+p-ASARM condition. $n = 3$, error bars +/− SD, * indicates significant difference ($p<0.05$) relative to NM condition. **B:** Sirius Red staining of collagen in deciduous tooth sections from a 3-year-old male XLH patient (upper right panel), permanent tooth sections from a 15-year-old female XLH patient (bottom right panel) and control patient (upper left panel) revealing an intact collagen distribution only where dentin has mineralized in the form of characteristic calcospherites (arrows), and not in the interglobular spaces (asterisks) in the dentin where mineralization is typically impaired in XLH and where matrix degradation occurs. Sirius Red staining of normal dentin (right panel) is generally homogeneous across the tubular dentin. Similarly, von Kossa staining counterstained with toluidine blue in the same XLH permanent tooth sections (bottom left panel) show lack of fusion of calcospherites (arrows) with large non-mineralized interglobular spaces (asterisks) in the dentin. o: odontoblast. pd: predentin. d: dentin. p: pulp.

doi:10.1371/journal.pone.0056749.g003

the MEPE mid-region at a 1/200 dilution and processed as described above in the immunohistochemistry section.

Human XLH Tooth Characterization

Patient characteristics are given in Table 2. All teeth were obtained with the informed and oral consent of the patients and the parents, according to ethical guidelines set by the French government (see above). Human deciduous incisors were collected from a 3-year-old male patient with XLH [26]. Immediately after extraction, teeth were fixed for 7 days at 4°C in a 4% paraformaldehyde solution buffered at pH 7.3 by PBS and processed after demineralization [7] for Sirius red staining.

Human permanent third molar germs were collected in the context of an orthodontic treatment plan from a 15-year-old female patient with XLH [26]. Immediately after extraction, teeth were fixed for 7 days at 4°C in 70% ethanol, included in methyl methacrylate [44] and processed for von Kossa and Sirius red staining.

Statistical Analysis

Values are represented as the mean +/− standard deviation (SD). Data were analyzed by one-way analysis of variance (ANOVA) followed by post hoc Fisher's least significant difference test.

Results

Dose-dependent Response of SHEDs to p-ASARM Peptide

SHEDs were cultured in a 3D collagen matrix enclosed within a tooth slice under mineralizing conditions (Fig. 1A). Cells were treated at concentrations ranging from 5 to 20 μM of phosphorylated MEPE-derived ASARM peptide (p-ASARM) for 21 days in mineralizing medium (Fig. 1B). p-ASARM peptide was shown to inhibit mineralization nodule formation in a dose-dependent manner with the highest inhibition occurring at the highest concentration (20 μM) of p-ASARM, which is in agreement with preliminary data obtained with 2D cultures of either human dental pulp stem cells or SHEDs (data not shown), and with previous studies [33,38]. This 20 μM concentration was subsequently used for all other experiments. In contrast, nonphosphorylated MEPE-derived ASARM peptide (np-ASARM) had no effect on mineralization as previously reported with other cell types [14,33].

p-ASARM Peptide Inhibits ECM Mineralization in a 3D Culture of SHEDs

To examine the role of p-ASARM on ECM mineralization, SHEDs were cultured for 21 days in the 3D model under mineralizing (M) or nonmineralizing (NM) conditions, or under mineralizing conditions with either 20 μM of p-ASARM (M+p-ASARM) or np-ASARM (M+np-ASARM). No mineralization was observed in the presence of p-ASARM, whereas readily distinguishable mineralized nodules were observed in the absence or the presence of np-ASARM (Figs. 1C). Calcium quantification from the cell cultures performed by flame atomic adsorption spectrometry confirmed the mineralized nodule counts by showing very low calcium levels in the M+p-ASARM treatment condition similar to the nonmineralizing condition calcium content (Fig. 1D).

Analysis of samples by scanning electron microscopy (SEM) of fractured collagen/tooth slice scaffolds showed mineralized nodules within the collagenous ECM in close association with neighboring cells (Figs. 2A, B). In all conditions, well-distinguishable cell processes were observed in contact with the tooth slice (Fig. S2). Calcium-to-phosphate ratios of mineralized nodules obtained by EDX spectroscopy were close to 1.67 for the two conditions permissive of mineralization (M, and M+np-ASARM, Fig. 2B), which is consistent with the formation of a hydroxyapatite-like mineral phase. In contrast, cell cultures treated under NM conditions, or with the M+p-ASARM condition, showed no evidence of mineralization (Fig. 2A). Under the conditions where mineral formed, analysis by light microscopy and by TEM of mineralized scaffold matrix regions showed a small nodular type of mineralization amongst the collagen fibrils, with some mineralization extending occasionally along collagen fibrils (Fig. 2C); no such mineralization was observed in cultures treated with p-ASARM (data not shown).

p-ASARM does not Modify Type I Collagen mRNA Expression but Upregulates Tissue-nonspecific Alkaline Phosphatase mRNA

The aim of seeding SHEDs in a 3D collagen matrix was to generate an ECM environment mimicking that found in vivo which favors the cell differentiation process of progenitor/stem cells [48,49,50]. We therefore investigated some of the major ECM components and marker proteins known to be expressed by SHEDs as they begin to differentiate towards the odontoblast phenotype. The number of transcripts encoding type I collagen − the major ECM protein of odontoblasts/dentin − increased under mineralizing conditions from day 7 to day 14 (approximately 2-fold), after which it returned at day 21 to the basal expression level of cells grown under the nonmineralizing condition (Fig. 3A); this induction was not modified by the presence of the ASARM peptides. Likewise, alkaline phosphatase mRNA expression was upregulated in all mineralizing conditions between days 7 and 14 (Fig. 3A). Thereafter, it remained stable up to day 21 in the presence of p-ASARM, but diminished to a level comparable to the nonmineralizing condition in the other conditions (M and M+np-ASARM).

As collagen has never been investigated in teeth from patients with XLH, we examined its distribution in tooth sections. Sirius red staining, which stains collagen fibrils, was associated predominantly with the calcospherites characteristic of this pathology, indicating that there was little or no collagen (degraded) in the interglobular spaces (Fig. 3B) as previously shown [12].

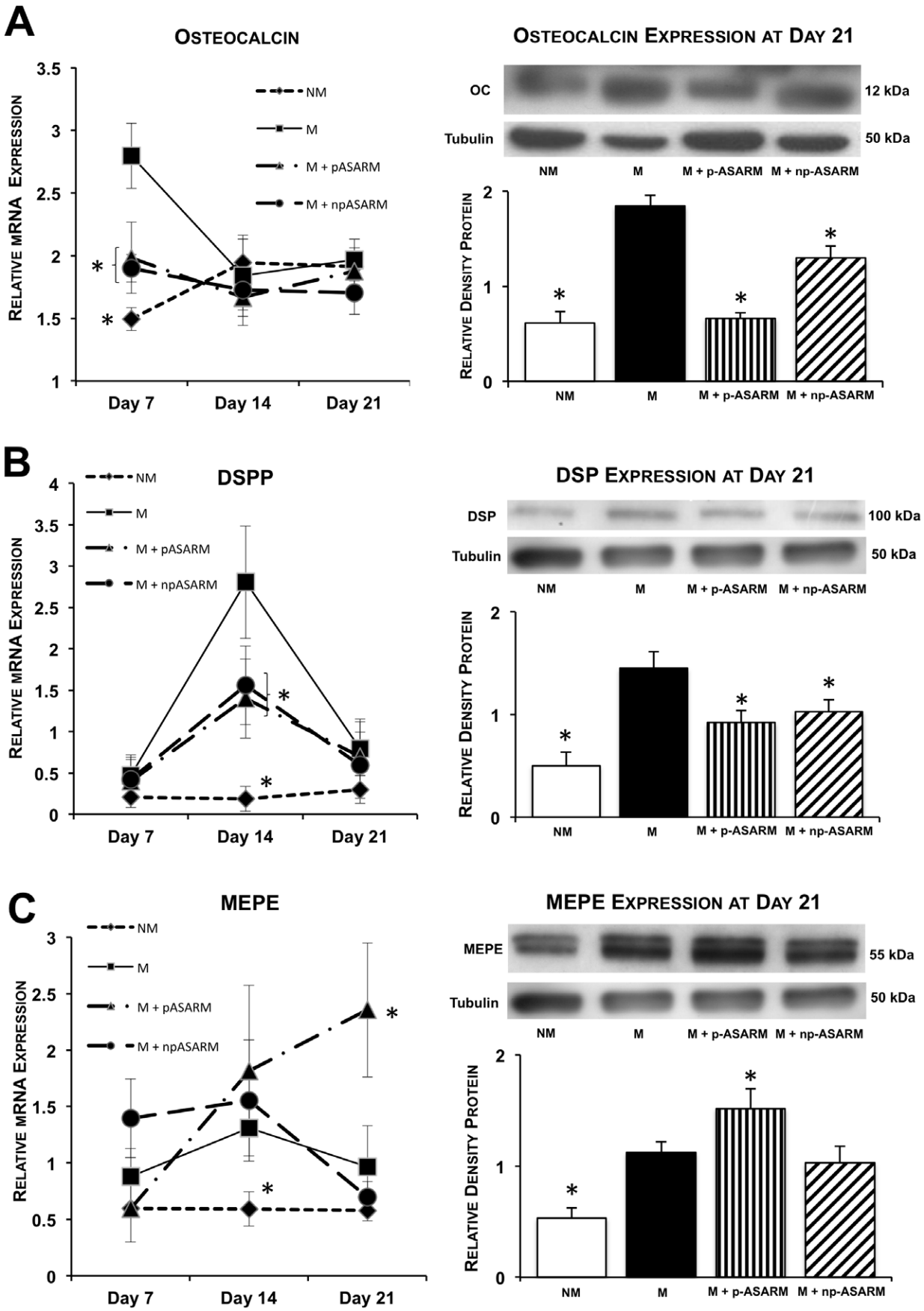
A
OSTEOCALCIN
RELATIVE MRNA EXPRESSION
NM
M
M + pASARM
M + npASARM
Day 7
Day 14
Day 21
OSTEOCALCIN EXPRESSION AT DAY 21
OC
12 kDa
Tubulin
50 kDa
NM
M
M + p-ASARM
M + np-ASARM
RELATIVE DENSITY PROTEIN
B
DSPP
DSP EXPRESSION AT DAY 21
DSP
100 kDa
C
MEPE
MEPE EXPRESSION AT DAY 21
55 kDa

Figure 4. Effect of MEPE-ASARM peptides on osteocalcin, DSPP and MEPE expression. SHED cell cultures were maintained in nonmineralizing (NM) or mineralizing (M) conditions in the absence or presence of 20 μM of either phosphorylated (p-ASARM) or nonphosphorylated (np-ASARM) ASARM peptide for 21 days. Quantitative real-time PCR at day 7, 14 and 21, and Western blotting at day 21, for osteocalcin, DSPP/DSP and MEPE were performed. **A,B:** Osteocalcin and DSPP/DSP expression are induced under the M condition both at the mRNA and protein levels. This induction is reduced in the presence of both the p-ASARM and np-ASARM peptides. **C:** mRNA and Western blot analysis for MEPE reveal increased expression of MEPE in all mineralizing conditions from day 7 to day 14 (expression was not detectable at baseline). At day 21, MEPE expression was still strongly upregulated in the M+p-ASARM condition. $n = 3$, error bars +/− SD, * indicates significant difference ($p<0.05$) relative to the mineralizing condition without peptides (M).
doi:10.1371/journal.pone.0056749.g004

Odontoblast Differentiation is Impaired in the Presence of ASARM Peptides

Differentiation of SHED cells to odontoblasts is associated with an increase in mineralization-regulating protein marker gene expression. Osteocalcin mRNA was increased in all mineralizing conditions at day 7 relative to the nonmineralizing condition, an expression pattern substantially reduced in the presence of the ASARM peptides (Fig. 4A). Western blot analysis confirmed a lower expression of the osteocalcin protein in the presence of the ASARM peptides and most particularly after addition of p-ASARM. Osteocalcin immunolocalization revealed variable levels of cell immunostaining under all conditions. In addition, mineralized nodules in the mineralizing conditions (M and M+np-ASARM) were stained for osteocalcin (Fig. 5, top row, arrows) whereas no ECM labeling was observed in the p-ASARM-treated samples and in the nonmineralizing condition. Analysis of the expression of the dentin sialoprotein protein (DSP) precursor protein DSPP, another marker of odontogenic differentiation [51], revealed an increase in its transcript number at day 14 in all mineralizing conditions as compared to the nonmineralizing condition (Fig. 4B). However, in the presence of the ASARM peptides, this upregulation was twice as low when compared to control mineralizing conditions. Such a differential expression pattern was confirmed at the protein level by Western blot analysis at day 21. For DSP, positive immunohistochemical staining was revealed in the mineralized nodules in the ECM (Fig. 5, middle row, arrows in M and M+np-ASARM conditions).

p-ASARM Peptide Upregulates MEPE Expression

Given the mineralization-inhibiting properties of the MEPE-derived p-ASARM peptide and also its effects on expression of odontoblast marker proteins, we next examined the expression of *MEPE* itself after the 3D cultures were treated with the ASARM peptides. As presented in Figure 4C, MEPE transcript expression was induced from day 7 to day 14 in all mineralizing conditions, regardless of the presence of the ASARM peptides. However, at

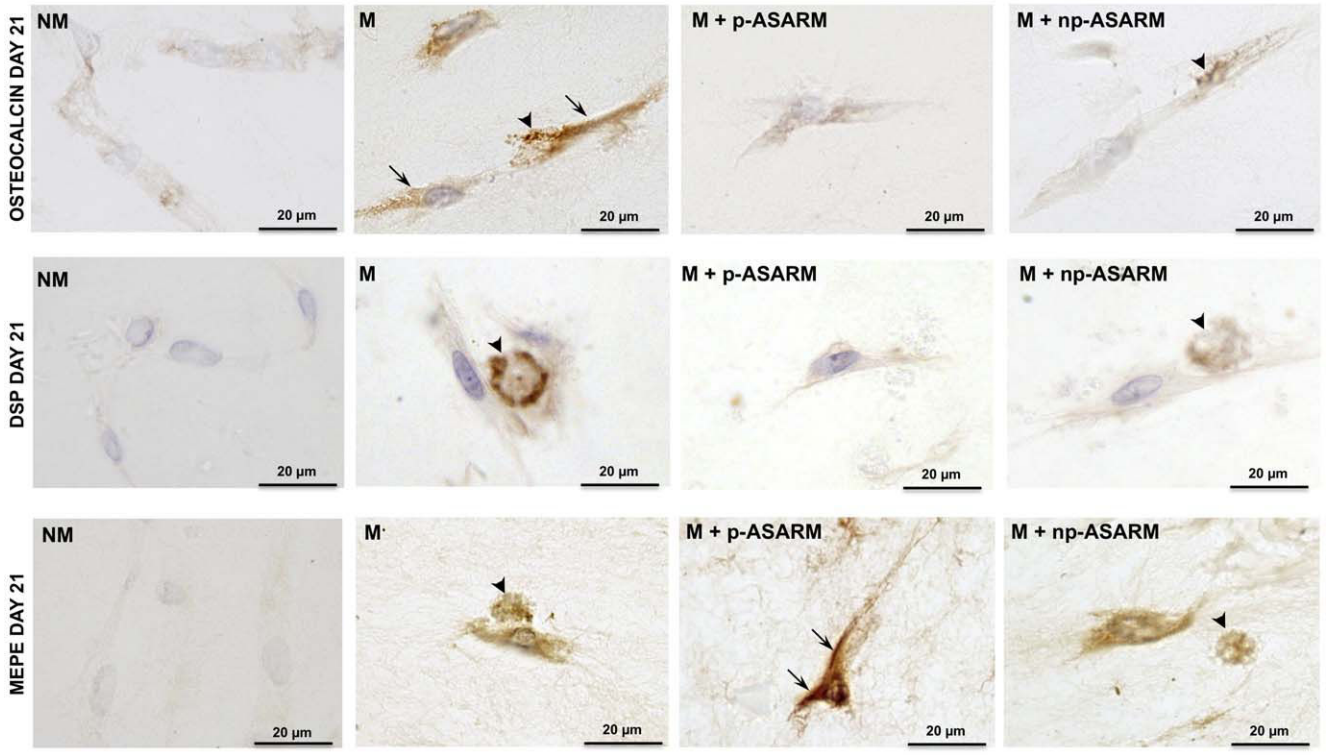

Figure 5. Immunohistochemical detection of osteocalcin, DSP and MEPE after treatment with MEPE-ASARM peptides. SHED cell cultures were maintained in nonmineralizing (NM) or mineralizing (M) conditions in the absence or presence of 20 μM of either phosphorylated (p-ASARM) or nonphosphorylated (np-ASARM) ASARM peptide for 21 days. Immunohistochemistry for osteocalcin, DSP and MEPE was performed on methyl methacrylate sections of 21-day cultures. Osteocalcin immunostaining (top row) is strong in SHEDs (arrows) and nodules (arrowheads) in the M and M+p-ASARM conditions. Immunohistochemistry for DSP shows strong staining in mineralized nodules in both the M and M+np-ASARM conditions. MEPE immunostaining is found in SHEDs and nodules in mineralizing conditions the (M and M+np-ASARM conditions) but is particularly strong in the cultures treated with p-ASARM that do not mineralize (M+p-ASARM). The images presented are representative of all sections examined.
doi:10.1371/journal.pone.0056749.g005

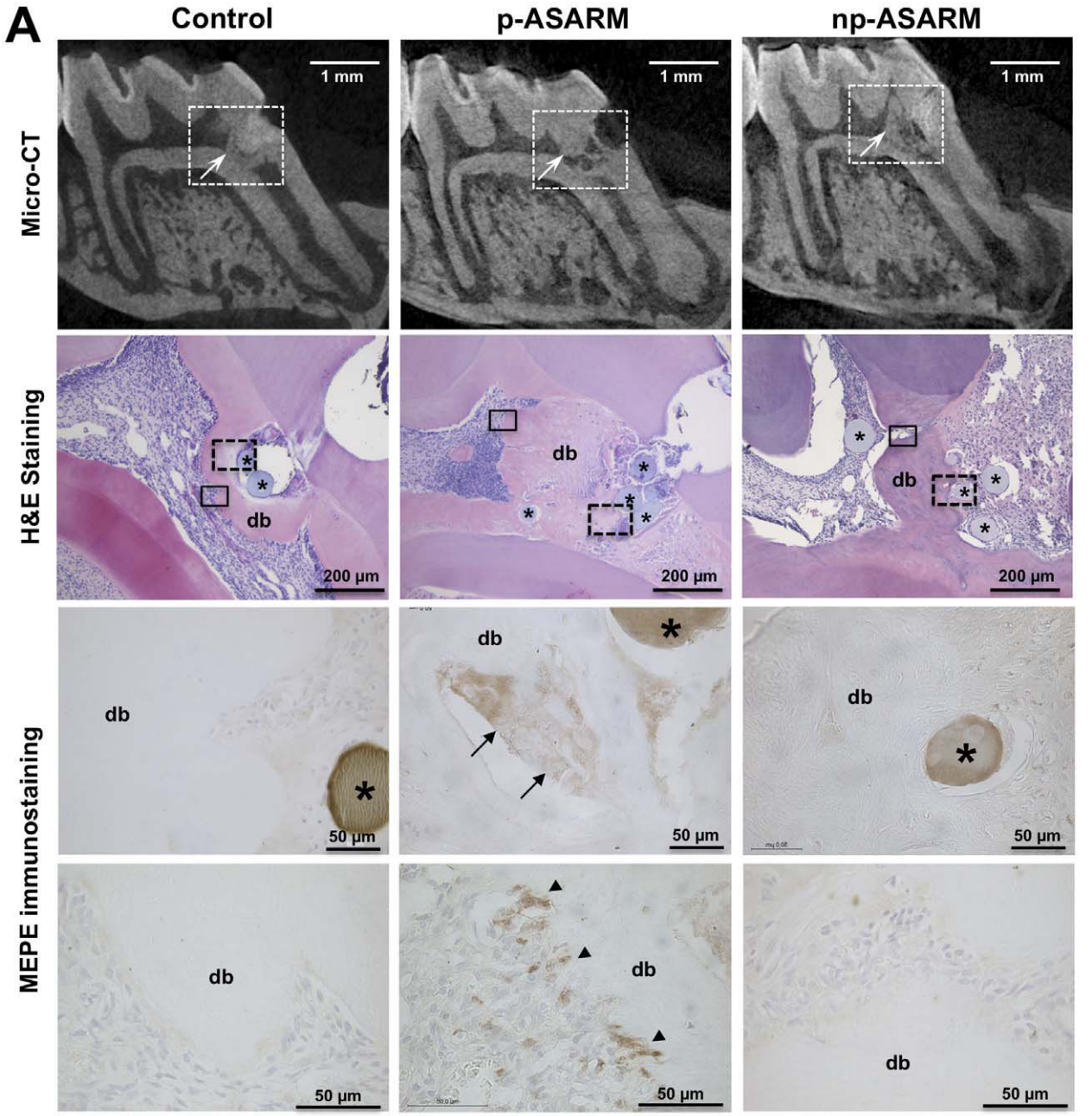
A
Control
p-ASARM
np-ASARM
Micro-CT
H&E Staining
MEPE immunostaining
1 mm
200 µm
50 µm
db
B
Serial micro-CT sections
Pulp areas selected from serial micro-CT sections (segmentation)
Pulp volume reconstructed from segmentation data
Pulp Volume (mm³)
1.2
1
0.8
0.6
0.4
0.2
0
Control
p-ASARM
np-ASARM

Figure 6. Effect of MEPE-ASARM peptides on reparative dentin mineralization and MEPE expression in a rat dentin/pulp wound model. This *in vivo* data is from rats sacrificed at 1 month after implantation of agarose beads soaked in either p-ASARM or np-ASARM, or buffer (control), into the pulp of the first upper molar. A: MEPE derived p-ASARM impairs reparative dentin mineralization and enhances MEPE expression. Micro-computed tomography (micro-CT) sections (top row) show mineralization (arrows) occurring in the pulp chamber as a reparative process (dentin bridge formation) near the pulp injury (white dashed box outline). The dentin bridge appears thinner and irregular with large voids (mineralization defects) in the p-ASARM treatment when compared to the control and np-ASARM treatment. Hematoxylin and eosin (H&E) staining of paraffin histology sections (second row) taken from the region outlined by the white dashed boxes show the irregular nature of the dentin bridge (db) in the vicinity of the beads (asterisks) soaked in p-ASARM as compared to the control and the np-ASARM treated wounds. Immunohistochemistry for MEPE (third row) in the region demarcated by the black dashed box outlines shows an accumulation of MEPE (arrows) in nonmineralized spaces of the reparative dentin bridge only in the case p-ASARM treatment. Immunohistochemistry for MEPE (bottom row) in the region demarcated by the black box outlines shows strong MEPE staining of cells (odontoblasts) secreting the dentin bridge. In control and np-ASARM-treated samples, the dentin bridge appears homogenous and with no or weak staining for MEPE. B: Quantification of the pulp volume (to indirectly measure mineralization volume "pulp fill") was performed by micro-CT of the bead-implanted molars. Semi-automatic segmentation (red area) of the pulp was performed from micro-CT serial sections in order to calculate the global volume of the pulp. The volume of the pulp from the p-ASARM-treated molars was significantly higher when compared to the control and np-ASARM treatment suggesting that mineralization in the reparative dentin process was impaired by p-ASARM. * indicates significant difference ($p<0.05$) relative to control.
doi:10.1371/journal.pone.0056749.g006

day 21, MEPE transcripts remained significantly increased (2.8-fold) in the presence of p-ASARM peptide, whereas they returned to levels in the other mineralizing conditions (M and M+np-ASARM) comparable to those observed in nonmineralizing conditions. This result was confirmed by Western blot analysis where MEPE protein expression increased in all mineralizing conditions (Fig. 4C), but its expression was significantly higher in the presence of p-ASARM. Consistent with this, immunohistochemistry for MEPE showed particularly strong cell staining for the p-ASARM treatment under mineralizing conditions (Fig. 5, bottom row, arrowheads). In contrast, in the presence of np-ASARM or in the mineralizing condition alone without added peptide, the staining was associated with the mineralized nodules in the ECM, with moderate staining of the cells (Fig. 5, bottom row, arrows). These results indicate that the p-ASARM peptide increases MEPE expression by differentiating SHEDs via a positive feedback mechanism. Given that MEPE has protein-protein interactions with PHEX, and given that its ASARM peptide is a substrate for PHEX enzymatic activity, we examined PHEX expression *in vitro* under our different treatment conditions applied to the SHED cells in 3D cell culture. In this collagen/tooth slice scaffold model, PHEX expression was not altered by ASARM treatment (Fig. S3).

p-ASARM Peptide Impairs Dentin Formation in a Rat Model of Pulp Repair

To evaluate whether ASARM peptides display similar properties on dentin mineralization in teeth *in vivo*, we implanted agarose beads soaked in either p-ASARM or np-ASARM peptide, or control buffer, into injured dental pulp in a tooth-wound model in young rats. In this model, the repair process is mediated by endogenous pulp cells undergoing odontoblast differentiation [47]. Micro-CT analysis and histology after hematoxylin and eosin staining at 1 month following surgery and peptide implantation showed a reparative mineralized dentin bridge in all samples (Fig. 6A); however, it appeared thicker in both control and np-ASARM treated pulps when compared to the p-ASARM treated teeth. To quantify this reparative process using micro-CT, the pulp volume was segmented in order to calculate its global volume (Fig. 6B). The pulp volume was significantly greater in the p-ASARM-treated samples (1.03 mm^3+/−0.04) (thus less mineralized dentin bridge tissue) than in both the control and np-ASARM conditions (0.88 mm^3+/−0.06 and 0.86 mm^3+/−0.05, respectively). These results in an animal model are consistent with our other *in vitro* SHED cell culture observations and show that the p-ASARM peptide impairs dentin neo-formation and its mineralization after pulp injury. Given our *in vitro* data indicating that mineralization inhibited by p-ASARM was accompanied by an increased expression of MEPE, we then evaluated MEPE expression in this *in vivo* model using an antibody directed against the mid-region of MEPE. Nonmineralized spaces within a heterogeneous dentin bridge stained positively for MEPE in the p-ASARM treated samples (Fig. 6A). In addition, cells adjacent to and likely secreting this dentin bridge were strongly stained for MEPE. In contrast, in control and np-ASARM samples, a homogenous reparative bridge was seen with no MEPE staining. Taken together, these results demonstrate that the p-ASARM peptide enhances MEPE expression by differentiating dental pulp stem cells both *in vivo* and *in vitro*.

Discussion

A MEPE-derived ASARM peptide was previously identified in human hypophosphatemic tooth dentin [12]. Together with the results of the present study, these data present evidence that this peptide (and potentially other similar ASARM peptides derived from other matrix SIBLING proteins) may be involved in impairing tooth dentin mineralization as observed in patients affected with XLH. Using a cell culture collagen/tooth slice 3D scaffold model, together with an *in vivo* wound healing animal model, the present study demonstrates that the MEPE-derived ASARM peptide inhibits odontogenic differentiation of deciduous dental pulp stem cells (SHEDs), enhances MEPE expression, and impairs dentin ECM mineralization.

Cell functions such as migration, adhesion and differentiation are routinely studied in 2D cultures. However, interpretations from these *in vitro* models are limited by the fact that they do not accurately recreate the appropriate, natural tissue architecture [48,52,53,54,55]. We have therefore developed and used a 3D collagen/tooth slice scaffold model where seeded cells can undergo differentiation in a more natural ECM environment [41], as demonstrated by the expression of several well-known odontoblast markers commonly used to identify this cell type (without the added tooth slice, no odontoblast marker expression was observed – data not shown). Based on our previous clinical and histologic findings [3,6] together with observations made by others [4,8] reporting severe abnormalities in deciduous teeth of patients with XLH (spontaneous dental abscesses associated with enamel cracks, poorly mineralized dentin, large pulp chamber and prominent pulp horns), we used 3D culture of dental pulp cells which displayed a typical SHED phenotype [56] as confirmed by polychromatic flow cytometry (Fig. S1), and a tooth/dentin wounding model in rats to examine further the causes of XLH tooth pathology, with a focus on the effects of the MEPE ASARM peptide. Under mineralizing culture conditions without added peptide, we observed von Kossa-stained mineralized nodules in

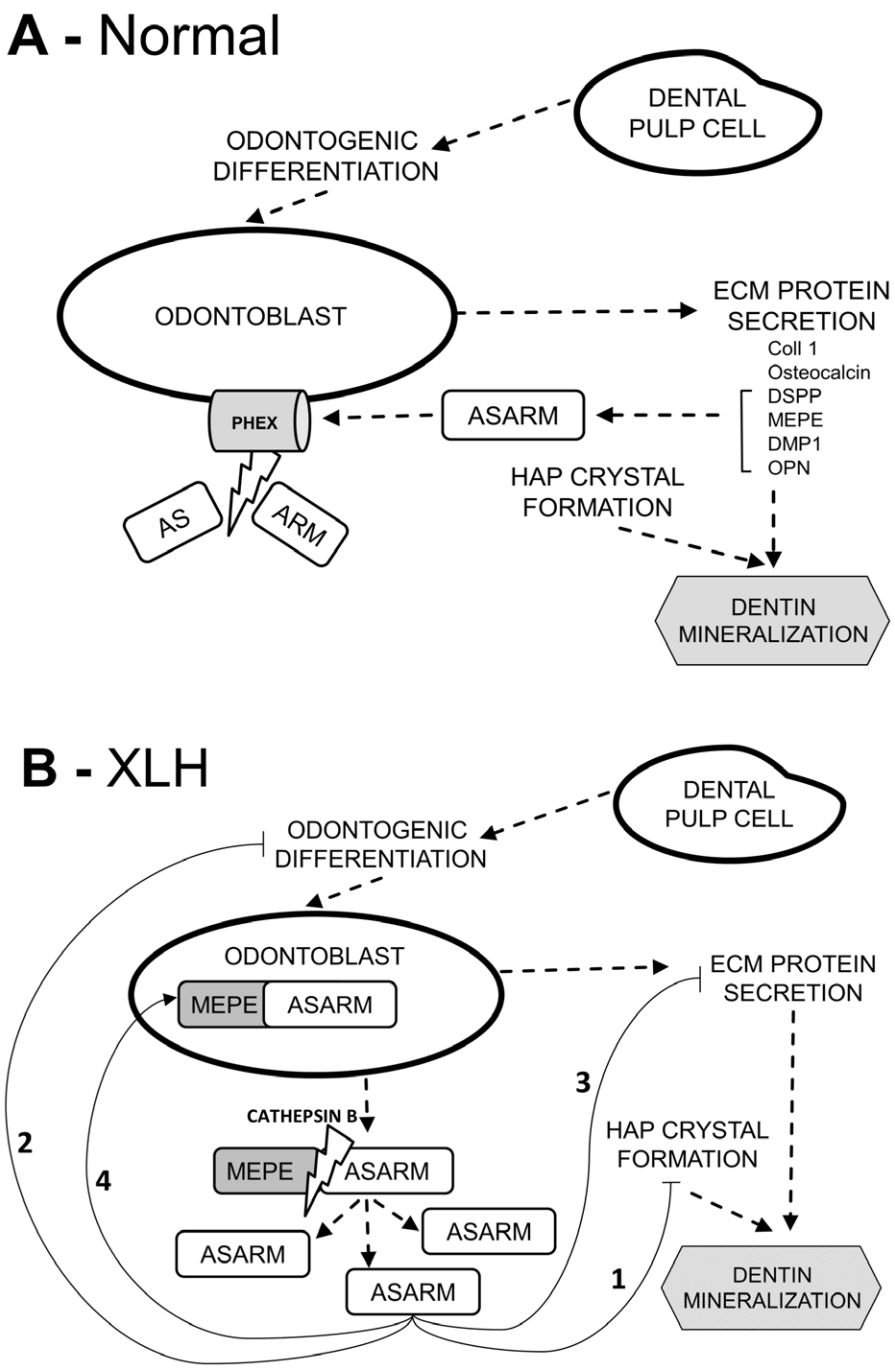

Figure 7. Summary of the role of the MEPE-derived ASARM peptide in the etiology of tooth dentin abnormalities in XLH patients. A: SIBLING proteins containing the ASARM peptide are processed by a multitude of proteolytic enzymes, some of which may release the ASARM peptide or larger protein fragments containing the ASARM peptide into the extracellular matrix (ECM). ASARM and ASARM-containing peptides are inhibitory for mineralization, binding directly to hydroxyapatite (HAP) mineral crystals in bones and teeth. In normal conditions, neutralizing PHEX cleavage of ASARM releases extracellular matrices from this inhibition and mineralization proceeds appropriately. B: In XLH tooth dentin, inactivating mutations in the *PHEX* gene result in nonfunctional PHEX enzyme that allows HAP crystal-binding, ASARM-containing peptides to accumulate in the dentin thus inhibiting tooth mineralization (pathway 1). Normal PHEX also protects full-length MEPE from cleavage by proteases (cathepsin B), thereby preventing release of mineralization-inhibiting ASARM. In XLH, excessive cleavage of MEPE by proteases (in the absence of functional PHEX) to release the inhibitory ASARM peptide might also contribute to the impaired mineralization of dentin. Finally, ASARM accumulation in XLH may impair dentinogenesis by decreasing odontoblast differentiation and downregulating genes encoding for secreted ECM proteins (pathways 2 and 3), while increasing MEPE expression (pathway 4) which in turn would further exacerbate the XLH hypomineralization tooth phenotype.
doi:10.1371/journal.pone.0056749.g007

the ECM which were in close proximity to the cells and not more distal in the collagen scaffold, suggesting that they resulted from a cell-mediated biomineralization process rather than from random (dystrophic) mineral deposition within the collagen scaffold. Collagen mineralization along collagen fibrils was confirmed morphologically by SEM and TEM analyses and by microana-

lytical EDX demonstrating high calcium and phosphorus levels within the nodules with calcium/phosphate ratios being comparable to those observed in human mineralized bone and tooth extracellular matrices [57,58,59. In addition, cells differentiated from normal SHEDs expressed a variety of mineralization-relevant biomarkers including PHEX, which demonstrates the utility of our collagen scaffold *in vitro* model in providing a suitable 3D matrix environment enabling odontoblast cell differentiation. Taken together, these observations confirm that the culture model used here was appropriate to evaluate SHED cell differentiation in response to addition of p-ASARM – a circumstance thought to be relevant to bone and tooth mineralization in the pathologic XLH condition where available evidence describes an accumulation of ASARM-containing (and other) peptides derived from the SIBLING proteins [14,32,33,36,37,60]. Whereas most of the studies reported to date describe the effects of ASARM peptides and their degradation by PHEX on mineralization in bone cell cultures, the present study is the first to extend these results to mineralization in odontoblast cultures, and to describe effects of ASARM on cell differentiation.

In terms of its effects on mineralization in the SHED/odontoblast 3D cultures, the phosphorylated form of the MEPE-derived ASARM peptide (p-ASARM) inhibits the formation of mineralization nodules in the collagenous ECM, whereas the non-phosphorylated form has no effect on mineralization. This observation is consistent with previous findings from bone cell cultures showing that the phosphorylation of MEPE- and OPN-derived ASARM peptides is necessary for the inhibition of ECM mineralization [14,32,33,37,60]. These previous bone cell studies demonstrated that the ASARM peptides inhibit mineralization in a phosphorylation-dependent manner via direct binding to hydroxyapatite crystals [14,33]. Interestingly, the p-ASARM dosage used by us and others to inhibit mineralization in cell culture (20 μM) is similar to the mean levels of ASARM peptide directly measured in the serum of patients with XLH, and in the serum of homolog Hyp mice (16 and 23 μM, respectively) [61].

In terms of its effects on cell differentiation in the SHED 3D cultures, we have made here the additional finding that ASARM peptide impairs dental pulp stem cell differentiation into odontoblast-like cells, an important observation with direct relevance to the pathologic mechanisms underlying XLH. The modified expression of odontoblast markers (DSPP, osteocalcin, alkaline phosphatase and MEPE) in the presence of ASARM peptides is a novel finding for tooth cells, and we further show that such an influence is more pronounced after exposure to the phosphorylated form of the peptide. Such observations are consistent with a previous study conducted on murine bone marrow stromal cells differentiating into osteoblasts, which reports a modification of osteoblast gene expression in the presence of MEPE-derived ASARM peptide [14]. Contrary to this, another study reported no effect of ASARM on cell differentiation using the murine MC3T3-E1 pre-osteoblast cell line [33]. This discrepancy may be explained by differences in cell characteristics (*e.g.* stem cells versus partially committed cells) and by the fact that these previous studies were carried out in 2D cell cultures.

In the present study, odontoblast differentiation was substantially impaired in the presence of p-ASARM as evidenced by the decrease (both at the mRNA and protein levels) of markers related to the odontoblast program such as DSPP and osteocalcin, whereas there was only a slight effect on these markers when np-ASARM was added.

The decreased osteocalcin expression reported here is consistent with those previously reported in bone cell cultures treated with p-ASARM [14], and also with our report on dentin matrix proteins in XLH deciduous human teeth where we showed by Western blot analysis of dentin extracts a decrease in osteocalcin and DSP compared to age-matched controls [7]. In contrast, type I collagen, the most prominent protein of dentin ECM, was not modified by the addition of the ASARM peptides in our present cell culture study. Indeed, type I collagen expression followed a pattern comparable to that previously reported for osteogenic cells cultured in a collagenous ECM-like 3D scaffold and treated with ascorbic acid [53]. In hypomineralized XLH human dentin, it appears that ECM matrix components are degraded at sites where the dentin does not mineralize [7].

Expression of tissue-nonspecific alkaline phosphatase (ALPL, TNAP) was up-regulated in our experiments in all mineralizing conditions from day 7 to day 14. This phosphatase catalyzes the hydrolysis of most phosphomonoesters – particularly cleavage of the potent mineralization-inhibiting small molecule pyrophosphate (PPi) found in serum, most tissue fluids and ECMs – releasing inorganic phosphate (Pi) which could contribute to local phosphate levels and mineralization [62]. In the present study, mRNA levels of alkaline phosphatase were upregulated prior to ECM mineralization and downregulated when mineralized nodules became apparent by bright field light microscopy after von Kossa staining. This expression pattern has been previously reported during the differentiation of human and murine osteogenic cell lines cultured within a dense collagen scaffold [53,63]. We additionally found that in the presence of the p-ASARM peptide, alkaline phosphatase mRNA levels remained elevated at the later culture time point (day 21). Such a difference might be explained by the fact that although most of the required conditions for mineralization *in vitro* have been met and are present in the cultures – including high levels of phosphate and calcium for mineralization, ascorbic acid for synthesis and secretion and assembly of collagen fibrils, and noncollagenous protein secretion – mineralization has not occurred in the presence of p-ASARM, and the cells are sensing that excess inhibitory PPi may need to be removed by continuing their ALPL expression. Interestingly, and similar to this observation, the serum of patients with XLH shows increased alkaline phosphatase activity, being especially high in children prior to their treatment (with vitamin D analogues and phosphate supplements) [64]. For example, in a group of 28 children affected with XLH and having a PHEX mutation, with a mean age of 2.2 ± 1.1 years, the mean $\pm$ SE alkaline phosphatase activity before any treatment was $1{,}320 \pm 910$ IU/L, being more than 4 times higher than the upper normal range (normal range is inferior to 300 IU/L); data from Centre de Référence des Maladies Rares du Métabolisme du Phosphore et du Calcium, AP-HP, Kremlin Bicêtre, France).

Our *in vivo* observations using a rat pulp injury model also support an inhibitory effect of phosphorylated MEPE-derived ASARM peptide on the formation of mineralized dentin. In this model, a reparative dentin bridge normally forms following injury and operates as a barrier to protect the dental pulp [39,47]. We previously reported abnormal dentin mineralization in the proximity of p-ASARM peptide soaked beads using this rat model [12]. Here we show in additional studies that only the phosphorylated form of the ASARM peptide impairs mineralization, and that immunohistochemistry for MEPE shows more intense staining of odontoblasts adjacent to the reparative dentin bridge after p-ASARM treatment than after np-ASARM treatment as applied by peptide-soaked agarose bead placement at the wound site. Moreover, here we have quantified pulp volume to show that it is significantly higher in rat molars treated with inhibitory p-ASARM, indicating decreased mineralization relative to controls. Paralleling this, when compared to age-matched

control patients with normal teeth, we previously reported a 2-fold higher pulp ratio (pulp chamber area/tooth area) in deciduous molars of children with XLH, and a 1.6-fold higher pulp ratio in permanent teeth of young adults with XLH [3].

The cleavage and protein-protein interactions of MEPE have been implicated in the pathogenicity of XLH [23]. Notably, it has been reported that MEPE is downregulated as odontoblasts differentiate [65,66]. In our *in vitro* experiments, p-ASARM significantly increased MEPE expression, both at the mRNA and protein levels. In addition, odontoblast-like cells producing reparative bridge dentin in rat dental pulps implanted with p-ASARM peptides strongly expressed MEPE. Thus, our *in vitro* and *in vivo* results indicate that the p-ASARM peptide enhances MEPE expression, which in turn might delay pulp stem cell differentiation as might be expected to occur in XLH patients. Moreover, accumulation of MEPE in the unmineralized heterogeneous dentin bridge regions identified in p-ASARM-treated rats is consistent with our previous observation showing that MEPE accumulates in the unmineralized interglobular spaces (between calcospherites) of dentin in patients with XLH [13]. Furthermore, the increased expression of MEPE we observed in the presence of p-ASARM both in the 3D culture model and in the wounded pulp rat model is consistent with previous publications reporting an upregulation of MEPE in osteoblasts of Hyp mice [16,20,23,37]. Thus, in XLH, overexpressed MEPE in osteoblasts (and shown here now in odontoblasts) results in the potential for more ASARM peptide to accumulate in the ECM of bone and dentin, which would not be cleaved away (as would normally occur by the enzymatic activity of PHEX) as a result of the inactivating PHEX mutations (summarized in Fig. 7). As the ASARM peptides are highly resistant to proteases and are only known to be degraded by PHEX [23,33], this positive-feedback loop on MEPE expression induced by ASARM peptides might exacerbate the disease and would thus be a mechanism contributing in part to the mineralization defect seen in XLH. Indeed, increased levels of ASARM peptide in serum have been reported in hypophosphatemic patients and in Hyp mice [31,61]. Furthermore, the ASARM peptide has been shown to accumulate in the renal tubules of Hyp mice [61], and recent evidence suggests that it may directly impair phosphate uptake and induce hypophosphatemia [31]. Studies are currently in progress using pulp cells derived from XLH patients to better understand the function of PHEX in this complex pathologic process.

In conclusion, using *in vitro* and *in vivo* models we demonstrate that the MEPE-derived ASARM peptide – previously identified in XLH dentin – inhibits both ECM mineralization and odontoblast differentiation, while increasing MEPE expression. These results provide for a partial mechanistic explanation of the pathogenesis of XLH whereby direct inhibition of mineralization by p-ASARM positively reinforced by increased MEPE expression induced by ASARM, together with decreased odontoblast differentiation to produce less dentin, leads to the mineralization defect and increased pulp chamber characteristic of teeth in XLH. Further studies are required to determine whether the MEPE-derived ASARM peptide affects odontoblast differentiation through indirect cell-signaling induced by defective ECM mineralization and/or by direct cell signaling with potential internalization of the peptide by cells. Collectively, these data appear promising in guiding the development of novel therapies for XLH through targeting the MEPE-ASARM system.

Supporting Information

Figure S1 Polychromatic flow cytometry analysis of dental pulp cells from deciduous teeth. More than 95% of cells at passage 2 were CD45-. In addition, most of them were CD90+/CD29+/CD44+/CD146+/CD105+/CD73+. About 10% were STRO-1+.
(TIFF)

Figure S2 Interaction of cells with the tooth dentin slice. Scanning electron microscopy of an interaction of SHEDs with the tooth dentin slice at day 21. Images show a close relationship between the cell processes (asterisks) and the dentin surface (containing many dentinal tubules). Higher magnification of the white dashed frame is shown in the right panel.
(TIFF)

Figure S3 MEPE-ASARM peptides do not affect PHEX expression. SHED cell cultures were maintained in nonmineralizing (NM) or mineralizing (M) conditions in the absence or presence of 20 μM of either phosphorylated (p-ASARM) or nonphosphorylated (np-ASARM) ASARM peptide for 21 days. Immunofluorescence microscopy (left panel) and Western blotting (right panel) were performed at day 21. Immunofluorescent staining for PHEX (arrows) is observed in the SHEDs under all conditions. Western blot analysis shows similar levels of PHEX protein without any significant differences between the different conditions, when normalized to cellular tubulin content.
(TIFF)

Acknowledgments

The authors thank Dr. Morad Benshidoum (UMR CNRS 7052 - Biomecanique et Biomateriaux Osteo-Articulaires B2OA) for his assistance with the micro-computed tomography. The authors greatly acknowledge Alain Schmitt and Jean-Marc Masse of the Cochin Imaging Facility, and Lydia Malynowsky, for assistance with the TEM. The authors are grateful to Jean-Luc Charrier, Marc Perrine and Henry Martinez for collecting third molars in odontology departments.

Author Contributions

Conceived and designed the experiments: BS CB SOV CC. Performed the experiments: BS CB MK JN BRC BB FL JL FD DLD AN. Analyzed the data: BS EH AL MDM CC AN. Contributed reagents/materials/analysis tools: FL AP PSR AL DLD. Wrote the paper: CC BS EH AP AL MDM.

References

1. Gorski JP (2011) Biomineralization of bone: a fresh view of the roles of non-collagenous proteins. Front Biosci 16: 2598–2621.
2. Opsahl Vital S, Gaucher C, Bardet C, Rowe PS, George A, et al. (2012) Tooth dentin defects reflect genetic disorders affecting bone mineralization. Bone 50: 989–997.
3. Chaussain-Miller C, Sinding C, Wolikow M, Lasfargues JJ, Godeau G, et al. (2003) Dental abnormalities in patients with familial hypophosphatemic vitamin D-resistant rickets: prevention by early treatment with 1-hydroxyvitamin D. J Pediatr 142: 324–331.
4. Seow WK, Needleman HL, Holm IA (1995) Effect of familial hypophosphatemic rickets on dental development: a controlled, longitudinal study. Pediatr Dent 17: 346–350.
5. Seow WK (1984) X-linked hypophosphataemic vitamin D-resistant rickets. Aust Dent J 29: 371–377.
6. Chaussain-Miller C, Sinding C, Septier D, Wolikow M, Goldberg M, et al. (2007) Dentin structure in familial hypophosphatemic rickets: benefits of vitamin D and phosphate treatment. Oral Dis 13: 482–489.
7. Boukpessi T, Septier D, Bagga S, Garabedian M, Goldberg M, et al. (2006) Dentin alteration of deciduous teeth in human hypophosphatemic rickets. Calcif Tissue Int 79: 294–300.
8. Murayama T, Iwatsubo R, Akiyama S, Amano A, Morisaki I (2000) Familial hypophosphatemic vitamin D-resistant rickets: dental findings and histologic study of teeth. Oral Surg Oral Med Oral Pathol Oral Radiol Endod 90: 310–316.

9. Fisher LW, Fedarko NS (2003) Six genes expressed in bones and teeth encode the current members of the SIBLING family of proteins. Connect Tissue Res 44 Suppl 1: 33–40.
10. Qin C, Baba O, Butler WT (2004) Post-translational modifications of sibling proteins and their roles in osteogenesis and dentinogenesis. Crit Rev Oral Biol Med 15: 126–136.
11. Suzuki S, Haruyama N, Nishimura F, Kulkarni AB (2012) Dentin sialophosphoprotein and dentin matrix protein-1: Two highly phosphorylated proteins in mineralized tissues. Arch Oral Biol.
12. Boukpessi T, Gaucher C, Leger T, Salmon B, Le Faouder J, et al. (2010) Abnormal presence of the matrix extracellular phosphoglycoprotein-derived acidic serine- and aspartate-rich motif peptide in human hypophosphatemic dentin. Am J Pathol 177: 803–812.
13. Gaucher C, Boukpessi T, Septier D, Jehan F, Rowe PS, et al. (2009) Dentin noncollagenous matrix proteins in familial hypophosphatemic rickets. Cells Tissues Organs 189: 219–223.
14. Martin A, David V, Laurence JS, Schwarz PM, Lafer EM, et al. (2008) Degradation of MEPE, DMP1, and release of SIBLING ASARM-peptides (minhibins): ASARM-peptide(s) are directly responsible for defective mineralization in HYP. Endocrinology 149: 1757–1772.
15. David V, Martin A, Hedge AM, Rowe PS (2009) Matrix extracellular phosphoglycoprotein (MEPE) is a new bone renal hormone and vascularization modulator. Endocrinology 150: 4012–4023.
16. Rowe PS, de Zoysa PA, Dong R, Wang HR, White KE, et al. (2000) MEPE, a new gene expressed in bone marrow and tumors causing osteomalacia. Genomics 67: 54–68.
17. Boskey AL, Chiang P, Fermanis A, Brown J, Taleb H, et al. (2010) MEPE's diverse effects on mineralization. Calcif Tissue Int 86: 42–46.
18. Rowe PS (2012) Regulation of bone-renal mineral and energy metabolism: the PHEX, FGF23, DMP1, MEPE ASARM pathway. Crit Rev Eukaryot Gene Expr 22: 61–86.
19. Staines KA, Mackenzie NC, Clarkin CE, Zelenchuk L, Rowe PS, et al. (2012) MEPE is a novel regulator of growth plate cartilage mineralization. Bone 51: 418–430.
20. Argiro L, Desbarats M, Glorieux FH, Ecarot B (2001) Mepe, the gene encoding a tumor-secreted protein in oncogenic hypophosphatemic osteomalacia, is expressed in bone. Genomics 74: 342–351.
21. Gowen LC, Petersen DN, Mansolf AL, Qi H, Stock JL, et al. (2003) Targeted disruption of the osteoblast/osteocyte factor 45 gene (OF45) results in increased bone formation and bone mass. J Biol Chem 278: 1998–2007.
22. Quarles LD (2003) FGF23, PHEX, and MEPE regulation of phosphate homeostasis and skeletal mineralization. Am J Physiol Endocrinol Metab 285: E1–9.
23. Rowe PS, Kumagai Y, Gutierrez G, Garrett IR, Blacher R, et al. (2004) MEPE has the properties of an osteoblastic phosphatonin and minhibin. Bone 34: 303–319.
24. Rowe PS, Garrett IR, Schwarz PM, Carnes DL, Lafer EM, et al. (2005) Surface plasmon resonance (SPR) confirms that MEPE binds to PHEX via the MEPE-ASARM motif: a model for impaired mineralization in X-linked rickets (HYP). Bone 36: 33–46.
25. Rowe PS, Oudet CL, Francis F, Sinding C, Pannetier S, et al. (1997) Distribution of mutations in the PEX gene in families with X-linked hypophosphataemic rickets (HYP). Hum Mol Genet 6: 539–549.
26. Gaucher C, Walrant-Debray O, Nguyen TM, Esterle L, Garabedian M, et al. (2009) PHEX analysis in 118 pedigrees reveals new genetic clues in hypophosphatemic rickets. Hum Genet 125: 401–411.
27. Lorenz-Depiereux B, Guido VE, Johnson KR, Zheng QY, Gagnon LH, et al. (2004) New intragenic deletions in the Phex gene clarify X-linked hypophosphatemia-related abnormalities in mice. Mamm Genome 15: 151–161.
28. Filisetti D, Ostermann G, von Bredow M, Strom T, Filler G, et al. (1999) Non-random distribution of mutations in the PHEX gene, and under-detected missense mutations at non-conserved residues. Eur J Hum Genet 7: 615–619.
29. Econs MJ, Friedman NE, Rowe PS, Speer MC, Francis F, et al. (1998) A PHEX gene mutation is responsible for adult-onset vitamin D-resistant hypophosphatemic osteomalacia: evidence that the disorder is not a distinct entity from X-linked hypophosphatemic rickets. J Clin Endocrinol Metab 83: 3459–3462.
30. Rowe PS (2004) The wrickkened pathways of FGF23, MEPE and PHEX. Crit Rev Oral Biol Med 15: 264–281.
31. David V, Martin A, Hedge AM, Drezner MK, Rowe PS (2011) ASARM peptides: PHEX-dependent and -independent regulation of serum phosphate. Am J Physiol Renal Physiol 300: F783–791.
32. Addison WN, Masica DL, Gray JJ, McKee MD (2010) Phosphorylation-dependent inhibition of mineralization by osteopontin ASARM peptides is regulated by PHEX cleavage. J Bone Miner Res 25: 695–705.
33. Addison WN, Nakano Y, Loisel T, Crine P, McKee MD (2008) MEPE-ASARM peptides control extracellular matrix mineralization by binding to hydroxyapatite: an inhibition regulated by PHEX cleavage of ASARM. J Bone Miner Res 23: 1638–1649.
34. Rowe PS (2012) The chicken or the egg: PHEX, FGF23 and SIBLINGs unscrambled. Cell Biochem Funct 30: 355–375.
35. Martin A, David V, Quarles LD (2012) Regulation and function of the FGF23/klotho endocrine pathways. Physiol Rev 92: 131–155.
36. Barros NM, Hoac B, Neves RL, Addison WN, Assis DM, et al. (2012) Proteolytic processing of osteopontin by PHEX and accumulation of osteopontin fragments in Hyp mouse bone, the murine model of X-linked hypophosphatemia. J Bone Miner Res.
37. Liu S, Rowe PS, Vierthaler L, Zhou J, Quarles LD (2007) Phosphorylated acidic serine-aspartate-rich MEPE-associated motif peptide from matrix extracellular phosphoglycoprotein inhibits phosphate regulating gene with homologies to endopeptidases on the X-chromosome enzyme activity. J Endocrinol 192: 261–267.
38. Atkins GJ, Rowe PS, Lim HP, Welldon KJ, Ormsby R, et al. (2011) Sclerostin is a locally acting regulator of late-osteoblast/preosteocyte differentiation and regulates mineralization through a MEPE-ASARM-dependent mechanism. J Bone Miner Res 26: 1425–1436.
39. Six N, Septier D, Chaussain-Miller C, Blacher R, DenBesten P, et al. (2007) Dentonin, a MEPE fragment, initiates pulp-healing response to injury. J Dent Res 86: 780–785.
40. Miura M, Gronthos S, Zhao M, Lu B, Fisher LW, et al. (2003) SHED: stem cells from human exfoliated deciduous teeth. Proceedings of the National Academy of Sciences of the United States of America 100: 5807–5812.
41. Cordeiro MM, Dong Z, Kaneko T, Zhang Z, Miyazawa M, et al. (2008) Dental pulp tissue engineering with stem cells from exfoliated deciduous teeth. J Endod 34: 962–969.
42. Rajan N, Habermehl J, Cote MF, Doillon CJ, Mantovani D (2006) Preparation of ready-to-use, storable and reconstituted type I collagen from rat tail tendon for tissue engineering applications. Nat Protoc 1: 2753–2758.
43. Huang GT, Yamaza T, Shea LD, Djouad F, Kuhn NZ, et al. (2010) Stem/progenitor cell-mediated de novo regeneration of dental pulp with newly deposited continuous layer of dentin in an in vivo model. Tissue Eng Part A 16: 605–615.
44. Baroukh B, Cherruau M, Dobigny C, Guez D, Saffar JL (2000) Osteoclasts differentiate from resident precursors in an in vivo model of synchronized resorption: a temporal and spatial study in rats. Bone 27: 627–634.
45. Roche PC, Ryan RJ, McCormick DJ (1992) Identification of hormone-binding regions of the luteinizing hormone/human corionic gonadotropin receptor using synthetic peptides. Endocrinology 131: 268–274.
46. Pfaffl MW (2001) A new mathematical model for relative quantification in real-time RT-PCR. Nucleic Acids Res 29: e45.
47. Chaussain C, Eapen AS, Huet E, Floris C, Ravindran S, et al. (2009) MMP2-cleavage of DMP1 generates a bioactive peptide promoting differentiation of dental pulp stem/progenitor cell. Eur Cell Mater 18: 84–95.
48. Bell E, Ivarsson B, Merrill C (1979) Production of a tissue-like structure by contraction of collagen lattices by human fibroblasts of different proliferative potential in vitro. Proc Natl Acad Sci U S A 76: 1274–1278.
49. Ortinau S, Schmich J, Block S, Liedmann A, Jonas L, et al. (2010) Effect of 3D-scaffold formation on differentiation and survival in human neural progenitor cells. Biomed Eng Online 9: 70.
50. Estes BT, Guilak F (2011) Three-dimensional culture systems to induce chondrogenesis of adipose-derived stem cells. Methods Mol Biol 702: 201–217.
51. Gronthos S, Mankani M, Brahim J, Robey PG, Shi S (2000) Postnatal human dental pulp stem cells (DPSCs) in vitro and in vivo. Proc Natl Acad Sci U S A 97: 13625–13630.
52. Coulomb B, Dubertet L, Merrill C, Touraine R, Bell E (1984) The collagen lattice: a model for studying the physiology, biosynthetic function and pharmacology of the skin. Br J Dermatol 111 Suppl 27: 83–87.
53. Pedraza CE, Marelli B, Chicatun F, McKee MD, Nazhat SN (2010) An in vitro assessment of a cell-containing collagenous extracellular matrix-like scaffold for bone tissue engineering. Tissue Eng Part A 16: 781–793.
54. Szpalski C, Wetterau M, Barr J, Warren SM (2011) Bone Tissue Engineering: Current Strategies and Techniques Part I-Scaffolds. Tissue Eng Part B Rev.
55. Wang J, Ma H, Jin X, Hu J, Liu X, et al. (2011) The effect of scaffold architecture on odontogenic differentiation of human dental pulp stem cells. Biomaterials 32: 7822–7830.
56. Kerkis I, Caplan AI (2012) Stem cells in dental pulp of deciduous teeth. Tissue Eng Part B Rev 18: 129–138.
57. Arnold WH, Gaengler P (2007) Quantitative analysis of the calcium and phosphorus content of developing and permanent human teeth. Ann Anat 189: 183–190.
58. Mishima H, Kozawa Y (1998) SEM and EDS analysis of calcospherites in human teeth. Eur J Oral Sci 106 Suppl 1: 392–396.
59. Barragan-Adjemian C, Nicolella D, Dusevich V, Dallas MR, Eick JD, et al. (2006) Mechanism by which MLO-A5 late osteoblasts/early osteocytes mineralize in culture: similarities with mineralization of lamellar bone. Calcif Tissue Int 79: 340–353.
60. Sakai VT, Cordeiro MM, Dong Z, Zhang Z, Zeitlin BD, et al. (2011) Tooth slice/scaffold model of dental pulp tissue engineering. Adv Dent Res 23: 325–332.
61. Bresler D, Bruder J, Mohnike K, Fraser WD, Rowe PS (2004) Serum MEPE-ASARM-peptides are elevated in X-linked rickets (HYP): implications for phosphaturia and rickets. J Endocrinol 183: R1–9.
62. Millan JL (2006) Alkaline Phosphatases : Structure, substrate specificity and functional relatedness to other members of a large superfamily of enzymes. Purinergic Signal 2: 335–341.
63. Bitar M, Brown RA, Salih V, Kidane AG, Knowles JC, et al. (2008) Effect of cell density on osteoblastic differentiation and matrix degradation of biomimetic dense collagen scaffolds. Biomacromolecules 9: 129–135.

64. Carpenter TO, Imel EA, Holm IA, Jan de Beur SM, Insogna KL (2011) A clinician's guide to X-linked hypophosphatemia. J Bone Miner Res 26: 1381–1388.
65. Liu H, Li W, Shi S, Habelitz S, Gao C, et al. (2005) MEPE is downregulated as dental pulp stem cells differentiate. Arch Oral Biol 50: 923–928.
66. Wang H, Kawashima N, Iwata T, Xu J, Takahashi S, et al. (2010) Differentiation of odontoblasts is negatively regulated by MEPE via its C-terminal fragment. Biochem Biophys Res Commun 398: 406–412.

Title: Periodontal Pathobiology and Defective Cell-Autonomous Mineralization in X-linked Hypophosphatemia

Abstract: X-linked hypophosphatemia (XLH) is a rare disorder caused by mutations in the *PHEX* gene. The impairment of PHEX leads to systemic loss of phosphate. The XLH skeleton displays rickets and osteomalacia, but little is known about the periodontal condition of XLH. Although the exact function of PHEX is not known, it has been shown that PHEX could interact with SIBLING proteins involved in the regulation of bone and dentin mineralization, but it is not yet clear if the defects in XLH are caused by systemic hypophosphatemia only, or also by local consequences of the absence of PHEX. The aim of this doctoral dissertation was to explore the pathobiology of the XLH periodontium and to determine the impact of PHEX deficiency at the local level in a model of human biomineralization. We examined 34 adults with XLH in a case-control study and observed that periodontitis frequency and severity were increased in case of incomplete supplementation in phosphate and vitamin D analogs. The periodontium was then analyzed in XLH dental roots and further characterized in the *Hyp* mouse, the murine analog of XLH. We performed a model of tooth movement adaptation and a model of periodontal breakdown and repair to investigate the impact of XLH on the pathobiology of periodontal tissues. Our results showed strongly affected XLH/*Hyp* periodontium and impaired pathobiology and suggested that the key role played by osteopontin (OPN) in bone could not be generalized to other mineralized tissues. In order to determine the role of PHEX in local human mineralization, dense collagen gels were seeded with dental pulp cells from XLH patients. Our results showed that despite normal phosphate concentrations, PHEX deficiency led to decreased quantity and quality of the mineral phase and a pathologic accumulation and processing of OPN. Overall, we showed that XLH patients were more prone to periodontitis, the *Hyp* mouse presented reduced adaptive capacities to tooth movement and alveolar bone repair and PHEX deficiency caused mineralization defects independently of hypophosphatemia in an *in vitro* model of human mineralization.

Keywords: PHEX, X-linked hypophosphatemia, mineralization, dental pulp cells, collagen hydrogels, periodontium, osteopontin, periodontal breakdown and repair, alveolar bone, overeruption

Titre : Physiopathologie parodontale et défauts intrinsèques de minéralisation dans le rachitisme hypophosphatémique lié à l'X

Résumé : Le rachitisme hypophosphatémique lié à l'X (XLH) est une maladie génétique rare causée par des mutations du gène *PHEX* qui entraine une hypophosphatémie. Le squelette des patients présente une ostéomalacie, mais leur statut parodontal est mal connu. Le substrat de la protéine PHEX n'est pas identifié. Il a été montré que PHEX avait la capacité d'interagir et de dégrader des protéines de la famille des SIBLINGs, impliquées dans la régulation de la minéralisation, mais on ne sait pas si *in vivo* les défauts de minéralisation observés résultent de l'hypophosphatémie systémique ou bien également d'effets locaux dus à l'absence de PHEX. Cette thèse s'est intéressée à la physiopathologie du parodonte XLH ainsi qu'à l'impact de la mutation de *PHEX* dans un modèle de biominéralisation où la concentration en phosphate pouvait être normalisée. Une étude clinique cas-témoins sur le statut parodontal de 34 patients XLH a montré que les malades dont la supplémentation en phosphate et vitamine D était incomplète présentaient une fréquence et une sévérité accrues de parodontite. Le parodonte XLH a été étudié sur des échantillons humains et sur la souris HYP, le modèle murin du XLH. Un modèle d'égression dentaire ainsi qu'un modèle de résorption et de réparation osseuses alvéolaires ont permis de caractériser la physiopathologie parodontale. Nos résultats ont montré que le parodonte XLH était très perturbé, nous avons aussi pu mettre en évidence que le rôle pathologique de l'ostéopontine dans le tissu osseux XLH ne pouvait pas être généralisé aux autres tissus minéralisés. La culture de cellules pulpaires de patients dans des matrices de collagène dense cultivées en concentrations normales en phosphate a montré que la perte de fonction de la protéine PHEX entrainait une diminution de la quantité et de la qualité de la phase minérale et une accumulation et une dégradation pathologiques de la protéine ostéopontine. Cette thèse doctorale a mis en évidence la susceptibilité accrue des patients XLH à la parodontite, une mauvaise adaptation de la souris HYP aux mouvements dentaires et à la réparation de l'os alvéolaire et a apporté la preuve d'un rôle pathologique de l'absence de PHEX indépendant de l'hypophosphatémie sur des cultures cellulaires primaires humaines.

Mots-clefs : Rachitisme hypophosphatémique lié à l'X, PHEX, hydrogels de collagène, cellules pulpaires, ostéopontine, parodonte, modèle de résorption et d'apposition parodontales, os alvéolaire, modèle d'égression